

A Synthetic and Computational Investigation of Trishomocubane-Amino Acid Derivatives

by


Terrence Raasch

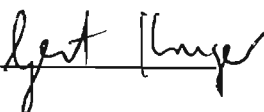
B.Sc. (Hons)

Submitted in fulfilment of the academic
requirements for the degree of
Master of Science in the
School of Pure and Applied Chemistry,
University of Natal,
Durban

June 2003

As the candidates supervisor I have approved this dissertation for submission.

Signed: 

Name: 

Date: 28/10/03

ABSTRACT

The class of polycyclic hydrocarbons including adamantane, pentacyclo [5.4.0.0^{2,6}.0^{3,10}.0^{5,9}]undecane (PCU) and trishomocubane have proven to be an exciting investigation for synthetic chemists. Many derivatives have been shown to possess excellent antiviral and antibacterial properties, as well as potent anti-Parkinson agents. Some improve the lipophilic nature of biologically active drugs, while others affect the three-dimensional structure of peptides once incorporated as amino acid analogues.

This investigation focussed on deriving routes to improve yields of racemic 4-amino-(D₃)-trishomocubane-4-carboxylic acid (tris-amino acid), the synthesis of enantiomerically pure tris-amino acid, the incorporation of tris-amino acid into a short peptide, as well as the simulation of the rearrangement of PCU to trishomocubane by using computational tools.

Research into developing a more efficient hydrolysis of trishomocubane-hydantoin (tris-hydantoin) to yield racemic tris-amino acid, led to the development of two novel compounds: the mono-Boc [**Novel Compound 1, (NC1)**] and bis-Boc [**Novel Compound 2, (NC2)**] protected hydantoin. Base hydrolysis of **NC2** quantitatively yielded the racemic tris-amino acid, which was a significant improvement on previously documented synthetic routes.

The first attempt to produce enantiomerically pure tris-amino acid was through the synthesis of diastereomeric derivatives of tris-hydantoin, chromatographic separation of the diastereomers, followed by base hydrolysis of the hydantoin ring to produce enantiomerically pure tris-amino acid. This research led to the development of two novel N-protected tris-hydantoin derivatives (**NC3** and **NC4**). Failure to chromatographically separate the diastereomers resulted in the abandonment of this particular route.

The use of enzymes was, therefore, attempted to produce enantiomerically pure tris-amino acid. A novel ester derivative of tris-amino acid (**NC5**) was synthesised, which was followed by the application of Pig Liver Esterase (PLE). PLE is an enzyme which cleaves ester functionalities. Some success was achieved but the extremely low yields of enantiomerically pure tris-amino acid did not warrant this enzyme as a viable route for production of the desired product.

Solid phase techniques were employed for the production of a tripeptide consisting of alanine-glycine-tris-amino acid (ala-gly-tris). Some difficulty was encountered in extending the amino acid sequence due to suspected Schiff base interaction between the free amino group of tris-amino acid and the carbonyl functionality of glycine in the second position.

A computational study, using *ab initio* methods, was performed on the rearrangement of the PCU diol to 7-fluoro-11-hydroxy-trishomocubane. Two mechanisms (**Proposed Mechanism 1** and **Proposed Mechanism 2**) were explored and both showed that the stereochemistry of the hydroxyl groups has only a marginal influence on the transition state

energies of the various isomers. Both mechanisms were also indicated to occur through an intramolecular S_N2 mechanism.

PREFACE

The experimental work described in this dissertation was carried out in the School of Pure and Applied Chemistry, University of Natal, Durban, from February 2002 to June 2003, under the supervision of Dr Hendrik G. Kruger.

These studies represent original work by the author and have not otherwise been submitted in any form for any degree or diploma to any tertiary institution. Where use has been made of the work of others it is duly acknowledged in the text.



Terrence Raasch

28 day of October 2003

LIST OF CONTENTS

	Page No.
List of Figures	vii
List of Tables	ix
List of Abbreviations	x
Acknowledgements.....	xiii
Chapter 1 Introduction	1
Chapter 2 Synthesis of 4-Amino-(D ₃)-Trishomocubane-4-Carboxylic Acid.....	5
Chapter 3 Diastereomers of Tris-Hydantoin	28
Chapter 4 Application of Enzymes to Cage Systems.....	35
Chapter 5 Peptide Synthesis	43
Chapter 6 Computational Chemistry.....	50
6.1 Introduction.....	50
6.1.1 Born-Oppenheimer Approximation.....	51
6.1.2 Hartree-Fock Approximation.....	52
6.1.3 LCAO Approximation	52
6.1.4 Roothaan-Hall Equations.....	52
6.2 Basis Sets for <i>Ab Initio</i> and DFT Calculations	54
6.2.1 Split-Valence Basis Set Incorporating Diffuse Functions (3-12+G).....	54
6.2.2 Polarisation Basis Set Incorporating Diffuse Functions [6-31+G(d)]	55
6.3 Other Models	55
6.3.1 Semi-Empirical Methods	55
6.3.2 Molecular Mechanics.....	56
6.3.3 Density Functional Theory	57
6.4 Transition State Modelling	57
6.5 Computational Tools.....	58
6.5.1 Gaussian 98 Program	58
6.5.2 Gauss View	58
6.6 Results for PCU Rearrangement to Trishomocubane.....	59

Chapter 7 Conclusion	68
Chapter 8 Experimental.....	70
References.....	79
Appendix 1 Spectra.....	84
Appendix 2 Commands for Gaussian 98	170
Appendix 3 Cartesian Co-ordinates for Computational Structures	173
Appendix 4 Compact Disk.....	181

LIST OF FIGURES

Figure 1.1: Enantiomers of serine	1
Figure 1.2: Role of angiotensin converting enzyme in regulating blood pressure	2
Figure 1.3: Structures of amantadine and adamantanine	3
Figure 1.4: Structure of pentacyclo[5.4.0.0 ^{2,6} .0 ^{3,10} .0 ^{5,9}]undecane and trishomocubane	3
Figure 2.1: Trishomocubane	5
Figure 2.2: “Diastereomers” of the quaternary substituted carbon of trishomocubane	6
Figure 2.3: Rearrangement of 2.4 to trishomocubane	7
Figure 2.4: Biologically active derivatives of trishomocubane	8
Figure 2.5: Bucherer-Bergs synthesis and hydantoin hydrolysis.....	9
Figure 2.6: Synthesis of 5,8-methano-4a,5,8,8a-tetrahydro-1,4-naphthoquinone (adduct, Spectra 1-3)	9
Figure 2.7: Synthesis of pentacyclo[5.4.0.0 ^{2,6} .0 ^{3,10} .0 ^{5,9}]undecane-8-11-dione via a classical, concerted [2+2] photocyclisation (dione, Spectra 4-6)	10
Figure 2.8: <i>Ab initio</i> calculated mechanism for adduct cyclisation.....	10
Figure 2.9: Synthesis of the keto-ketal (Spectra 7-9)	11
Figure 2.10: Nucleophilic attack on the keto functional group of cage systems	12
Figure 2.11: Synthesis of the hydroxy-ketal (Spectra 10-12)	12
Figure 2.12: Synthesis of the hydroxy-ketone (Spectra 13-15)	13
Figure 2.13: Synthesis of the <i>endo</i> -pentacyclo[5.4.0.0 ^{2,6} .0 ^{3,10} .0 ^{5,9}] undecane-8-ol (Spectra 16-18)	14
Figure 2.14: Synthesis of trishomocubane-4-ol (Spectra 19-21).....	15
Figure 2.15: Synthesis of trishomocubanone (Spectra 22-24).....	16
Figure 2.16: Synthesis of tris-hydantoin proposed by Bucherer (continued on following page)	17
Figure 2.16: Continuation of the synthesis of tris-hydantoin proposed by Bucherer (Spectra 25-32)	18
Figure 2.17: Alternative proposed mechanism for the synthesis of tris-hydantoin	19
Figure 2.18: DFT optimised tris-hydantoin	21
Figure 2.19: Synthesis of tris-amino acid (2.13) and Fmoc-tris-amino acid (2.65)	23
Figure 2.20: Novel Compound 1 (NC1, Spectra 37-44).....	24
Figure 2.21: Novel Compound 2 (Spectra 45-52)	25
Figure 2.22: Summary of novel synthetic work	27
Figure 3.1: Example of diastereomers	28
Figure 3.2: Strategy to produce diastereomers of tris-hydantoin.....	29
Figure 3.3: Synthesis of Novel Compound 3 (NC3)	31
Figure 3.4: Novel Compound 3 (NC3)	32
Figure 3.5: Novel Compound 4 (NC4)	33
Figure 4.1: Energetics of an enzyme-catalysed <i>versus</i> a non-enzyme catalysed reaction..	35
Figure 4.2: Lock and key mechanism	36
Figure 4.3: Hydrolysis of tris-hydantoin by hydantoinase enzyme	36
Figure 4.4: PLE catalysed hydrolysis of ester substrate	37

Figure 4.5: Novel Compound 5 (NC5)	37
Figure 4.6: Stereochemistry reversals exhibited by PLE.....	39
Figure 4.7: Side and top view of cubic space models of PLE active site	40
Figure 4.8: Effect of pH on activity of PLE	41
Figure 4.9: Effect of temperature on activity of PLE	42
Figure 5.1: Biologically important cage structures.....	43
Figure 5.2: Proposed tripeptide of ala-gly-tris	44
Figure 5.3: MBHA resin (5.5) and FmocAM linker (5.6)	45
Figure 5.4: Dehydrating action of DIPCDI	45
Figure 5.5: Fmoc deprotection using piperidine.....	46
Figure 5.6: Formation of a Schiff base bond	48
Figure 5.7: Summary of peptide synthesis.....	49
Figure 6.1: Restricted Hartree-Fock <i>versus</i> Unrestricted Hartree-Fock	53
Figure 6.2: Example of orbitals used in a split-valence set	54
Figure 6.3: Schematic representation of the five key contributions to a molecular force field.....	56
Figure 6.4: Proposed Mechanism 1	60
Figure 6.5: Proposed Mechanism 2	61
Figure 6.6: Transition state for the protonated trishomocubanol.....	62
Figure 6.7: Transition state for the <i>exo-endo</i> PCU diol.....	63
Figure 6.8: Transition state for the <i>exo-exo</i> PCU diol	63
Figure 6.9: Reaction pathway for Proposed Mechanism 1	64
Figure 6.10: Reaction pathway for Proposed Mechanism 2.....	65
Figure 6.11: Transition state for 8- <i>exo</i> -fluoro-11- <i>exo</i> -hydroxy-PCU	66
Figure 6.12: Transition state for 8- <i>exo</i> -fluoro-11- <i>endo</i> -hydroxy-PCU	66

LIST OF TABLES

Table 2.1: Force-field calculations for PCU and trishomocubane at 25 °C6

Table 2.2: NMR data for tris-hydantoin22

Table 3.1: Uses of bis(trichloromethyl)carbonate30

LIST OF ABBREVIATIONS

ACE	angiotensin converting enzyme
Aib	aminoisobutyric acid
ala	alanine
AlBr ₃	aluminium bromide
a.u.	atomic units
β	beta
Boc ₂ O	di- <i>tert</i> -butyl dicarbonate
<i>bs</i>	basis functions
CDCl ₃	deuterated chloroform
¹³ C NMR	carbon-13 nuclear magnetic resonance
COSY	correlation spectroscopy
CPU	central processing unit
<i>c_μ</i>	molecular orbital coefficient
C _x	carbon-x
d	doublet
DFT	density functional theory
DIPCDI	N,N-diisopropylcarbodiimide
DMAP	4-dimethylaminopyridine
DMF	N,N-dimethylformamide
DMSO	dimethyl sulphoxide
D ₂ O	deuterium oxide
<i>e</i>	charge of an electron
<i>E</i>	electron energies
E _a	energy of activation
<i>elec</i>	electrons
eq.	equivalent
etc.	etcetera
Et ₃ N	triethylamine
<i>F</i>	Fock matrix
FAB	fast atom bombardment
FmocAM	(<i>p</i> -[(R,S)- α -[1-(9H-fluoren-9-yl)methoxy-formamido]-2,4-dimethylbenzyl]-phenoxyacetic acid
Fmoc(-Cl)	9-fluorenylmethyl (chloro)formate
g	gram
G98	Gaussian 98
ΔG	change in Gibbs energy

gly	glycine
GUI	graphical user interface
HCl	hydrochloric acid
HF	hydrofluoric acid
HI	hydriodic acid
H _L	large hydrophobic region
HMBC	heteronuclear multiple bond coherence
¹ H NMR	hydrogen-1 nuclear magnetic spectroscopy
HNO ₂	nitrous acid
HNO ₃	nitric acid
HOBt	1-hydroxybenzotriazole
HPLC	high pressure liquid chromatography
H _{SM}	small hydrophobic region
HSQC	heteronuclear single quantum coherence
<i>h</i>	Planck's constant
hν	electromagnetic radiation
H _x	hydrogen-x
Hz	Hertz
I.D.	internal diameter
I.R.	infrared
KBr	potassium bromide
KH ₂ PO ₄	potassium dihydrogen phosphate
KOH	potassium hydroxide
LCAO	linear combination of atomic orbitals
LiOH	lithium hydroxide
m	multiplet
<i>m</i>	mass of electron
M	molarity
<i>M</i>	nuclear mass
MBHA	4-methylbenzhydramine
MgSO ₄	magnesium sulfate
MHz	Mega Hertz
mmol	millimole
mol	mole
m.p.	melting point
MP2	second order Møller-Plesset model
MP4	fourth order Møller-Plesset model
M.S.	mass spectroscopy
MS-TOF	mass spectroscopy-time of flight
m/z	mass per charge
NaOH	sodium hydroxide
NMR	nuclear magnetic resonance
NOESY	nuclear Overhauser effect spectroscopy
N _x	nitrogen-x
<i>nu</i>	nuclei

<i>occM.O.s</i>	occupied molecular orbitals
O_x	oxygen-x
P	density matrix
p	para
P_B	polar region at back of active site
PCU	pentacyclo[5.4.0.0 ^{2,6} .0 ^{3,10} .0 ^{5,9}]undecane
P_F	polar region at front of active site
PLE	pig liver esterase
ppm	parts per million
R	<i>rectus</i>
R_{AB}	distance separating nuclei
r_{ab}	distance separating electrons
r_{Aa}	distance separating electrons and nuclei
RHF	restricted Hartree-Fock
S	<i>sinister</i>
S	overlap matrix
s	singlet
SCF	self-consistent field
ser	serine
t	triplet
TFA	trifluoroacetic acid
THF	tetrahydrofuran
TS	transition state
UHF	unrestricted Hartree-Fock
UND	University of Natal, Durban
U.V.	ultra violet
Z	nuclear charge
ψ	wavefunction describing motion of electrons
\AA	Angstrom
α	alpha
ν_{\max}	frequency of maximum absorption
$^{\circ}\text{C}$	degrees Celsius
1°	primary
2°	secondary
\sim	approximately
$\%$	percent
∇^2	del squared
ϕ	atomic orbitals
ϵ	orbital energies
σ	sigma
π	pi

ACKNOWLEDGEMENTS

I would like to thank Dr H.G. Kruger, my supervisor at the University of Natal, Durban for allowing me to join his research team, and for giving me the freedom to explore chemistry that captured my imagination. I am extremely thankful to Mr T. Govender and Mr A. Singh at the University of Natal, Durban for all their support in and out of the laboratory.

I would like to thank Dr G. Maguire from the University of Natal, Durban for assisting in my understanding of chemical processes as well as Prof. Martincigh from the University of Natal, Durban for scrutinising the final draft of this dissertation.

I am thankful to Dr L. Fourie from Potchefstroom University for Christian Higher Education for all my mass spectroscopy data, Mr D. Jagjivan from the University of Natal, Durban for processing all the nuclear magnetic resonance data, and Mr A. M. Salim from the University of Natal, Durban for assisting me with the high performance liquid chromatography instrument.

I would like to thank Sasol, South Africa for upgrading the computational facilities at the University of Natal. A word of appreciation is also extended to the National Computational Science Alliance (USA) under grant number CHE000031N (NCSA SGI/CRAY Origin 2000) for computational support during this study. I would also like to thank the National Research Fund and the University of Natal, Durban for their generous financial support.

This work is dedicated to my family and friends for all their support throughout my journey into the world of chemistry.

CHAPTER 1

INTRODUCTION

The word protein is derived from the Greek word *proteios*, which means first. This is an appropriate name considering that proteins are primary building blocks for all life on earth.¹ Proteins are fundamental to all living cells as they are principal components of enzymes, hormones, antibodies and tissue.

Proteins are polymers of natural α -amino acids, which, except for glycine, contain at least one chiral centre.[†] A chiral molecule cannot be superimposed upon its mirror image (enantiomers, **Fig. 1.1, No. 1.1** and **1.2**). Those amino acids with chiral centres can naturally co-exist as enantiomers (**R** or **S** configuration) since they possess identical chemical and physical properties in the absence of an external chiral influence.

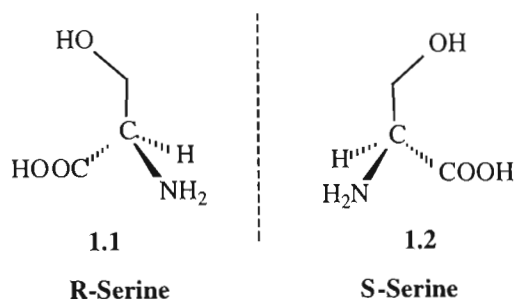


Figure 1.1: Enantiomers of serine

Amino acids found in eukaryotic organisms are mainly of the **S**-configuration.² This is key information to a chemist involved in asymmetric synthesis, since only one enantiomer of the synthesised racemate is likely to be biologically active. This is the challenge that has encouraged synthetic organic chemists to develop techniques that afford enantiopure molecules.³

In 1820 glycine was first isolated from gelatin hydrolyzates.⁴ In the 100 years that followed, the remaining 20 essential amino acids, which are normally found in proteins, were isolated. Since 1956 well over 500 naturally occurring amino acids have been identified due to the improvement of detection and elucidation techniques.⁴ There has also been extensive research into the asymmetric synthesis of non-natural amino acids since many have shown capacity to modify the biological activity of medically important peptides and have also been used extensively in the field of peptidomimetics.^{5,6} One example is the asymmetric synthesis of various substituted prolines. They have been used to alter the conformational behaviour of flexible, small peptides as well as inhibit angiotensin converting enzyme (ACE).⁶ ACE is a metalloprotease, which plays a vital role

[†] A chiral centre is a carbon atom with four different groups attached.

in blood pressure regulation.^{6,7} Captopril, which is an oral drug containing an enantiopure derivative of proline, has been successful in reducing blood pressure and preventing heart failure through the inhibition of ACE activity (**Fig. 1.2**).⁶ ACE is involved in cleaving off a dipeptide from the inactive decapeptide, angiotensin I, to give the biologically active octapeptide, angiotensin II. This peptide is involved in activating various systems that lead to increasing blood pressure. Captopril inhibits the actions of ACE, therefore, not allowing the production of angiotensin II (**Fig. 1.2**).

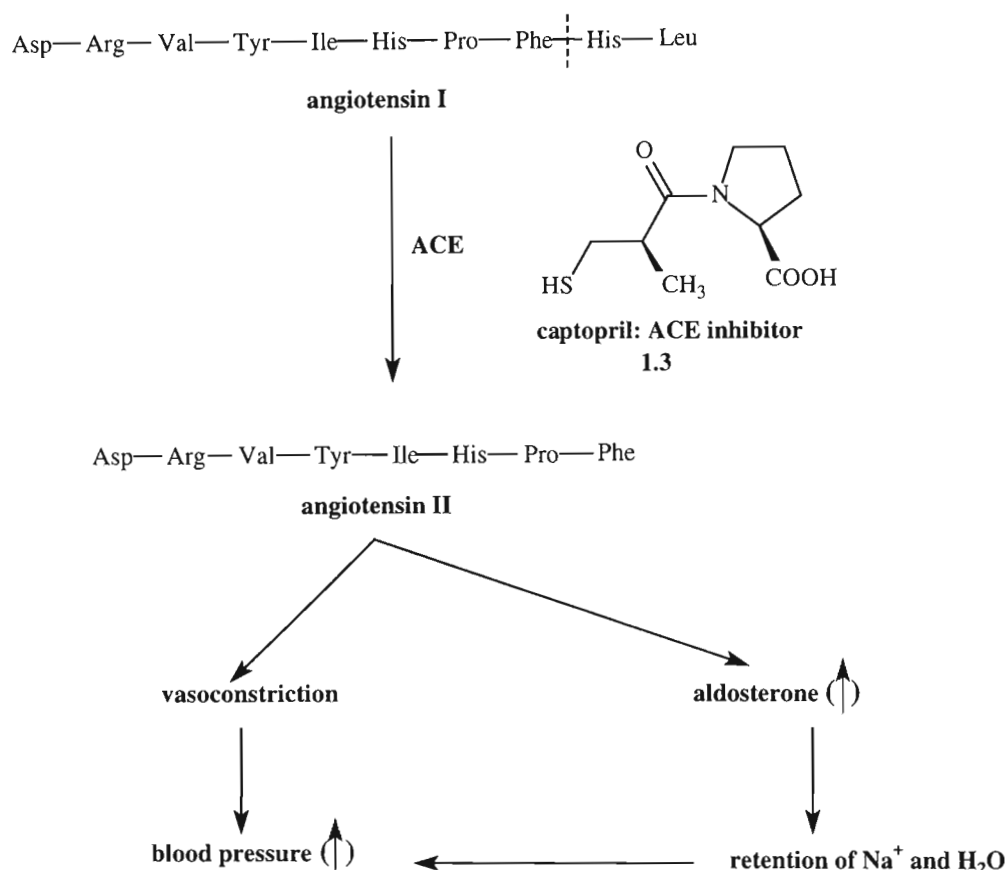


Figure 1.2: Role of angiotensin converting enzyme in regulating blood pressure

The synthetic organic chemistry research group of the University of Natal, Durban (UND) has followed suit in this growing field of non-natural amino acid synthesis.

The incorporation of cage molecules into various drugs has proven to aid biological activity.^{8,9,10,11} 1-Aminoadamantane, also known as amantadine (**Fig. 1.3, No. 1.4**), has proven to be an effective antiviral and anti-Parkinson agent.¹² Adamantanine (**Fig. 1.3, No. 1.5**) has displayed success as a biologically active species, with the capacity to reduce transport of methionine and leucine into Ehrlich ascites carcinoma cells *in vitro*.^{8,13} There have also been reports of polycyclic cage hydrocarbons improving lipophilicity, therefore, enhancing drug and ion transport across cellular membranes.^{9,14,15} A computational study, involving Ramachandran plots of short peptides containing a non-natural cage amino acid,

has suggested that the bulky cage is likely to influence secondary folding of the peptide.¹⁶ This synthetic study may contribute towards a mechanical synthetic tool to modify the three-dimensional structure of proteins.¹⁶ Our long term goal is to enhance the understanding of the manipulation of the three-dimensional structure of peptides and ultimately to design peptides/drugs to fit a required receptor site.

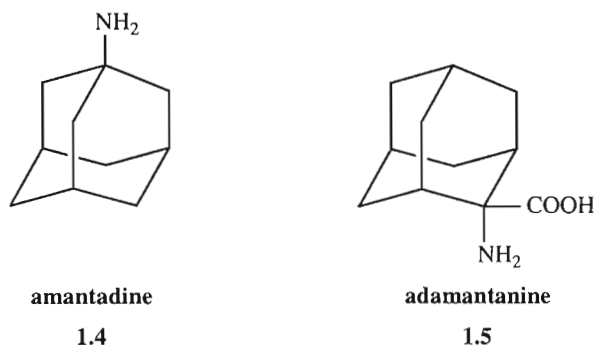


Figure 1.3: Structures of amantadine and adamantanine

Our research group is actively involved in asymmetric synthesis, solid phase peptide synthesis, and computational studies of polycyclic cage derivatives. The group pays particular attention to the chemistry of pentacyclo[5.4.0.0^{2,6}.0^{3,10}.0^{5,9}]undecane (PCU, **Fig. 1.4, No. 1.6**) and pentacyclo[6.3.0.0^{2,6}.0^{3,10}.0^{5,9}]undecane (trishomocubane, **Fig. 1.4, No. 1.7**) and their amino acid derivatives, since various cage amino derivatives have been cited as pharmaceutically important.^{13,17,18,19,20}

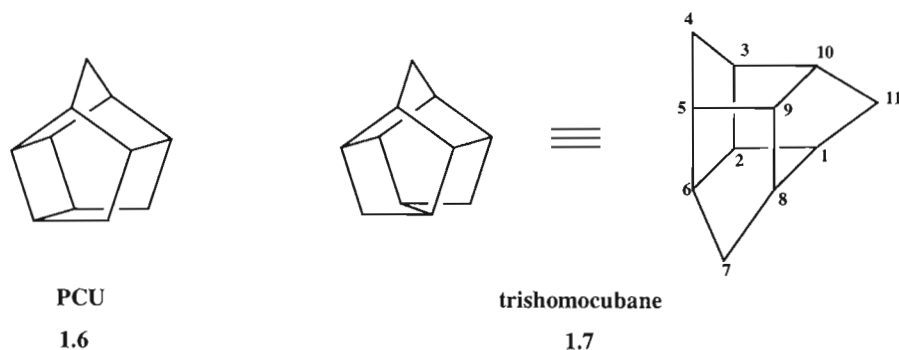


Figure 1.4: Structure of pentacyclo[5.4.0.0^{2,6}.0^{3,10}.0^{5,9}]undecane and trishomocubane[‡]

This project had four aims: (a) to improve the synthesis of racemic 4-amino-(D₃)-trishomocubane-4-carboxylic acid (tris-amino acid), (b) to synthesise enantiopure tris-amino acid, (c) to incorporate racemic tris-amino acid into a short peptide, and (d) to perform a computational investigation on the rearrangement of the PCU skeleton to trishomocubane.

[‡] The numbering system for trishomocubane was adopted from the paper published by Dekker *et al*, *Journal of Organic Magnetic Resonance.*, **1981**, 15, 188-192.

Many researchers have reported synthetic routes to afford enantiopure trishomocubane and various derivatives thereof,^{21,22} yet before a recent study,²³ there has been no attempt to synthesise tris-amino acid. Govender reported the successful synthesis of racemic tris-amino acid.²³ Research was, therefore, also undertaken to synthesise enantiopure tris-amino acid through the chromatographic separation of diastereomers, as well as the use of enzymes. The results are reported in the following chapters.

CHAPTER 2

SYNTHESIS OF 4-AMINO-(D₃)-TRISHOMOCUBANE-4-CARBOXYLIC ACID

Pentacyclo[6.3.0.0^{2,6}.0^{3,10}.0^{5,9}]undecane (trishomocubane) was first reported by Eaton *et al.* in 1968, as a keto-derivative.²⁴ Two years later, Ramamoorthy and Underwood were successful in synthesising the underivatised C₁₁H₁₄ polycyclic hydrocarbon, which they proposed the trivial name trishomocubane (**Fig. 2.1, No. 1.7 and 2.1**).²⁴

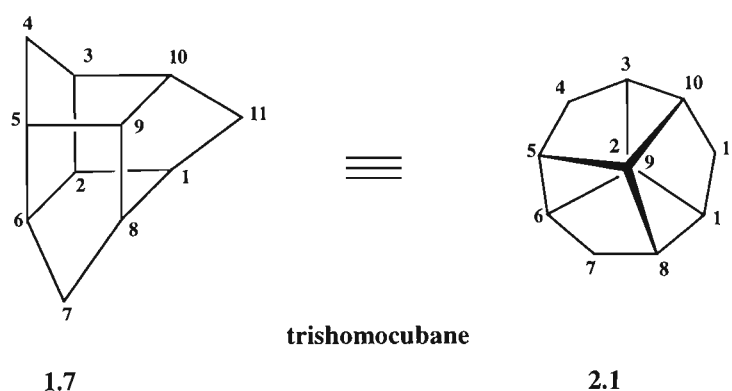


Figure 2.1: Trishomocubane

Trishomocubane can be regarded as a molecule of six fused, equivalent cyclopentane rings.²⁵ It is the only C₁₁H₁₄ pentacycle that does not contain highly strained three or four membered rings, and is a rare organic molecule belonging to the point group D₃.²⁶ Trishomocubane possesses three C₂ axes of symmetry (through each of the methylene groups and the centre of the opposite C-C bond), as well as an axis of symmetry passing through C₂ and C₉. It is also a chiral molecule.²⁵ Trishomocubane can, therefore, be termed a gyrochiral molecule.²¹ This describes the symmetry of a shape which is chiral but not asymmetric and of the point groups C_n (n≠1), D_n, T, O and I.²⁷ The D₃ symmetry of the cage ensures only two enantiomers for a quaternary substituted carbon instead of the usual set of four diastereomers (**Fig. 2.2**).

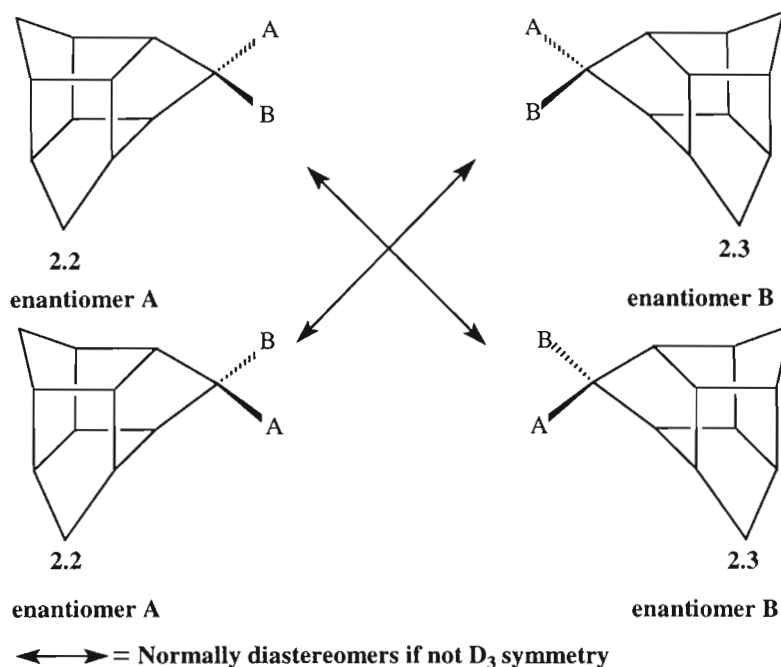


Figure 2.2: “Diastereomers” of the quaternary substituted carbon of trishomocubane

Empirical force field calculations using Allinger and Engler force-fields predicted trishomocubane to possess the greatest stability over any of the other C₁₁H₁₄ isomers.^{28,29} It is, for example, 10 kcal mol⁻¹ (ΔH) more stable than the PCU skeleton (also C₁₁H₁₄), making PCU an excellent starting material for the synthesis of trishomocubane (Table 2.1)^{26,28} since the rearrangement is exothermic.

Table 2.1: Force-field calculations for PCU and trishomocubane at 25 °C^{28,29}

	ΔH_f (kcal mol ⁻¹)	ΔH_f (kcal mol ⁻¹)	Strain energy (kcal mol ⁻¹)	Strain energy (kcal mol ⁻¹)
Compound	Engler	Allinger	Engler	Allinger
trishomocubane (1.7)	3.38	11.32	42.05	44.13
PCU (1.6)	19.62	21.93	52.29	54.74

Rearrangement of PCU to trishomocubane is thought to occur via a 1,2 alkyl shift of an intermediate secondary cation (Fig. 2.3).²⁶ It is not clear from the literature whether the mechanism occurs via a S_N1 or S_N2 intramolecular attack.

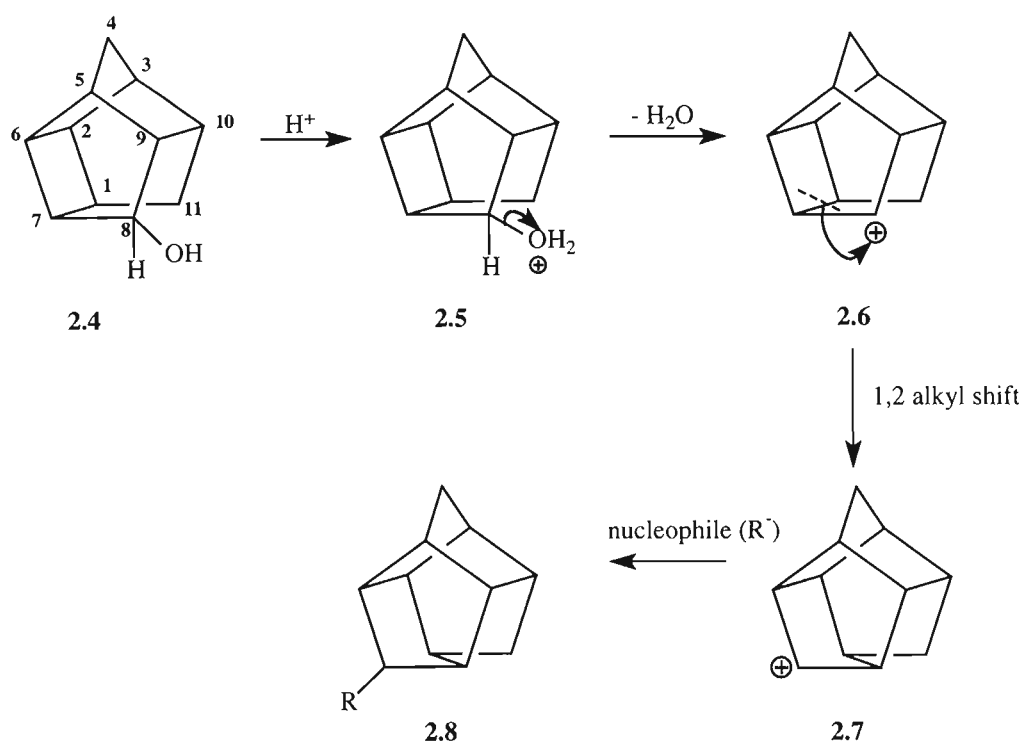


Figure 2.3: Rearrangement of 2.4 to trishomocubane

Kent *et al.* used force field calculations to predict the stability of various D₃-trishomocubyl cations (**Fig. 2.3, No. 2.6**) with respect to the aluminium bromide catalysed rearrangement of PCU to trishomocubane.²⁶ Cations at C₁, C₃, C₄, C₆, were predicted to be unfavourable. A cation at C₉ was predicted to be not prohibitively strained but all possible 1,2 alkyl shifts involving an initial carbocation at C₉ lead to products with four membered rings. A cation at the C₈/C₁₁ position was the thermodynamically most suitable position predicted, being the energetically most favourable, as well as the only 1,2 alkyl shift that did not result in the formation of a four membered ring.²⁶ The above mentioned results were reported for the AlBr₃ catalysed bromination in carbon disulfide. The synthesis yielded trishomocubane (93 %), 2,4-ethanonoradamantane (5 %) and 2,8-ethanonoradamantane (2 %). There are many alternative routes for the synthesis of trishomocubane, such as the Wolff-Kishner reduction of PCU with sodium, in diethylene glycol.²⁶ This synthesis also afforded unwanted side products due to the strain energy associated with the PCU molecule. Treatment of the PCU diol with hydriodic acid (HI) also leads to cage rearrangement, resulting in 7-iodo-trishomocuban-4-ol.²⁶ The mechanism for this rearrangement is more closely studied in **Chapter 6**, using computational tools.

Dekker *et al.* reported, through isotopic labelling experiments, that the rearrangement does not proceed exclusively via migration of the 1,7 bond as expected.³⁰ They did not offer a mechanism for the unexpected result and did not seem to report a follow-up study as they indicated.³⁰ There is, however, universal agreement that trishomocubane is the current

$C_{11}H_{14}$ stabilomer, which is the isomer that possesses the greatest thermodynamic stability at 25 °C in the gas phase.²⁶

By 1970, when Ramamoorthy and Underwood had synthesised and reported trishomocubane, biological applications for adamantane derivatives had already been discovered.¹¹ They foresaw a similar future for their $C_{11}H_{14}$ hydrocarbon. Their vision has become reality, with various trishomocubane derivatives exhibiting potential pharmacological properties¹³ as well as possible solar energy storage systems.³¹

As an example of the biological importance of trishomocubane derivatives, Oliver *et al.* synthesised various 4-amino-(D₃)-trishomocubane derivatives.¹³ These were tested as potential anticataleptic and anticholinergic agents. Many of the derivatives displayed promising results. One derivative (**Fig. 2.4, No. 2.9**) in particular, exhibited equipotency to amantadine (known anti-Parkinson agent) with regard to anticataleptic activity as well as mild anticholinergic activity.¹³ It also displayed excellent activity against Influenza A₂. An analogous compound (**Fig. 2.4, No. 2.10**) displayed activity against Herpes Simplex Type II. The difference in activity is attributed to the primary amine as opposed to a secondary amine.¹³

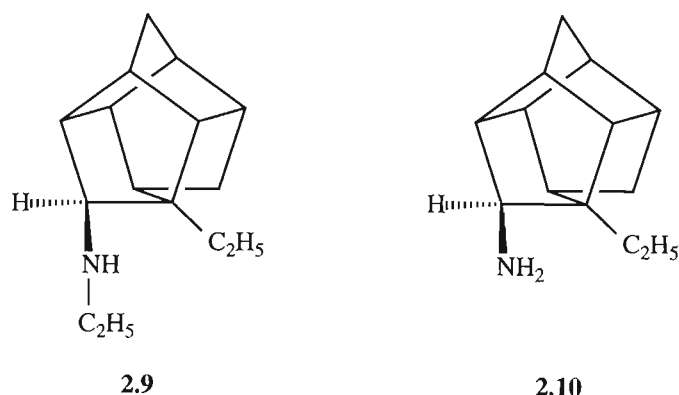


Figure 2.4: Biologically active derivatives of trishomocubane¹³

There has also been a great deal of research involving the incorporation of cage compounds into short peptide sequences. Many peptides containing non-proteinogenic or non-natural amino acids have been reported to exhibit biological activity.^{5,6,7,32,33} The incorporation of adamantyl cage amino acids into short peptides has yielded very promising results with regard to biological activity.¹⁰ The incorporation of tris-amino acid (**Fig. 2.5, No. 2.13**) into a short peptide may also prove to be a candidate for biological testing. Synthesis of the tris-amino acid involved numerous, well documented reactions, therefore, the work presented in this chapter deals with the synthesis of tris-amino acid, the starting material for the peptide work presented in **Chapter 5**.

The synthesis of the tris-amino acid (**Fig. 2.5, No. 2.13**) was achieved via a Bucherer-Bergs^{23,34} conversion of trishomocubanone (**Fig. 2.5, No. 2.11**) to its corresponding hydantoin (**Fig. 2.5, No. 2.12**). Subsequent base hydrolysis yields the corresponding tris-

amino acid (**Fig. 2.5, No. 2.13**).²³ This method was previously successfully applied to adamantanone³⁵ as well as to pentacyclo-undecanone.³⁶

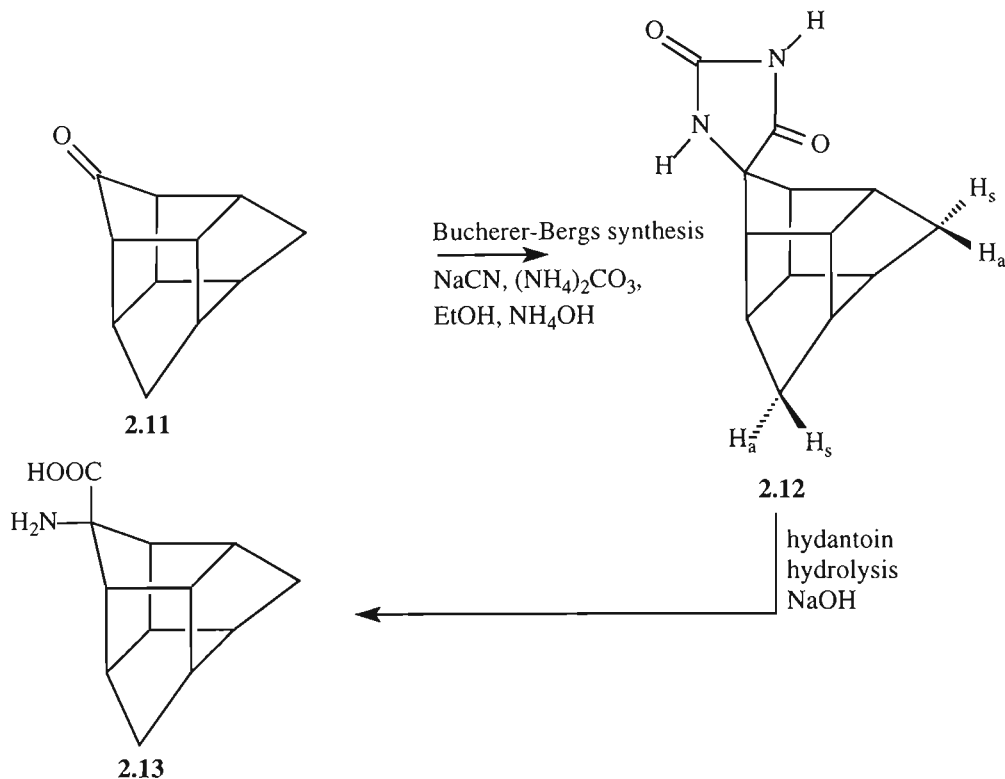


Figure 2.5: Bucherer-Bergs synthesis and hydantoin hydrolysis

The synthesis of trishomocubane began with the synthesis of the PCU skeleton, followed by cage rearrangement to yield the desired product. The PCU skeleton was synthesised in a two step Diels-Alder reaction. First, 5,8-methano-4a,5,8,8a-tetrahydro-1,4-naphthoquinone (adduct, **Fig. 2.6, No. 2.17**) was synthesised via a slow Diels-Alder reaction between cyclopentadiene (**Fig. 2.6, No. 2.14**) and *p*-benzoquinone (**Fig. 2.6, No. 2.15**).³⁷

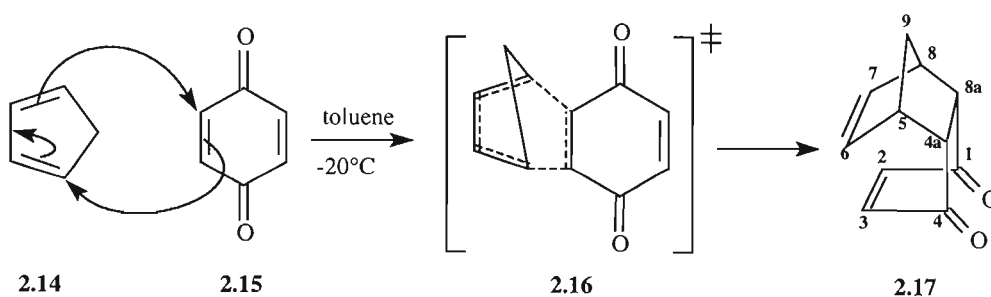


Figure 2.6: Synthesis of 5,8-methano-4a,5,8,8a-tetrahydro-1,4-naphthoquinone (adduct, Spectra 1-3)³⁸

The adduct was, subsequently, dissolved in 10 % (v/v) acetone in hexane solution and placed in direct sunlight. It was previously believed that photochemically induced intramolecular [2+2] cyclisation of compound 2.18 (**Fig. 2.7**) yielded pentacyclo

[5.4.0.0^{2,6}.0^{3,10}.0^{5,9}]undecane-8-11-dione (Cookson diketone or dione, **Fig. 2.7, No. 2.19**).^{37,39,40}

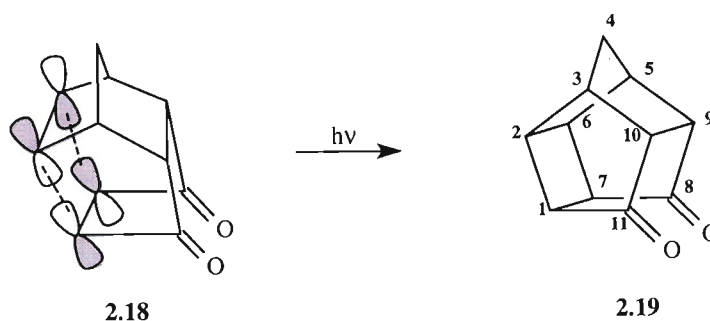


Figure 2.7: Synthesis of pentacyclo[5.4.0.0^{2,6}.0^{3,10}.0^{5,9}]undecane-8-11-dione via a classical, concerted [2+2] photocyclisation (dione, Spectra 4-6)

Recent *ab initio* investigations, however, have discovered that the cyclisation of the adduct proceeds via a stepwise diradical mechanism, through a triplet excited state rather than a concerted [2+2] cycloaddition (**Fig. 2.8**).⁴¹

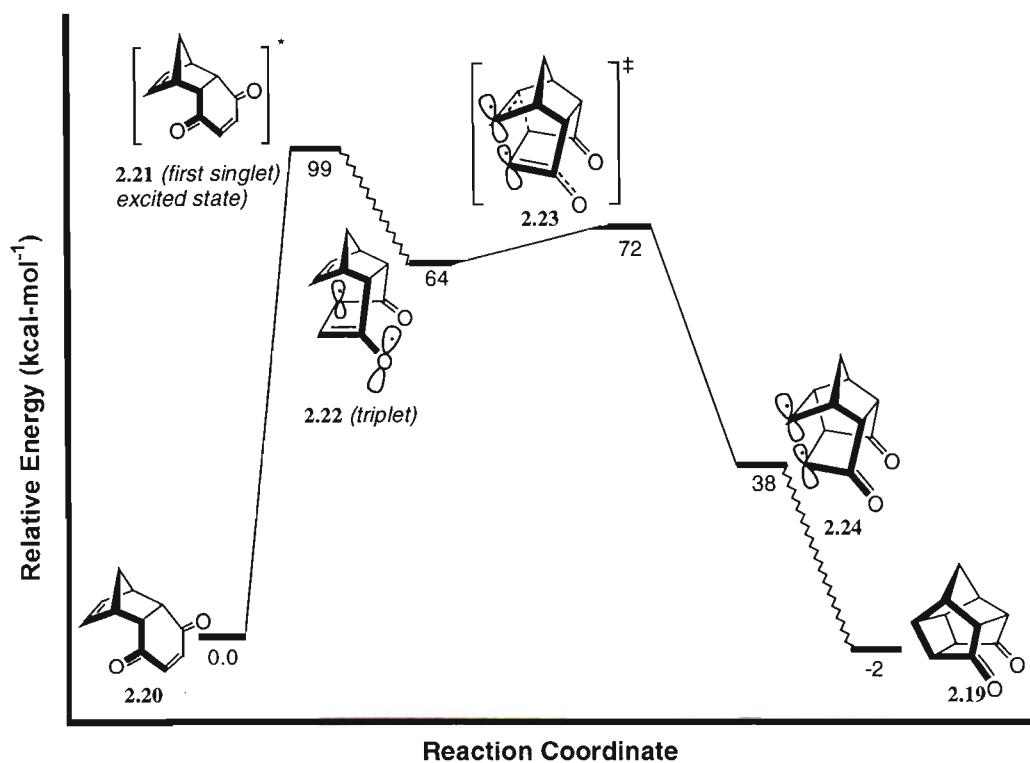


Figure 2.8: *Ab initio* calculated mechanism for adduct cyclisation⁴¹

Synthesis of trishomocubanone from the dione (**Fig. 2.9, No. 2.19**) involved protection of the free ketone via ketal formation for the purpose of mono-keto reduction in the following synthetic step. Ketal protection was achieved by refluxing (Dean and Stark apparatus) with 1,2-ethanediol and *p*-toluenesulfonic acid in toluene.^{42,43} The proximity of the two keto groups of (2.27) ensured mono protection due to steric hindrance. Even with excess 1,2-

ethanediol (1:1.5), only the mono protected dione (**Fig. 2.9, No. 2.33**) was obtained. Note, that it is well established^{44,45} that nucleophilic attack on the ketone groups of the PCU skeleton will almost exclusively occur from the *exo* face (**Fig. 2.10**). The mechanism of conversion to pentacyclo[5.4.0.0^{2,6}.0^{3,10}.0^{5,9}]undecane-8-11-dione-monoethylene ketal (keto-ketal) is illustrated in **Fig. 2.9**.⁴²

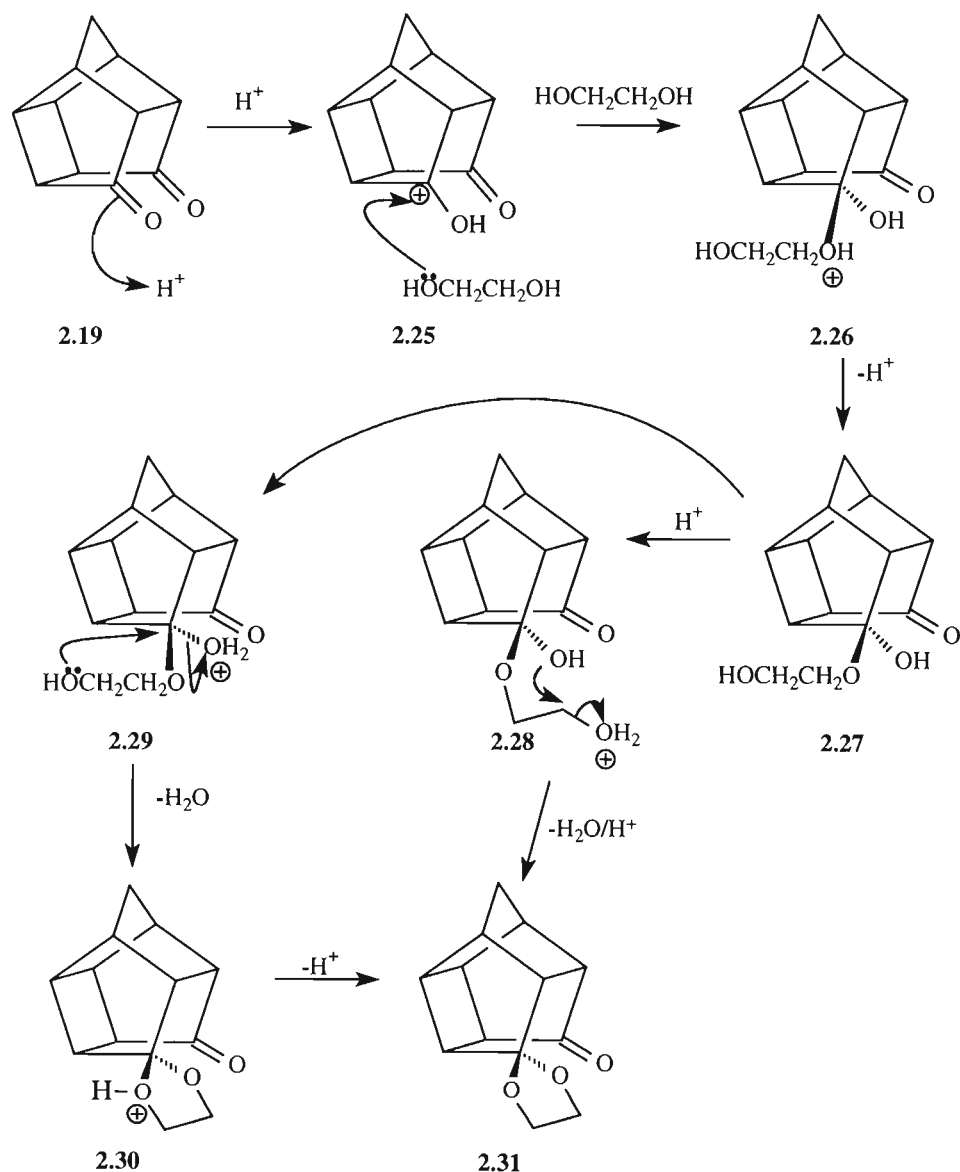


Figure 2.9: Synthesis of the keto-ketal (Spectra 7-9)⁴⁶

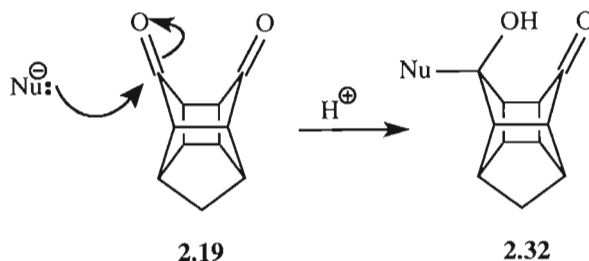


Figure 2.10: Nucleophilic attack on the keto functional group of cage systems

The keto-ketal (**Fig. 2.11, No. 2.33**) was dissolved in ethanol and the free ketone reduced with sodium borohydride. This resulted in the formation of 11-hydroxypentacyclo[5.4.0.0^{2,6}.0^{3,10}.0^{5,9}]undecane-8-one-ethylene ketal (hydroxy-ketal, **Fig. 2.11, No. 2.35**).^{37,42,43} An accepted mechanism of reduction is illustrated in **Fig. 2.11**.

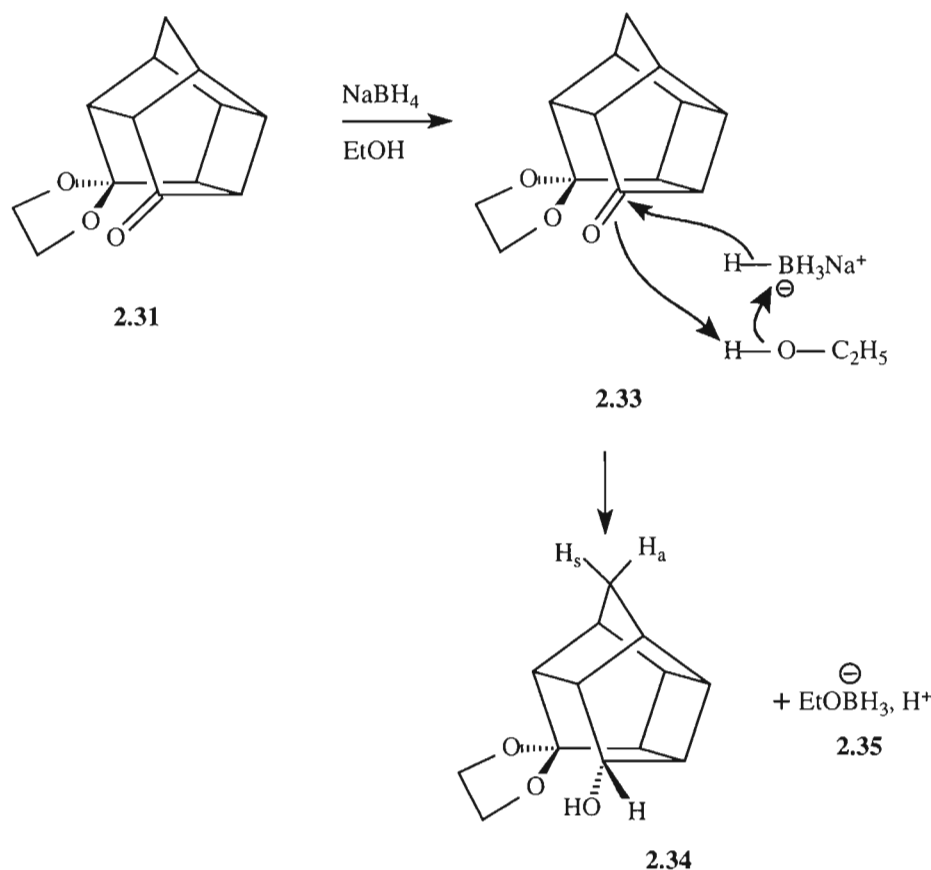


Figure 2.11: Synthesis of the hydroxy-ketal (Spectra 10-12)³⁸

The successful reduction of the ketone allowed removal of the ketal protective group in the next synthetic step to reintroduce the former keto functional group. Hydrolysis of the ketal was achieved through the addition of a 10 % (v/v) HCl solution, yielding 11-hydroxypentacyclo[5.4.0.0^{2,6}.0^{3,10}.0^{5,9}]undecane-8-one (hydroxy-ketone, **Fig. 2.12, No. 2.40**).⁴³ The mechanism of deprotection is illustrated in **Fig. 2.12**.

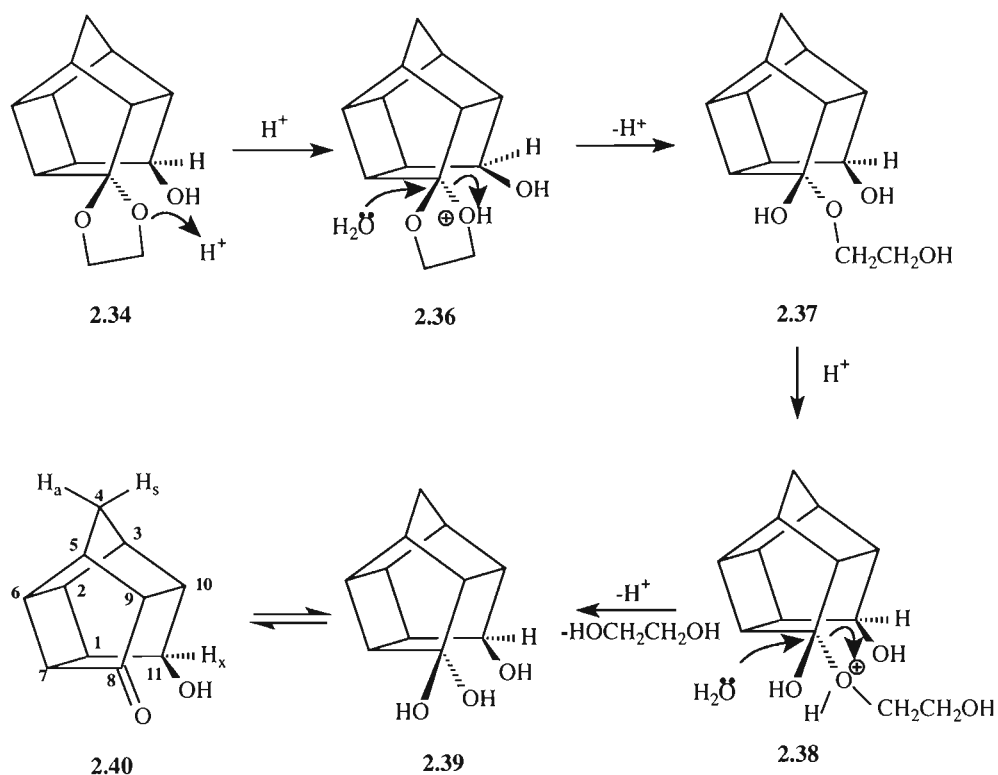


Figure 2.12: Synthesis of the hydroxy-ketone (Spectra 13-15)⁴⁶

The subsequent synthetic step involved the reduction of the keto functional group to a methylene functional group. This was achieved through refluxing (**Fig. 2.13, No. 2.40**) with hydrazine hydrate in diethylene glycol, and subsequent addition of excess KOH (Modified Huang-Minlon conditions).⁴³ Removal of volatile products from the high boiling diethylene glycol was achieved via steam distillation, which yielded *endo*-pentacyclo[5.4.0.0^{2,6}.0^{3,10}.0^{5,9}] undecane-8-ol (*endo*-PCU alcohol, **Fig. 2.13, No. 2.46**).⁴³

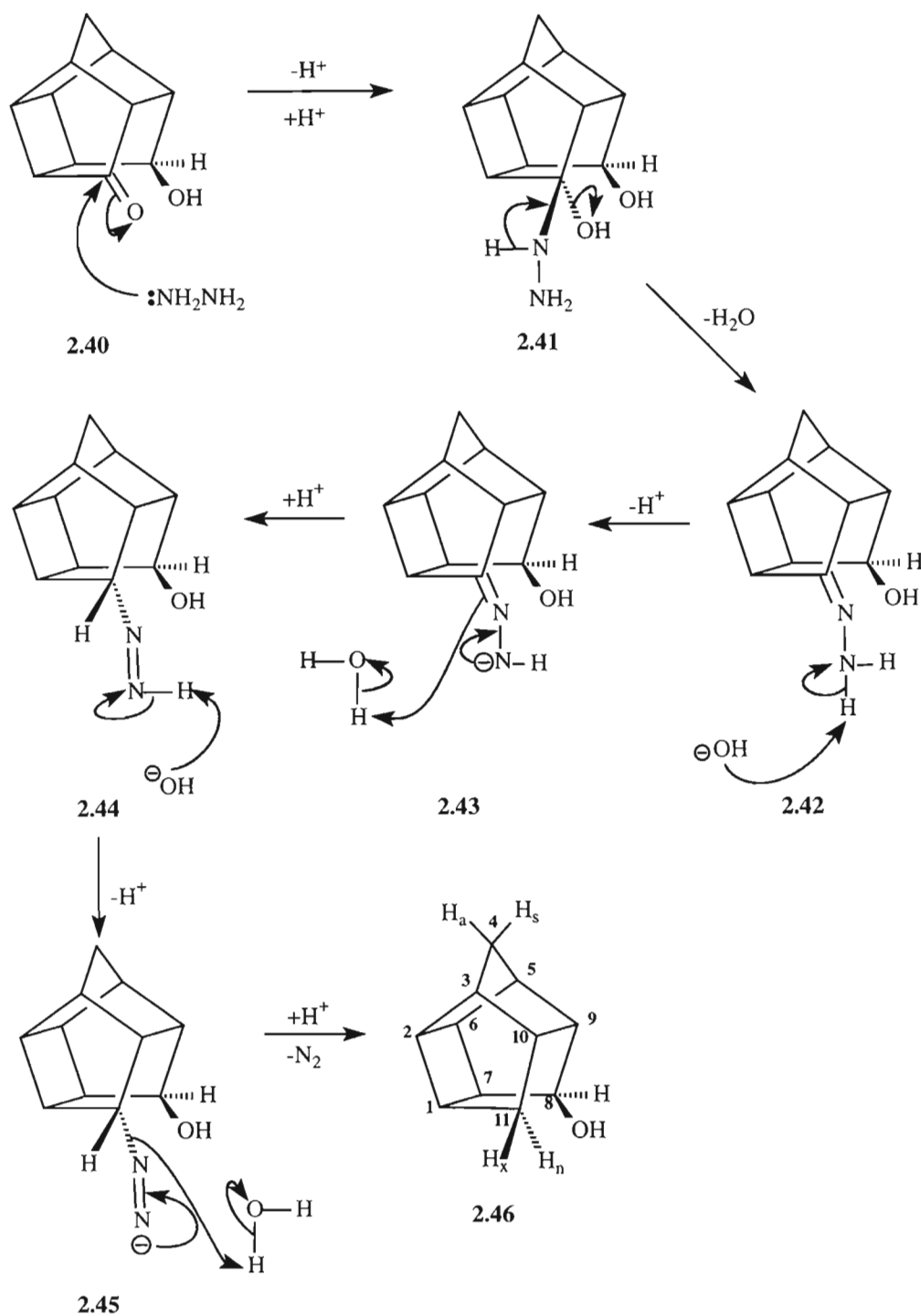


Figure 2.13: Synthesis of the *endo*-pentacyclo[5.4.0.0^{2,6}.0^{3,10}.0^{5,9}] undecane-8-ol (Spectra 16-18)³⁸

At this stage rearrangement of the PCU alcohol to trishomocuban-4-ol was possible. This was achieved through the dissolution of the alcohol (**Fig. 2.14, No. 2.46**) in glacial acetic acid and concentrated sulphuric acid, followed by reflux conditions. The acidic medium induced rearrangement of the PCU skeleton to yield trishomocubane as an acetate derivative (**Fig. 2.14, No. 2.49**). The acetate was carried directly to the next step. Dissolution of the crude acetate in methanol and potassium carbonate, with subsequent stirring at room temperature for 24 hours, hydrolysed the acetate to yield trishomocubane-4-ol (**Fig. 2.14, No. 2.52 and 2.53**).⁴³ The PCU diol can also be induced to rearrange to trishomocubane through the use of hydriodic acid (HI).⁴³ It follows a very similar mechanism to the one proposed for the PCU mono-alcohol (**Fig. 2.14**).²⁶

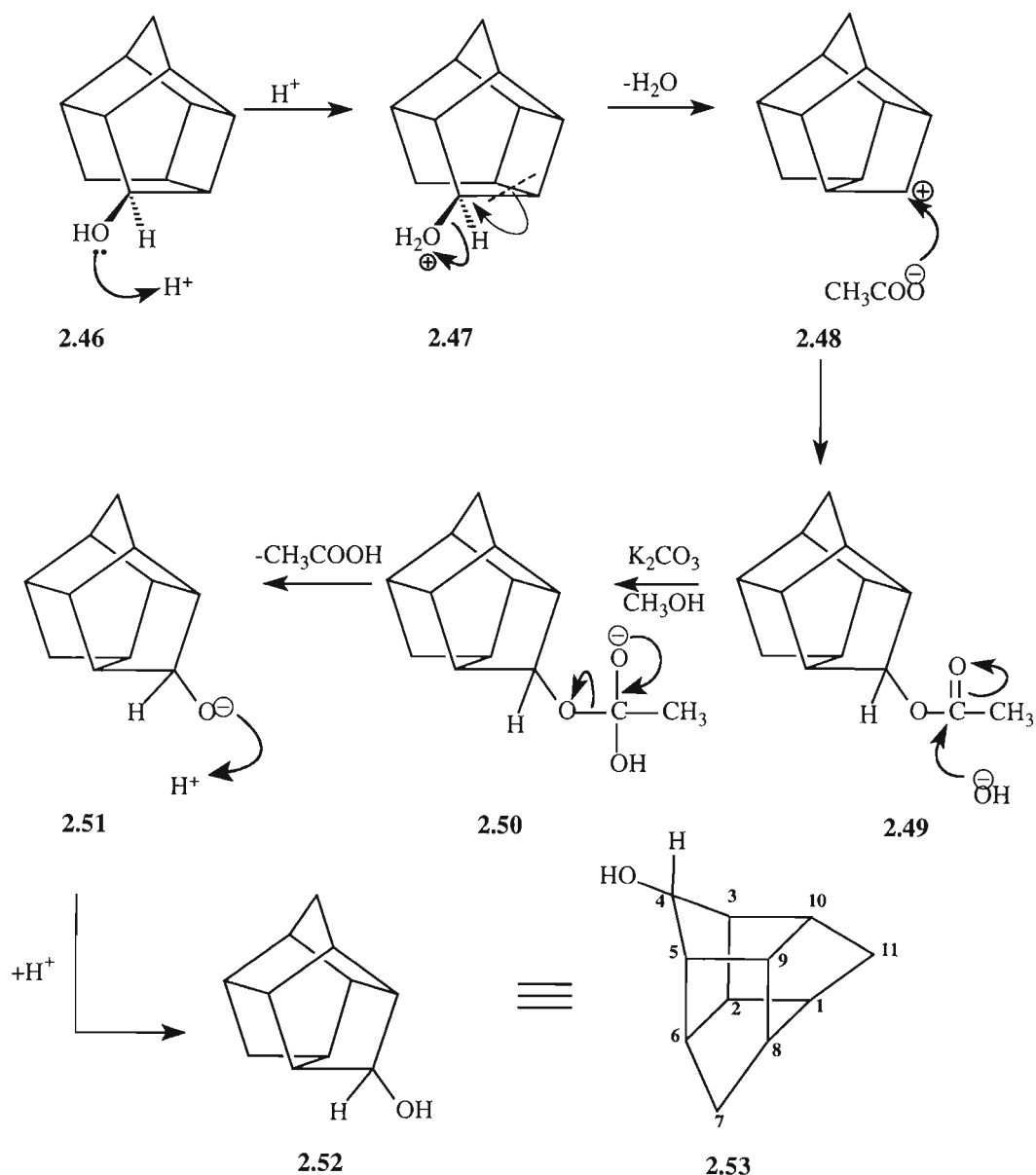


Figure 2.14: Synthesis of trishomocubane-4-ol (Spectra 19-21)

At this stage it was necessary to convert the alcohol back to a ketone as this was required for subsequent hydantoin formation (Bucherer-Bergs). The alcohol (**Fig. 2.15, No. 2.53**) was oxidised using the Jones oxidation to yield pentacyclo[6.3.0.0^{2,6}.0^{3,10}.0^{5,9}]undecanone (trishomocubanone, **Fig. 2.15, No. 2.55**).^{30,43}

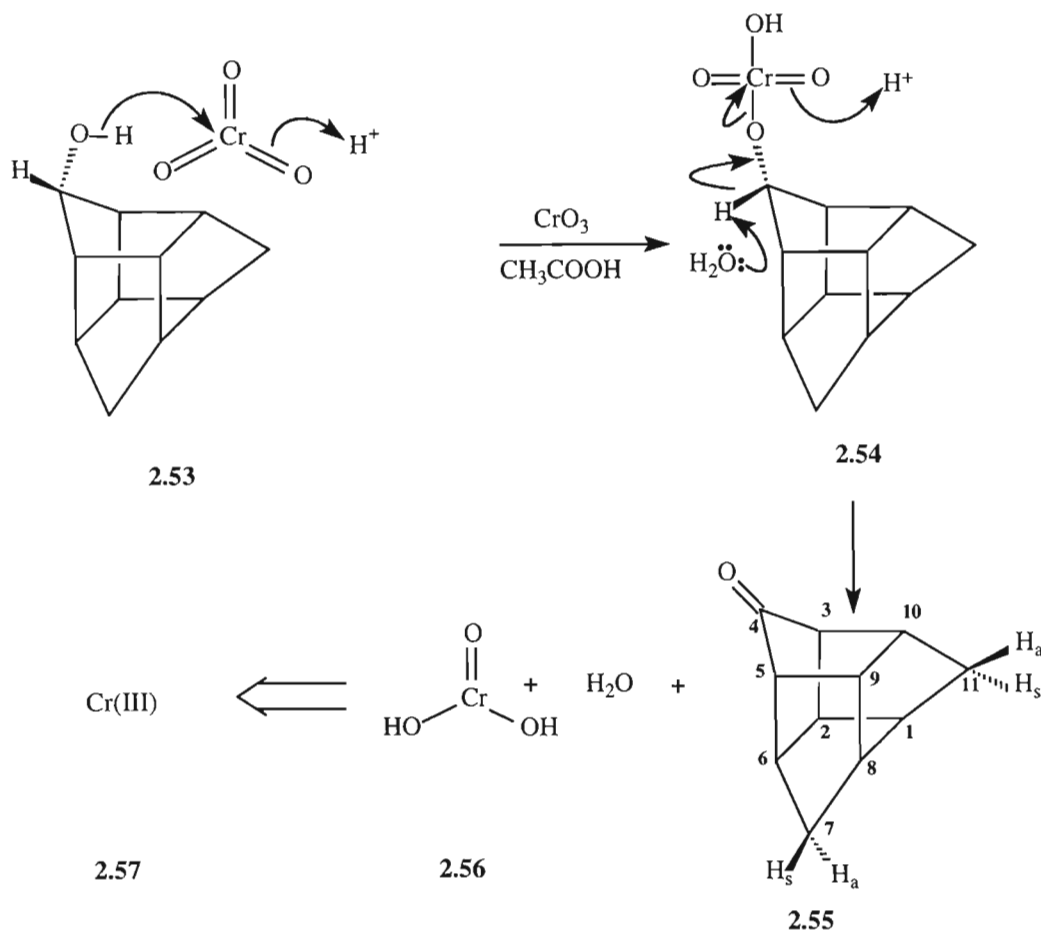


Figure 2.15: Synthesis of trishomocubanone (Spectra 22-24)³⁸

The monoketone (**Fig. 2.16, No. 2.55**) was subjected to the Bucherer-Bergs method for hydantoin formation, the precursor to the target amino acid. The reaction conditions for the conversion of the monoketone were optimised by Govender,²³ who first reported the synthesis of tris-hydantoin (**Fig. 2.16, No. 2.12**). The hydantoin was synthesised as a racemate due to the possible $\text{S}_{\text{N}}2$ attack of the nitrile group from both sides of the sp^2 hybridised keto functional group. It is, therefore, important to note that although the hydantoin is represented as one enantiomer in the following illustrations, it is in fact a racemic mixture. The mechanism of hydantoin formation, as proposed by Bucherer³⁴ is illustrated in **Fig. 2.16**.

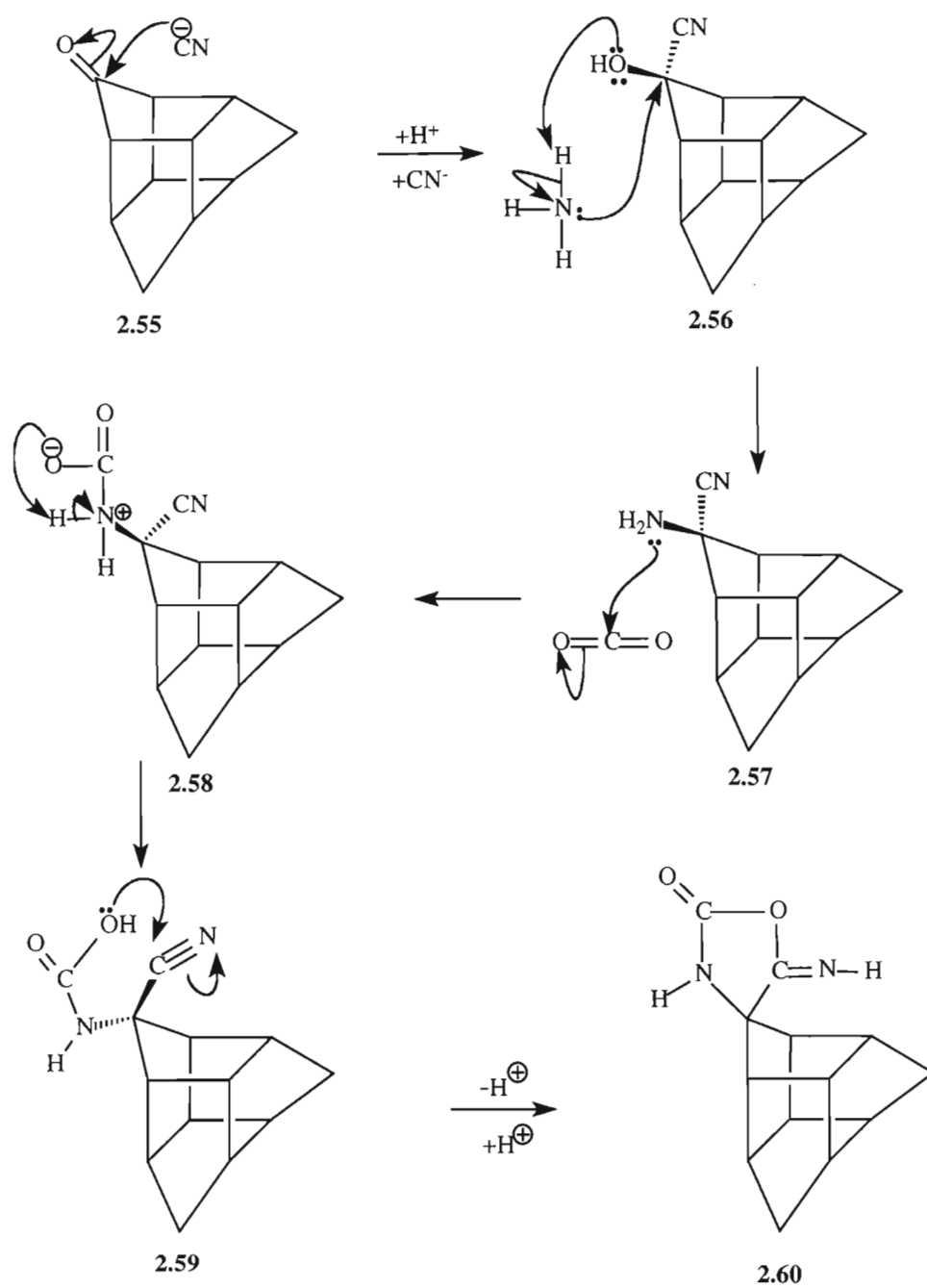


Figure 2.16: Synthesis of tris-hydantoin proposed by Bucherer³⁴
(continued on following page)

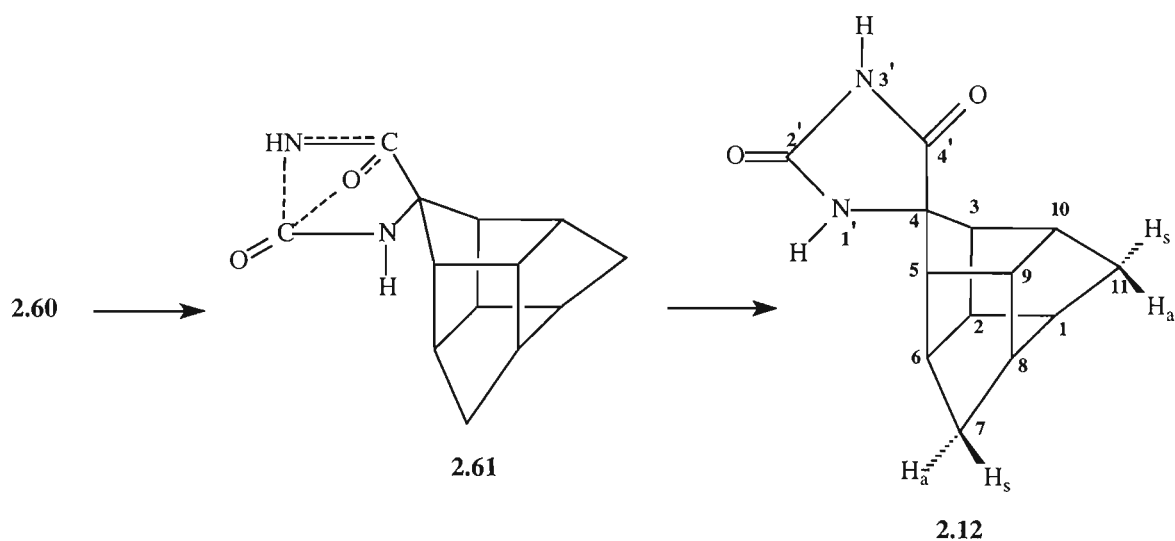


Figure 2.16: Continuation of the synthesis of tris-hydantoin proposed by Bucherer (Spectra 25-32)³⁴

The above proposed mechanism seems feasible, although the structure (**2.61**) is not clearly understood. There is, however, speculation of an alternative mechanism as from the intermediate **2.60** above. The alternative mechanism is represented in **Fig. 2.17**.

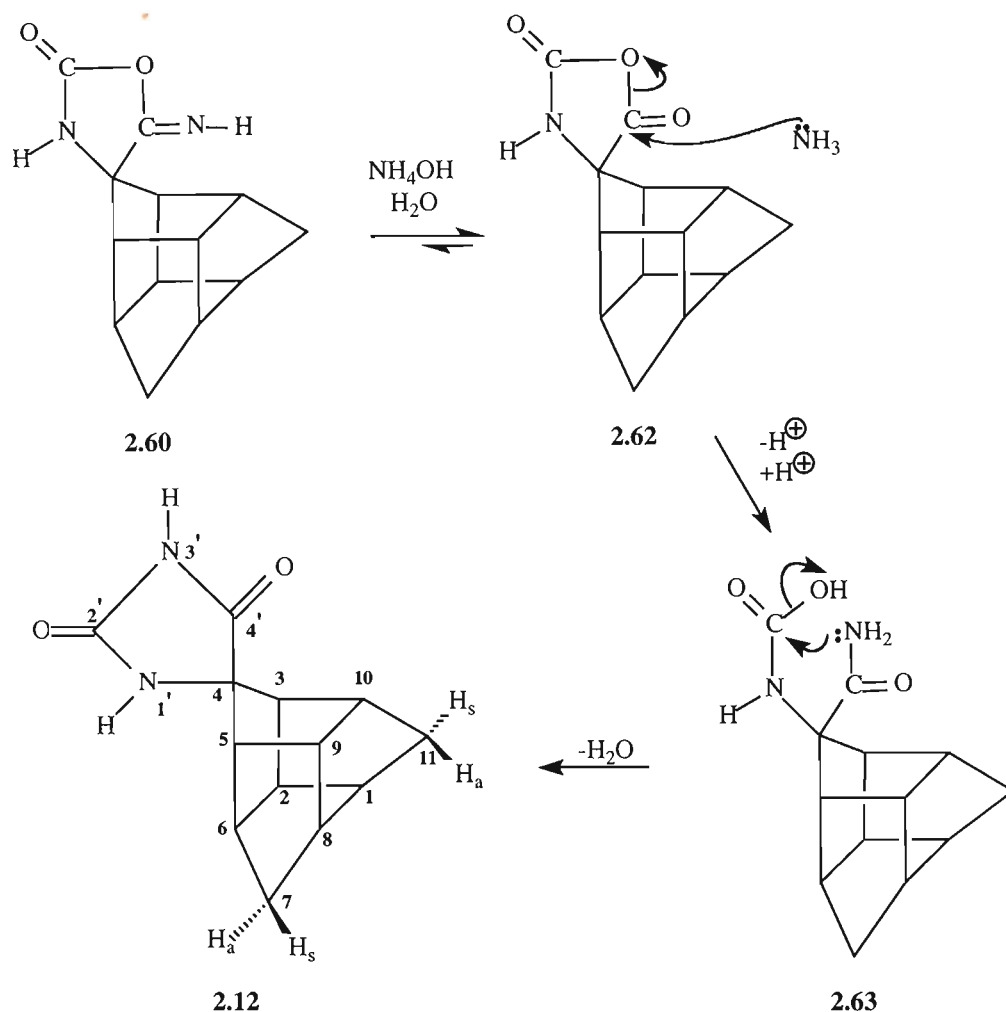


Figure 2.17: Alternative proposed[§] mechanism for the synthesis of tris-hydantoin

The mechanism proposed in **Fig. 2.17** is more likely since the imine (**2.60**) is readily hydrolysed to a carbonyl compound in aqueous acidic solution. The conversion of intermediate (**2.63**) to the hydantoin (**2.12**) is analogous to the synthesis of phthalamide from phthalic anhydride and ammonia.⁴⁷

Although Govender²³ successfully synthesised tris-hydantoin (**2.12**), it was not structurally elucidated. This prompted efforts to fully elucidate the hydantoin through the use of one- and two-dimensional nuclear magnetic resonance (NMR) spectroscopy.

The successful synthesis of tris-hydantoin was first evident from the infrared spectrum (**Spectrum 31**), with the presence of two carbonyl absorption bands at 1766 and 1720 cm^{-1} and a N-H absorption band at 3314 cm^{-1} . The correct molecular ion peak of m/z 231 $[\text{M}+\text{H}]^+$ in the mass spectrum (**Spectrum 32**) was also confirmation of tris-hydantoin. The presence of two D_2O exchangeable proton peaks at 7.88 ppm and 10.54 ppm in the ^1H

[§] Mechanism proposed by the author of this dissertation, T Raasch.

NMR spectrum (**Spectrum 25**) was evidence of the amide ($H_{1'}$) and imide ($H_{3'}$) protons of the hydantoin ring respectively. The ^{13}C NMR spectrum (**Spectrum 26**) enabled a quick review of the molecule, with the presence of a characteristic amide carbonyl signal at 177.50 ppm ($C_{4'}$) and an urea carbonyl group at 157.05 ppm ($C_{2'}$),^{36,39} the eight methine carbons of the cage between 39.57 and 55.67 ppm and the presence of two methylene carbons at 32.95 and 33.49 ppm. Two-dimensional NMR techniques were essential for the full elucidation of the tris-hydantoin molecule.

The numbering system of tris-hydantoin and the novel derivatives thereof were adopted from the numbering system used by Dekker *et al.* during their structural elucidation of trishomocubanol and trishomocubanone.³⁰

The C_4 carbon of the cage was assigned to 73.48 ppm in the ^{13}C NMR spectrum due to it being an integral part of the electron withdrawing hydantoin system. This assignment was confirmed by the absence of heteronuclear single quantum coherence (HSQC) correlations (**Spectrum 29**), and visible heteronuclear multiple bond coherence (HMBC) correlations (**Spectrum 30**) with $H_{1'}$ of the hydantoin ring. The C_3 and C_5 carbons were assigned as the next most downfield shifted carbons (54.82 and 55.67 ppm) due to their direct attachment to the deshielded C_4 carbon. At this point it was essential to confirm other functional groups of the cage before it was possible to more accurately assign the C_3 and C_5 carbons, but at least it was possible to deduce their proton peaks to the region 1.90-1.98 ppm in the HSQC spectrum.

The positions of $NH_{1'}$ and $O_{4'}$ oxygen with respect to the trishomocubane skeleton were determined next. This would assist with the elucidation of the rest of the cage skeleton. The positions of $NH_{1'}$ and $O_{4'}$ were chosen as indicated in **Fig. 2.17**.

The position of $NH_{1'}$ and $O_{4'}$ with respect to the cage skeleton were confirmed from the nuclear Overhauser effect spectroscopy spectrum (NOESY, **Spectrum 28**) of **2.64**. Correlations of $NH_{1'}$ were observed with four proton signals, which should be H_2 , H_3 , H_5 and H_6 . Oxygen $O_{4'}$ should, therefore, be pointing towards protons H_9 and H_{10} . The strongest NOESY interaction of $NH_{1'}$ should be with the nearest neighbouring proton (largest spot on the NOESY spectrum – correlation at 7.88 ppm with 2.45 ppm).

The extreme downfield shifted methine proton at 2.84 ppm in the ^1H NMR spectrum was assigned to the carbon peak at 42.75 ppm in the HSQC spectrum. This proton peak could have represented H_6 or H_{10} due to their close spatial proximity to the hydantoin ring. The H_{10} proton was confirmed to be the closest to the $C_{4'}$ carbonyl by measuring the bond distances between the cage methine protons and the various functionalities of the hydantoin ring of an optimised model of tris-hydantoin (**Fig. 2.18, No. 2.64**).^{**} The tris-hydantoin was optimised using density functional theory (DFT) at the B3LYP level of theory, using a 6-31+G(d) basis set. The hydantoin ring interacts through space with these protons and causes considerable deshielding of these two protons. The proton closest to the hydantoin ring in the PCU hydantoin analogue also experienced similar deshielding.³⁶ This

^{**} A more detailed description of computational chemistry is presented in Chapter 6.

assignment to either H₆ or H₁₀ was confirmed by HMBC correlations with C₄. The proton was eventually successfully assigned to H₁₀ due to the absence of NOESY correlations (Spectrum 28) with H₁.

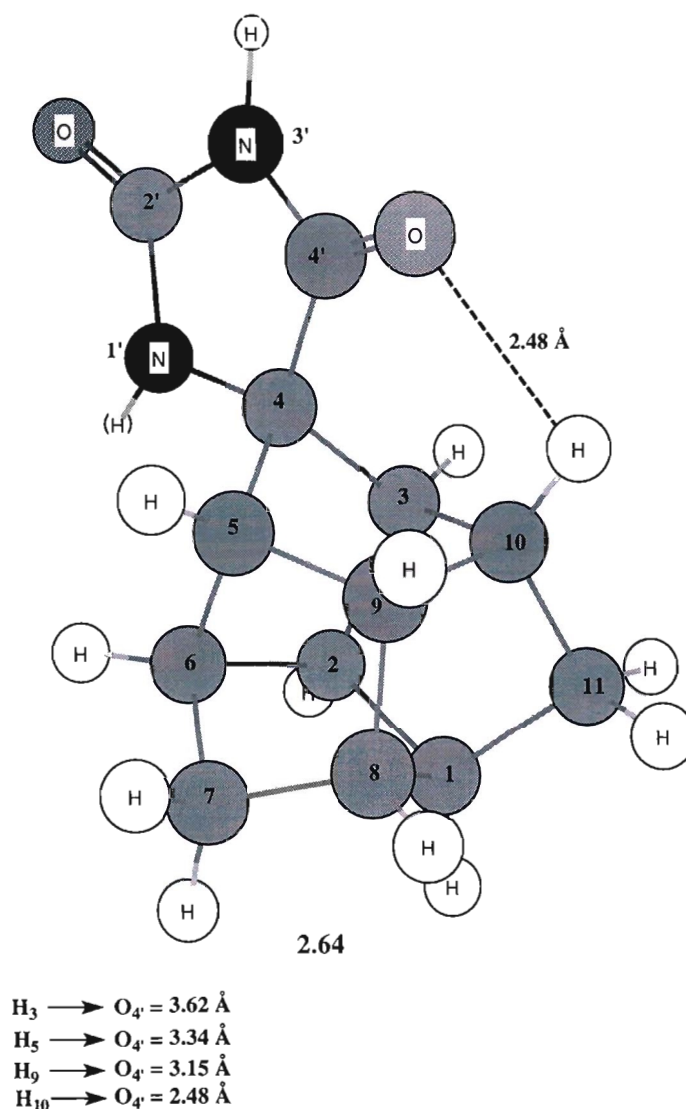


Figure 2.18: DFT optimised tris-hydantoin

The assignment of H₁₀ allowed the assignment of H₆ to 2.45 ppm in the ¹H NMR spectrum due to visible NOESY correlations with H₁ of the hydantoin ring. At this point it was evident from the NOESY correlations of H₆ and H₁₀ with the relevant methylene functional groups of the cage that the peaks between 1.19-1.27 ppm and 1.36-1.39 ppm represented both H₇ and H₁₁ protons. A more accurate assignment was achieved at a later stage, but first it was important to successfully assign the H₃ and H₅ protons of the cage. The H₃ methine proton was assigned to 1.97 ppm in the correlation spectroscopy (COSY) spectrum (Spectrum 27) due to correlations with H₁₀. This allowed assignment of H₅ to 1.91 ppm in the COSY spectrum. It was now possible to make a more accurate elucidation of the two methylene groups. The proton peaks 1.19-1.22 ppm in the ¹H NMR spectrum were

assigned to H_{11s} due to NOESY correlations with H₃. The proton peaks 1.24-1.27 ppm were assigned to H_{7s} due to NOESY correlations with H₅.

The H₂ methine proton was assigned to 2.18 ppm in the COSY spectrum due to correlations with H₃ and H₆. This allowed the assignment of H₁ to 2.10 ppm in the COSY spectrum due to correlations with H₂ and H_{11s}. The H₉ methine proton was assigned to 2.13 ppm in the COSY spectrum due to correlations with H₅ and H₁₀. This allowed the H₈ methine proton, which was the last unassigned methine proton of the cage, to be assigned to 2.10 ppm in the COSY spectrum. This was confirmed by NOESY correlations with both the H₇ and H₁₁ methylene protons.

Since the H_{7s} proton had already been assigned, it was possible to assign H_{7a} to 1.36-1.39 ppm in the COSY spectrum due to correlation with H₆. The previous assignment of H_{11s} also allowed the assignment of H_{11a} to 1.36-1.39 ppm in the COSY spectrum due to correlation with H₁₀. These assignments were confirmed by Dekker *et al.*, who reported that the methylene protons of trishomocubanol and trishomocubaneone are significantly coupled to only one of the vicinal protons³⁰. They reported coupling between H₆-H_{7a}, H₁₀-H_{11a}, H₁-H_{11s} and H₈-H_{7s}.³⁰ These coupling assignments are in agreement with the above reported couplings. These assignments completed the structural elucidation of tris-hydantoin.

The rest of the carbon atoms were assigned through correlation with the established proton signals using the HSQC spectrum. A summary of the NMR data is available in **Table 2.2**.

Table 2.2: NMR data for tris-hydantoin

Atom Number	¹ H (ppm)	<i>J</i> (Hz)	¹³ C (ppm)
1	2.10		46.66
2	2.18		43.69
3	1.97		55.67
4			73.48
5	1.91		54.82
6	2.45		45.66
7 _a	1.36-1.39	10.26	32.95
7 _s	1.24-1.27	10.26	
8	2.10		47.10
9	2.13		42.20
10	2.84		42.75
11 _a	1.36-1.39	10.26	33.49
11 _s	1.19-1.22	9.89	
1'	7.88		
2'			157.05
3'	10.54		
4'			177.50

The next synthetic step in pursuit of tris-amino acid involved hydrolysis of the hydantoin ring (Fig 2.19, No. 2.12), resulting in the racemic tris-amino acid (Fig. 2.19, No. 2.13, Spectrum 33). The hydrolysis required harsh conditions (1.25 M NaOH, 170 °C).²³ The amino acid was precipitated from the basic medium by adjusting the pH to the approximate isoelectric point (pH 6.5) using concentrated hydrochloric acid. Previous work had determined the PCU-amino acid's isoelectric point as pH 6.5.³⁹ This has not been determined for tris-amino acid, yet from experimental results the amino acid precipitated from the aqueous solution between pH 6.5-7.0. The Fmoc derivative was subsequently prepared in order to compare NMR data to authentic spectra that had previously been confirmed (Fig 2.19, No. 2.65, Spectra 34-36).²³

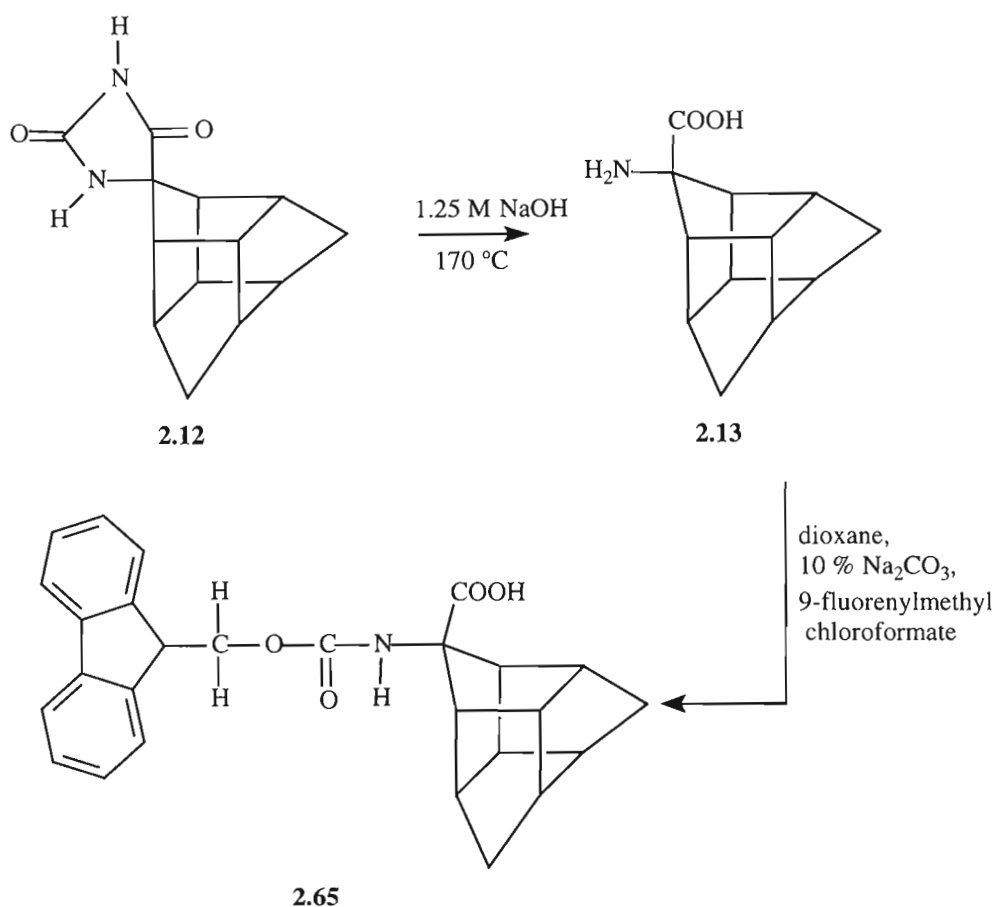
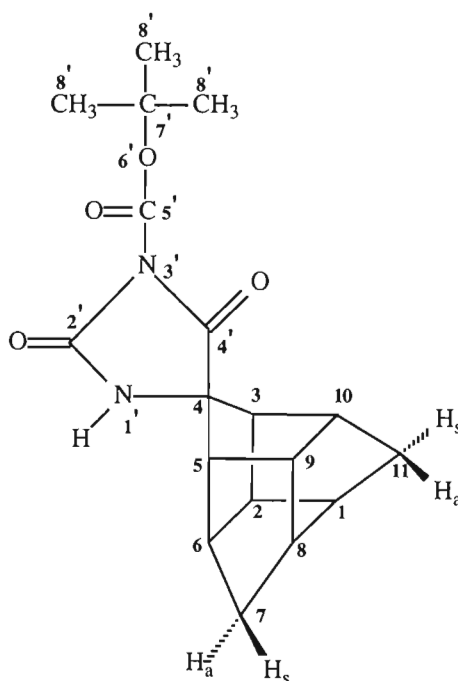


Figure 2.19: Synthesis of tris-amino acid (2.13) and Fmoc-tris-amino acid (2.65)

The poor yields (~60%) of amino acid obtained in the above-mentioned hydrolysis of tris-hydantoin prompted a search for a more efficient method of hydrolysis. Rebek⁴⁸ modified a method that hydrolysed lactams and secondary amides⁴⁹ and developed an efficient, facile method for hydrolysis of α,α -disubstituted hydantoins. It has been postulated that hydrolysis of mono and disubstituted hydantoins proceeds *via* different mechanisms.⁵⁰ Rebek's method involved Boc protection of the amide and imide nitrogens on the hydantoin ring, followed by lithium hydroxide aided hydrolysis at room temperature. Boc

protection enables milder hydrolysis conditions due to the carbonyl groups becoming more susceptible to nucleophilic attack, and converts the nitrogens to better leaving groups.⁴⁸

Rebek's method of Boc addition to the hydantoin ring was applied to the pre-synthesised tris-hydantoin. It was clearly visible from the NMR data that the method only resulted in the monoprotected hydantoin [**Novel Compound 1, (NC1), Fig. 2.20, No. 2.66**]. Addition had also, surprisingly, occurred on the imide nitrogen (N_3). The imide nitrogen is positioned between two electron withdrawing carbonyl functional groups. One would, therefore, expect this nitrogen to be far more electron deficient and 'hang-on' to its proton far more than the corresponding amide nitrogen (N_1). The attachment of the Boc group to N_3 may have been due to steric hindrance from the cage, which did not energetically favour attack on the more nucleophilic (N_1) nitrogen.



2.66

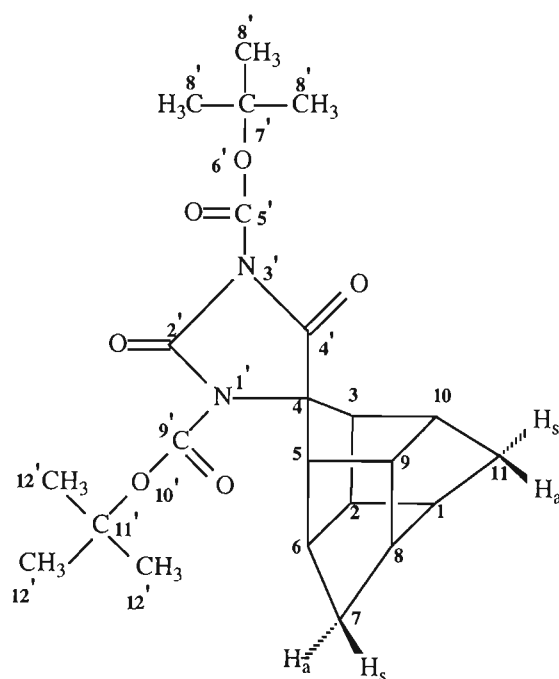
Figure 2.20: Novel Compound 1 (NC1, Spectra 37-44)

The previous structural elucidation of tris-hydantoin was essential in elucidating the structure of NC1 (**Fig. 2.20, No. 2.66**) since a similar method was used to identify the various functional groups. It was possible to assign all the relevant carbons and protons of the cage and hydantoin system by following the logic described for the elucidation of tris-hydantoin. A more detailed description is available in the experimental section (**Chapter 8**). Confirmation of the Boc group is, however, presented in the following paragraph.

It was evident that the Boc derivative of the tris-hydantoin had been synthesised with the appearance of three carbonyl peaks in the ^{13}C NMR spectrum (**Spectrum 38**) and the appearance of the expected molecular ion peak of m/z 331 $[\text{M}+\text{H}]^+$ in the mass spectrum (**Spectrum 44**). The presence of a proton peak (1.56 ppm) in the ^1H NMR spectrum (**Spectrum 37**), which integrated to nine protons could, therefore, be assigned to the three

methyl groups (H_8) of the Boc group. The absence of the imide proton ($H_{3'}$) at about 10 ppm and the presence of the amide proton ($H_{1'}$) at 6.40 ppm in the 1H NMR spectrum was evidence that the Boc group had attached to the imide nitrogen. The assignment of the $H_{1'}$ proton to 6.40 ppm in the 1H NMR spectrum was later confirmed by NOESY correlation (**Spectrum 40**) with the H_6 methine proton of the cage. The C_7 carbon of the Boc group was assigned to 85.31 ppm in the HMBC spectrum (**Spectrum 42**) due to correlation with the H_8 methyl protons. A more comprehensive assignment of the **NC1** functionalities is available in the experimental section (**Chapter 8**).

In an attempt to add a Boc functional group to both the amide and imide nitrogens of the hydantoin ring, a method published by Hammer *et al.*⁵¹ for derivatising the hydantoin ring of α,α -disubstituted amino acids was applied to tris-hydantoin. It was similar to Rebek's method, except triethylamine was also added to the reaction mixture. The electrophilic nature of the base aided in activating the amide nitrogen ($N_{1'}$) for derivatisation, enabling the bis-Boc derivative [**Novel Compound 2**, (**NC2**), **Fig. 2.21**, **No. 2.67**] to be successfully synthesised.



2.67

Figure 2.21: Novel Compound 2 (Spectra 45-52)

Although **NC2** could not be fully structurally elucidated due to major overlap of the NMR signals, it was evident that **NC2** had been synthesised due to the presence of four carbonyl groups present in the ^{13}C NMR spectrum (**Spectrum 46**). The absence of the amide and imide hydrogens of the hydantoin ring at ~6 and ~10 ppm, respectively, in the 1H NMR spectrum (**Spectrum 45**), and the presence of the expected molecular ion peak of m/z 431 $[M+H]^+$ in the mass spectrum (**Spectrum 52**), further supported the presence of two Boc groups. This was further supported by the presence of two proton peaks in the 1H NMR

spectrum, that each integrated to the nine protons of the methyl groups on the Boc functionality.

Due to the absence of the $H_{1'}$ proton, a different strategy was employed for elucidating the structure of **NC2** from that which was previously used for tris-hydantoin and **NC1**. Previous assignments of the methylene groups during the elucidation of tris-hydantoin and **NC1**, as well as reported couplings between the methylene protons and their respective vicinal protons of trishomocubanol and trishomocubanone,³⁰ proved to be a helpful starting point in analysing the two-dimensional NMR spectra of **NC2**.

The C_4 carbon of **NC2** was easily recognisable at 76.55 ppm in the HSQC spectrum (**Spectrum 49**) as it displayed no HSQC correlations. It was also expected to be the most downfield shifted cage carbon due to its direct attachment to the electron withdrawing hydantoin ring. The next most downfield shifted carbons (54.03 and 58.15 ppm) were assigned to either C_3 or C_5 due to their direct attachment to C_4 . Through HSQC correlations their protons were located at either 2.16-2.17 or 2.52-2.53 ppm. A more precise assignment was only possible at a more advanced stage of **NC2** elucidation.

The next stage of elucidation relied on the previous assignments of the methylene (H_{7a} , H_{7s} , H_{11a} , H_{11s}) protons of tris-hydantoin and **NC1** as well as the reported couplings between $H_6(H_{10})$ and $H_{7a}(H_{11a})$ and between $H_1(H_8)$ and $H_{11s}(H_{7s})$ of trishomocubanol and trishomocubanone.³⁰ This allowed the assignment of the downfield shifted proton peak at 3.12 ppm in the COSY spectrum (**Spectrum 47**) to be assigned to the H_{10} methine proton. This was due to correlations with the H_{11a} proton at 1.44-1.46 ppm. The H_6 (2.28 ppm), H_1 (2.09-2.13 ppm) and H_8 (2.14-2.15 ppm) methine protons were assigned due to corresponding COSY correlations with H_{7a} (1.46-1.48 ppm), H_{11s} (1.27-1.30 ppm) and H_{7s} (1.30-1.33 ppm) protons respectively.

This allowed the assignment of H_2 to 2.38-2.40 ppm in the COSY spectrum due to correlation with H_1 . Similarly the H_3 proton was assigned to 2.52-2.53 ppm in the COSY spectrum due to correlation with H_2 , which is one of the predicted shifts for H_3 mentioned above. This allowed the assignment of H_5 to 2.16-2.17 ppm, the other predicted shift mentioned above. This was confirmed by visible COSY correlation with H_6 . This led to the assignment of the last methine proton, H_9 of the cage to 2.29 ppm due to COSY and NOESY correlations (**Spectrum 48**) with H_{10} .

The C_7 carbon was assigned to 33.02 ppm due to HMBC correlations (**Spectrum 50**) with H_5 , and C_{11} to 32.94 ppm due to HMBC correlation with C_2 . The $H_{12'}$ protons of the Boc group were assigned to 1.53 ppm in the NOESY spectrum due to correlation with H_2 and H_6 , therefore, allowing the H_8' Boc protons to be assigned to 1.55 ppm. This led to the assignment of $C_{7'}$ to 86.11 ppm in the HMBC spectrum due to correlation with H_8' . The HMBC correlation between $H_{12'}$ and the carbon peak at 84.95 ppm allowed this carbon peak to be assigned to $C_{11'}$. The C_4' carbonyl was assigned to 169.58 ppm in the ^{13}C NMR spectrum, while the C_2' carbonyl was assigned to 145.74 ppm due to more electron delocalisation from $N_{1'}$ and $N_{3'}$ at C_2' . Based on the same analogy the C_5' and C_9' carbonyl

groups were assigned to 149.67 and 149.03 ppm respectively. A more comprehensive description of **NC2** is available in the experimental section (**Chapter 8**).

Rebek's method of hydrolysis of the hydantoin ring was applied to **NC2**.⁴⁸ This involved addition of lithium hydroxide (8 mole equivalents) in aqueous solution, followed by stirring at room temperature overnight. Adjustment of the pH to 6.5 resulted in precipitation of the amino acid. The product was obtained by filtration and washed successively with deionised water, acetone and diethyl ether. This method quantitatively resulted in the tris-amino acid (**Fig. 2.22, No. 2.13**), which was confirmed through successful synthesis of the Fmoc derivative. The NMR data was identical to authentic data.²³ This method proved to be a milder method of hydantoin hydrolysis, with improved yields, despite the additional step. The base hydrolysis of tris-hydantoin, which was reported by Govender,²³ only resulted in a 60 % yield of tris-amino acid. The base hydrolysis of the bis-Boc derivative of tris-hydantoin, which is reported in this dissertation, resulted in a 100 % yield of tris-amino acid.

Two novel derivatives (**NC1** and **NC2**) of tris-hydantoin were synthesised during an attempt to improve the yield of tris-amino acid from the base hydrolysis of tris-hydantoin. The base hydrolysis (LiOH) of **NC2** quantitatively yielded tris-amino acid, which was a significant improvement in yield compared to the yields reported by Govender.²³ A summary of the novel synthetic work is illustrated in **Fig. 2.22**.

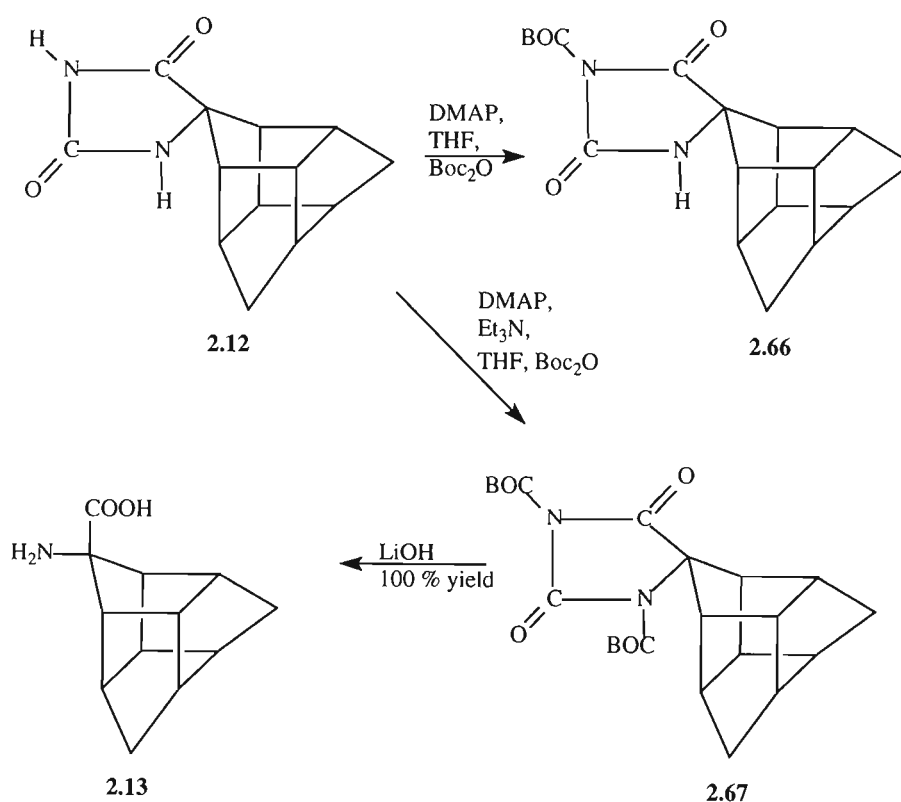


Figure 2.22: Summary of novel synthetic work

CHAPTER 3

DIASTEREOMERS OF TRIS-HYDANTOIN

Solid phase peptide synthesis using tris-amino acid has, thus far, only involved the racemic amino acid²³ since synthesising enantiomerically pure tris-amino acid has proven to be a formidable task. An attempt was, therefore, made in this study, to produce enantiopure tris-amino acid through the separation of diastereomeric trishomocubane derivatives.

Stereoisomers that are not mirror images of each other are called diastereomers¹ (**Fig. 3.1**). Since they are not mirror images of each other, they may differ in all properties, whether chiral or achiral.⁵² Diastereomers may differ in melting point, boiling point and solubility, therefore, sometimes be separable by fractional distillation or fractional crystallisation.¹ Differences in molecular shape and polarity results in a difference in adsorption, which may also allow separation of diastereomers by chromatographic techniques.¹

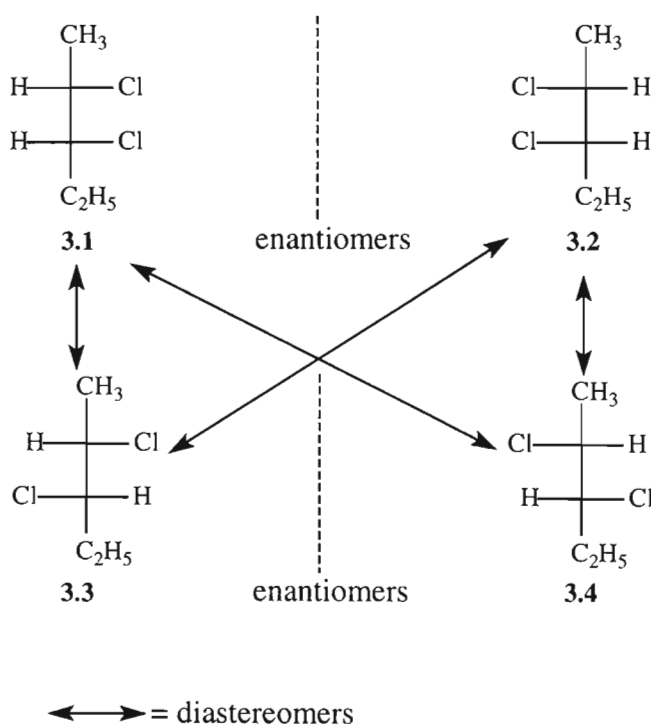


Figure 3.1: Example of diastereomers

Tris-hydantoin already possesses nine chiral centres and is one synthetic step from the amino acid (NaOH hydrolysis). Attaching an enantiopure starting material possessing one

chiral centre to the hydantoin ring would produce diastereomers of tris-hydantoin. This, in principle, could afford chromatographic separation of the resulting diastereomers, and could ultimately lead to the isolation of enantiopure tris-amino acid.

A route was devised to prepare the corresponding chloroformic ester (**Fig. 3.2, No. 3.6**) from R-(-)-2-butanol (**Fig. 3.2, No. 3.5**). This would be added onto the hydantoin ring of tris-hydantoin to form diastereomers (**Fig. 3.2, No. 3.7**).

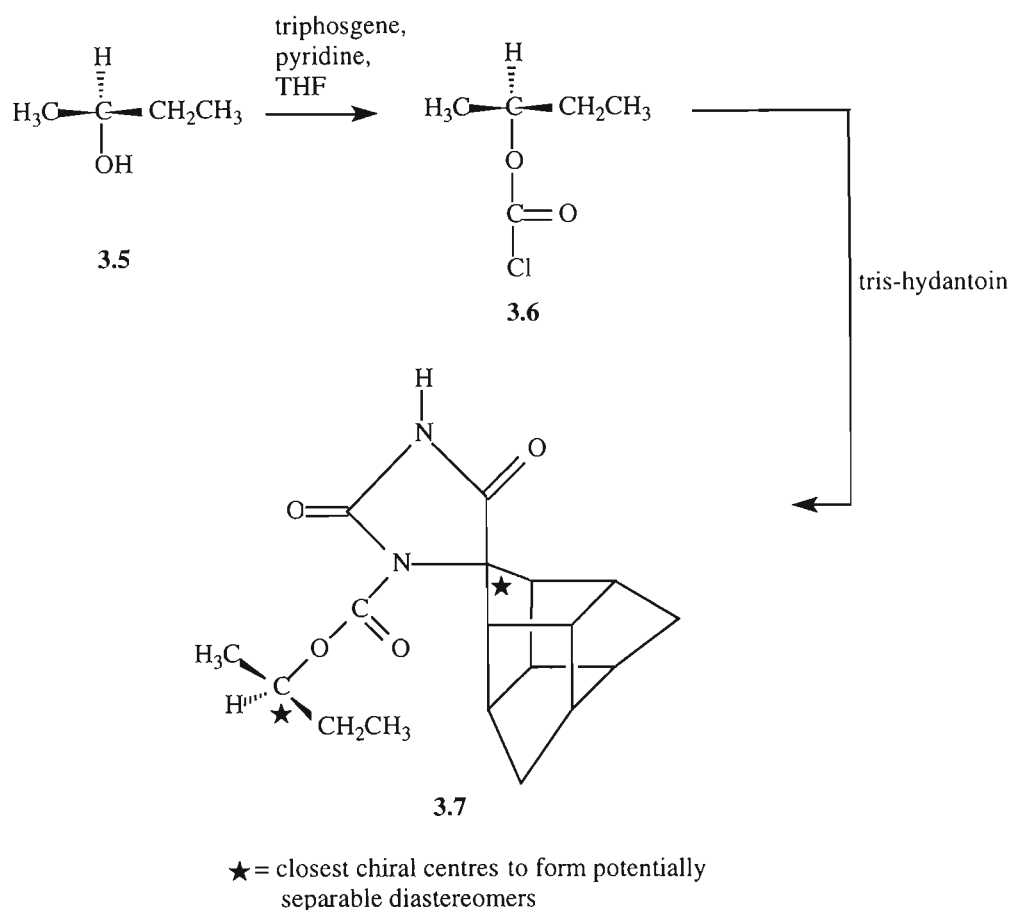


Figure 3.2: Strategy to produce diastereomers of tris-hydantoin

It was hoped to separate the diastereomers by using column chromatography since it is a less expensive technique compared to preparative high performance liquid chromatography (HPLC). Once separated, the side chain would be removed by methods similar to those used to cleave Boc groups (TFA or HNO_3).^{52,53} Hydrolysis of the hydantoin ring would result in enantiomerically pure tris-amino acid.

A common method to form chloroformate esters from alcohols is the use of phosgene gas or triphosgene [bis(trichloromethyl)carbonate, **Fig. 3.3, No. 3.8**].⁵⁴ Triphosgene is a white, crystalline solid that is soluble in common organic solvents such as dichloromethane, tetrahydrofuran, ether and chloroform. Many diverse applications have been discovered for triphosgene, the safe cogener of phosgene gas⁵⁵ (**Table 3.1**).

Table 3.1: Uses of bis(trichloromethyl)carbonate

Uses of triphosgene	References
Preparing acid chlorides and anhydrides from carboxylic acids	55
Chlorination of 1° and 2° alcohols to alkyl chlorides	55
Preparing chloroformic esters from alcohols	54,56
Protecting diols, aminols and thiols	55
Esterification of amino acids and mono acids	55
Synthesis of peptide coupling agents	57

The procedure for chloroformate formation was first tested with isopropanol due to the cost of enantiopure alcohols. The chloroformic ester (**Fig. 3.3, No. 3.12**) was prepared *via* slow, cannular addition of dry pyridine to an ice-cooled, stirred solution of isopropanol, triphosgene and dry THF under nitrogen gas. The reaction mixture was subsequently filtered, under nitrogen gas, into an ice-cooled, stirred solution of tris-hydantoin in dry THF. This resulted in the synthesis of **Novel Compound 3** [(NC3), **Fig. 3.3, No. 3.13**].

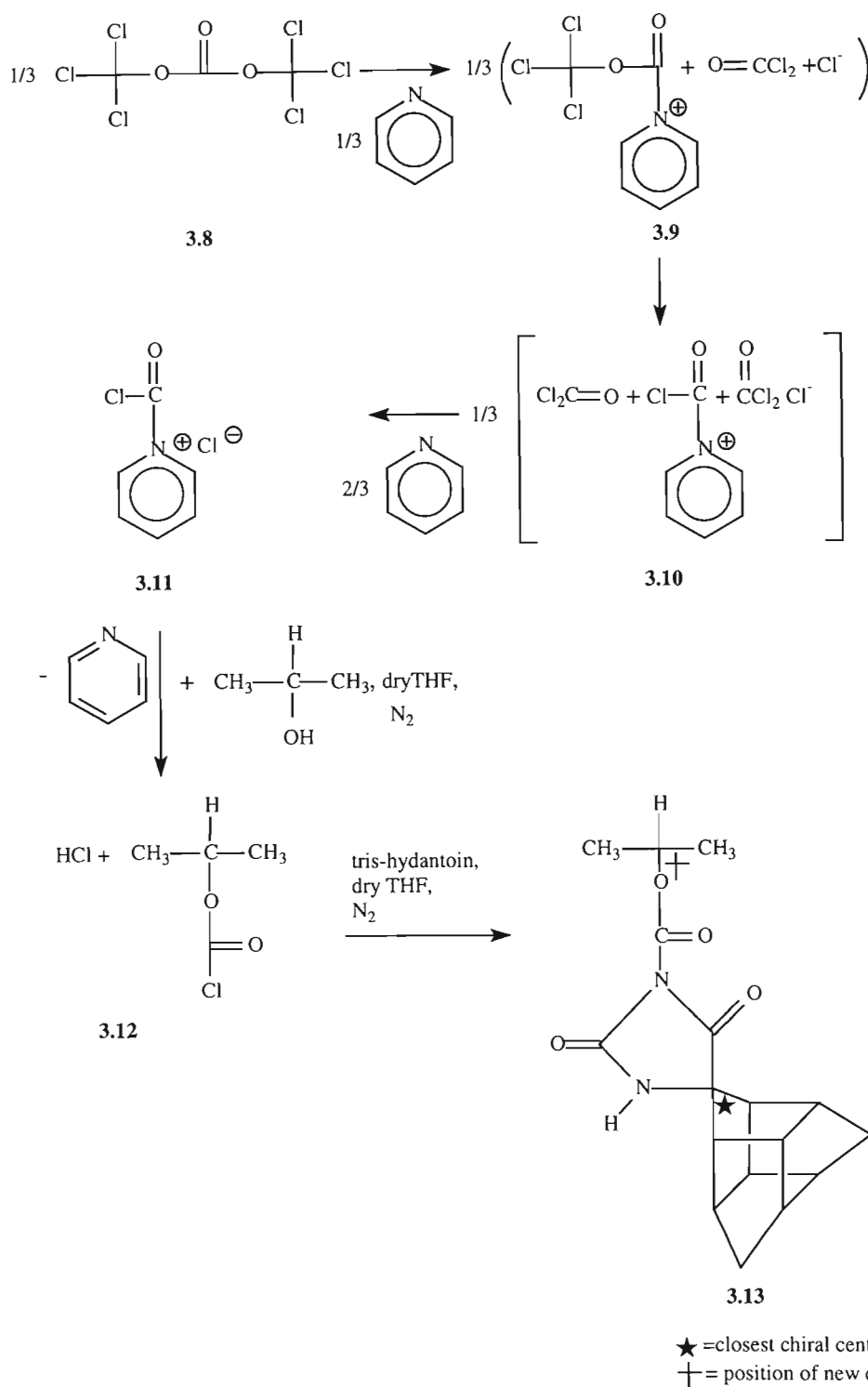
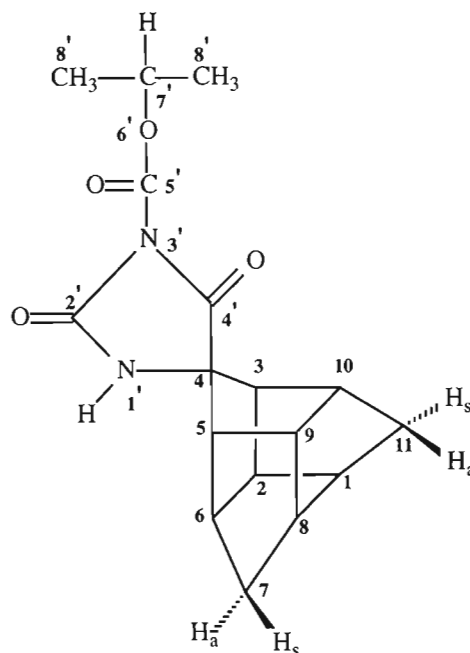


Figure 3.3: Synthesis of Novel Compound 3 (NC3)

It was hoped that the attack of the chloroformate would be on the amide nitrogen (N_1) of the hydantoin ring (**Fig. 3.3, No. 3.13**), resulting in the chiral centres being separated by only three atoms when applying the chiral chloroformate. The attachment of the

chloroformate to the imide nitrogen ($N_{3'}$) of the hydantoin ring would result in the separation of the chiral centres by four atoms. The greater the distance between chiral centres, the less probability of separating the diastereomers. NMR studies ultimately revealed that attack had taken place on the imide nitrogen, resulting in **Novel Compound 3** [(NC3), Fig. 3.4, No. 3.14].



3.14

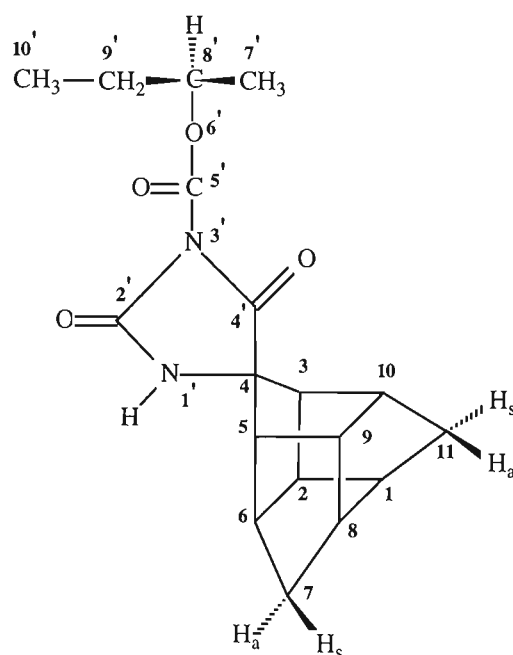
Figure 3.4: Novel Compound 3 (NC3)

It was evident from the ^1H NMR spectrum (**Spectrum 53**) that attack had been on the imide nitrogen due to the presence of the amide proton ($H_{1'}$) at 6.98 ppm. The presence of three carbonyl peaks in the ^{13}C NMR spectrum (**Spectrum 54**) and the molecular ion peak of m/z 331 $[\text{M}+\text{H}]^+$ in the mass spectrum (**Spectrum 60**) was evidence of product formation. The proton peaks at 1.35 and 1.36 ppm in the ^1H NMR spectrum ($H_{8'}$) integrating to six protons, and the multiplet at 5.15 ppm of the $H_{7'}$ proton was also evidence that the product had been formed. The assignment of $H_{8'}$ was confirmed by COSY correlations (**Spectrum 55**) with the H_9 methyl protons.

The various NMR spectra for **NC3** were very similar to those of tris-hydantoin and **NC1** (**Chapter 2**), which was useful in assigning the peaks of this novel compound. The same strategy for elucidating the structure of tris-hydantoin and **NC1** was used to fully elucidate the structure of **NC3**. A more detailed description is available in the experimental section (**Chapter 8**). Note, the H_{7s} proton peaks are obscured by the $H_{8'}$ proton peaks between 1.35-1.36 ppm in the ^1H NMR spectrum. The $H_{1'}$ and $H_{8'}$ proton peaks are indistinguishable and their respective carbons are represented by a single peak (46.74 ppm) in the ^{13}C NMR spectrum.

Although attack had unexpectedly taken place on the imide nitrogen ($N_{3'}$), the chiral chloroformate was still prepared and added to tris-hydantoin. It was hoped that separation of the diastereomers would still be possible, despite the chiral centres being separated by four atoms (**Fig. 3.3, No. 3.13**). The method used by Hammer *et al.*⁵¹ was also used in an attempt to add the chiral chloroformate to the amide nitrogen of tris-hydantoin but it was not successful.

The procedure used to synthesise [chlorocarbonic acid-((-)(R)-*sec*-butyl ester), **Fig. 3.2, No. 3.6**] from R(-)-2-butanol (**Fig. 3.2, No. 3.5**), and the subsequent addition to tris-hydantoin, was identical to that used for the preparation **NC3**. This yielded **Novel Compound 4** [(**NC4**), **Fig. 3.5, No. 3.15**].



3.15

Figure 3.5: Novel Compound 4 (NC4)

It was evident that **NC4** had been synthesised by the presence of the expected molecular ion peak of m/z 331 $[M+H]^+$ in the mass spectrum (**Spectrum 68**) and the presence of three carbonyl peaks in the ^{13}C NMR spectrum (**Spectrum 62**). The appearance of the amide proton ($H_{1'}$) of the hydantoin ring at 7.19 ppm, and the absence of the imide proton ($H_{3'}$) at ~10 ppm in the 1H NMR spectrum (**Spectrum 61**), was evidence that the chloroformate had added onto the imide nitrogen.

The various NMR spectra for **NC4** were very similar to those of tris-hydantoin, **NC1** and **NC3**, which was useful in assigning the peaks of this novel compound. The same strategy for elucidating the structure of tris-hydantoin, **NC1**, and **NC3** was used to fully elucidate the structure of **NC4**. A more detailed description is available in the experimental section (**Chapter 8**). Note, the H_{7s} proton peaks are obscured by the H_7 proton peaks between 1.32-1.35 ppm in the 1H NMR spectrum. The H_1 and H_8 proton peaks are indistinguishable

and their respective carbons are represented by a single peak (46.73 ppm) in the ^{13}C NMR spectrum.

The $\text{C}_{2'}$ (171.50 ppm) and $\text{C}_{4'}$ (152.62 ppm) carbons of the hydantoin ring were assigned with the same reasoning used for the elucidation of tris-hydantoin, **NC1** and **NC3**. Hence, the $\text{C}_{5'}$ carbonyl carbon was assigned to the peak at 147.74 ppm in the ^{13}C NMR spectrum. The $\text{H}_{8'}$ protons were assigned to 5.00 ppm from HMBC correlation (**Spectrum 66**) with $\text{C}_{5'}$. The $\text{H}_{7'}$ methyl protons were assigned to 1.32-1.35 ppm in the COSY spectrum (**Spectrum 63**) due to correlation with the $\text{H}_{8'}$ proton. This allowed the assignment of the methyl protons ($\text{H}_{10'}$) to 0.94-0.99 ppm in the ^1H NMR spectrum, which integrated to three protons. The $\text{H}_{9'}$ methylene protons were lastly assigned to the multiplet at 1.60-1.75 ppm in the COSY spectrum due to correlation with $\text{H}_{10'}$. A more complete summary of the NMR data is provided in the experimental section (**Chapter 8**).

The ^{13}C results provided convincing evidence that diastereomers were present. The carbon centres closest to the chiral centres and including the chiral centres (C_3 , C_4 , C_5 , $\text{C}_{7'}$ and $\text{C}_{9'}$) exhibited two carbon peaks. This was expected considering diastereomers may differ in NMR shifts, and peaks closest to the diastereomeric chiral centres would be split in the ^{13}C NMR spectrum. Numerous attempts to separate the diastereomers by thin layer chromatography and column chromatography failed, thus, this particular route to produce enantiomerically pure tris-amino acid was abandoned. Future work should attempt to generate diastereomers where the chiral centres are not so far apart.

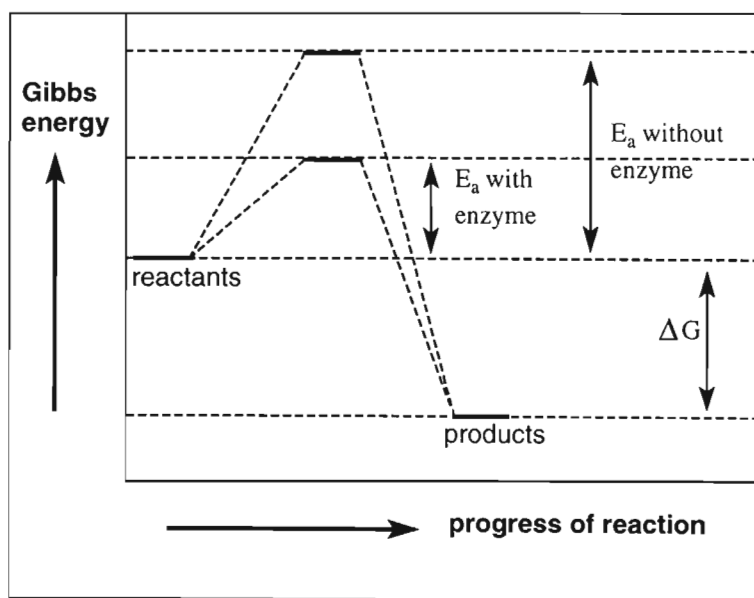
Although this particular project failed, the synthetic investigation resulted in two novel tris-hydantoin derivatives (**NC3** and **NC4**). There are also alternative routes for the synthesis of enantiopure tris-amino acid. **Chapter 4** deals with the use of enzymes for the synthesis of enantiopure tris-amino acid.

CHAPTER 4

APPLICATION OF ENZYMES TO CAGE SYSTEMS

Enzymes are catalytic proteins, which regulate the chemistry of cells and organisms.⁵⁸ A catalyst is a substance which increases the rate of a chemical reaction, without itself being changed in the overall process. To date, there are over 2000 known enzymes, with an enzyme available for most organic reactions.^{59,60} There are currently several hundred commercially available enzymes and they are often very expensive. The cost should in no way demotivate a chemist once the numerous advantages of enzyme-catalysed reactions are fully recognised. Enzymes are usually very versatile and catalyse a broad spectrum of reactions and often operate under mild conditions (room temperature and neutral pH). This minimises problems of isomerisation, racemisation and rearrangement. Many are highly efficient catalysts, generally very specific with respect to structure and stereochemistry of substrate and product.⁵⁹ Unfortunately, enzymes might, therefore, be substrate specific and would not work for all available analogous substrates.

The role of a catalyst is to lower the energy of activation (E_a) of a reaction, and ultimately induce a faster reaction⁵⁸ (Fig. 4.1). This is often achieved by the catalyst nursing the reacting molecule into a conformation that resembles the transition state, but is of lower energy due to the favourable energetics of binding to the catalyst.²



4.1

Figure 4.1: Energetics of an enzyme-catalysed *versus* a non-enzyme catalysed reaction

An enzyme binds the substrate into a region called the active site to form an enzyme-substrate complex⁵⁸ (**Fig. 4.2**). This is usually a pocket or cleft surrounded by amino acid side chains that either help bind the substrate or play a role in catalysis. The specific stereochemistry of the pocket accounts for the specificity of the enzyme and is often alluded to as a lock and key mechanism² (**Fig. 4.2**). The enzyme not only demands a specific substrate but also demands the substrate to be distorted into an orientation that resembles its transition state. This is the induced fit hypothesis proposed by Daniel Koshland in 1958.² Induced fit also implies distortion of the enzyme, which may be localised at the active site, or may also demand a major change in the enzyme's conformation.² Once the catalytic process is complete, the enzyme releases the substrate and returns to its original state, ready for another round of catalysis (**Fig. 4.2**).

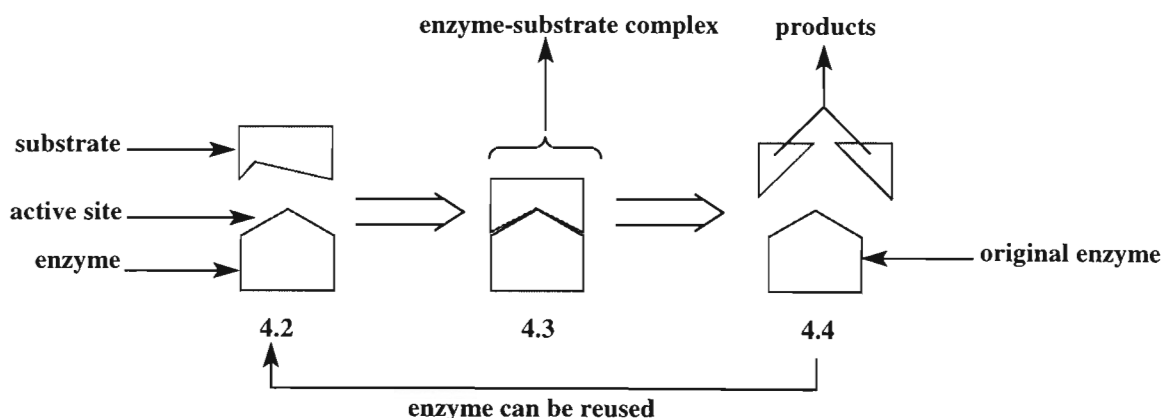
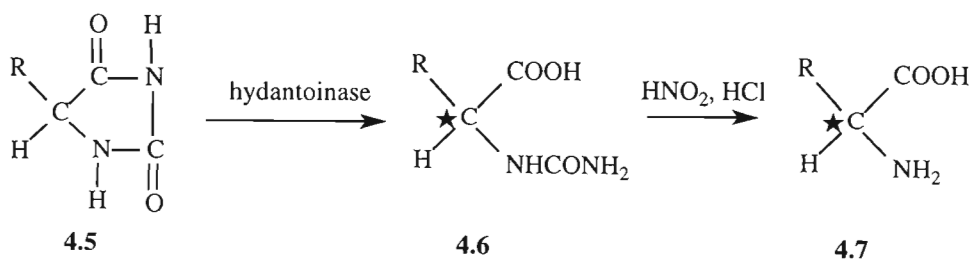


Figure 4.2: Lock and key mechanism

According to Marchand,⁶¹ many enzymes fail to catalyse cage-related substrates. Despite this lack of success, it was decided to pursue an enzyme-catalysed reaction on a trishomocubane substrate with the hope of some positive results. There was an obvious choice of two types of enzymes with regard to their application to the various trishomocubane derivatives. Hydantoinase⁶² could have been applied to tris-hydantoin to hydrolyse one enantiomer of the hydantoin, resulting in an enantiomerically pure form of tris-amino acid (**Fig. 4.3, No. 4.7**).



★=enantiopure chiral centre

Figure 4.3: Hydrolysis of tris-hydantoin by hydantoinase enzyme⁶²

Pig liver esterase (PLE), the alternative choice of enzyme, has the ability to hydrolyse esters, resulting in a free carboxylic acid group (**Fig. 4.4, No. 4.9**). Since PLE was readily available in the laboratory, it was decided to test this enzyme on an ester derivative of

trishomocubane. It was, therefore, necessary to synthesise such a derivative. Researchers have reported some success with the application of PLE to α,α -disubstituted α -amino acid esters, which falls in the same category of compounds as an ester derivative of trishomocubane.⁶³ Future work could investigate the applicability of hydantoinase enzyme to tris-hydantoin.

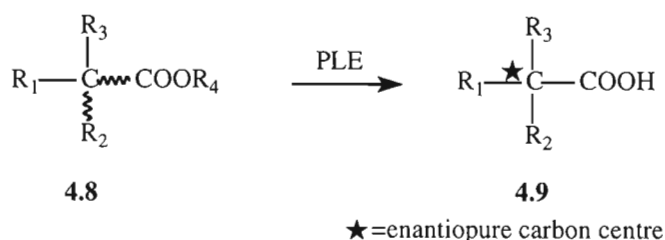


Figure 4.4: PLE catalysed hydrolysis of ester substrate⁶³

The tris- α -amino acid ester [**Novel Compound 5**, (NC5), **Fig. 4.5**, **No. 4.10**] was synthesised by the addition of tris-amino acid to ethanol and thionyl chloride under reflux conditions. The structure was fully elucidated before it was used as a PLE substrate. It was the most difficult of the trishomocubane derivatives to elucidate due to major overlap of the NMR signals.

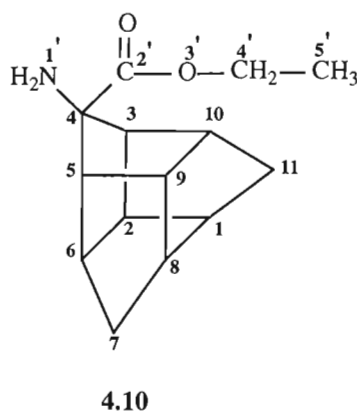


Figure 4.5: Novel Compound 5 (NC5)

It was evident that **NC5** had been synthesised due to the $[M+H]^+$ peak of m/z 234 in the mass spectrum (**Spectrum 76**), the presence of the carbonyl peak (C_2) at 175.74 ppm in the ^{13}C NMR spectrum (**Spectrum 70**), and the D_2O exchangeable proton at 1.80 ppm in the 1H NMR spectrum (**Spectrum 69**) arising from the amino group ($H_{1'}$). The multiplet at 4.12-4.18 ppm in the 1H NMR spectrum, which could be assigned to the downfield shifted methylene group ($H_{4'}$) of the ester was further evidence of successful ester synthesis.

The C_4 carbon was assigned to 69.07 ppm in the HSQC spectrum (**Spectrum 73**) due to the absence of HSQC correlations and also because it is the most deshielded carbon due to its proximity to the carbonyl functionality. The next most deshielded carbons of the cage (54.04 and 56.20 ppm) were recognised as C_3 or C_5 due to their direct attachment to C_4 . The HMBC correlation (**Spectrum 74**) of H_{11a} (1.37-1.39 ppm, the splitting patterns of the cage methylene protons were identical to those seen for tris-hydantoin) with the carbon

peak at 56.20 ppm allowed this peak to be assigned to C₃. A similar correlation was visible between H_{7a} (1.39-1.42 ppm) and C₅. HSQC correlations, therefore, allowed the identification of the H₃ proton at 1.94-1.95 ppm, and the H₅ proton at 2.07-2.10 ppm. The H₆ proton was identified at 2.60 ppm in the COSY spectrum (**Spectrum 71**) due to correlation with H₅. This assignment was confirmed by the visible NOESY correlation (**Spectrum 72**) with the N₁ protons as well as COSY correlations with both the H_{7a} and H_{7s} (1.30 ppm) protons. The C₆ carbon (45.30 ppm) was identified due to HMBC correlation with H_{7a}.

The H₂ proton (2.15-2.18 ppm) was identified due to NOESY correlation with H₆ and HMBC correlation with C₅. The assignment of H₂ allowed the assignment of H₁₀ (2.10-2.11 ppm) due to NOESY correlation with H₃. The C₁₀ carbon was distinguished from the C₆ carbon due to HMBC correlation with the H_{11a} proton. The H₁ proton (2.10-2.11 ppm) was assigned from the COSY correlations with both the H_{11a} and H_{11s} (1.30 ppm) protons. It was, unfortunately, not possible to assign its carbon peak to either 46.92 or 46.96 ppm due to indistinguishable correlations. The H₈ proton (2.10-2.11 ppm) was assigned from NOESY correlations with both the H₇ and H₁₁ methylene protons. Its carbon peak, however, was indistinguishable from the C₁ carbon peak due to reasons mentioned above. The last unassigned methine proton of the cage (H₉, 2.12-2.15 ppm) was identified from the COSY correlation with H₈. The H₄ (4.12-4.18 ppm) protons were correctly assigned due to COSY correlations with the H₅ methyl protons. A more detailed elucidation of **NC5** is available in the experimental section (**Chapter 8**).

Pig Liver Esterase (PLE) is a serine hydrolase, which catalyses the hydrolysis of a wide range of ester structures.⁶⁴ Hydrolytic enzymes are one of the most useful class of enzymes as they possess broad substrate specificities, are usually highly stereoselective in their catalysis, do not require expensive and unstable co-enzymes, and are often stable in organic and aqueous media.⁶⁵

Previously, PLE posed a few problems to chemists as the enzyme's stereochemistry appeared to be somewhat fickle towards certain substrate groups⁶⁴ (**Fig. 4.6**).

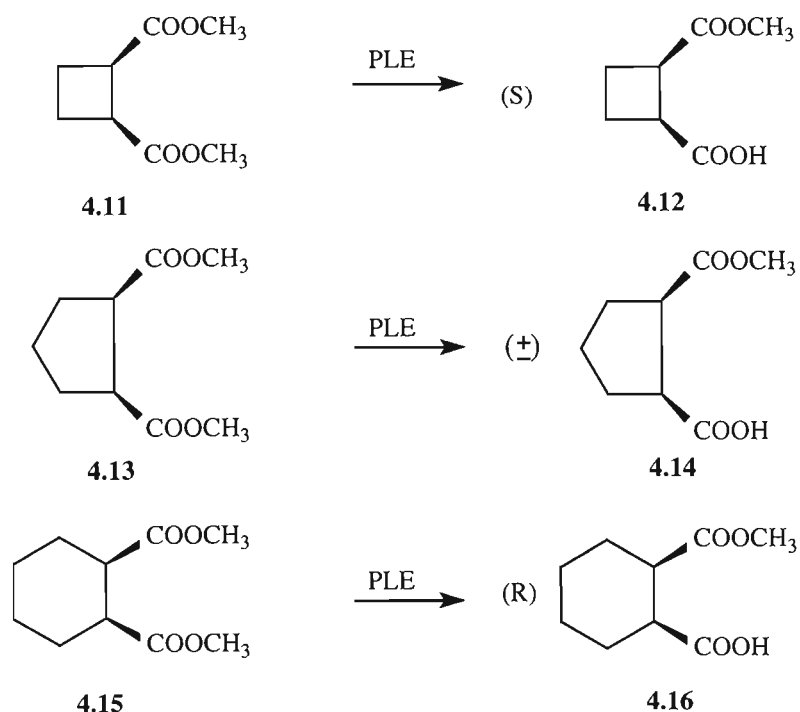


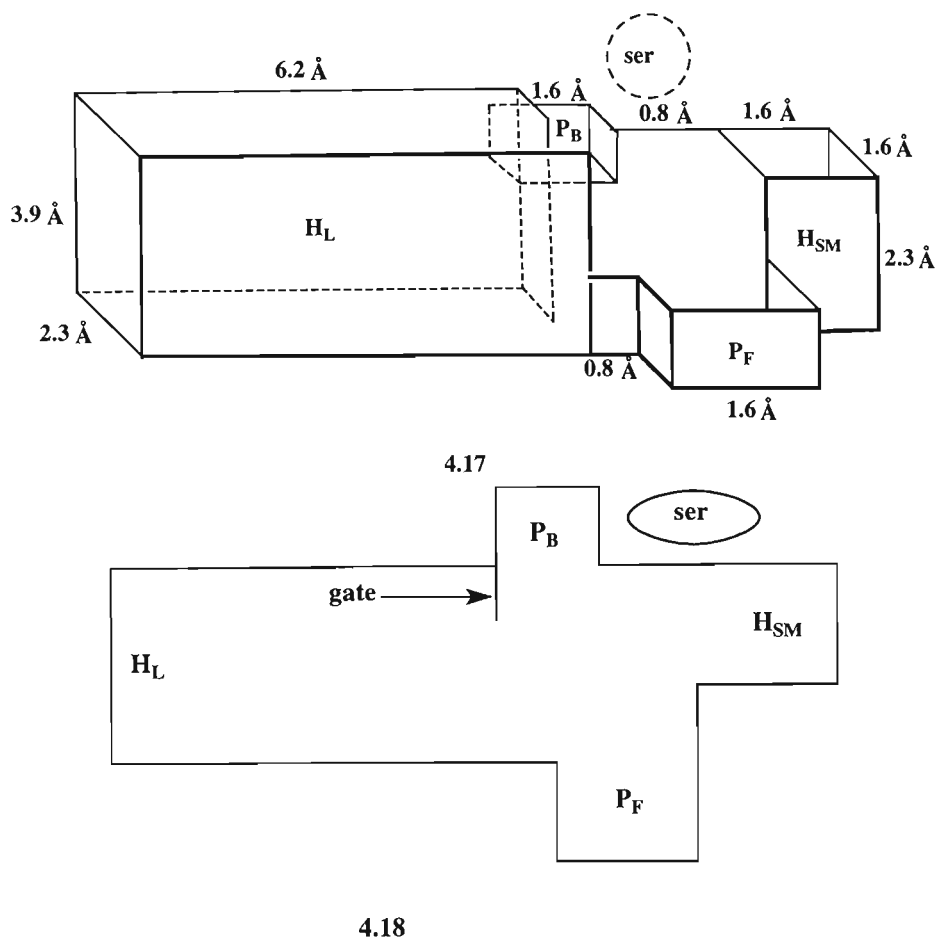
Figure 4.6: Stereochemistry reversals exhibited by PLE⁶⁴

If an enzyme is to be universally approved as a routine catalyst, it is important for it to be unwavering in its stereochemical specificity. The results in **Fig. 4.6** were first thought to be attributed to the fact that commercially available PLE consists of a mixture of isozymes. Separation of these isozymes and individual testing concluded that, although PLE is a mixture, it behaves as if it were a single species.^{64,65} The inconsistency in stereoselectivity was, therefore, attributed to the active site of PLE. This prompted research into the development of a suitable model for the active site of PLE.

The absence of an X-ray structure for PLE prompted chemists into seeking an alternative means to developing a model for the PLE active site. Many models have been proposed but the model proposed by Jones has proven to be the most successful.^{65,66,67} Jones⁶⁵ opted for an empirical approach when creating a model for the active site. The model was created in a cubic space form for various reasons. The empirical approach has been successful for many enzymes, it is the easiest to visualise and use, and any biochemical statement regarding the presence or absence of specific amino acids is avoided. There is also no temptation to align the bonds of the structure along the lines of the framework of the model, as in the case of diamond lattice models, for example.⁶⁵

Jones's model is comprised of five binding loci, with the boundaries representing the physical restrictions that amino acids of the enzyme place on the substrate (**Fig. 4.7, No. 4.17** and **4.18**). The catalytically essential region is the area encircling the serine (**ser**) residue. It initiates hydrolysis by attack on the carbonyl group of the ester. This nucleophilic site is best represented as a zone (1 Å diameter) since dissimilar substrates orientate differently in the active site. The binding regions controlling specificity are composed of two hydrophobic and two other more hydrophilic regions, which are

represented in the side (Fig. 4.7, No. 4.17) and top (Fig. 4.7, No. 4.18) view of the computed enzyme pocket.⁶⁵



H_L - large hydrophobic region
 H_{SM} - small hydrophobic region
 P_B - back hydrophilic region
 P_F - front hydrophilic region
 ser - serine residue

Figure 4.7: Side and top view of cubic space models of PLE active site⁶⁵

The two hydrophobic regions are the large (H_L) and small (H_{SM}) regions. They interact with the aliphatic or aromatic portions of the substrate. The H_L region has a total volume of $\sim 56 \text{ \AA}^3$, while the H_{SM} region has a total volume of 5.5 \AA^3 .⁶⁶ There is also a “gate” at the entrance to the H_L region, which incorporates some restrictions on the steric disposition of groups near the ester functionality.⁶⁷ Double bonds and small rings near the ester can be expected to slow the rate of hydrolysis and may lead to regioselective transformations. There is preferential binding of the hydrophobic portion of the substrate to the H_{SM} region. If the moiety is too large then binding will take place in the H_L region. This is the basis of size-induced reversals of the enzyme’s stereoselectivity and explains the results in Fig.

4.6.⁶⁴ Both H_L and H_{SM} regions exclude polar groups such as hydroxyl, amino, carbonyl and nitro functional groups. They can, however, accommodate less polar heteroatom functional groups, such as halogen, ether or ketal oxygen atoms.⁶⁵

The other two specified regions are more polar (P) or hydrophilic. These areas are designated P_B (B - back of active site) and P_F (F - front of active site), respectively. The P_F site binds the second, non-hydrolysed ester functionality in the case of diester substrates. It can also accommodate non-polar groups. The P_B site interacts well with hydrogen bond donors. A variety of alcohol, ether and carbonyl functional groups can also comfortably locate here. The P_B site is, however, too polar to accept hydrophobic moieties. The rear boundary of P_B as well as the space above the model is open, allowing groups to extend beyond the active site if necessary.⁶⁵

Computational chemistry*, using Gaussian 98⁶⁸ and a 3-21+G basis set was utilised to calculate the volume of the trishomocubane skeleton. This was performed to assess the steric constraints of the cage and predict the success and applicability of PLE to the tris- α -amino acid ester (**NC5**). The volume of trishomocubane was calculated to be 351.97 \AA^3 . This volume is supposedly far too great to fit in either the H_L or H_{SM} binding region of PLE. Although poor results were expected, PLE was still tested on **NC5** since some enzyme studies on cage systems have achieved success. For example, horse liver alcohol dehydrogenase was successful in catalysing the reduction of pentacyclo-[5.4.0.0^{2,6}.0^{3,10}.0^{5,9}]undecane-8,11-dione, which yielded (-)-11-hydroxy-pentacyclo-[5.4.0.0^{2,6}.0^{3,10}.0^{5,9}]undecan-8-one.⁶⁹

The PLE enzyme was applied to **NC5** to test the efficiency of ester hydrolysis. PLE was added to a stirred solution of **NC5** in 0.05 M KH_2PO_4 buffer at pH 8 and 28 °C. Researchers have determined that the above mentioned conditions are required for optimum activity of PLE.^{63,70} **Figure 4.8** and **Figure 4.9** shows the effect of varying pH and temperature on the activity of PLE, using α -hydroxy esters as substrates, respectively.

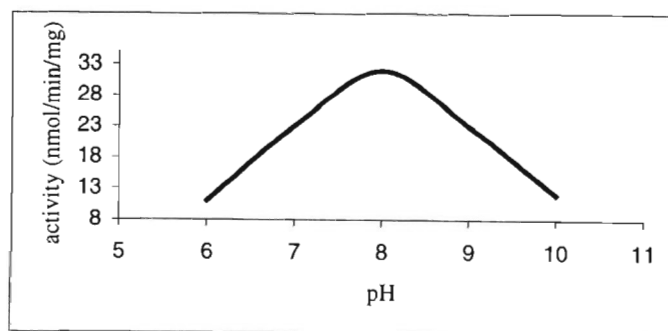


Figure 4.8: Effect of pH on activity of PLE⁷⁰

* Chapter 6 describes the theoretical basis of computational chemistry.

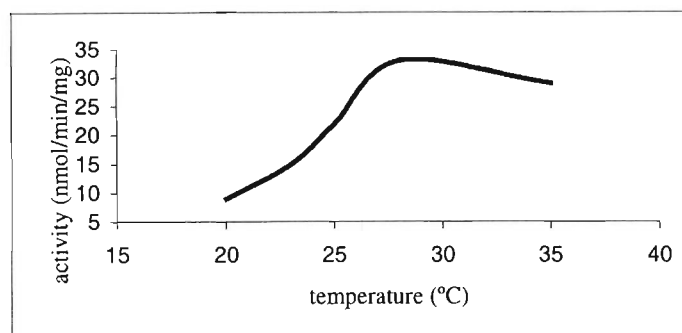


Figure 4.9: Effect of temperature on activity of PLE⁷⁰

The reaction was run over a two-week period due to a few unanticipated difficulties. The poor solubility of **NC5** in the buffer solution and the possible steric problems induced by the bulky cage forced a longer reaction time. After two weeks the reaction mixture was filtered through a sintered glass funnel to remove the enzyme, followed by washing with buffer solution. The aqueous filtrate was extracted with ethyl acetate to remove any unreacted starting material. Unreacted ester was recovered from the organic layer, which was evidence of a very slow reaction possibly amplified by poor solubility. The aqueous layer was acidified to pH 6.5 by adding concentrated hydrochloric acid. This solution was placed on a hot plate to reduce the volume, which resulted in the tris-amino acid precipitating out of solution. The tris-amino acid was isolated by filtering off the aqueous layer and was subsequently washed with acetone and diethyl ether. A 10 % yield of tris-amino acid was obtained, indicating that PLE is a highly unfavourable enzyme for hydrolysing cage related esters. The Fmoc derivative of tris-amino acid was synthesised to obtain NMR data and confirm the presence of the trishomocubane cage. The NMR data was identical to authentic data.²³ The application of a chiral shift reagent (Europium tris[3-(heptafluoropropyl-hydroxymethylene)-(+)-camphorate] did not induce any splitting in the ¹H or ¹³C NMR spectra (the spectra were identical to **Spectra 34** and **35**) which was a clear indication that enantiomerically pure Fmoc-tris-amino acid was present. This was evidence that PLE had successfully produced enantiomerically pure tris-amino acid. Unfortunately, the low yields only afforded enough material to produce NMR data. Future investigations should attempt to record the optical rotation of the product.

The poor yields (10 %) from the enzyme reaction did not warrant any further investigation. The results confirm the private communication with Marchand⁶¹ stating the poor success rate of various enzymes on cage-related compounds. It is, however, worth investigating the application of hydantoinase to tris-hydantoin, which could yield more promising results.

CHAPTER 5

PEPTIDE SYNTHESIS

Govender²³ has reported the synthesis of a dipeptide consisting of glycine and tris-amino acid. He, however, failed to extend the dipeptide or isolate a pure sample for structural elucidation by NMR techniques. Research was, therefore, undertaken to incorporate tris-amino acid into a longer peptide as well as isolate a pure sample for NMR analysis.

The synthesis of non-natural amino acids^{71,72,73} and their incorporation into short peptides^{8,10,74} has been the focus of many research groups due to their various biological applications. Incorporating cage structures into short peptides for pharmaceutical use has been proven to induce some positive effects,^{8,9,10,11} such as improved lipophilicity for transport across cellular membranes. The bulkiness of the cage has also been shown to retard metabolic degradation.

Adamantane (**Fig. 5.1, No. 5.1**) is one particular non-natural cage, which has exhibited some successful biological activity.^{8,10} Various adamantanine peptides have proved stable in *in vivo* experiments (**Fig. 5.1, No. 5.2**).⁸ This has been attributed to the steric hindrance of the peptide bonds involved, inhibiting enzymatic degradation. This type of system may be applicable to active substances which encounter bioavailability or transport problems.⁸ Various adamantyl peptides have also been proven to enhance lipophilicity and penetration through the blood brain barrier¹⁰ as well as significant antiviral activity.⁷⁵ These results have prompted research into incorporating cage compounds such as tris-amino acid²³ (**Fig. 5.1, No. 2.13**) and PCU amino acid⁷⁶ (**Fig. 5.1, No. 5.3**) into short peptides.

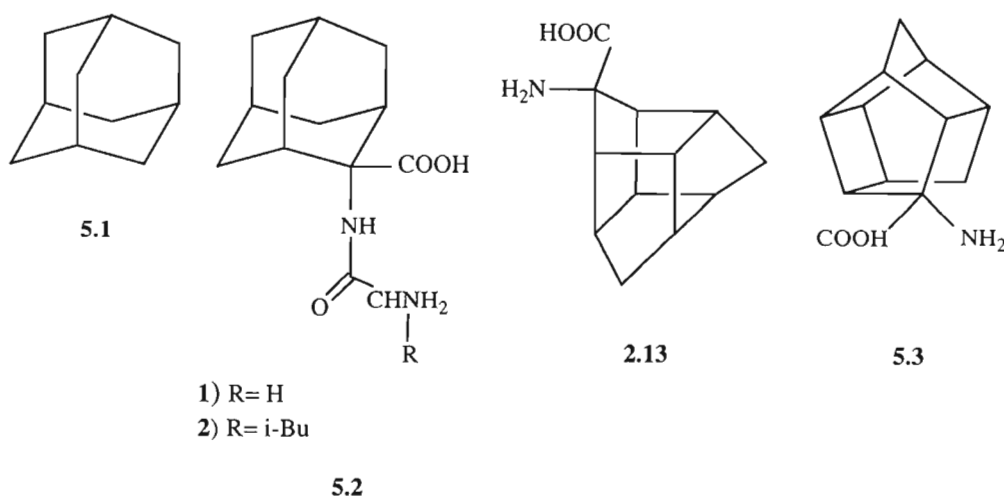
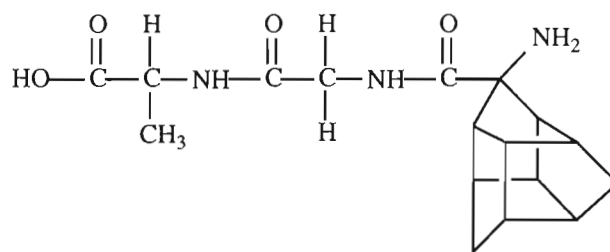


Figure 5.1: Biologically important cage structures

An attempt was made to incorporate the racemic α,α -disubstituted tris-amino acid (**Fig. 5.1, No. 2.13**, synthesis is described in detail in **Chapter 2**) into a tripeptide of ala-gly-tris (**Fig. 5.2, No. 5.4**) *via* solid phase techniques. $C^{\alpha,\alpha}$ -disubstituted- α -amino acids display a propensity to induce secondary folding to short peptides,⁷⁷ which may be an interesting investigation following the successful synthesis of the tripeptide.



5.4

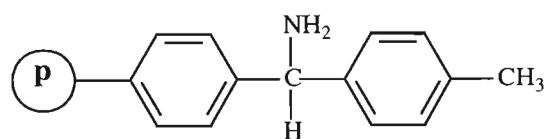
Figure 5.2: Proposed tripeptide of ala-gly-tris

There are two reasons why glycine was chosen: (a) it serves as an achiral linker between the racemic tris-amino acid and (S)-Ala, to minimise diastereomeric effects visible during NMR analysis, and (b), it is the smallest amino acid, which may assist the coupling to the very bulky tris-amino acid.

It was Emil Fischer who first prepared a peptide of 18 amino acid residues.¹ Early peptide work relied on solution chemistry techniques. This classical method of peptide synthesis was successful in the preparation of several active peptides,⁷⁸ however, the techniques often encountered difficulties with solubility and purification. R.B. Merrifield's method of solid phase peptide synthesis, which was reported in 1963, revolutionised the field of peptide chemistry.⁷⁹ The attachment of amino acid residues to an insoluble polymer proved to be an efficient method as excess reagents and by-products could easily be removed through filtration.

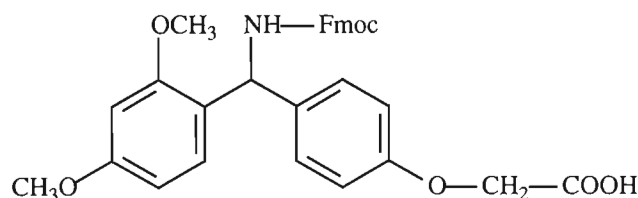
The procedure for the tripeptide synthesis involved the attachment of a linker to the resin, synthesis of a dipeptide: ala-gly by their successive attachment to the linker, followed by the addition of the tris-acid fluoride.

The 4-methylbenzhydrylamine resin (MBHA, 0.7 mmol NH_2/g , **Fig. 5.3, No. 5.5**) was prepared by swelling in N,N-dimethylformamide (DMF). This was performed to increase the surface area of free amino groups attached to the polymeric support for coupling to the Fmoc protected linker. Coupling to the linker (*p*-[(R,S)- α -[1-(9H-fluoren-9-yl)methoxyformamido]-2,4-dimethylbenzyl]-phenoxyacetic acid (FmocAM linker, **Fig. 5.3, No. 5.6**) was achieved through the addition of N,N-diisopropylcarbodiimide (DIPCDI) and 1-hydroxybenzotriazole (HOBt) in DMF.



P = polymer

5.5



5.6

Figure 5.3: MBHA resin (5.5) and FmocAM linker (5.6)

DIPCDI (**Fig. 5.4, No. 5.9**) is a dehydrating agent, which favours the formation of peptide bonds (**Fig. 5.4, No. 5.10**) and in the process is converted to a soluble urea co-product (**Fig. 5.4, No. 5.11**). HOBt is an additive, which accelerates carbodiimide-mediated couplings and suppresses racemisation of the amino acid.⁸⁰ Note that racemisation is not a problem with the tris-amino acid due to the lack of an acidic α -hydrogen. The resulting mixture was stirred over a 24 hour period. The excess reagents were filtered from the mixture, followed by successive washing with DMF. A negative Kaiser test⁸¹ proved the successful attachment of the Fmoc protected linker to the resin.

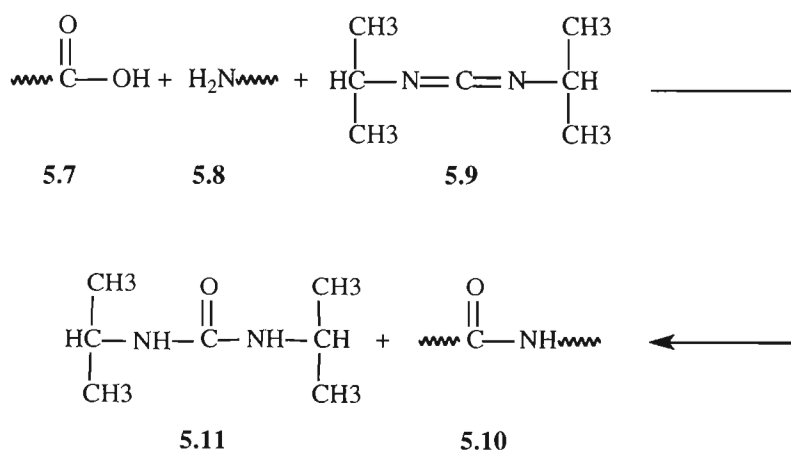


Figure 5.4: Dehydrating action of DIPCDI⁵²

The Fmoc group on the linker (**Fig. 5.5, No. 5.12**) was removed by the addition of 20 % (v/v) piperidine (**Fig. 5.5, No. 5.13**) in DMF and subsequent stirring for two hours.²³ The resin was washed with DMF and the Fmoc removal was verified by a positive Kaiser test.

The resin was washed with 1 % (v/v) TFA in DMF before addition of the Fmoc-alanine to ensure complete absence of piperidine.

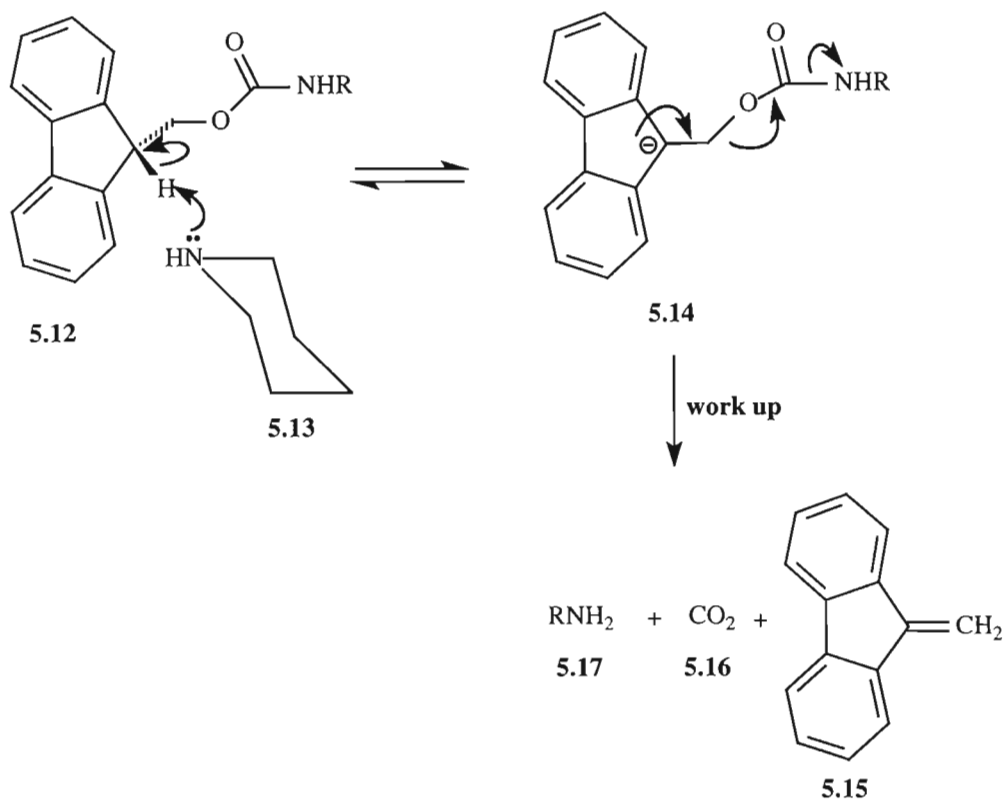


Figure 5.5: Fmoc deprotection using piperidine³⁸

The attachment procedure for the first and second amino acids (Fmoc-ala and Fmoc-gly) also required the addition of DPCDI and HOBT in DMF. The cleavage procedure for removal of the Fmoc group again required addition of a 20 % (v/v) piperidine in DMF solution.

NMR data (**Spectrum 81**) was useful in verifying the successful synthesis of the dipeptide (ala-gly). HPLC (**Chromatogram 82**) was used to determine the purity of the products. The presence of one peak at 12.70 minutes in the chromatogram was proof of a pure dipeptide. At this stage, addition of the tris-acid fluoride to the dipeptide was possible. Previous attempts to couple the tris-amino acid failed and partial success was achieved by activating the acid to the acid fluoride using cyanuric fluoride.²³

It was first essential to synthesise the acid halide derivative of tris-amino acid before coupling to the dipeptide. This was to ensure successful coupling of the sterically hindered α,α -disubstituted tris-amino acid.^{82,83} There has been much success with the use of amino acid chlorides,^{84,85} yet there have also been some disadvantages. N-protected amino acid chlorides are often very highly reactive and sensitive to hydrolysis. They, therefore, need to be used immediately after preparation and often in large excesses.⁸⁶ There has also been difficulty in preparing stable Fmoc-amino acid chlorides from trifunctional amino acids.⁸⁷

There has, therefore, been much attention paid to acid fluorides due to their high reactivity in coupling, partly due to the small size of the fluoride leaving group.⁸⁵ The acid fluorides also display numerous advantages over the analogous chlorides. They have proven to be more stable, often storable for up to six months under normal conditions. Oxazolone formation in the presence of a tertiary base is not observed and has often exhibited coupling in the absence of base.⁸⁸ It has also been proven, due to the nature of the C-F bond, that acid fluorides possess a greater stability towards neutral oxygen nucleophiles such as water and methanol but equal reactivity to anionic nucleophiles and amines.⁸⁷ Acid fluorides are effective in the coupling of α,α -dialkyl substituents and highly sterically hindered units such as alamethicin acid (eight aminoisobutyric acid (Aib) and two proline residues).⁸²

It was, therefore, decided to synthesise the Fmoc-tris-amino acid fluoride by mixing Fmoc-tris-amino acid, dry pyridine and cyanuric fluoride in dry dichloromethane for four hours at room temperature. This was followed by the addition of ice water. The precipitated cyanuric acid was filtered off. Removal of the organic phase resulted in pure Fmoc-tris-amino acid fluoride (**Spectra 77-80**).⁸⁹

The Fmoc-tris-amino acid fluoride was added to the dipeptide along with DMF and pyridine as a fluoride ion scavenger. This was necessary since hydrofluoric acid is effective in cleaving MBHA linkages.⁹⁰ The resulting solution was left to stir for 24 hours. The successful addition was confirmed by a negative Kaiser test. The Fmoc group was removed by addition of 20 % (v/v) piperidine in DMF. Confirmation of Fmoc removal was very difficult since it was impossible to achieve a positive Kaiser test. It was speculated that the base had failed to remove the Fmoc group and so a 30 % (v/v) piperidine in DMF solution was applied and left overnight. A negative Kaiser test was still obtained. The peptide was, therefore, cleaved from the resin and linker to perform NMR analysis.

The tripeptide was prepared for cleavage by washing successively with dichloromethane, methanol and diethyl ether, followed by drying *in vacuo*. The cleavage mixture of 95 % (v/v) trifluoroacetic acid, 2.5 % (v/v) water and 2.5 % (v/v) triisopropylsilane was subsequently added. The resin was removed by filtration, while the application of nitrogen gas to the filtrate removed most of the TFA. Diethyl ether was subsequently added to precipitate the peptide from solution. Decanting the diethyl ether served to remove the linker from the peptide.^{23,91} NMR analysis (**Spectrum 83**) of the peptide confirmed the removal of the Fmoc protecting group. The fact that a negative Kaiser test was obtained may be due to the formation of a reversible Schiff base bond (**Fig. 5.6, No. 5.19**), where the free amine of the cage attacks the carbonyl functionality of the glycine residue. This is a reasonable explanation since the absence of steric hindrance from the glycine residue in the second position enables the peptide to fold back on itself to form a reversible six membered ring (**Fig. 5.6**). Computational studies⁹² suggest that tris-amino acid possesses strong β -turn characteristics,¹⁶ which would assist the formation of the six-membered Schiff base.

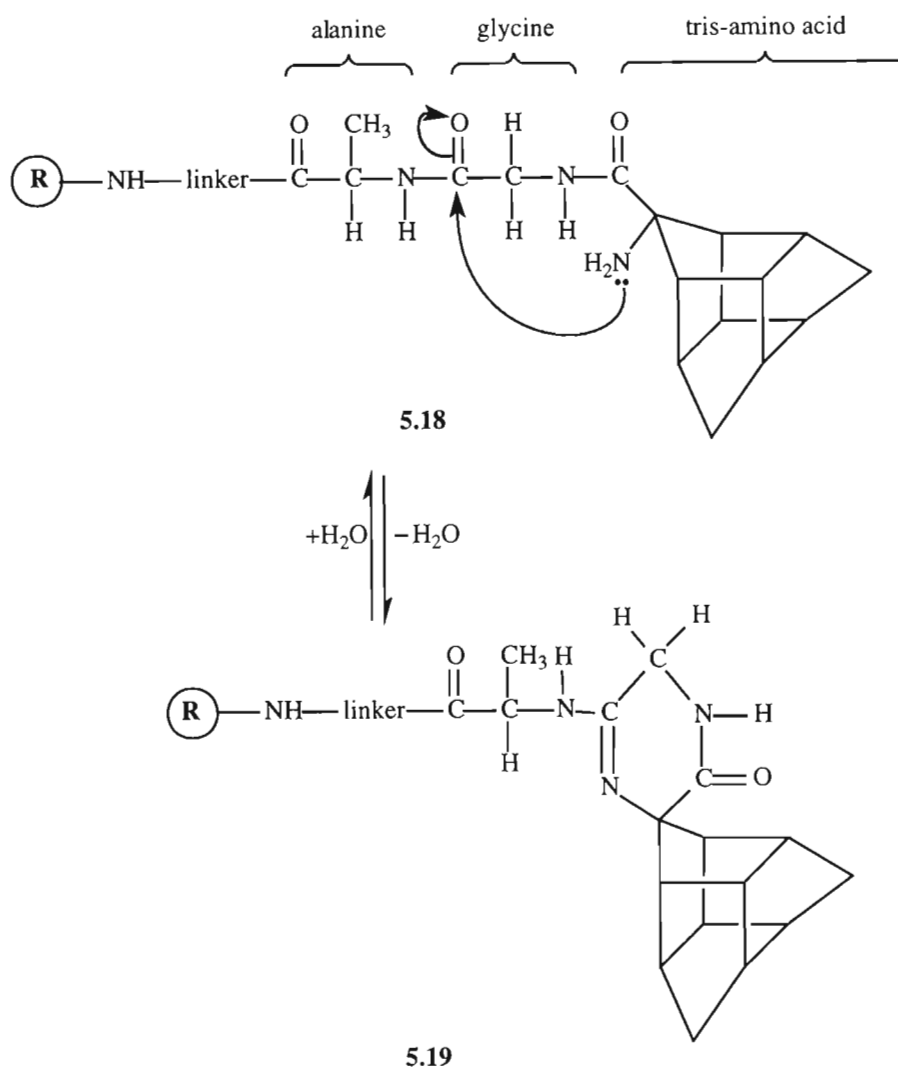


Figure 5.6: Formation of a Schiff base bond

The NMR analysis of the tripeptide also showed that it contained impurities, which was confirmed by HPLC results (**Chromatogram 84**). The fact that the peptide was present as a mixture of diastereomers [(*S*)-ala-gly-(*R*)-tris and (*S*)-ala-gly-(*S*)-tris] accounted for the broad peak representing the tripeptide (31.22-39.72 minutes), which exhibited identical ultraviolet spectra (**Chromatogram 84**). This broad peak could not be resolved. Mass spectrometry (**Spectrum 85**) was useful in confirming the synthesis of the tripeptide by the presence of the molecular ion peak at m/z 334 $[M+H]^+$. A summary of the peptide synthesis is depicted in **Fig. 5.7**.

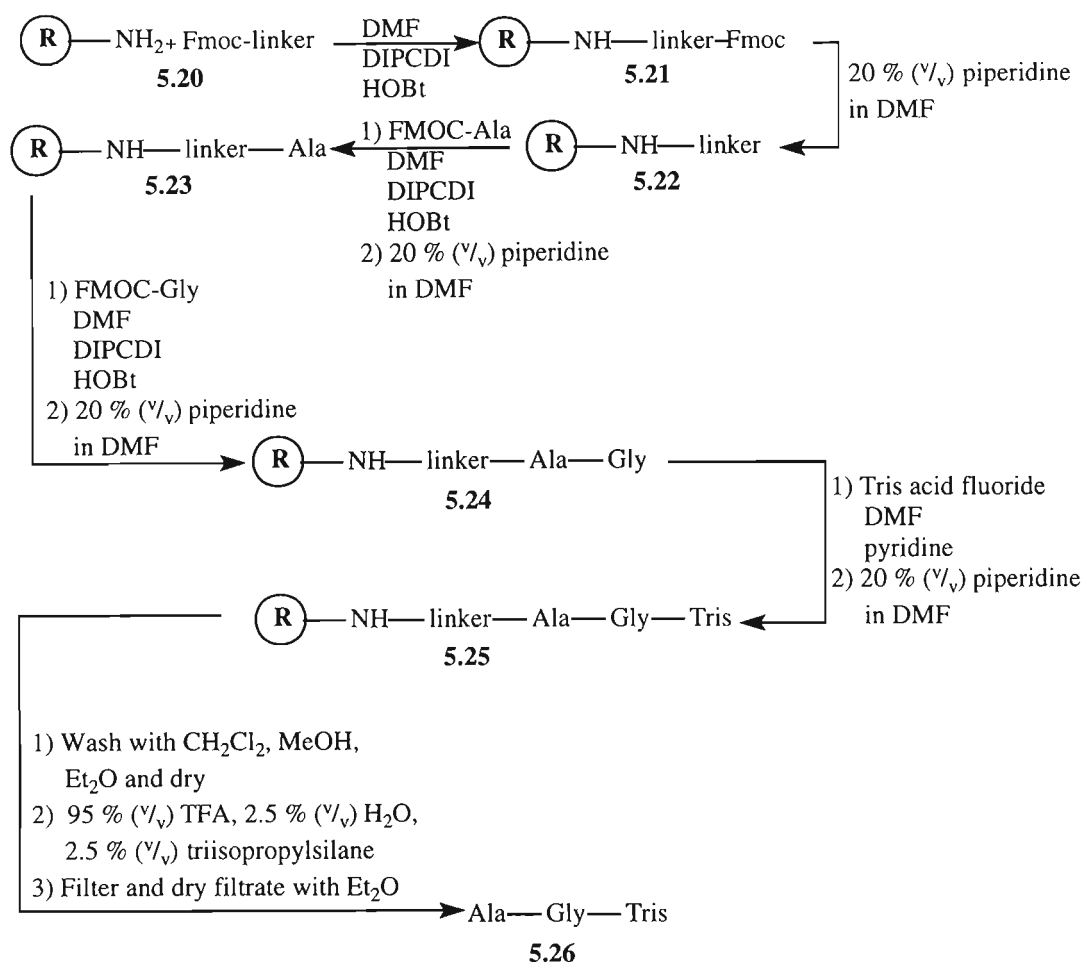


Figure 5.7: Summary of peptide synthesis

The tripeptide was successfully synthesised according to mass spectrometry results. The product proved difficult to purify, and consequently a full structural elucidation by NMR techniques was not possible. In order to prevent the back turning of the tris-amino acid and prevent some of the problems experienced, would be to avoid glycine insertion at the $i+1$ position. Optically pure tris-amino acid would also be required to avoid diastereomeric effects.

CHAPTER 6

COMPUTATIONAL CHEMISTRY

The synthetic work described in the previous chapters relied on the formation of trishomocubane from the rearrangement of the PCU skeleton. A computational investigation was, therefore, undertaken to gain insight into the mechanism for the rearrangement.

6.1 Introduction

Many of the mathematical algorithms necessary for computational chemistry have been available for many years, yet the discipline has only recently become accessible to the average chemist with the improvement of computer hardware and software. Computational chemistry is, therefore, a fairly new discipline and has become a useful tool to chemists, enabling a more comprehensive understanding of chemical reactions and processes. It has allowed chemists to predict the stability of chemical reactions, to estimate energy differences between different states and to explain reaction mechanisms.⁹³ This information is invaluable, particularly in research, where laboratory-based experiments are expensive and time-consuming.

Computational chemistry simulates chemical structures and reactions numerically and is based on the fundamental laws of physics.⁹⁴ There are two categories within computational chemistry: *molecular mechanics* and *electronic structure theory*.

Ab initio methods, a class within electronic structure theory, perform calculations based on the fundamental laws of quantum mechanics and on the values of a few physical constants: the speed of light, the masses and charges of electrons and nuclei, and Planck's constant.⁹⁴ *Ab initio* methods are derived directly from theoretical principles with no inclusion of experimental data.

Ab initio methods were used to examine the rearrangement mechanism of the PCU-diol to 7-fluoro-11-hydroxy-trishomocubane *via* two proposed mechanisms. Before the discussion of the two proposed mechanisms, a short overview on computational chemistry will be presented.

Ab initio methods compute solutions to the Schrödinger equation (**Eq. 6.1**) by using a series of rigorous mathematical approximations and provide high quality quantitative predictions for a broad range of atomic and molecular systems.⁹⁴ The Schrödinger equation is represented as:

$$H\psi = E\psi \tag{6.1}$$

where H is the Hamiltonian operator. This is represented as:

$$\begin{aligned}
& -\frac{h^2}{8\pi^2} \sum_A \frac{1}{M_A} \nabla_A^2 - \frac{h^2}{8\pi^2 m} \sum_a \nabla_a^2 - e^2 \sum_A \sum_a \frac{Z_A}{r_{Aa}} + e^2 \sum_A \sum_{>B} \frac{Z_A Z_B}{R_{AB}} + \\
& e^2 \sum_a \sum_{>b} \frac{1}{r_{ab}}
\end{aligned} \tag{6.2}$$

where M are the nuclear masses, a are electrons, A are nuclei, R_{AB} are the distances separating nuclei, r_{ab} are the distances separating electrons and r_{Aa} are the distances separating electrons and nuclei. The first two terms represent the kinetic energy of the nuclei and the electrons, while the last three terms represent the Coulombic interactions between particles.

The Shrödinger equation is a combination of the differential equation describing the profile of a simple harmonic standing wave and de Broglie's relation between matter and waves.¹⁶ Manipulations of this equation allow the description of molecules in terms of interactions among nuclei and electrons, and molecular geometry in terms of minimum energy arrangements of nuclei.⁹⁵ Unfortunately, this many electron equation cannot be solved exactly for systems that involve three or more interacting particles, therefore, some approximations need to be introduced.⁹⁶ These will be briefly described in sections 6.1.1-6.1.4.

6.1.1 Born-Oppenheimer Approximation

In this method it is assumed that the nuclei of a system do not move.⁹⁵ The mass of a nucleus is thousands of times greater than that of an electron, therefore, nuclei move slowly with respect to electrons and electrons respond instantaneously to changes in nuclear positions.¹⁶ Consequently, the energy of a molecule in its ground state can be considered a function of the nuclear co-ordinates only. The electronic wavefunction thus depends only on the positions of the nuclei and not on their momenta.¹⁶ This approximation leads to the "electronic" Shrödinger equation (Eq. 6.3), where the nuclear kinetic energy is excluded and the nuclear-nuclear Coulomb term is constant.

$$H^{elec} \psi^{elec} = E^{elec} \psi^{elec} \tag{6.3}$$

$$H^{elec} = -\frac{h^2}{8\pi^2 m} \sum_a \nabla_a^2 - e^2 \sum_A \sum_a \frac{Z_A}{r_{Aa}} + e^2 \sum_a \sum_{>b} \frac{1}{r_{ab}} \tag{6.4}$$

$$E_{total} = E^{elec} + e^2 \sum_A \sum_{>B} \frac{Z_A Z_B}{R_{AB}} \tag{6.5}$$

6.1.2 Hartree-Fock Approximation⁹⁵

This approximation involves the replacement of the many electron wavefunction by a product of one-electron wavefunctions, termed spin orbitals. Each spin orbital is written as a product of a space part, ψ , and is termed a molecular orbital with one of two possible spin parts, α or β . Only two electrons may occupy a given molecular orbital and must be of opposite spin.¹⁶

The Hartree-Fock level of theory is the entry level of *ab initio* techniques. There are better levels of theory such as DFT, MP2, MP4, *etc.*, but they are very expensive with regard to hardware resources and time.

6.1.3 LCAO Approximation

Molecular orbitals are expressed as linear combinations of a finite set (a basis set) of prescribed functions: known as basis functions, ϕ (Eq. 6.6):

$$\psi_i = \sum_{\mu}^{bs} c_{\mu i} \phi_{\mu} \quad (6.6)$$

where $c_{\mu i}$ is the molecular orbital coefficient (often incorrectly referred to as molecular orbitals), ϕ_{μ} are the atomic orbitals because they are usually centred at the nuclear position and bs are the basis functions.

Hartree-Fock theory takes advantage of the variational principle to solve for the set of molecular orbital expansion co-efficients by finding the set of co-efficients that minimise the energy of the resultant wavefunction.⁹⁴

6.1.4 Roothaan-Hall Equations⁹⁵

The application of Hartree-Fock and LCAO approximations to the electronic Schrödinger equation leads to the Roothaan-Hall equations (Eq. 6.7):

$$\sum_{\nu}^{bs} (F_{\mu\nu} - \epsilon_i S_{\mu\nu}) c_{\nu} = 0 \quad (6.7)$$

where ϵ_i are the orbital energies, S is the overlap matrix (extent to which basis functions “see each other”) and F is the Fock matrix (average effects of the field of all the electrons on each orbital), which is represented in atomic units as:

$$F_{\mu\nu} = \left\langle \phi_{\mu} \left| -\frac{1}{2} \nabla^2 - \sum_A^{nu} \frac{Z_A}{r_A} \right| \phi_{\nu} \right\rangle + \sum_{\lambda}^{bs} \sum_{\sigma}^{bs} P_{\lambda\sigma} \left[(\phi_{\mu} \phi_{\nu} | \phi_{\lambda} \phi_{\sigma}) - \frac{1}{2} (\phi_{\mu} \phi_{\lambda} | \phi_{\nu} \phi_{\sigma}) \right] \quad (6.8)$$

The first term represents the kinetic energy and potential energy of individual electrons, the second term represents the interactions among electrons, P is the density matrix (energy of a single electron in the field of the bare nuclei) and $P_{\lambda\sigma}$ is represented as:

$$P_{\lambda\sigma} = 2 \sum_i^{occM.O.s} c_{\lambda i}^* c_{\sigma i} \quad (6.9)$$

where *occM.O.s* are the occupied molecular orbitals.

The solutions of the Roothaan-Hall equations are termed *ab initio* models. These models treat the motions of individual electrons as independent of one another. This leads to an overestimation of the electron-electron repulsion energy. This results in an overestimation of the total energy since electrons “get in each others way” to a greater extent than they should. The problem is solved by the self-consistent field (SCF) approximation. Through SCF any instantaneous electron-electron repulsions are neglected. Each electron is considered to interact with the average field generated by the global charge distribution of all the other electrons in the system, rather than with other electrons taken as distinct particles. An adjustment in one orbital changes the SCF effective potential and may lead to an adjustment in the form of another orbital, and so on.⁹⁴ One of the problems of using molecular orbital theory with the SCF approximation is how to treat molecules with and without unpaired electrons: closed or open shell systems. Restricted Hartree-Fock (RHF) or closed shell calculations force each electron pair into a single spatial orbital (**Fig 6.1, a**), while Unrestricted Hartree-Fock (UHF) or open shell systems use separate spatial orbitals for the spin-up and spin-down electrons (α and β respectively, **Fig. 6.1, b**).⁹⁴

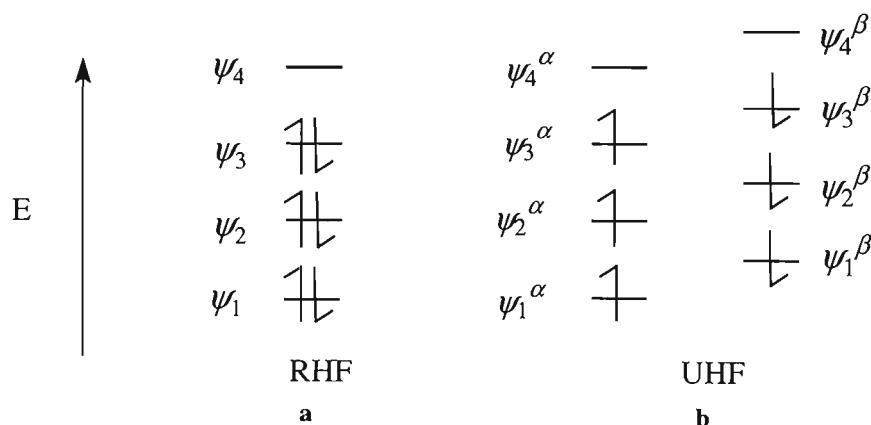


Figure 6.1: Restricted Hartree-Fock versus Unrestricted Hartree-Fock

With UHF, the two sets of orbitals are similar but not necessarily identical. By convention, any unpaired electrons are designated *alpha* spin.¹⁶ UHF is more flexible than RHF because the formally paired *alpha* and *beta* orbitals, which correspond to double occupied molecular orbitals in RHF, need not be identical, and can be independently adjusted to achieve a lower energy.¹⁶ UHF is generally a much more time consuming tool, but is the most appropriate way to deal with molecules near the dissociation limit.⁹⁶

6.2 Basis Sets for *ab initio* and DFT Calculations

A basis set is a mathematical description of the orbitals within the system used to perform the theoretical calculations.⁹⁴ The number of atomic orbitals determines the quality of the molecular orbital. If there are many electrons in a molecule then the number of atomic integrals required increases rapidly.¹⁶ The Gaussian 98⁶⁸ program offers a range of pre-defined basis sets, classified by the number of types of functions they contain.¹⁶ Minimal basis sets are characterised by fixed size atomic orbitals, and contain the minimum number of basis functions needed for each atom,⁹⁴ for example, hydrogen only contains an 1s orbital, while carbon is allowed 1s, 2s, 2p_x, 2p_y and 2p_z orbitals.

Minimal basis sets are well known to have several deficiencies. Atoms such as oxygen and fluorine are described using the same number of basis functions as the atoms at the beginning of the period, despite the fact that they have more electrons. The functions cannot expand or contract in size in accordance with the molecular environment. They cannot describe non-spherical aspects of the electron distribution.⁹⁶

Split-valence basis sets increase the number of basis functions per atom and introduce two or more sizes of basis functions for each valence orbital, for example, hydrogen is allowed an 1s and 1s' orbital, and carbon an 1s, 2s, 2s', 2p_x, 2p_y, 2p_z, 2p_x', 2p_y', 2p_z' orbital. The primed and unprimed orbitals differ in size but not in shape.⁹⁵

Split-valence basis sets allow for the fact that the p-orbitals, which make up a “tight” σ bond, need to be more contracted than the p-orbitals, which make up a “looser” π bond (Fig. 6.2).⁹⁵

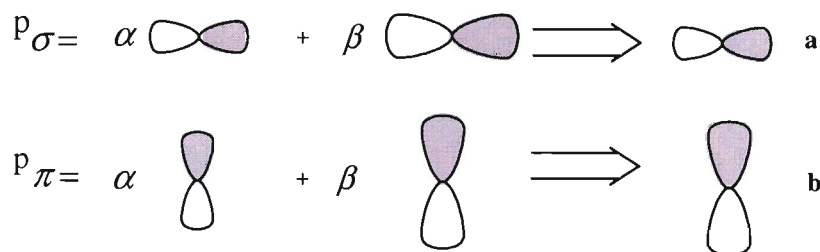


Figure 6.2: Example of orbitals used in a split-valence set

6.2.1 Split-Valence Basis Set Incorporating Diffuse Functions (3-21+G)

This basis set represents inner shell atomic orbitals by a single set of functions, which, in turn, is written in terms of three Gaussians. Basis functions representing inner and outer components of valence atomic orbitals are written in terms of expansions of two and one Gaussians respectively.⁹⁵ Heavy atoms are provided with diffuse functions (which is designated by the “+” sign). Diffuse functions are large size versions of s and p-type functions, and allow orbitals to occupy a larger region of space. This is important for systems where electrons are relatively far from the nucleus, molecules with lone pairs, anions, systems in excited states and systems with low ionisation potentials.⁹⁴

6.2.2 Polarisation Basis Set Incorporating Diffuse Functions [6-31+G(d)]

This basis set represents inner shell atomic orbitals by a single set of functions, written in terms of six Gaussians. The inner and outer components of the valence atomic orbitals are written in terms of three and one Gaussians respectively. Diffuse functions as well as a set of six d-type polarisation functions are included for each heavy (non-hydrogen) atom.⁹⁵

Ab initio methods offer the advantage that they may eventually converge to the exact solution once all approximations become sufficiently small. They are also disadvantageous: they are often expensive regarding CPU time, memory and disk space. In general they are an excellent qualitative tool, becoming more quantitative for smaller molecules. As hardware and software develop, ever increasing molecular sizes will be studied with improved accuracy.

6.3 Other Models

6.3.1 Semi-Empirical Methods

Semi-empirical methods follow directly from Hartree-Fock methods. Semi-empirical methods introduce various approximations, which reduce the computational effort characteristic of *ab initio* methods. They may also incorporate parameters derived from experimental data or high level *ab initio* calculations to simplify the computation.

Semi-empirical methods only consider the valence electrons of the system and considers inner shell electrons to be part of the nuclear core.^{93,94,95} This is rationalised by the fact that the electrons involved in chemical bonding are those in the valence shell. The second approximation is that the basis set is restricted to a minimal representation. For main group elements, this comprises a single s-type function and a set of p-type functions, for example, 2s, 2p_x, 2p_y, 2p_z.

For transition metals, a set of d-type functions, a s-type function and a set of p-type functions are included, for example, 3d_{x²-y²}, 3d_{z²}, 3d_{xy}, 3d_{xz}, 3d_{yz}, 4s, 4p_x, 4p_y, 4p_z.

A feature common to semi-empirical methods is that some of the elements that correspond to the overlap between two atomic orbitals on different atoms are set to zero. This serves to simplify the Roothaan-Hall equations. It is, however, important to include some of the overlaps in even the simplest semi-empirical models.

With the exception of modelling transition states, semi-empirical methods can reproduce a variety of experimental data, such as heats of formation, dipole moments and ionisation potentials.⁹³ Accuracy is, however, limited, largely because the models are parameterised, often upon the results from relatively low-level *ab initio* calculations.⁹⁴ In general, semi-empirical methods are faster than *ab initio* methods, yet results can be erratic if the molecule is significantly different from the parameterisation set.

6.3.2 Molecular Mechanics

Many molecular modelling systems are too large to be considered by quantum mechanical methods. Quantum mechanics deals with electrons within a system and, even if some are ignored (semi-empirical), a large number of particles must still be considered. Molecular mechanics (empirical force field calculations) ignore electronic motions and calculate the energy of a system as a function of the nuclear positions only.⁹⁴ Different molecular mechanics methods are each characterised by a particular force field. A force field comprises a set of equations defining how the potential energy of a molecule varies with the locations of its component atoms. Molecular mechanics force fields describe molecules in terms of “connected atoms”, and molecular geometry in terms of distortions from “ideal” bond distances, bond angles and dihedral angles, together with an account of non-bonded van der Waals and Coulombic interactions (Eq. 6.1.9, also see Fig. 6.3).⁹³ The total energy is given by:

$$E^{total} = \sum_i^{bonds} E_i^{stretch} + \sum_i^{bond\ angles} E_i^{bend} + \sum_i^{dihedral\ angles} E_i^{torsion} + \sum_i \sum_j^{nonbonded\ atoms} E_{ij}^{nonbonded} \quad (6.10)$$

The first three summations are over all bonds, all bond angles and all dihedral angles respectively, while the last summation is over all pairs of atoms which are non-bonded.⁹³

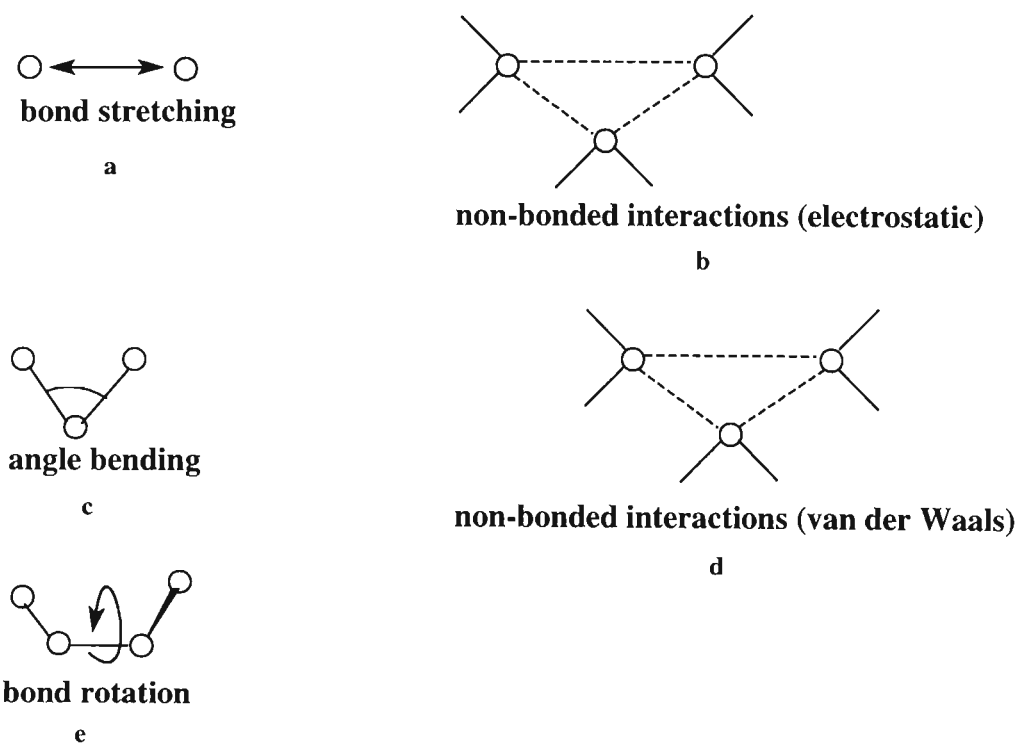


Figure 6.3: Schematic representation of the five key contributions to a molecular force field

Molecular dynamic methods can produce very accurate results with respect to geometry and energies of very large systems, at a fraction of the time compared to *ab initio* methods. The method, however, can be prone to huge error if the force field is not specifically designed for a specific system. The method is also not applicable to transition state calculations.

6.3.3 Density Functional Theory

Density functional theory (DFT) methods are very similar to *ab initio* methods, in that they require similar resources but are not as expensive. Electrons in a molecular system react to one another's motion and attempt to 'keep out of each others way'. DFT accounts for the effect of electron correlation and is, therefore, a more attractive method than *ab initio*. DFT is based on the theory that the ground state energy of any molecule can be described in terms of the electron density, that is, each molecule has a unique functional which exactly determines its geometry. This system differs to the wave function approach of *ab initio* methods, where the complexity of the wave function increases by a factor of $3N$ for an N electron system. The complexity of the DFT function is less dependant on the system size since electron density has the same number of variables. The advantage of DFT methods is that only total electron density needs to be considered.⁹⁷

The accuracy of results from DFT calculations vary from poor to fairly good, depending on the choice of basis set and density functional. DFT tends to give energy values that are lower than the expected energy, whereas *ab initio* methods asymptotically approach the expected energy as the basis set is improved. DFT has been improved with the use of hybrid functionals such as B3LYP. B3LYP with a 6-31G(d) basis set is the most widely used due to the accurate results obtained for organic molecules⁹⁸ and was used to optimise tris-hydantoin in **Chapter 2**.

6.4 Transition State Modelling

The 3-21+G basis set is the minimum basis set for *ab initio* calculations that still provides a reasonable answer for transition state geometries and energies. It is relatively inexpensive in terms of CPU time and is a logical choice when one is still in a learning phase. Upgrading of results to a better level of theory and basis set is trivial after one has determined all possible reaction details.

A transition state is a molecular species that is represented by the maximum on a potential energy curve in a simple one-dimensional reaction co-ordinate diagram. It is difficult to predict the geometry of a transition state without the aid of computational chemistry, yet, experimentally it has recently become possible by femtosecond pulsed laser spectroscopy.⁹⁹ Unfortunately, this method is currently only available to a limited number of very specific systems and we still have to rely largely on computational methods to gain insight into the mechanistic detail of most reactions.

In order to determine a transition state computationally, a modelling program could be used to perform a linear step search for the lowest maximum on the energy surface between reactant and product. This is achieved by performing a SCAN calculation (Gaussian 98),

where the transition state is found at the top of the potential curve. A SCAN job can be performed if one knows which bond will break or form during the reaction. SCAN jobs typically increase/decrease a bond length (angle or dihedral angle) in a stepwise manner. At each step the molecule is optimised while only constraining the specified SCAN parameter. A frequency calculation is performed on this structure to verify it as the correct transition state. A frequency calculation determines the number of imaginary frequencies and the normal modes corresponding to the imaginary frequencies. Imaginary frequencies are stored in the output file as negative eigenvalues. A structure which has n imaginary frequencies is an n^{th} order saddle point. A transition state is usually characterised by one imaginary frequency since it is a first order saddle point. The movement of atoms associated with the imaginary frequency should follow the atoms on the reaction co-ordinate between reactant and product.

A less mechanical approach to finding a transition state involves guessing a transition state starting structure and then performing a full, unrestricted transition state optimisation. The output file of the calculation is closely followed to detect any changes that may need to be made to the reaction co-ordinates. This method can be complicated by using constrained reaction co-ordinates, while the rest of the structure is optimised using a transition state optimisation algorithm. This approach is able to find a better starting structure for a full, unconstrained transition state optimisation, yet requires experience and a good knowledge of transition state reaction co-ordinates for a specific system.

6.5 Computational Tools

6.5.1 *Gaussian 98 Program*⁶⁸

This is a program capable of performing *ab initio* Hartree-Fock molecular orbital calculations, dealing mainly with Gaussian-type orbitals based on a LCAO approach. It is capable of computing energies, molecular structures and vibrational frequencies in the gas phase or in solution. The input section of the program requires the molecular charge, multiplicity, the symbols of the constituent atoms and a definition of the molecular structure in terms of Cartesian co-ordinates. This information must be accompanied by an appropriate instruction with regard to basis set and level of theory. All calculations reported here were performed with the Gaussian 98 program (G98).

6.5.2 *Gauss View*

This is a Graphical User Interface (GUI), used in conjunction with G98. It is used to build molecules that are to be submitted to G98 as well as view results from G98. Its animation abilities allow transition states to be viewed that are associated with the negative eigenvalues of the transition state.

6.6 Results for PCU Rearrangement to Trishomocubane

Ab initio (RHF) methods using a 3-21+G basis set were employed to determine the starting structures, transition states and products for the two proposed mechanisms: **Proposed Mechanism 1** (**Fig. 6.4**) and **Proposed Mechanism 2** (**Fig. 6.5**) of the PCU-diol (**Fig. 6.4**, No. 6.1 and **Fig. 6.5**, No. 6.5) to the fluorotrishomocubyl alcohol (**Fig. 6.4**, No. 6.4 and **Fig. 6.5**, No. 6.10). The synthesis²⁶ requires refluxing the diol in hydriodic acid (HI) at 100 °C for two hours to yield the iodotrishomocubyl alcohol. In order to simplify the computational simulation for the assigned basis set, it was decided to employ hydrofluoric acid (HF) instead of HI for the PCU diol rearrangement. The synthetic procedure utilised in **Chapter 2** made use of the PCU mono alcohol and acetic acid.⁴³ A similar mechanism for rearrangement should hold for this system as that described in this chapter for the PCU-diol.

The **Proposed Mechanism 1** (**Fig. 6.4**) for the rearrangement of the PCU-diol to trishomocubane involved the protonation of O₈ on the hydroxyl group of 8-*exo*-hydroxy-11-*exo*-hydroxy PCU. This transition state was omitted from the results since it yielded unrealistic energy values. This was due to the fact that it is a charged molecule and the calculation is performed under gas phase conditions. The transition state (**Fig. 6.4**, No. 6.3) that followed, involved the breaking of the C_{1,7} PCU bond, the formation of the C_{1,8} bond to induce cage rearrangement through an intramolecular S_N2 mechanism, and attachment of a fluorine atom to the C₇ *exo* position to yield 7-*exo*-fluoro-11-*exo*-hydroxy-trishomocubane. This exact procedure was followed for 8-*exo*-hydroxy-11-*endo*-hydroxy PCU to yield 7-*exo*-fluoro-11-*endo*-hydroxy-trishomocubane (**Fig. 6.4**). Note that the chemical procedure yields a racemate. Since enantiomers have the same geometry* in space, as well as identical energies, only one enantiomer was chosen for the computational model. All reported transition states are available on CD attached at the back of this dissertation (**Appendix 4**).

* The Cartesian co-ordinates of enantiomers differ only in the sign (+ versus -).

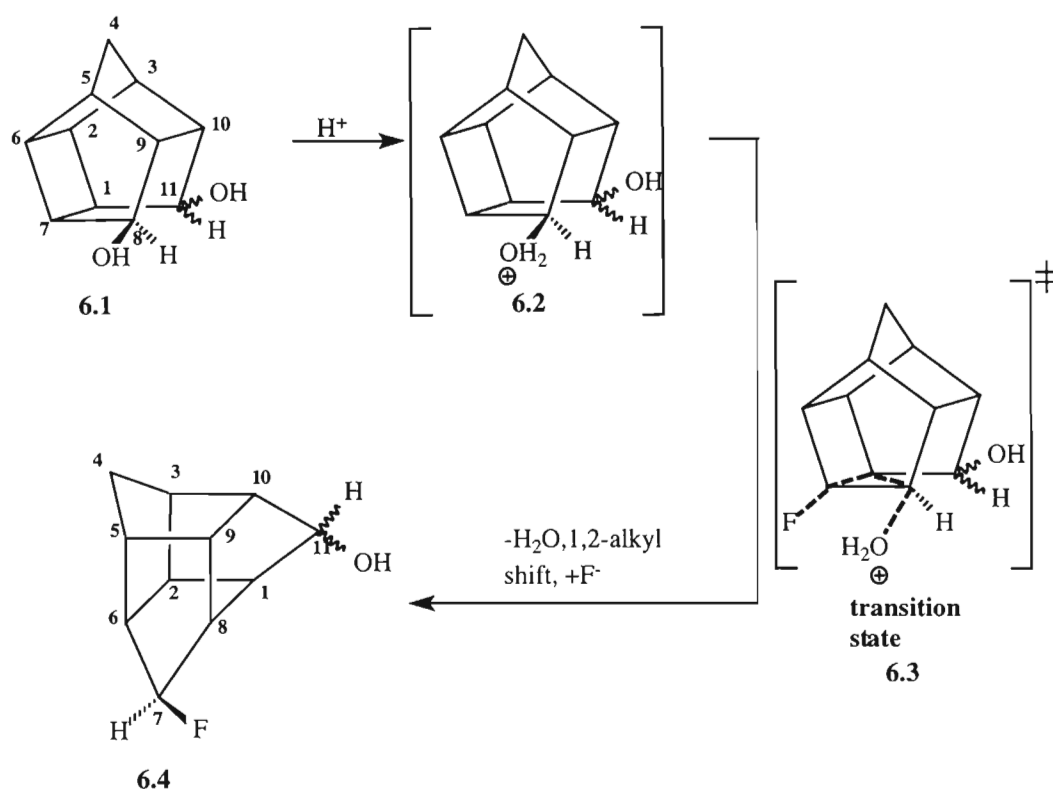


Figure 6.4: Proposed Mechanism 1

The **Proposed Mechanism 2** (Fig. 6.5) involved the addition of fluorine through the $\text{S}_{\text{N}}2$ displacement of the protonated form of the alcohol at C₈ (Fig. 6.5, No. 6.7). This was followed by cage rearrangement as described in **Proposed Mechanism 1** to yield the identical products mentioned in the description of **Proposed Mechanism 1** in Fig. 6.4.

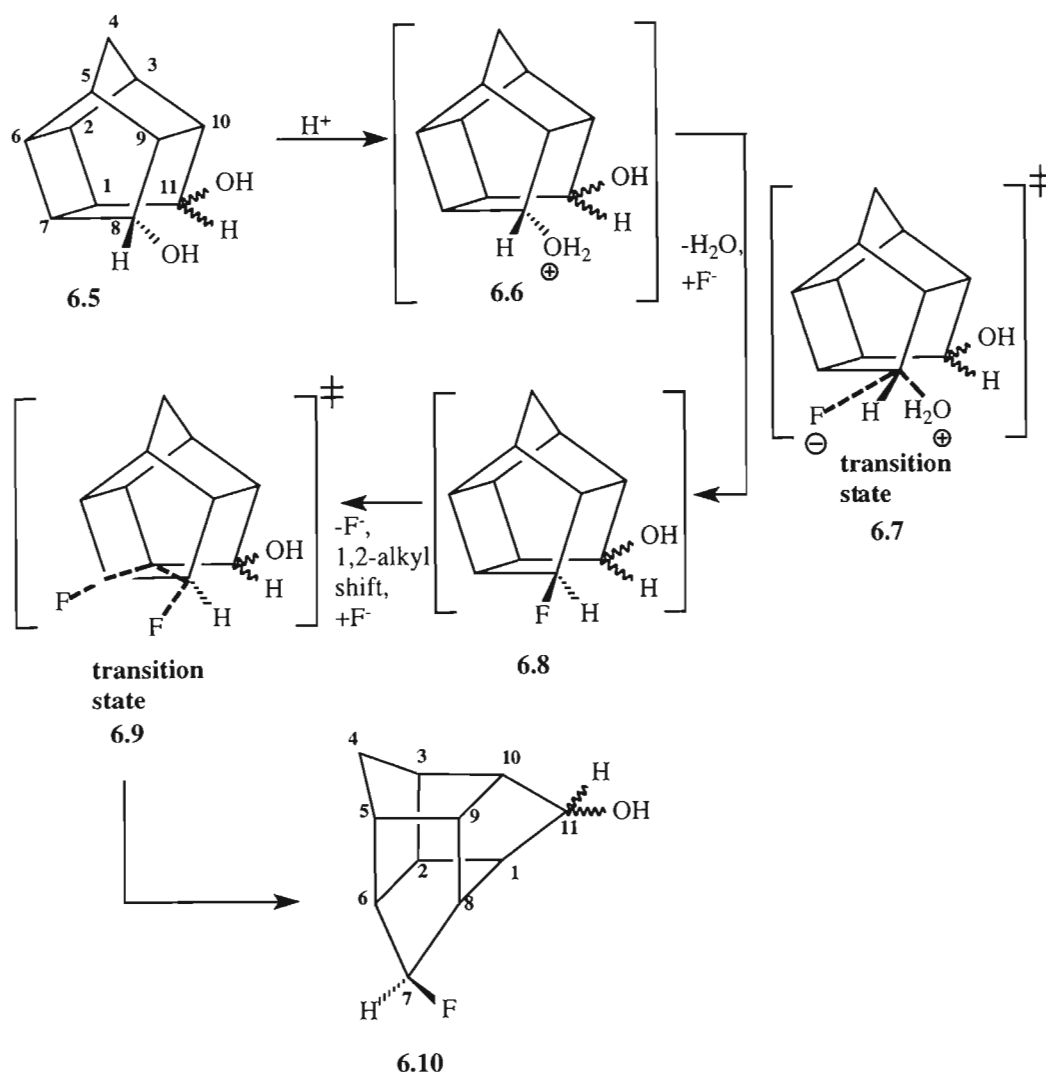


Figure 6.5: Proposed Mechanism 2

The project began by first attempting to find the transition state of the protonated form of trishomocubanol (**Fig. 6.6, No. 6.11**) to get a feel for the mechanism. This was achieved by performing a SCAN calculation: scanning the C_1 and C_8 carbon atoms closer together, since these are the atoms involved in cage rearrangement. A simple plot of energy from each SCANNED step versus the corresponding bond distance revealed a maximum where the C_1 and C_8 atoms were 1.92 \AA apart. The co-ordinates for this structure were saved as an input file for an unconstrained transition state optimisation, followed by a frequency calculation. One negative eigenvalue was obtained and the movement of atoms associated with the negative eigenvalue was evidence of cage rearrangement. These cage co-ordinates provided the skeleton upon which the remaining transition state calculations were performed. Many of the transition states that were subsequently calculated proved to possess very similar cage geometries to the first calculated transition state.

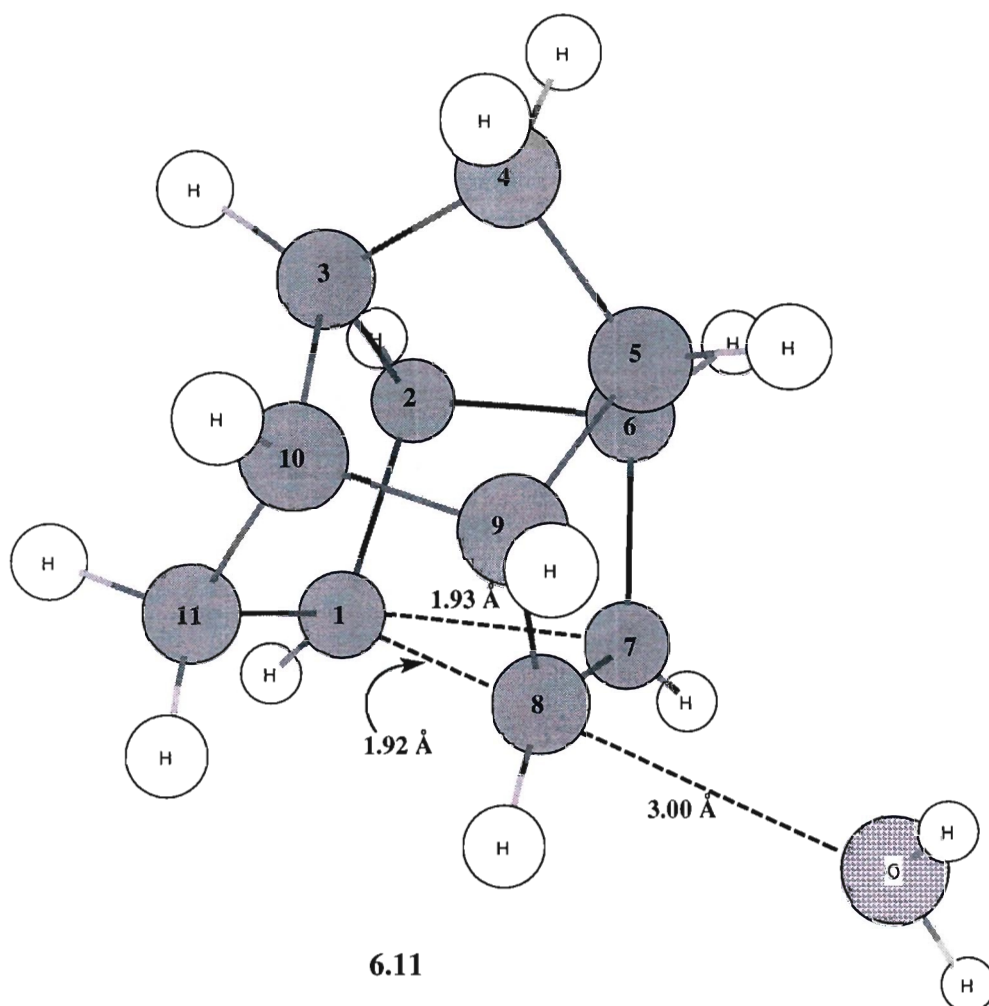


Figure 6.6: Transition state for the protonated trishomocubanol

The transition states for **Proposed Mechanism 1** were achieved by adding the relevant functional groups in the relevant stereochemistry to the input structure of **6.11**, optimising the structure, and lastly, scanning the fluorine atom towards C₇ until a maximum on the potential energy curve was obtained. The structure was subsequently used as an input file and a frequency calculation performed in order to verify the structure as a transition state. The transition state structures for the *exo-endo* protonated diol (**Fig. 6.7. No. 6.12**) and *exo-exo* protonated diol (**Fig. 6.8, No. 6.13**) are shown in **Fig. 6.7** and **Fig. 6.8**. It is clear from **Fig. 6.7** and **Fig. 6.8** that the stereochemistry of the hydroxy group attached to C₁₁ has very little influence on the geometry of the transition states.

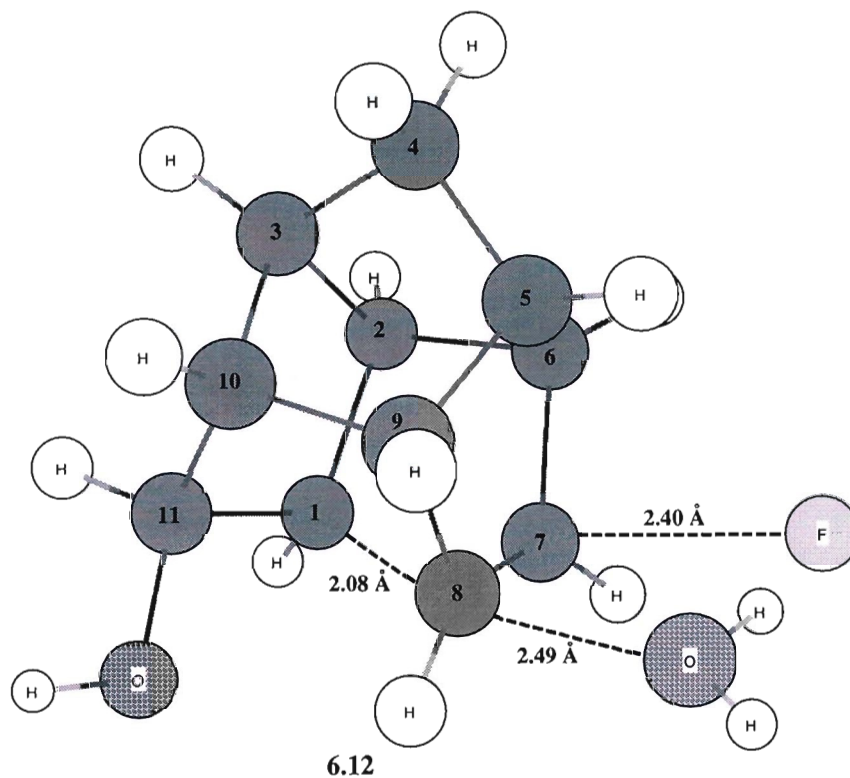


Figure 6.7: Transition state for the *exo-endo* PCU diol

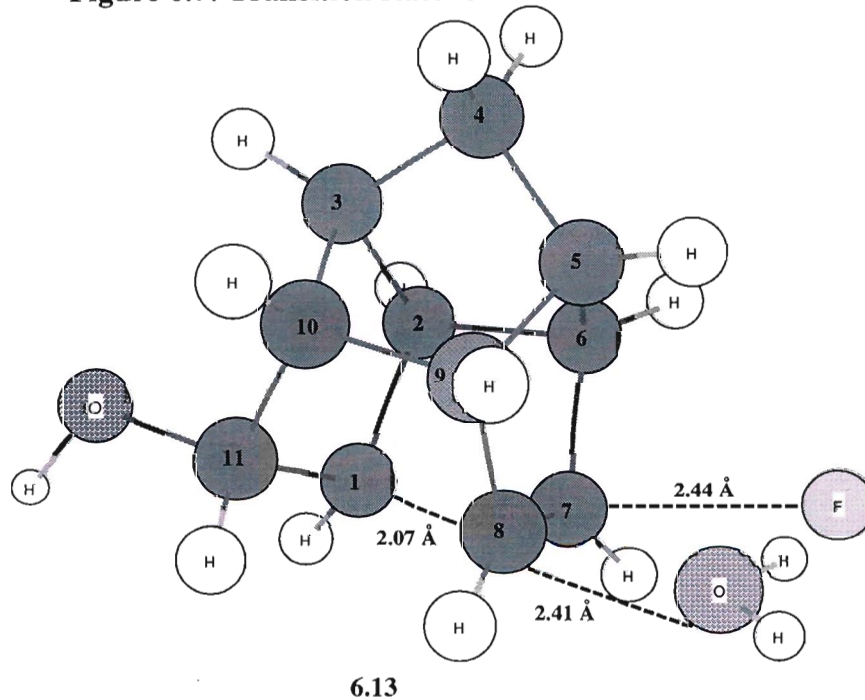


Figure 6.8: Transition state for the *exo-exo* PCU diol

A simple one-dimensional plot of relative energy *versus* reaction pathway (Fig. 6.9) of the two relative pathways revealed a very small difference in transition state energies. The

exo-endo PCU diol proved to be a slightly better starting material for rearrangement as its transition state proved to be $2.6 \text{ kcal mol}^{-1}$ lower than the *exo-exo* diol analogue (**Fig. 6.9**). Since the reaction is performed under reflux conditions, using aqueous HI,⁴³ the difference of $2.6 \text{ kcal mol}^{-1}$ in activation energy would probably not prevent both isomers (**6.12** and **6.13**) from simultaneously forming. Molecules have enough thermal and kinetic energy at room temperature to allow processes requiring $15 \text{ to } 20 \text{ kcal mol}^{-1}$.¹⁰⁰

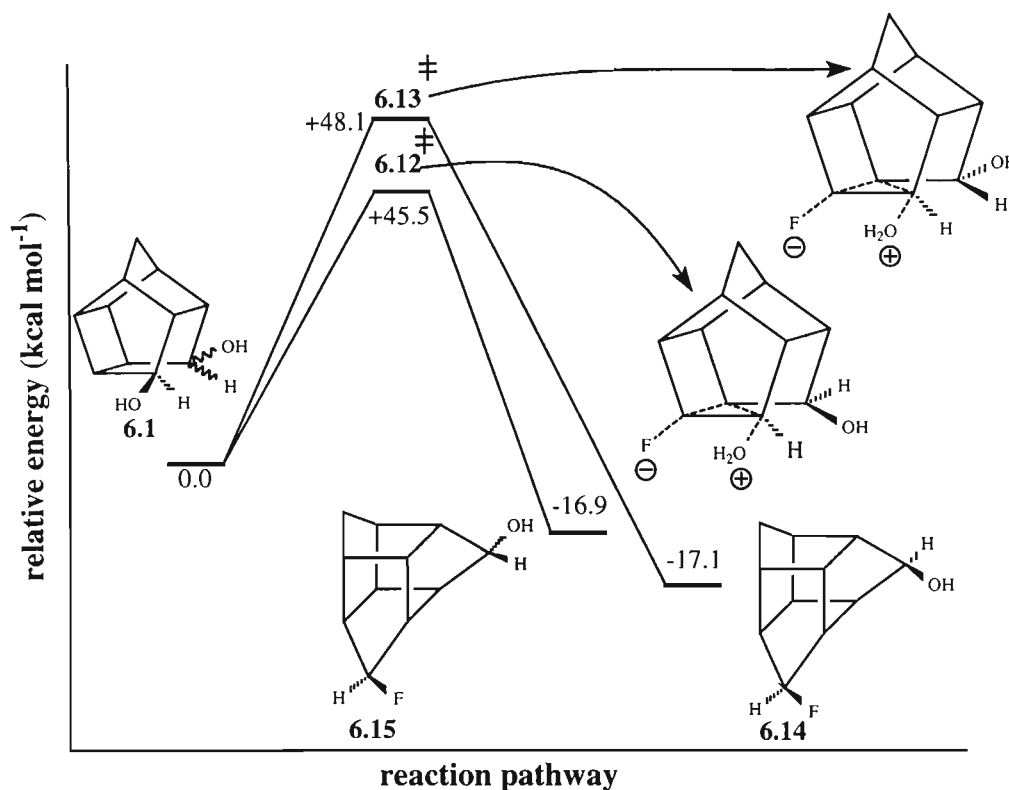
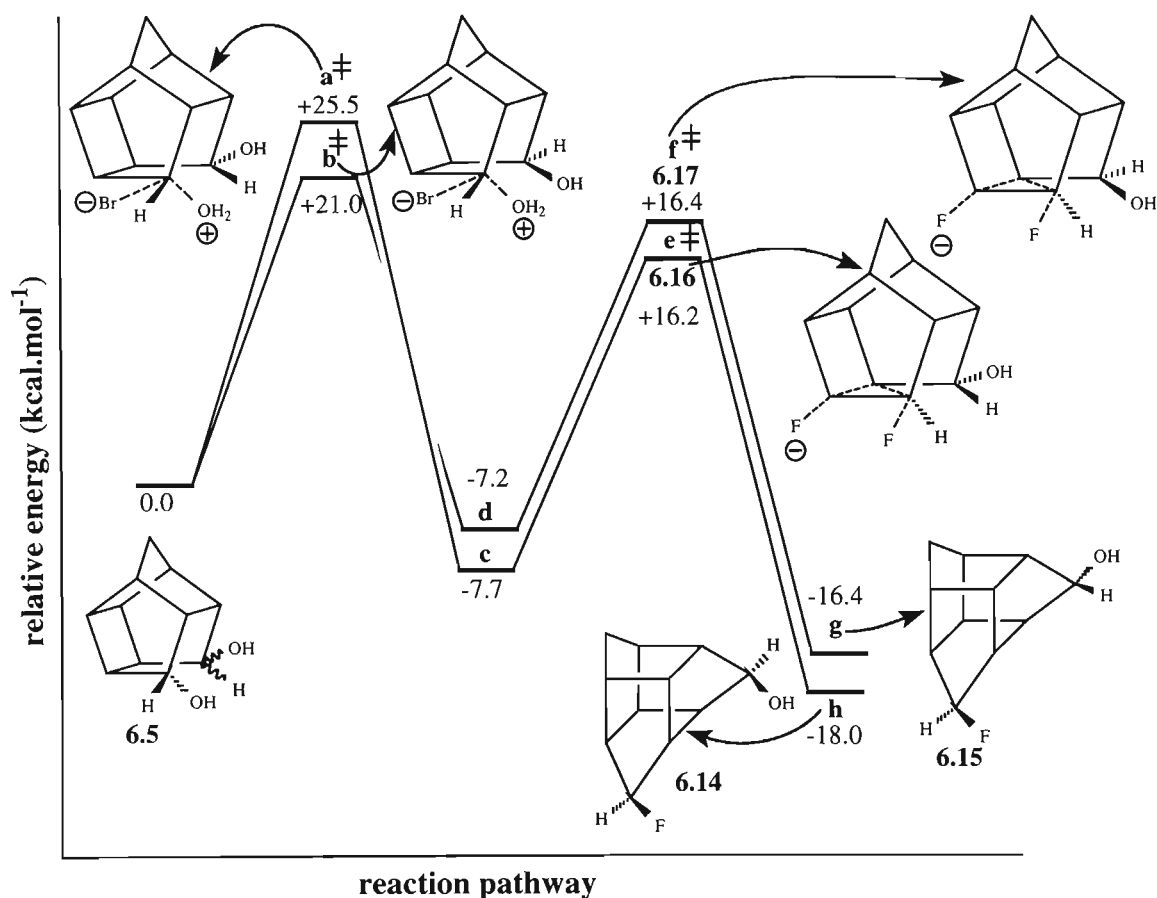


Figure 6.9: Reaction pathway for Proposed Mechanism 1

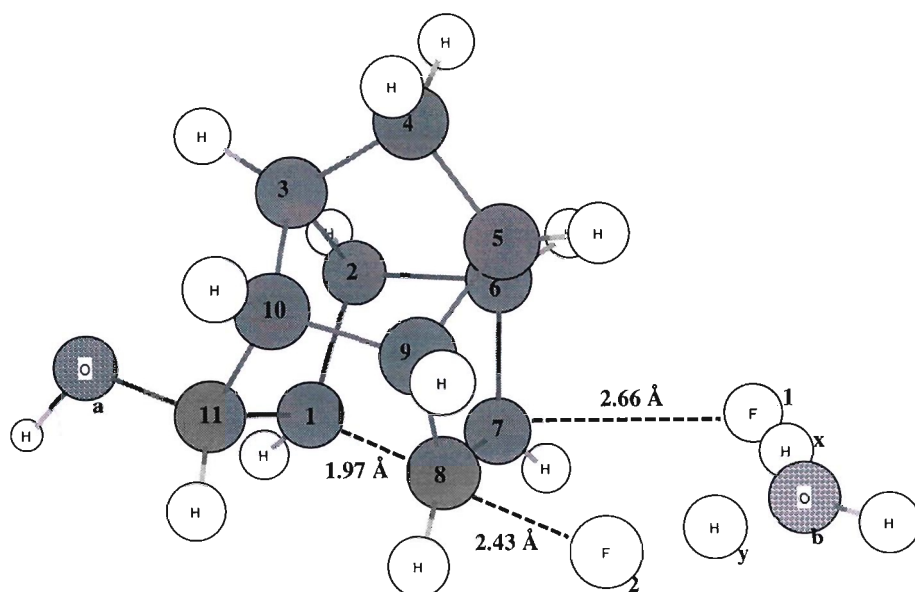
As far as **Proposed Mechanism 2** is concerned, it proved very difficult to find the transition state for the S_N2 displacement of water by a fluorine ion (**Fig. 6.5, No. 6.7**). Note that fluorine was chosen to minimise the computational model with respect to time and resources, as mentioned before. Even a SCAN job failed to isolate the optimum structure for transition state analysis. To overcome this problem with fluorine, the S_N2 displacement of water by a bromine ion was modelled and easily found. Bromine was therefore, used to calculate the energy of the first transition states (**Fig. 6.10, a and b**). This would at least give an idea of the order of energy involved.



- a=endoOH₂-exoOH + Br⁻
 b=endoOH₂-endoOH + Br⁻
 c=exoF-exoOH
 d=exoF-endoOH
 e=exoF-exoOH + HF + H₂O
 f=exoF-endoOH + HF + H₂O
 g=7-*exo*-fluoro-11-*endo*-hydroxy-trishomocubane
 h=7-*exo*-fluoro-11-*exo*-hydroxy-trishomocubane

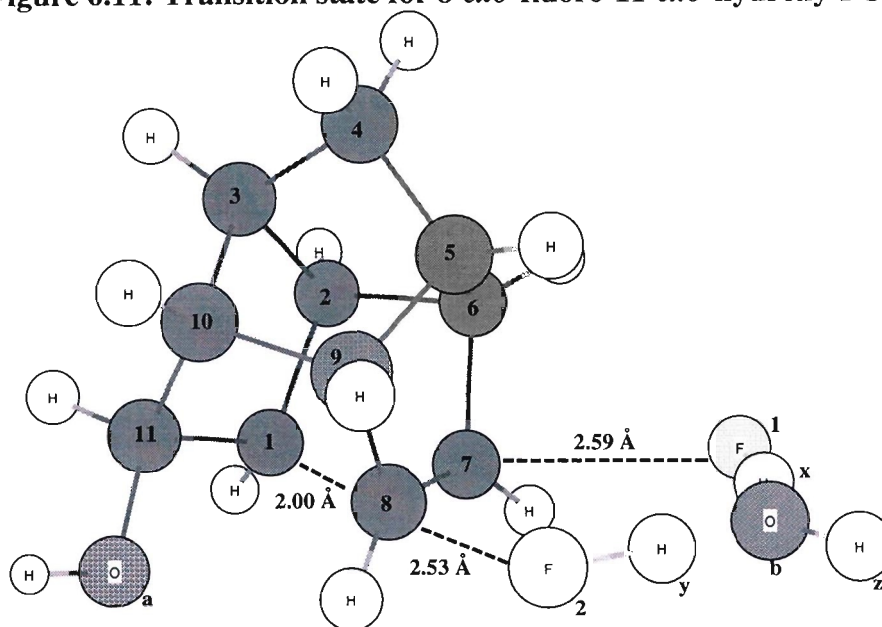
Figure 6.10: Reaction pathway for Proposed Mechanism 2

The transition states for cage rearrangement of the two isomers (**Fig. 6.11** and **Fig. 6.12**) were subsequently calculated by performing frequency calculations on the optimised cage structures of the two isomers of 8-fluoro-11-hydroxy-trishomocubane, hydrofluoric acid and water. The movement of atoms associated with the corresponding negative eigenvalues confirmed cage rearrangement. As the C_{1,8} bond formed there was migration of the F₁ atom to C₇ and H_x to the O_b atom. This was accompanied by migration of the F₂ atom to the H_y atom of the water molecule to ultimately yield 7-hydroxy-11-fluoro-trishomocubane, hydrofluoric acid and water as products (**Fig. 6.11** and **Fig. 6.12**).



6.16

Figure 6.11: Transition state for 8-*exo*-fluoro-11-*exo*-hydroxy-PCU



6.17

Figure 6.12: Transition state for 8-*exo*-fluoro-11-*endo*-hydroxy-PCU

It is again clear from **Fig. 6.11** and **Fig. 6.12** that the stereochemistry of the hydroxy group attached to C₁₁ has very little influence on the geometry of the transition state. A one-dimensional plot of relative energy *versus* reaction pathway (**Fig. 6.10**) of the two relative pathways revealed a very small difference in transition state energies. The *exo-exo* analogue (**Fig. 6.11**, No. 6.16) proved to be a slightly better starting material for

rearrangement as its transition state proved to be 0.2 kcal mol⁻¹ lower than the *exo-endo* analogue (**Fig. 6.12, No. 6.17**).

The rate-determining step in **Proposed Mechanism 2** involves the S_N2 displacement of the protonated *endo*-hydroxy group by the halogen in the *exo* orientation. The rest of the process is downhill.

This computational investigation revealed that the stereochemistry of the hydroxyl group at the C₁₁ position has little effect on the transition state energy during cage rearrangement. It was also evident from the movement of atoms associated with the transition states that the PCU skeleton may rearrange to trishomocubane through an intramolecular S_N2 mechanism.

CHAPTER 7

CONCLUSION

This project had four aims: (a) to improve the synthesis of racemic 4-amino-(D₃)-trishomocubane-4-carboxylic acid (tris-amino acid), (b) to synthesise enantiopure tris-amino acid, (c) to incorporate racemic tris-amino acid into a short peptide, and (d) to perform a computational investigation on the rearrangement of the PCU skeleton to trishomocubane.

Two novel derivatives of tris-hydantoin (**NC1** and **NC2**) were synthesised during an investigation that was aimed at improving the yields of tris-amino acid. The base (LiOH) hydrolysis of **NC2** quantitatively yielded tris-amino acid. This was a significant improvement on previous methods, which required base (NaOH) hydrolysis of tris-hydantoin (60 % yield).

Two novel tris-hydantoin derivatives (**NC3** and **NC4**) were also synthesised in an attempt to produce separable diastereomers. The investigation was aimed at separating the diastereomers, followed by base hydrolysis of the hydantoin ring to yield enantiopure tris-amino acid. The diastereomers, however, were inseparable by column chromatography, so this particular route to produce enantiopure tris-amino acid was abandoned.

A novel ester derivative of tris-amino acid (**NC5**) was synthesised in an attempt to produce enantiopure tris-amino acid by the application of PLE enzyme. The poor solubility of **NC5** in the buffer solution and the bulky nature of the cage may have been the reason for the low yield (10 %) of enantiopure tris-amino acid. Due to the low yield, only NMR analysis was possible. The application of a chiral shift reagent to the tris-amino acid during NMR analysis did not result in any splitting of the NMR peaks. This was a clear indication that enantiopure tris-amino acid was present. Future investigation should attempt to record the optical rotation of the enantiopure tris-amino acid. Alternative enzymes, such as hydantoinase should also be considered for future enzyme work on trishomocubane derivatives.

Previous research managed to incorporate tris-amino acid into a dipeptide, consisting of glycine and tris-amino acid, yet they failed to further extend the peptide or obtain a suitably pure sample for two-dimensional NMR analysis. An attempt was, therefore, made to synthesise a longer peptide and obtain a pure sample for two-dimensional analysis. A tripeptide consisting of alanine, glycine and tris-amino acid was successfully synthesised, yet difficulty was experienced in extending the peptide due to a possible Schiff base interaction between the amino group of tris-amino acid and the carbonyl functionality of glycine. A pure sample of the tripeptide could not be obtained for two-dimensional NMR analysis.

The mechanism of the PCU rearrangement to form trishomocubane is not well understood, therefore, a computational investigation of this was pursued. The investigation revealed that the stereochemistry of the hydroxyl group at the C₁₁ position of the PCU-diol had little effect on the transition state energies of the various isomers. The movement of atoms associated with the transition states also indicated that the rearrangement of PCU to trishomocubane may proceed through an intramolecular S_N2 mechanism.

CHAPTER 8

EXPERIMENTAL

Melting points were recorded using a Bombay 400 013 instrument from Shital Scientific Industries. All melting points are uncorrected. Infrared spectra were obtained using a Nicolet Impact 410 spectrometer. The one-dimensional NMR spectra were recorded on a Varian Gemini 300 MHz spectrometer, while the two-dimensional NMR spectra were recorded on a Varian Unity Inova 400 MHz spectrometer. The fast atom bombardment (FAB) mass spectra were obtained from a Micromass VG70-70E mass spectrometer, equipped with an In tech FAB gun. The samples were bombarded with xenon atoms (1 mA at 8 keV), with *m*-nitrobenzyl alcohol as the matrix. Electron impact (EI) mass spectra (70eV) were obtained from a Micromass Autospec-TOF mass spectrometer. Elemental analyses were obtained from a Leco CHNS 932 instrument. HPLC analysis was performed using a Waters 600 solvent delivery system, equipped with a Perkin Elmer series 700 autosampler, a Waters 996 photodiode array detector and Millenium software. A Nucleosil 100 C₁₈ column (5 µm particle size, 250 mm x 4.6mm i.d.) was also used.

Synthesis of 5,8-methano-4a,5,8,8a-tetrahydro-1,4-naphthoquinone (2.17, adduct)^{37,40,101}

p-Benzoquinone was dissolved in dry toluene (4.00 l) and placed in an ice/salt bath within a dark fumehood. Cold, freshly cracked cyclopentadiene (132.00 ml, 1.96 mols) was added over two hours *via* a dropping funnel. The slow addition and cool temperatures allowed a successful Diels-Alder reaction, without polymerisation of the cyclopentadiene. The reaction was left to stir overnight. The solution was removed from the ice/salt bath, wrapped in tin foil and left in the dark fumehood to allow complete evaporation of the toluene to leave yellow crystals of adduct (229.68g, 74 %). m.p. 77 °C. IR (KBr) 3315 (w), 1667 (vs, C=O), 1596 (s, conjugated C=C), 1293 (m), 1280 (m), 1053cm⁻¹ (m). ¹H NMR [CDCl₃, 300 MHz]: δ_H 1.50 (m, 2H, methylene bridge protons), 3.20 (m, 2H, H_{4a}, H_{8a}), 3.50 (m, 2H, bridgehead protons), 6.02 (m, 2H, ethylene bridge protons), 6.50 (s, 2H, enone vinyl protons). ¹³C NMR [CDCl₃, 300 MHz]: δ_C 48.35 (d), 48.72 (t), 48.78 (d), 135.30 (d), 142.06 (d), 199.45 (s). M.S. was identical to an authentic sample.

Synthesis of pentacyclo[5.4.0.0^{2,6}.0^{3,10}.0^{5,9}]undecane-8-11-dione (2.19)^{37,102}

The synthesised adduct was added to a volumetric flask (5.00 l) and dissolved in 10 % (v/v) acetone in hexane solution (5.00 l). The volumetric flask was exposed to direct sunlight until a colourless solution was obtained. The solvent was evaporated *in vacuo* to give a white, microcrystalline solid (183.74g, 80 %). m.p. 240 °C. IR (KBr) ν_{max} 2974, 1709 cm⁻¹ (vs, C=O). ¹H NMR [CDCl₃, 300 MHz]: δ_H 1.83-2.03 (AB quartet, 2H, methylene bridge protons), 2.66-3.14 (broad absorption, 8H, methine protons). ¹³C NMR [CDCl₃, 300 MHz]:

δ_C 38.74 (C₂, C₆), 40.49 (C₄), 43.79 (C₃, C₅), 44.62 (C₉, C₁₀), 54.72 (C₁, C₇), 212.21 (C₈, C₁₁). M.S. M.S. was identical to an authentic sample.

Synthesis of pentacyclo[5.4.0.0^{2,6}.0^{3,10}.0^{5,9}]undecane-8-11-dione-mono-ethylene ketal (2.31)^{42,43}

A mixture of the diketone (183.00 g, 1.05 mol), ethylene glycol (81.20 ml, 1.45 mol), *p*-toluenesulfonic acid (6.11 g, 3.21x10⁻² mol) and A4 molecular sieves (2 g) in dry toluene (800 ml) was refluxed with stirring in a Dean and Stark trap for four days. The reaction mixture was left to cool and poured slowly into ice-cold 10 % (v/v) aqueous sodium carbonate (1.00 l). This was extracted with dichloromethane (3 x 500 ml). The combined organic extracts were dried over anhydrous sodium sulphate. The mixture was filtered and the solvent evaporated *in vacuo*. The resulting brown residue was recrystallised from hexane to give the mono-ketal as white crystals (170.04 g, 74 %). IR (KBr) ν_{\max} 1747 cm⁻¹ (vs, C=O). ¹H NMR [CDCl₃, 300 MHz]: δ_H 1.51-1.84 (2H, methylene bridge protons), 2.35-2.92 (8H, methine protons), 3.78-3.91 (4H, ketal protons). ¹³C NMR [CDCl₃, 300 MHz]: δ_C 36.35 (d), 38.74 (t), 41.33-53.02 (d), 64.52-65.71 (t, ketal carbons), 113.92 (s), 215.14 (s). M.S. was identical to an authentic sample.

Synthesis of 11-hydroxypentacyclo[5.4.0.0^{2,6}.0^{3,10}.0^{5,9}]undecane-8-one-ethylene ketal (2.34)^{42,43,103}

The mono-ketal (10.00 g, 4.59x10⁻² mol) was dissolved in ethanol (100 ml) and placed in an ice-bath to cool. An ethanolic solution of sodium borohydride (3.50 g in 50 ml) was added, with stirring, over a 10 minute period. The mixture was left to stir for two hours in the ice-bath, and an additional two hours at room temperature. Some sample (5 ml) was withdrawn to confirm complete reduction of the keto functional group. The solvent of this sample was removed *in vacuo*, and the residue extracted using dichloromethane (50 ml). The organic extracts were combined, thereafter, the solvent was removed *in vacuo* to leave the hydroxy-ketal as a homogenous oil (7.70 g, 77 %). m.p. 250 °C. IR (KBr) ν_{\max} 3452 (s), 2956 (s), 1114cm⁻¹ (s). ¹H NMR [CDCl₃, 300 MHz]: δ_H 1.04 (H_a, J_{AB} 8.91 Hz), 1.54 (H_s, J_{AB} 8.79 Hz), 2.10-2.60 (m, 8H, methine protons), 3.49-3.91 (m, 5H, 4 protons of ketal, OH), 5.25 [1H, t, *J* ~5 Hz, HC₁-H(*exo*)C₁₁-HC₁₀]. ¹³C NMR [CDCl₃, 300 MHz]: δ_C 35.01 (t), 38.88 (d), 39.07(d), 39.27 (d), 39.91 (d), 43.62 (d), 44.65 (d), 46.77 (d), 47.24 (d), 63.00 (t), 65.54 (t), 72.36 (d), 115.82 (s). M.S. was identical to an authentic sample.

Synthesis of 11-hydroxypentacyclo[5.4.0.0^{2,6}.0^{3,10}.0^{5,9}]undecane-8-one (2.40)⁴³

The hydroxy-ketal was placed in an ice-bath to cool at which stage 10 % (v/v) hydrochloric acid (200 ml) was cautiously added. This was left, with stirring, to warm to room temperature for 18 hours. The mixture was extracted with dichloromethane (150 ml) to yield the hydroxy-ketone (4.84 g, 60 %). IR (KBr) ν_{\max} 3407 (m, OH), 2975, 1738 cm⁻¹ (s, vs, C=O). ¹H NMR [CDCl₃, 300 MHz]: δ_H 1.47 (1/2H, d, J_{4a,4s} 10.56 Hz, H_{4a}), 1.51 (1/2H, d, J_{4a,4s} 10.56 Hz, H_{4a}), 1.86 (1H, d, J_{4a,4s} 11.00 Hz, H_{4s}), 2.37-2.97 (8H, H₁, H₂, H₃, H₅, H₆,

H₇, H₉, H₁₀), 4.04 (1/2H, t, J 4 Hz, H₈), 4.35, (1H, t, J 5 Hz, D₂O exchangeable OH), 4.56 (1H, t, J 5 Hz, H₈). ¹³C NMR [CDCl₃]: 36.84, 38.32, 40.79, 41.59 (2C), 41.75, 41.90, 42.47, 42.76, 43.94, 44.15, 44.25, 45.00, 45.12, 50.02, 53.56, 54.45, 54.56, 75.26, 81.40, 122.01, (O-C-O) and 218 (C=O). M.S. was identical to an authentic sample.

Synthesis of *endo*-pentacyclo[5.4.0.0^{2,6}.0^{3,10}.0^{5,9}]undecane-8-ol (2.46)^{30,43,104}

A mixture of the hydroxy-ketone (15.00 g, 8.52x10⁻² mol) and hydrazine hydrate (23.10 ml, 0.74 mol) in diethylene glycol (200 ml) was refluxed, with stirring, at 120 °C for two hours. The mixture was allowed to cool to 80 °C at which stage excess KOH (12.00 g, 0.21 mol) was added. Excess hydrazine hydrate and water was distilled from the mixture until the temperature reached 185 °C, thereafter, refluxed for a further three hours at 185 °C. The mixture was cooled, diluted with water (300 ml) and extracted with dichloromethane (3x100 ml). The combined organic phases were removed *in vacuo*. The yellow residue was distilled by steam distillation to yield the alcohol as a colourless oil with a camphor-like odour (8.02 g, 58.10 %). m.p. 231 °C. IR (KBr) ν_{max} 3403 (m, OH), 2952 cm⁻¹. ¹H NMR [CDCl₃, 300 MHz]: δ_H 1.05 (1H, dd, J 4Hz, H_{11x}), 1.14 and 1.67 (2H, AB system, J_{4a,4s} 10 Hz, H_{4a}, H_{4s}), 1.58 (1H, s, D₂O exchangeable OH), 2.26 (1H, d, J_{11n,11x} 12 Hz, H_{11n}, obscured by env.), 2.18-2.73 (8H, env., H₁, H₂, H₃, H₅, H₆, H₇, H₉, H₁₀) and 3.91 (1H, m, H₈). ¹³C NMR [CDCl₃]: δ_C 28.78 (C₁₁), 35.16 (C₄), 35.92 (C₁), 38.82 (C₇), 39.91 (C₆), 42.01 (C₂,C₁₀), 43.11 (C₅), 45.73 (C₉), 47.02 (C₃) and 74.36 (C₈). M.S. was identical to an authentic sample.

Synthesis of pentacyclo[6.3.0.0^{2,6}.0^{3,10}.0^{5,9}]undecane-4-ol (2.53)^{30,43}

Pentacyclo[5.4.0.0^{2,6}.0^{3,10}.0^{5,9}]undecane-8-ol (20.00 g, 0.12 mol) was dissolved in a solution of glacial acetic acid (300 ml) and concentrated sulphuric acid (7.00 g). The solution was refluxed, with stirring, for 12 hours. The resulting black solution was cooled, diluted with deionised water (1200 ml) and extracted with dichloromethane (500 ml). The organic extract was washed successively with deionised water, a saturated solution of sodium hydrogen carbonate and water. Activated charcoal was subsequently added, and the solution heated for a few minutes. This was filtered, while hot, through celite, which yielded an orange solution. The solvent was removed *in vacuo*. The resulting orange oil was added to a stirring solution of methanol (330 ml) and potassium carbonate (18.00 g), and left overnight. The reaction mixture was concentrated *in vacuo*. Deionised water was added and extracted with dichloromethane. Removal of the organic solvent yielded pentacyclo[6.3.0.0^{2,6}.0^{3,10}.0^{5,9}]undecane-4-ol as a white solid (14.00 g, 72 %). m.p. 165 °C. IR (KBr) ν_{max} 3412, 2951, 2859cm⁻¹. ¹H NMR [CDCl₃, 300 MHz]: δ_H 1.31 (2H, s, 2 x H₁₁), 1.44 and 1.48 (2H, AB system, J 10.44 Hz, 2 x H₇), 1.54 (1H, s, D₂O exchangeable, OH), 1.91-2.11 (7H, env, H₁, H₂, H₃, H₅, H₈, H₉, H₁₀), 2.56 (1H, s, H₆) and 4.15 (1H, s, H₄). ¹³C NMR [CDCl₃, 300 MHz]: δ_C 33.00 (C₇), 33.68 (C₁₁), 40.67 (C₂), 41.23 (C₉), 43.14 (C₁₀), 44.21 (C₆), 47.14 (C₈), 47.45 (C₁), 52.22 (C₅), 53.49 (C₃), 77.45 (C₄). M.S. was identical to an authentic sample.

Synthesis of pentacyclo[6.3.0.0^{2,6}.0^{3,10}.0^{5,9}]undecanone (2.55)^{30,43,105}

Chromium trioxide (32.00 g, 0.32 mol) was prepared in deionised water (30 ml) and added to acetic acid (320 ml). The alcohol (20.00 g, 0.12 mol) was dissolved in acetic acid (100 ml) and added drop-wise to the prepared mixture. The reaction was refluxed at 90 °C overnight. The successful oxidation (Jones oxidation) of the alcohol was evident through reduction of Cr⁶⁺ (dark red) to Cr³⁺ (green). The reaction mixture was cooled, diluted with deionised water (1000 ml) and extracted with dichloromethane (800 ml). The organic extract was washed successively with water (2 x 500 ml), a saturated bicarbonate solution (2 x 500 ml) and water (500 ml). The organic solution was dried, using anhydrous sodium sulphate. The mixture was filtered, and the solvent removed *in vacuo* to yield pentacyclo[6.3.0.0^{2,6}.0^{3,10}.0^{5,9}]undecanone (15.55 g, 81 %). m.p. 165 °C. IR (KBr) ν_{\max} 3433, 2949, 1770, 1750 cm⁻¹. ¹H NMR [CDCl₃, 300 MHz]: δ_{H} 1.40-1.75 (H_{7a}, H_{7s}, H_{11a}, H_{11s}), 2.35-2.43 (8H, env., H₁, H₂, H₃, H₅, H₆, H₈, H₉, H₁₀). ¹³C NMR [CDCl₃, 300 MHz]: δ_{C} 35.52 (C₇, C₁₁), 40.94 (C₂, C₉), 41.09 (C₆, C₁₀), 47.69 (C₁, C₈), 50.20 (C₃, C₅), 217.45 (C₄). M.S. was identical to an authentic sample.

Synthesis of tris-hydantoin (2.12)²³

A mixture of the mono-ketone (1.00 g, 6.25x10⁻³ mol), NaCN (1.00 g, 2.04x10⁻² mol), (NH₄)₂CO₃ (2.00 g, 2.08x10⁻² mol), ethanol (10 ml) and NH₄OH (15 ml) were sealed in a glass pressure vessel. This was sealed in a metal pressure vessel, containing water. The reaction was placed in an oil bath and heated at 60 °C for two hours, 100 °C for two hours and 120 °C overnight. The cooled reaction was diluted with deionised water (100 ml) and extracted with ethyl acetate (150 ml). The solvent was removed *in vacuo* to yield the crude hydantoin. The product was washed successively with acetone and diethyl ether, thereafter, recrystallised with tetrahydrofuran to yield pure hydantoin as a white solid (1.32 g, 92 %). m.p. 325 °C. IR (KBr) ν_{\max} 3314, 2944, 1766, 1720, 1403 cm⁻¹. ¹H NMR [CDCl₃, 400 MHz]: δ_{H} 1.19-1.22 (1H, H_{11s}, *J* 9.89 Hz), 1.24-1.27 (1H, H_{7s}, *J* 10.26 Hz), 1.36-1.39 (2H, H_{7a}, H_{11a}, *J* 10.26 Hz), 1.91 (H₅), 1.97 (H₃), 2.10 (H₁, H₈), 2.13 (H₉), 2.18 (H₂), 2.45 (H₆), 2.84 (H₁₀), 7.88 (D₂O exchangeable H₁), 10.54 (D₂O exchangeable H₃). ¹³C NMR [CDCl₃, 400 MHz]: δ_{C} 32.95 (C₇), 33.49 (C₁₁), 42.20 (C₉), 42.75 (C₁₀), 43.69 (C₂), 45.66 (C₆), 46.66 (C₁), 47.10 (C₈), 54.82 (C₅), 55.67 (C₃), 73.48 (C₄), 157.05 (C₂) and 177.50 (C₄). M.S-TOF [M+H]⁺ 231 m/z.

Synthesis of 4-amino-(D₃)-trishomocubane-4-carboxylic acid (tris-amino acid, 2.13)²³

The hydantoin (1.00 g, 4.35x10⁻³ mol) was dissolved in a 1.25 M NaOH solution and placed in a metal pressure vessel. The vessel was sealed, placed in an oil bath and heated with stirring at 170 °C overnight. The cooled reaction was diluted with deionised water (100 ml) and placed on a hotplate to reduce the volume to 80 ml. The reaction was subsequently adjusted to pH 6.5, which induced precipitation of the amino acid. The volume of the reaction was again reduced to 50 ml. The amino acid was recovered through

filtration and successively washed with acetone and diethyl ether to yield the amino acid as a white solid (0.47 g, 52 %). IR (KBr) ν_{\max} 3199, 1590, 1496 cm^{-1} . The amino acid was characterised as the Fmoc derivative (**2.65**).

Improved yield of 4-amino-(D₃)-trishomocubane-4-carboxylic acid (tris-amino acid, **2.13**)⁴⁸

Novel Compound 2 (0.2 g, 4.65×10^{-4} mol) was added to an aqueous lithium hydroxide (8 mol equivalents) solution and left to stir for 24 hours. The solution was adjusted to pH 6.5 using concentrated HCl. This resulted in the tris-amino acid precipitating out of solution. The mixture was filtered to isolate the tris-amino acid, which was subsequently washed with acetone and diethyl ether. This resulted in pure tris-amino acid (0.1 g, 4.87×10^{-4} mol). The infrared spectrum was identical to an authentic sample. The amino acid was characterised as the Fmoc derivative (**2.65**).

Synthesis of Fmoc-tris-amino acid (**2.65**)²³

To an ice cooled solution of amino acid (0.10 g, 4.88×10^{-4} mol) in 1,4-dioxane (7.50 ml) and 10 % (v/v) Na_2CO_3 (20 ml) was added, with stirring, a solution of 9-fluorenylmethyl chloroformate (Fmoc, 0.15 g, 5.80×10^{-4} mol) in 1,4-dioxane (5.00 ml). This was left to stir in the ice-bath for four hours and at room temperature for a further eight hours. The solution was diluted with deionised water (50 ml) and extracted with diethyl ether (100 ml). The aqueous layer was cooled to 10 °C in an ice-bath and acidified to pH 2 with concentrated HCl. The solution was subsequently extracted with ethyl acetate (150 ml). The organic solvent was evaporated *in vacuo* to give the crude Fmoc derivative. Purification was achieved through silica gel column chromatography (dichloromethane) (0.16 g, 75 %). m.p. 213 °C. IR (KBr) ν_{\max} 3360, 2952, 1748, 1702, 1294 cm^{-1} . ^1H NMR [DMSO, 400 MHz]: δ_{H} 1.15-1.50 (m, 4H), 1.90-2.30 (m, 7H), 2.47 (m, 1H), 3.35 (s, 1H, D_2O exchangeable), 4.10-4.43 (m, 3H), 7.22-8.08 (m, 8H), 12.17 (s, 1H, D_2O exchangeable). ^{13}C NMR [DMSO, 400 MHz]: δ_{C} 31.70 (t), 32.70 (t), 42.50 (d), 42.60 (d), 42.80 (d), 43.80 (d), 46.10 (d), 46.40 (d), 46.70 (d), 52.80 (d), 53.30 (d), 65.10 (s), 68.60 (t), 120.00 (d), 125.10 (d), 125.20 (d), 126.90 (d), 127.90 (d), 140.60 (s), 140.70 (s), 143.70 (s), 143.80 (s), 155.30 (s), 174.00 (s). M.S. was identical to an authentic sample.

Synthesis of Novel Compound 1 (NC1, **2.66**)⁴⁸

A solution of tris-hydantoin (0.50 g, 2.17×10^{-3} mol), di-*tert*-butyl-dicarbonate (0.71 g, 3.26×10^{-3} mol), 4-dimethyl-aminopyridine (DMAP) (3.00 mg, 2.17×10^{-5} mol) in dry THF (50 ml) was left to stir under nitrogen gas for 24 hours. The solution was concentrated *in vacuo* to yield the crude product. Purification was achieved through silica gel column chromatography (dichloromethane) to yield the product as a white powder (0.53 g, 74 %). m.p. 206 °C. IR (KBr) ν_{\max} 3220, 1770, 1712 cm^{-1} . ^1H NMR [CDCl_3 , 400 MHz]: δ_{H} 1.26-1.29 (1H, $\text{H}_{11\text{s}}$, J 10.44 Hz), 1.34-1.37 (1H, $\text{H}_{7\text{s}}$, J 10.44 Hz), 1.46-1.49 (2H, $\text{H}_{7\text{a}}$, $\text{H}_{11\text{a}}$, J 10.44 Hz), 1.56 (9H, H_8), 2.08 (H_5), 2.09 (H_3), 2.18 (H_1), 2.19 (H_8), 2.27 (H_2), 2.33 (H_9),

2.39 (H₆), 2.95 (H₁₀), 6.40 (H₁). ¹³C NMR [CDCl₃, 400 MHz]: δ_C 27.82 (C₈), 32.80 (C₇), 33.16 (C₁₁), 41.98 (C₁₀), 42.78 (C₂), 43.20 (C₉), 45.32 (C₆), 46.69 (C₁), 46.76 (C₈), 55.12 (C₅), 56.08 (C₃), 71.78 (C₄), 85.31 (C₇), 146.29 (C₂), 152.20 (C₅), 171.80 (C₄). M.S. [M+H]⁺ 331 m/z. Elemental analysis. Experimental: C, 65.54, H, 6.41, N 8.27 %. Calculated: C, 65.45, H, 6.67, N, 8.48 %.

Synthesis of Novel Compound 2 (NC2, 2.67)⁵¹

A solution of tris-hydantoin (0.50 g, 2.17x10⁻³ mol), di-*tert*-butyl-dicarbonate (1.19 g, 5.43x10⁻³ mol), 4-dimethyl-aminopyridine (DMAP) (1.3 mg, 1.09x10⁻⁴ mol) and triethylamine (0.35 ml, 2.60x10⁻³ mol) in dry THF (50 ml) was left to stir under nitrogen gas for 24 hours. The solution was concentrated *in vacuo* to yield the crude product. Purification was achieved through silica gel column chromatography (dichloromethane) to yield the product as a white powder (0.77 g, 98 %). m.p. 227 °C. IR (KBr) ν_{max} 2965, 1771 cm⁻¹. ¹H NMR [CDCl₃, 400 MHz]: δ_H 1.27-1.30 (H_{11s}, *J* 11.17 Hz), 1.30-1.33 (H_{7s}, *J* 11.17 Hz), 1.44-1.46 (H_{11a}, *J* 7.69 Hz), 1.46-1.48 (H_{7a}, *J* 8.06 Hz), 1.53 (9H, H₁₂), 1.55 (9H, H₈), 2.09-2.13 (H₁), 2.14-2.15 (H₈), 2.16-2.17 (H₅), 2.28 (H₆), 2.29 (H₉), 2.38-2.40 (H₂), 2.52-2.53 (H₃), 3.12 (H₁₀). ¹³C NMR [CDCl₃, 400 MHz]: δ_C 27.52 (C₁₂), 27.72 (C₈), 32.94 (C₁₁), 33.02 (C₇), 41.94 (C₉), 42.91 (C₁₀), 45.27 (C₆), 45.93 (C₁), 46.11 (C₈), 46.23 (C₂), 54.03 (C₃), 58.15 (C₅), 76.55 (C₄), 84.95 (C₁₁), 86.11 (C₇), 145.74 (C₂), 149.67 (C₅), 149.03 (C₉), 169.59 (C₄). M.S. [M+H]⁺ 431 m/z. Elemental analysis. Experimental: C, 63.91, H, 6.70, N, 6.39 %. Calculated: C, 64.19, H, 6.98, N, 6.51 %.

Synthesis of Novel Compound 3 (NC3, 3.14)^{54,56}

A solution of isopropanol (0.27 ml, 3.56x10⁻³ mol) and triphosgene (0.35 g, 1.19x10⁻³ mol) in 50 ml of dry THF was stirred under nitrogen gas in an ice-bath. Once the reaction mixture had reached 0 °C, dry pyridine (0.58 ml, 7.12x10⁻³ mol) was added *via* cannular over a 30 s period. A white precipitate of pyridinium hydrochloride was immediately visible. The reaction was allowed to slowly warm to room temperature and left to stir overnight. The solution was filtered directly into an ice-cooled, stirred solution of tris-hydantoin (0.46 g, 2.00x10⁻³ mol) and dry THF (50 ml). This was performed under nitrogen gas. This resulted in a pale yellow solution, which was allowed to warm to room temperature over 24 hours. The solution was evaporated to dryness *in vacuo* and the resulting yellow precipitate was dissolved in dichloromethane (100 ml) and extracted with deionised water (100 ml). The organic layer was subsequently dried over anhydrous sodium sulphate and filtered. Evaporation of the organic solvent resulted in the crude product, which was purified by silica gel column chromatography (dichloromethane). This resulted in white crystals of product (0.44 g, 70 %). m.p. 175 °C. IR (KBr) ν_{max} 3304, 1822, 1771 cm⁻¹. ¹H NMR [CDCl₃, 400 MHz]: δ_H 1.25-1.28 (H_{11s}, *J* 10.44 Hz), 1.35-1.36 (6H, H₈), 1.45-1.48 (2H, H_{7a} and H_{11a}, *J* 10.44 Hz), 2.07-2.08 (H₅), 2.08-2.10 (H₃), 2.17-2.18 (2H, H₁ and H₈), 2.27-2.30 (H₉), 2.30-2.33 (H₂), 2.44 (H₆), 2.94 (H₁₀), 5.15 (1H, H₇), 6.98 (H₁). ¹³C NMR [CDCl₃, 400 MHz]: δ_C 21.54, 21.56 (C₉), 32.78 (C₁₁), 33.13 (C₇), 41.96 (C₉), 42.75 (C₈), 43.22 (C₂), 45.30 (C₆), 46.71 (C₁), 55.22 (C₅), 56.13 (C₃), 71.92

(C₄), 72.69 (C₈), 147.53 (C₅), 152.46 (C₄), 171.44 (C₂). M.S. [M+H]⁺ 317 m/z. Elemental analysis. Experimental: C, 64.22, H, 6.30, N, 8.72 %. Calculated: C, 64.56, H, 6.33, N, 8.86 %.

Synthesis of Novel Compound 4 (NC4, 3.15)^{54,56}

A solution of R-(-)-2-butanol (0.32 ml, 3.50x10⁻³ mol) and triphosgene (0.35g, 1.17x10⁻³ mol) in 50 ml of dry THF was stirred under nitrogen gas in an ice-bath. Once the reaction mixture had reached 0 °C, dry pyridine (0.57 ml, 7.00x10⁻³ mol) was added *via* cannular over a 30 s period. A white precipitate of pyridinium hydrochloride was immediately visible. The reaction was allowed to slowly warm to room temperature and left to stir overnight. The solution was filtered directly into an ice-cooled, stirred solution of tris-hydantoin (0.46 g, 2.00x10⁻³ mol) and dry THF (50 ml). This was performed under nitrogen gas. This resulted in a pale yellow solution, which was allowed to warm to room temperature over 24 hours. The solution was evaporated to dryness *in vacuo* and the resulting yellow precipitate was dissolved in dichloromethane (100 ml) and extracted with deionised water (100 ml). The organic layer was subsequently dried over anhydrous sodium sulphate and filtered. Evaporation of the organic solvent resulted in the crude product, which was purified by silica gel column chromatography (dichloromethane). This resulted in white crystals of product (0.48 g, 73 %). m.p. 215 °C. IR (KBr) ν_{\max} 3439, 1802, 1757, 1718 cm⁻¹. ¹H NMR [CDCl₃, 400 MHz]: δ_{H} 0.94-0.99 (H₁₀'), 1.26-1.28 (H_{11s}, *J* 10.62 Hz), 1.32-1.35 (H₇'), 1.45-1.48 (2H, H_{7a} and H_{11a}, *J* 10.62 Hz), 1.60-1.75 (H₉'), 2.07-2.09 (H₅'), 2.09-2.11 (H₃'), 2.17 (2H, H₁ and H₈'), 2.28-2.31 (H₂'), 2.31-2.33 (H₉'), 2.45 (H₆'), 2.95 (H₁₀'), 5.00 (H₈'), 7.19 (H₁'). ¹³C NMR [CDCl₃, 400 MHz]: δ_{C} 9.45 (C₁₀'), 19.21, 19.28 (C₇'), 28.55, 28.58 (C₉'), 32.79 (C₁₁'), 33.15 (C₇'), 41.98 (C₉'), 42.75 (C₁₀'), 43.23 (C₂'), 45.34 (C₆'), 46.73 (C₁ and C₈'), 55.21, 55.25 (C₅'), 56.12, 56.17 (C₃'), 71.96, 72.00 (C₄'), 77.32 (C₈'), 147.74 (C₅'), 152.62 (C₄'), 171.50 (C₂'). M.S. [M+H]⁺ 331 m/z. Elemental analysis. Experimental: C, 65.35, H, 6.79, N, 8.50 %. Calculated: C, 65.45, H, 6.67, N, 8.48 %.

Synthesis of Novel Compound 5 (NC5, 4.10)¹⁰⁶

A solution of tris-amino acid (0.41 g, 2.00x10⁻³ mol) in ethanol was treated with thionyl chloride (0.50 ml, 6.85x10⁻³ mol) and refluxed for 24 hours. The solution was evaporated to dryness under reduced pressure to yield the crude product. This was extracted with dichloromethane and deionised water. The organic solvent was removed *in vacuo* to yield the amino acid ester, which was purified by silica gel chromatography (dichloromethane) to yield the pure product (0.33 g, 71 %). m.p. 56 °C. IR (KBr) ν_{\max} 3427, 2954, 2869, 1730 cm⁻¹. ¹H NMR [CDCl₃, 400 MHz]: δ_{H} 1.25-1.28 (3H, H₅'), 1.30 (H_{7s}, H_{11s}'), 1.37-1.39 (H_{11a}, *J* 11.72 Hz), 1.39-1.42 (H_{7a}, *J* 11.72 Hz), 1.80 (H₁', D₂O exchangeable protons), 1.94-1.95 (H₃'), 2.07-2.10 (H₅'), 2.10-2.11 (H₁, H₈, H₁₀'), 2.12-2.15 (H₉'), 2.15-2.18 (H₂'), 2.60 (H₆'), 4.12-4.18 (H₄'). ¹³C NMR [CDCl₃, 400 MHz]: δ_{C} 14.19 (C₅'), 32.68, 33.60 (C₇, C₁₁'), 42.10 (C₂'), 43.22 (C₁₀'), 44.64 (C₆'), 46.91, 46.92 (C₁, C₈'), 54.04 (C₅'), 56.20 (C₃'), 60.47 (C₄'), 69.07 (C₄'), 175.74 (C₂'). M.S. [M+H]⁺ 234 m/z. Elemental analysis. Experimental: C, 72.37, H, 8.27, N, 6.08 %. Calculated: C, 72.10, H, 8.15, N, 6.01 %.

Hydrolysis of Novel Compound 5 (NC5) using PLE^{63,70}

PLE (12 mg) was added to a stirring suspension of NC5 (0.20 g, 8.58×10^{-4} mol) in 0.05 M KH_2PO_4 buffer (11.00 ml) of pH 8 and 25 °C. The pH was maintained by adding 0.1 M NaOH dropwise and the temperature was maintained by an electronic probe. The reaction was run over a two-week period. The mixture was filtered through a sintered glass funnel and washed with buffer solution. The resulting solution was extracted with ethyl acetate (100 ml). The aqueous layer was acidified to pH 6.5 with concentrated HCl. The volume was reduced by heating on a heating mantle, which resulted in the amino acid precipitating out of solution. The amino acid was recovered by filtration and washed successively with acetone and diethyl ether (17.50 mg, 10 %). The IR spectrum was identical to that of tris-amino acid. The Fmoc derivative was subsequently synthesised. The NMR data was identical to previously synthesised Fmoc-tris-amino acid.

Coupling of linker to MBHA resin (5.22)^{23,91}

The MBHA resin (0.50 g, 0.70 mmol NH_2/g) was swelled using DMF. The FmocAM linker (0.47 g, 8.75×10^{-4} mol), DIPCDI (0.14 ml, 8.75×10^{-4} mol) and HOBt (0.12 g, 8.75×10^{-4} mol) were added at room temperature to the resin in DMF. This was left to stir for 24 hours. Successful attachment was confirmed by a negative Kaiser test. The Fmoc group was cleaved by the application of a 20 % (v/v) piperidine in DMF solution for two hours. Cleavage of the Fmoc group was confirmed by positive Kaiser test. The Fmoc by-product was removed from the solution by filtration, followed by washing the resin with isopropanol and DMF.

Washing procedure for solid phase peptide synthesis^{23,91}

The resin was washed with DMF (5 x 10 ml), isopropanol (3 x 10 ml) and DMF (3 x 10 ml).

Coupling of glycine and alanine to the linker (5.24, 5.25)^{23,91}

The Fmoc protected amino acid, DIPCDI (0.14 ml, 8.75×10^{-4} mol) and HOBt (0.12 g, 8.75×10^{-4} mol) were added at room temperature to the resin in DMF. This was left to stir for 24 hours. Successful attachment was confirmed by a negative Kaiser test. The Fmoc group was cleaved by the application of a 20 % (v/v) piperidine in DMF solution for two hours. Cleavage of the Fmoc group was confirmed by positive Kaiser test. The Fmoc group was removed from the solution by filtration, followed by washing the resin with isopropanol and DMF.

Synthesis of Fmoc-tris-acid fluoride^{23,89}

Cyanuric fluoride (40.50 μl , 4.68×10^{-4} mol) was added to a suspension of Fmoc-tris-amino acid (0.20 g, 4.68×10^{-4} mol) and dry dichloromethane (50 ml). Dry pyridine was subsequently added (37.80 μl , 4.68×10^{-4} mol) and the resulting solution was left to stir under nitrogen for 12 hours. The mixture, which now contained a white suspension of water-soluble cyanuric acid was extracted with ice water (40 ml). The organic phase was dried over MgSO_4 , filtered and subsequently removed *in vacuo*. The resulting white solid was recrystallised from dichloromethane/hexane to give the pure acid fluoride as a white solid (0.17 g, 87 %). IR (KBr) ν_{max} 2966, 1724, 1504, 1277 cm^{-1} . ^1H NMR [CDCl_3 , 300 MHz]: δ_{H} 1.16-1.18 (m, 4H), 1.96-2.46 (m, 7H), 2.73 (br s, 1H), 4.22 (t, J 6.6 Hz, 1H), 4.75 (d, J 6.2 Hz, 2H), 5.38 (s, 1H, D_2O exchangeable), 7.25-7.48 (m, 4H), 7.59 (d, J 7 Hz, 2H), 7.77 (d, J 7 Hz, 2H). ^{13}C NMR [CDCl_3 , 300 MHz]: δ_{C} 32.00 (t), 33.0 (t), 42.7 (d), 42.9 (d), 43.2 (d), 44.2 (d), 46.9 (d), 47.0 (d), 47.2 (d), 53.7 (d), 54.1 (d), 66.7 (t), 68.1 (s), 69.2 (s), 119.3 (d), 124.8 (d), 127.0 (d), 127.6 (d), 141.3 (s), 143.5 (s), 155.2 (s), 158.6 (s), 166.0 (s). ^{19}F NMR [CDCl_3 , 400 MHz]: δ_{F} 234.09. M.S. and infrared spectra were identical to an authentic sample.

Coupling of Fmoc-tris-acid fluoride to the dipeptide (5.26)²³

The tris-amino acid fluoride (0.67 g, 1.56×10^{-3} mol) and dry pyridine (151.00 μl , 1.87×10^{-3} mol) was added to the resin in DMF and left to stir for 24 hours. Successful attachment was confirmed by a negative Kaiser test. The Fmoc group was cleaved by the application of a 20 % (v/v) piperidine in DMF solution for two hours. The Fmoc group was removed from the solution by filtration, followed by washing the resin with isopropanol and DMF.

Cleavage of the tripeptide from the resin and linker (5.27)^{23,91}

The resin was washed several times with dichloromethane, methanol and diethyl ether and dried overnight in a vacuum pump. The dry resin was placed in a flask containing the cleavage mixture of 95 % (v/v) trifluoroacetic acid, 2.5 % (v/v) water and 2.5 % (v/v) triisopropylsilane. The mixture was left to stir for 12 hours. The resin was removed by filtration and washed several times with TFA. The application of nitrogen gas served to evaporate the TFA. Diethyl ether was subsequently added to precipitate the tripeptide as a white solid. Decanting the diethyl ether served to remove the linker from the peptide. M.S. $[\text{M}+\text{H}]^+$ 334 m/z.

REFERENCES

- 1) Morrison, R.T., Boyd, R.W, *Organic Chemistry*, 6th Ed., Prentice Hall, Inc., Englewood Cliffs, New Jersey, **1992**, p.p. 144, 145, 1205, 1221
- 2) Mathews, C.K., Van Holde, K.E., *Biochemistry*, 2nd Ed., The Benjamin Cummings Publishing Company, Inc., California, **1996**, p.p. 133, 368, 369
- 3) Chandrasekhar, S., Raza, A., Takhi, M., *Tetrahedron: Asymmetry.*, **2002**, 13, 423-428
- 4) Wagner, I., Musso, H., *Angew. Chem. Int. Ed. Engl.*, **1983**, 22, 816-828
- 5) Tanaka, K., Sawanishi, H., *Tetrahedron: Asymmetry.*, **1998**, 9, 71-77
- 6) Gante, J., *Angew. Chem. Int. Ed. Engl.*, **1983**, 22, 816-828
- 7) Van Betsbrugge, J., Van Den Nest, W., Verheyden, P., Tourwé, D., *Tetrahedron.*, **1998**, 54, 1753-1762
- 8) Nagasawa, H.T., Elberling, J.A., Shiota, F.N., *J. Med. Chem.*, **1975**, 18, 826-830
- 9) Brooks, K.B., Hickmott, P.W., Jutle, K.K., Schreyer, C.A., *S. Afr. J. Chem.*, **1992**, 45, 8-11
- 10) Kitagawa, K., Mizobuchi, N., Hama, T., Hibi, T., Konishi, R., Futaki, S., *Chem. Pharm. Bull.*, **1997**, 45, 1782-1787
- 11) Schwab, R.S., England, A.C., Poskanzer, D.C., Young, R.R., *J. Am. Med. Assoc.*, **1969**, 208, 1168-1170
- 12) Bailey, E.V., Stone, T.W., *Arch. Int. Pharmacodyn.*, **1975**, 216, 246-262
- 13) Oliver, D.W., Dekker, T.G., Snyckers, F.O., Fourie, T.G., *J. Med. Chem.*, **1991**, 34, 851-854
- 14) Gerzon, K., Kau, D., *J. Med. Chem.*, **1967**, 10, 189-199
- 15) Ranganathan, D., Haridas, V., Madhusudanan, K.P., Roy, R., Nagaraj, R., John, G.B., Sukhaswami, M.B., *Angew. Chem. Int. Ed. Engl.*, **1996**, 35, 1105-1107
- 16) Bisetty, K., Ph.D. thesis, *University of Natal, Durban*, **2002**
- 17) Oliver, D.W., Dekker, D.G., Snyckers, F.O., *Eur. J. Med. Chem.*, **1991**, 26, 375-379
- 18) Oliver, D.W., Dekker, D.G., Snyckers, F.O., *Drug. Res.*, **1991**, 41, 549-552
- 19) Inamoto, Y., Aiyami, K., Tasaishi, N., Fujikura, Y.J., *J. Med. Chem.*, **1967**, 19, 536
- 20) Inamoto, Y., Aiyami, K., Kadono, T., Makayama, H., Takatsuki, A., Tumura, G., *J. Med. Chem.*, **1977**, 20, 1371
- 21) Nakazaki, M.; Naemura, K.; Arashiba, N., *J. Org. Chem.*, **1978**, 43, 689-692
- 22) Helmchen, G., Staiger, G., *Angew. Chem. Int. Ed. Engl.*, **1977**, 16, 116-117
- 23) Govender, T. M.Sc. dissertation, *University of Natal, Durban*, **2001**
- 24) Underwood, G.R., Ramamoorthy, B., *Tet. Lett.*, **1970**, 4125-4127
- 25) Oliver, D.W. Dekker, D.G., *S. Afr. J. Chem.*, **1988**, 84, 407-409
- 26) Kent, G.J., Godleski, S.A., Ōsawa, E., von R. Schleyer, P., *J. Org. Chem.*, **1977**, 42, 3852-3859
- 27) Nakazaki, M., Naemura, K., Kadowaki, H., *J. Org. Chem.*, **1976**, 41, 3725-3730
- 28) Engler, E.M., Andose, J.D., von R. Schleyer, P., Ōsawa, E., Kent, G.J., *J.A.C.S.*, **1973**, 95, 8005-8025

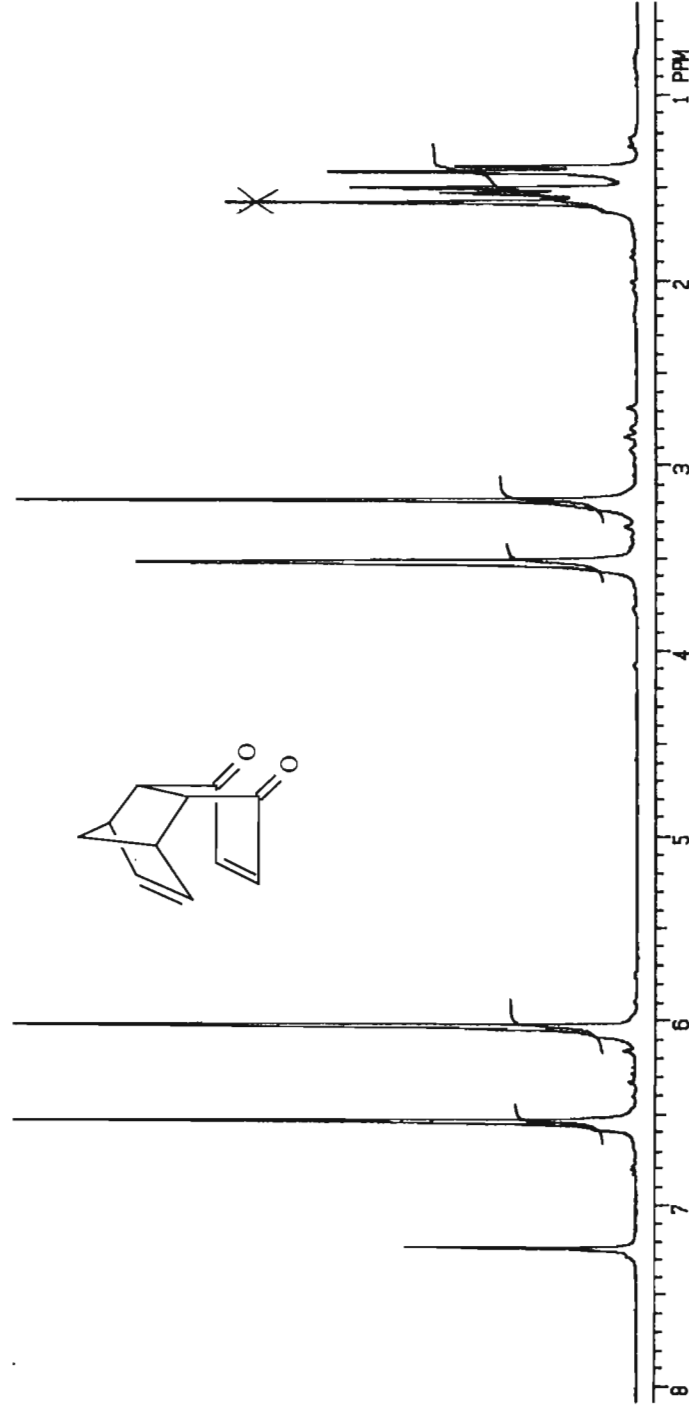
-
- 29) Godleski, S.A., von R. Schleyer, P., *J. C.S. Chem. Comm.*, **1974**, 976-977
 - 30) Dekker, T.G., Oliver, D.W., Pachler, K.G.R., Wessels, P.L., Woudenberg, M. *Journal of Organic Magnetic Resonance.*, **1981**, 15, 188-192.
 - 31) Mehta, G., Srikrishna, A., *J. C. S. Chem. Comm.*, **1982**, 218-219
 - 32) Jouin, P., Poncet, J., Dufour, M-N., Pantaloni, A., Castro, B., *J. Org. Chem.*, **1989**, 54, 617-627
 - 33) Pettit, G.R., Singh, S.B., Herald, D.L., Lloyd-Williams, P., Kantoci, D., Burkett, D.D., Barkóczy, J., Hogan, F., Wardlaw, T.R., *J. Org. Chem.*, **1994**, 59, 6287-6295
 - 34) Bucherer, H.T., Steiner, W., *J. Prakt. Chem.*, **1934**, 291-314
 - 35) Nagasawa, H.T., Elberling, J.A., Shiota, F.N., *J. Med. Chem.*, **1973**, 16, 823
 - 36) Martins, F.J.C., Viljoen, A.M., Kruger, H.G., Fourie, L., Roscher, J., Joubert, A.J., Wessels, P.L., *Tetrahedron*, **2001**, 57, 1601-1607
 - 37) Marchand, A.P., Allen, R.W., *J. Org. Chem.*, **1974**, 39, 1596
 - 38) The mechanisms presented in this thesis were adopted from classical organic chemistry textbooks. Clayden, J., Greeves, N., Warren, S., Wothers, P., *Organic Chemistry*, Oxford University Press, New York, **2001**, p.p. 140, 617, 618, 627, 638, 906
 - 39) Kruger, H.G., Ph.D. thesis, *Potchefstroom University for C.H.E.*, **1996**
 - 40) Cookson, R.C., Crundwell, R., Hill, R., Hudec J., *J.Org. Chem.*, **1964**, 3062-3075
 - 41) Marchand, A.P., Power, T.D., Kruger, H.G., *Croatica Chemica Acta*, **2001**, 265-270
 - 42) Eaton, P.E., Cassar, L., Hudson, R.A., Hwang, D.R., *J. Org. Chem.*, **1976**, 41, 1445-1448
 - 43) Dekker, T.G. and Oliver, D.W., *S. Afr. J. Chem.* **1979**, 45-48
 - 44) Marchand, A.P., La Roe, W.D., Sharma, G.V.M., Shur, S.C., Reddy, D.S., *J. Org. Chem.*, **1986**, 51, 1622
 - 45) Dekker, J., Dekker, J.J., Fourie, L., Wenteler, G.L., *J. S. Afr. Chem. Inst.*, **1975**, 28, 321
 - 46) The mechanisms involved were adapted from general mechanisms in classical organic textbooks: March, J., *Advanced Organic Chemistry, Reactions, Mechanisms and Structure*, 4th Ed., John Wiley and Sons, Inc., New York, **1992**, p.p. 889, 1209
 - 47) Furniss, B.S., Hannaford, A.J., Smith, P.W.G., Tatchell, A.R., *Vogel's Textbook of Practical Organic Chemistry*, 5th Ed., Longman Scientific and Technical, England, **1989**, p.p. 1276
 - 48) Kubik, S., Meissner, R.S., Rebek Jr., J., *Tet. Lett.*, **1994**, 35, 6635-6638
 - 49) Flynn, D.A., Zelle, R.E., Grieco, P.A., *J. Org. Chem.*, **1983**, 48, 2424-2426
 - 50) Scott Yokum, Tungaturthi, P.K., T., McLaughlin, M.L., *Tet. Lett.*, **1997**, 38, 5111-5114
 - 51) Wysong, C.L., Scott Yokum, T., Morales, G.A., Gundry, R.L., McLaughlin, M.L., Hammer, R.P., *J. Org. Chem.*, **1996**, 61, 7650-7651
 - 52) Hart, H., Hart, D.J., Craine, L.E, *Organic Chemistry, A Short Course*, 9th Ed., Houghton Mifflin Co., Boston, **1995**, 509
 - 53) Strazzolini, P., Melloni, T., Giumanini, A.G., *Tetrahedron*, **2001**, 57, 9033-9043

-
- 54) Hoffman, H.M.R., Iranshahi, L., *J. Org. Chem.*, **1984**, 49, 1174-1176
 - 55) Krishnaswamy, D., *Synlett.*, **2000**, 1860
 - 56) Goren, Z., Heeg, M.J., Mobashery, S., *J. Org. Chem.*, **1991**, 56, 7186-7188
 - 57) Rivero, I.A., Somanathan, R., Hellberg, L.H., *Synthetic Communications*, **1995**, 25, 2185-2188
 - 58) Campbell, N.A., *Biology*, 4th Ed., Benjamin/Cummings Publishing Co., Inc. California, **1996**, p.p. 97-100
 - 59) Jones, J.B., *Tetrahedron*, **1986**, 42, 3351-3403
 - 60) Wong C.H., Whitesides, G.M., *Enzymes in Synthetic Organic Chemistry*, Tetrahedron Organic Chemistry Series, Vol., 12, Elsevier Science Ltd., **1994**, p.p. 1
 - 61) Marchand, A.P., personal communication, University of North Texas, USA. (www.chem.unt.edu/faculty/research/apmres.htm)
 - 62) Takahashi, S., Ohashi, T., Kii, Y., Kumagai, H., Yamada, H., *J. Ferment. Technol.*, **1979**, 57, 328-332
 - 63) Kaptein, B., Boesten, W.H.J., Broxterman, Q.B., Peters, P.J.H., Schoemaker, H.E., Kamphuis, J., *Tetrahedron: Asymmetry*, **1993**, 4, 1113-1116
 - 64) Jones, J.B., *Can. J. Chem.*, **1993**, 71, 1273-1282
 - 65) Toone, E.J., Werth, M.J., Jones, J.B., *J.A.C.S.*, **1990**, 4946-4952
 - 66) Provencher, L., Wynn, H., Jones, J.B., *Tetrahedron: Asymmetry*, **1993**, 4, 2025-2040
 - 67) Basak, A., Bhattacharya, G., Palit, S.K., *Bull. Chem. Soc. Jpn.*, **1997**, 70, 2509-2513
 - 68) Gaussian 98, Revision A.9, Frisch, M.J., Trucks, G.W., Schlegel, H.B., Scuseria, G.E., Robb, M.A., Cheeseman, J.R., Zakrzewski, V.G., Montgomery, Jr., J.A., Stratmann, R.E., Burant, J.C., Dapprich, S., Millam, J.M., Daniels, A.D., Kudin, K.N., Strain, M.C., Farkas, O., Tomasi, J., Barone, V., Cossi, M., Cammi, R., Mennucci, B., Pomelli, C., Adamo, C., Clifford, S., Ochterski, J., Petersson, G.A., Ayala, P.Y., Cui, Q., Morokuma, K., Malick, D.K., Rabuck, A.D., Raghavachari, K., Foresman, J.B., Cioslowski, J., Ortiz, J.V., Baboul, A.G., Stefanov, B.B., Liu, G., Liashenko, A., Piskorz, P., Komaromi, I., Gomperts, R., Martin, R.L., Fox, D.J., Keith, T., Al-Laham, M.A., Peng, C.Y., Nanayakkara, A., Challacombe, M., Gill, P.M.W., Johnson, B., Chen, W., Wong, M.W., Andres, J.L., Gonzalez, C., Head- / Gordon, M., Replogle, E.S., Pople, J.A., Gaussian, Inc., Pittsburgh PA, **1998**.
 - 69) Naemura, K., Fujii, T., Chikamatsu, H., *Chemistry Letters*, **1986**, 923-926
 - 70) Moorlag, H., Kellogg, R.M., *J. Org. Chem.*, **1990**, 55, 5878-5881
 - 71) Chen, X., Du, D-A., Hua, W-T., *Tetrahedron: Asymmetry*, **2002**, 13, 43-46
 - 72) Teetz, V., Saul, H., *Tet. Lett.*, **1984**, 25, 4483-4486
 - 73) Wang, W., Xiong, C., Zhang, J., Hruby, J., *Tetrahedron*, **2002**, 58, 3101-3110
 - 74) Stavropoulos, G., Karagiannis, K., Vynios, D., Papaioannou, D., Aksnes, D.W., Frøystein, N.Å., Francis, G.W., *Acta Chemica Scandinavica*, **1991**, 45, 1047-1054
 - 75) Vranešić, B., Tomašić, J., Smerdel, S., *Helvetica Chimica Acta*, **1993**, 76, 1752-1758
 - 76) Singh, A., M. Sc., *University of Natal, Durban*, Personal Communication
 - 77) Fu, Y., Hammarström, G.J., Miller, T.J., Fronczek, F.R., McLaughlin, M.L., Hammer, R.P., *J. Org. Chem.*, **2001**, 66, 7118-7124

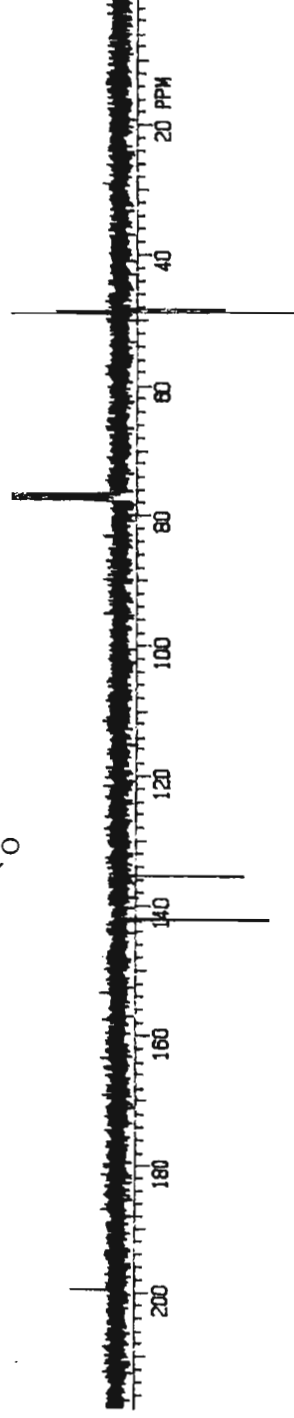
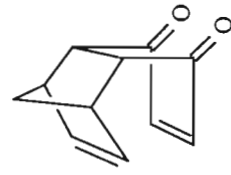
-
- 78) du Vigneaud, V., Ressler, C., Swan, J.M., Roberts, C.W., Katsoyannis, P.G., Gordon, S., *J.A.C.S.*, **1953**, 4879-4880
 - 79) Merrifield, R.B., *J.A.C.S.*, **1963**, 85, 2149-2154
 - 80) Mojsov, S., Mitchell, A.R., Merrifield, R.B., *J. Org. Chem.*, **1980**, 45, 555-560
 - 81) Kaiser, E., Colescott, R.L., Bossinger, C.D., Cook, P.I., *Anal. Biochem.*, **1970**, 34, 595-598
 - 82) Wenschuh, H., Beyermann, M., Krause, E., Brudel, M., Winter, R., Schümann, M., Carpino, L.A., Bienert, M., *J. Org. Chem.*, **1994**, 59, 3275-3280
 - 83) Wenschuh, H., Beyermann, M., Krause, M., R., Carpino, L.A., Bienert, M., *Tet. Lett.*, **1993**, 34, 3733-3736
 - 84) Carpino, L.A., Chao, H.G., *J. Org. Chem.*, **1991**, 56, 2635-2642
 - 85) Perlow, D.S., Erb, J.M., Gould, N.P., Tung, R.D., Freidinger, R.M., Williams, P.D., Veber, D.F., *J. Org. Chem.*, **1992**, 57, 4394-4400
 - 86) Bertho, J-N., Loffet, A., Pinel, C., Reuther, F., Sennyey, G., *Tet. Lett.*, **1991**, 1301-1306
 - 87) Carpino, L.A., Sadat-Aalae, D., Chao, H.G., DeSelms, R.H., *J.A.C.S.*, **1990**, 112, 9651-9652
 - 88) Wenschuh, H., Beyermann, M., R., El-Faham, A., Ghassemi, S., Carpino, L.A., Bienert, M., *J. C. S. Chem. Comm.*, **1995**, 669-670
 - 89) Carpino, L.A., El-Sayed, M., Mansour, E., Sadat-Aalae, D., *J. Org. Chem.*, **1991**, 56, 2611-2614
 - 90) Tam, J.P., Merrifield, R.B., *Strong Acid Deprotection of Synthetic Peptides: Mechanisms and Methods. In the Peptides, Vol. 9.*, Academic Press, New York, **1987**, p.p. 185-248
 - 91) General procedure from Novabiochem catalogue.
 - 92) Govender, P., M. Tech., *Durban Institute of Technology*, Personal Communication
 - 93) *Hyperchem, Computational Chemistry*, Hypercube, Inc. **1996**
 - 94) Foresman, J.B., Frisch, A.E., *Exploring Chemistry with Electronic Structure Methods, 2nd Ed.*, Gaussian, Inc., **1996**, p.p. 3, 5, 6, 10, 98, 99, 262
 - 95) Hehre, W.J., Yu, J., Klunzinger, P.E., Lou, L., *A Brief Guide to Molecular Mechanics and Quantum Chemical Calculations*, Wavefunction, Inc., **1998**, p.p. 10-14, 19, 20
 - 96) Leach, A.R., *Molecular Modelling, Principles and Applications*, Addison Wesley Longman Ltd., England, **1996**, p.p. 4, 34, 35, 73, 78, 90, 91, 99, 131-133
 - 97) Singh, T., M.Tech., *Durban Institute of Technology*, Personal Communication
 - 98) Young, D., *Computational Chemistry: A Practical Guide for Applying Techniques to Real World Problems*, John Wiley and Sons, Inc., **2001**
 - 99) Atkins, P.W., *Physical Chemistry, 6th Ed.*, Oxford University Press, Great Clarendon Street, Oxford OX2 6DP, pp 834
 - 100) Kruger, H.G., *J. Mol. Struct. (Theochem.)*, **2002**, 577, 281
 - 101) O'Brien, D.F., Gates, Jr., J.W., *J. Org. Chem.*, **1965**, 2593-2601
 - 102) Bishop, R., *Aust. J. Chem.*, **1984**, 37, 319-325
 - 103) Marchand, A.P., Wang, Y., Ren, C-T., Vidyasagar, V., Wang, D. *Tetrahedron.*, **1996**, 52, 6063-6072

-
- 104) Aleksandrov, A.M.; Kashyap, R.P., Pehk, T.J., Petrenko, A.E., Watson, W.H., *J. Org. Chem.*, **1993**, 58, 1831-1834
- 105) Eaton, P.E.; Hudson, R.A.; Giordano, C. *J.C.S. Chem. Comm.*, **1974**, 978
- 106) Moloney, G.P., Martin, G.R., Mathews, N., Hobbs, H., Dodsworth, S., Sang, P.Y., Knight, C., Maxwell, M., Glen, R.C., *J. Chem., Perkin Trans. 1.*, **1999**, 2699-2711

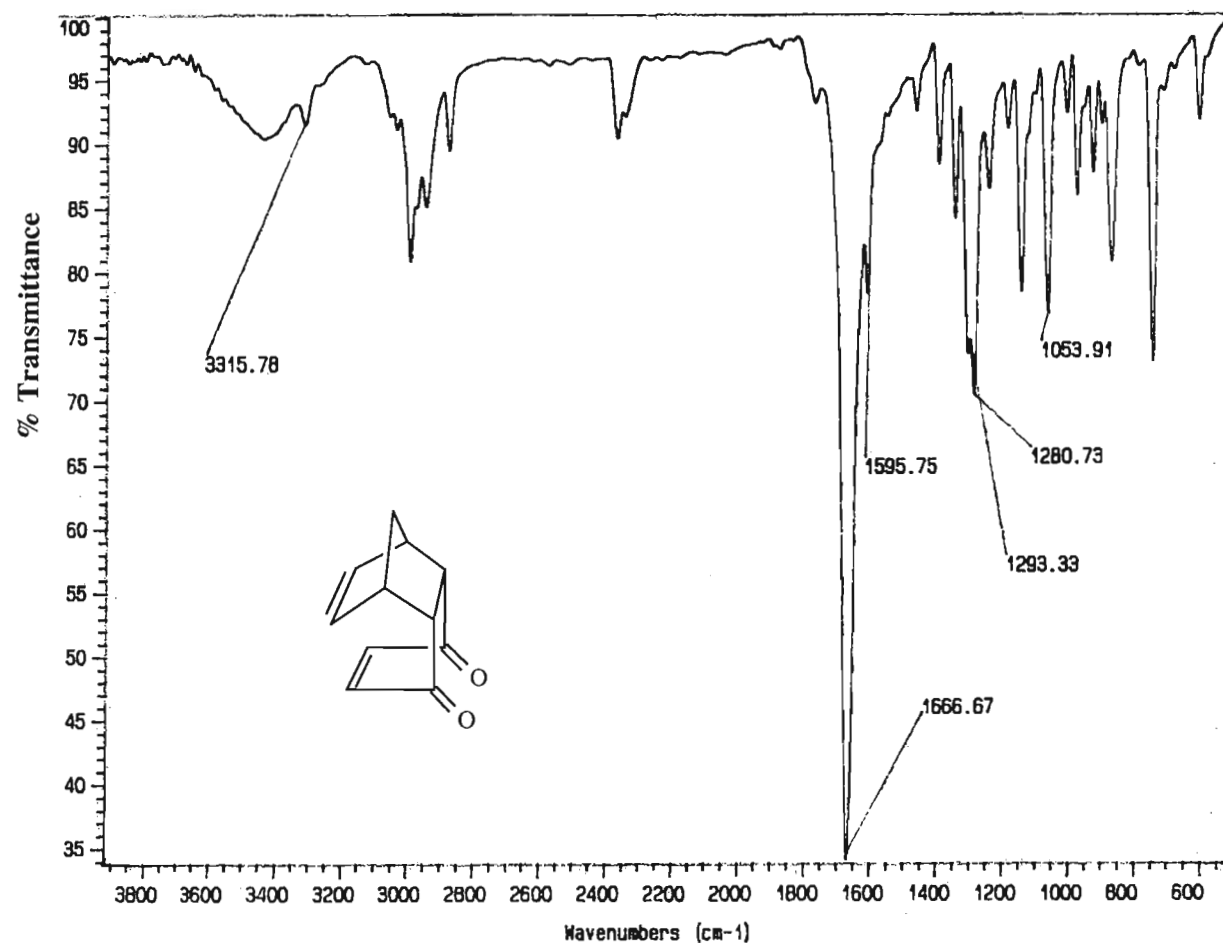
Appendix 1
Spectra



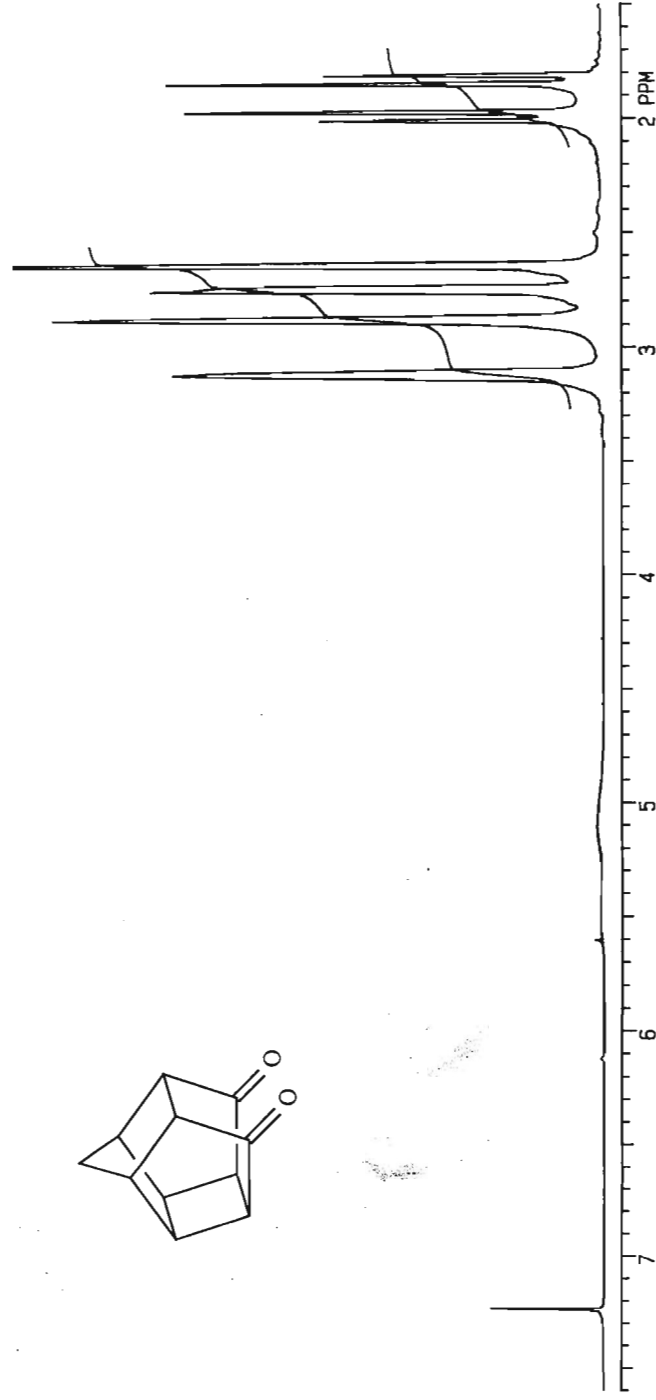
Spectrum 1: ^1H NMR spectrum of adduct in CDCl_3 (2.17)



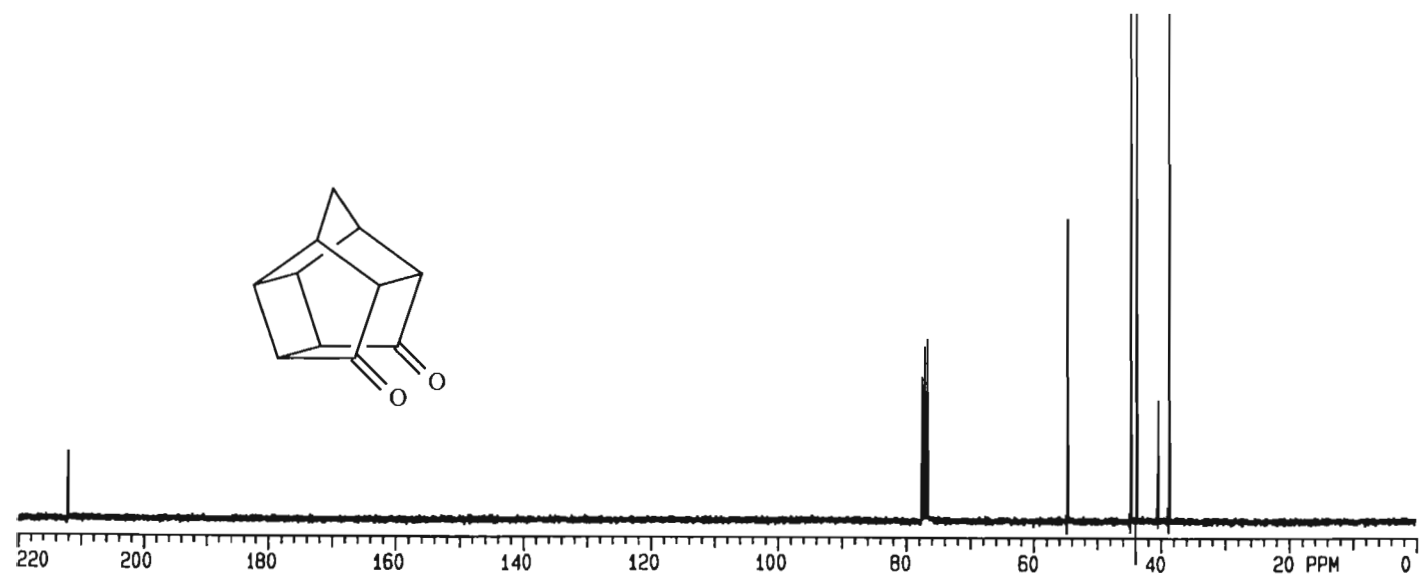
Spectrum 2: ^{13}C NMR spectrum of adduct in CDCl_3 (2.17)



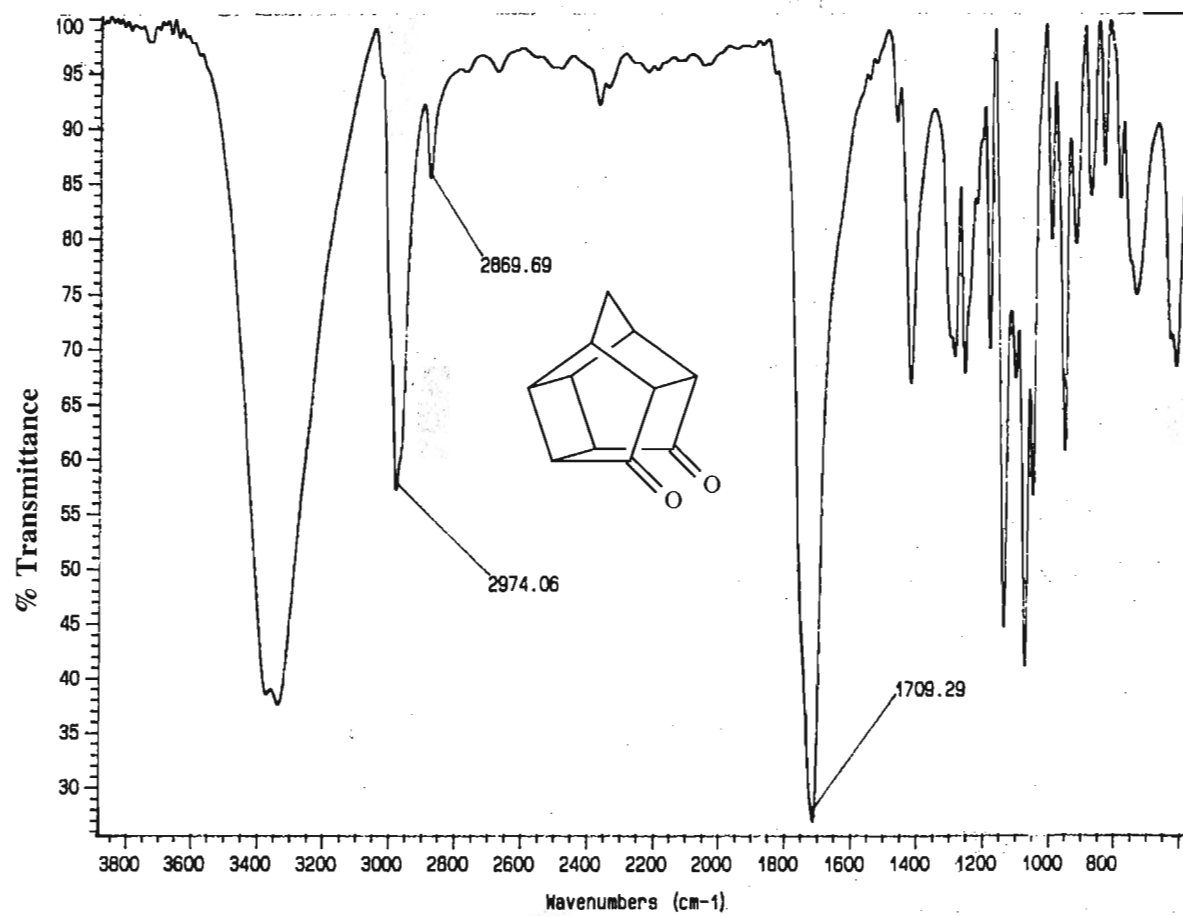
Spectrum 3: Infrared spectrum (KBr) of adduct (2.17)



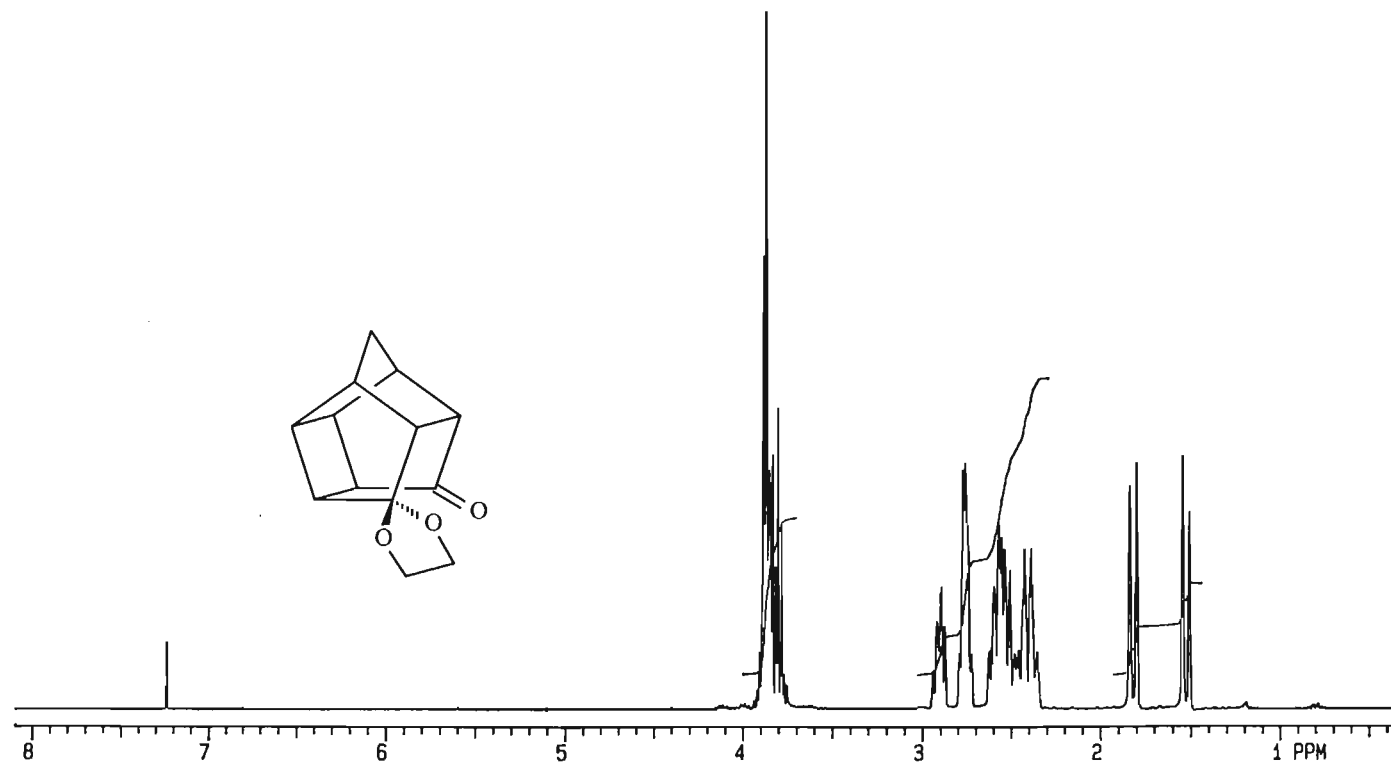
Spectrum 4: ^1H NMR spectrum of dione in CDCl_3 (2.19)



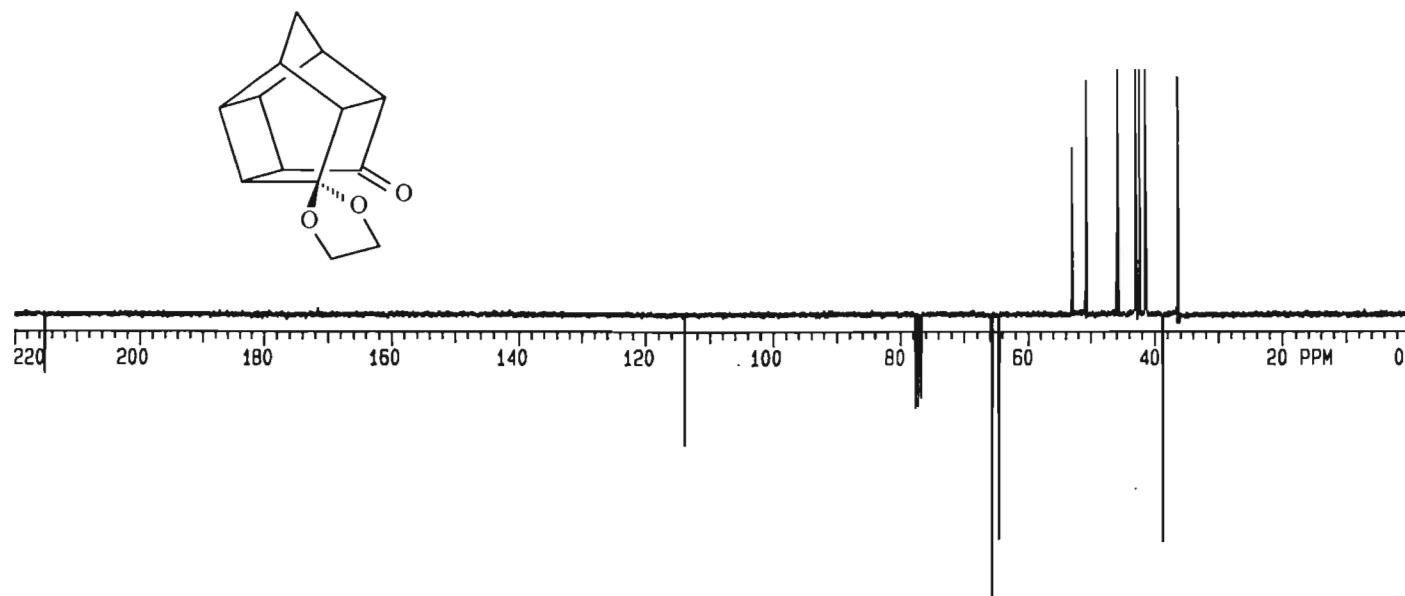
Spectrum 5: ^{13}C NMR spectrum of dione in CDCl_3 (2.19)



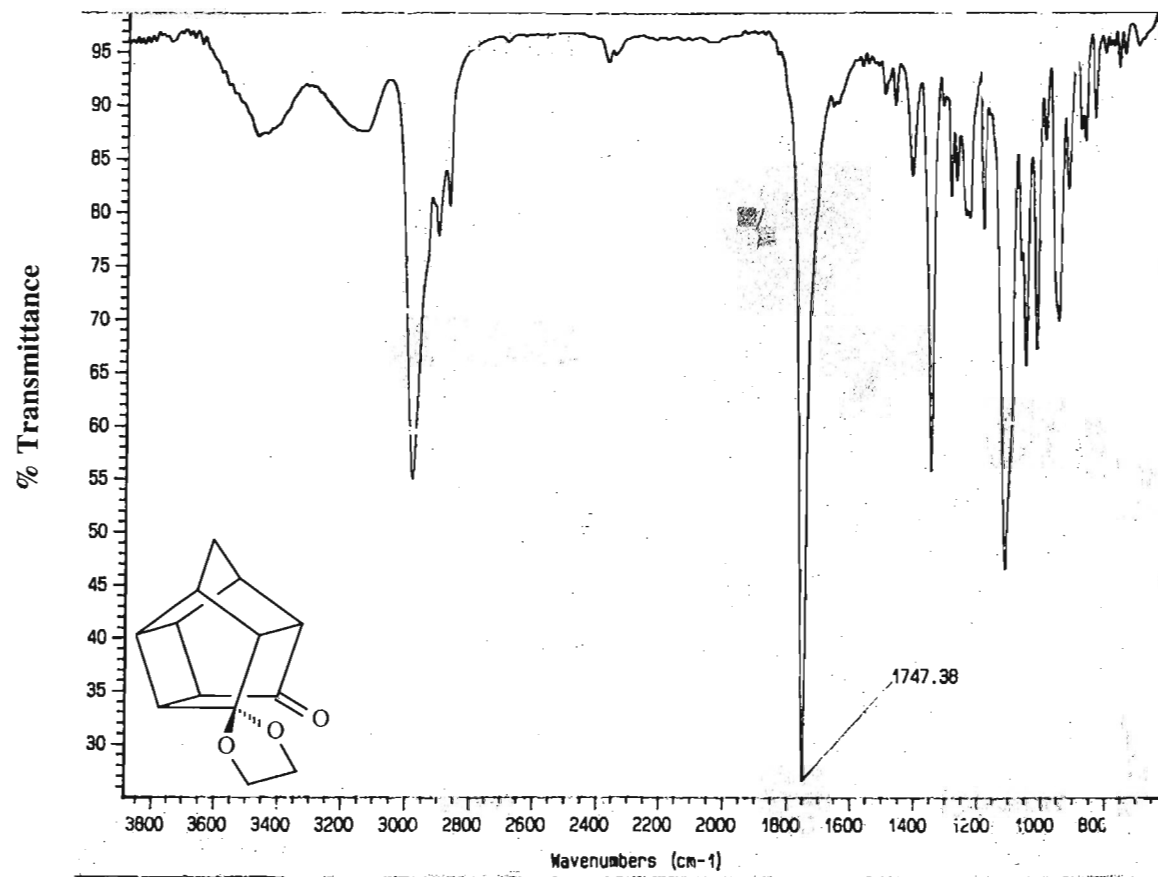
Spectrum 6: Infrared spectrum (KBr) of dione (2.19)



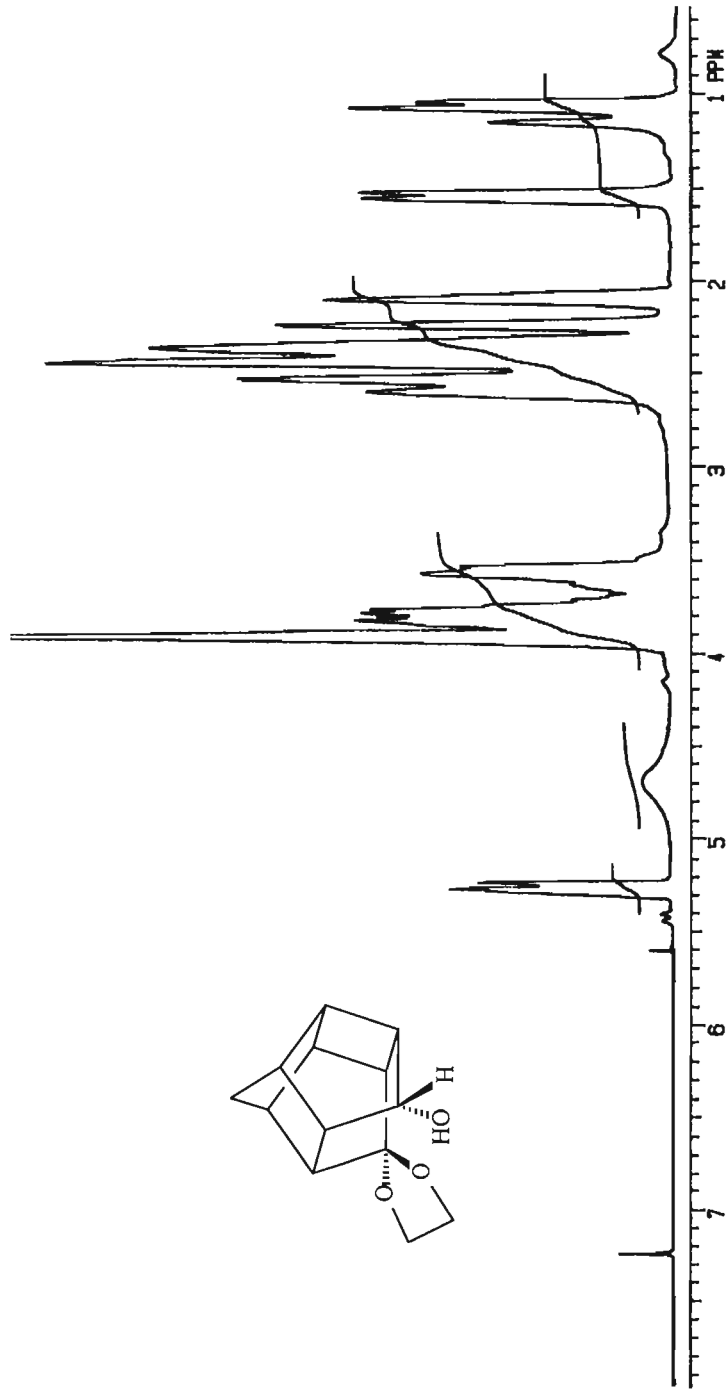
Spectrum 7: ^1H NMR spectrum of the keto-ketal in CDCl_3 (2.31)



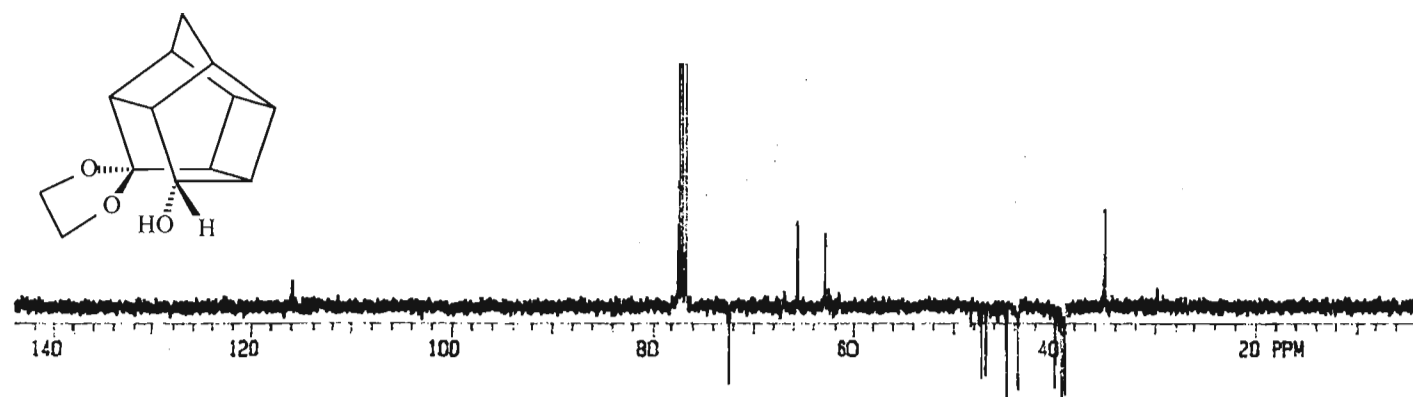
Spectrum 8: ^{13}C NMR spectrum of the keto-ketal in CDCl_3 (2.31)



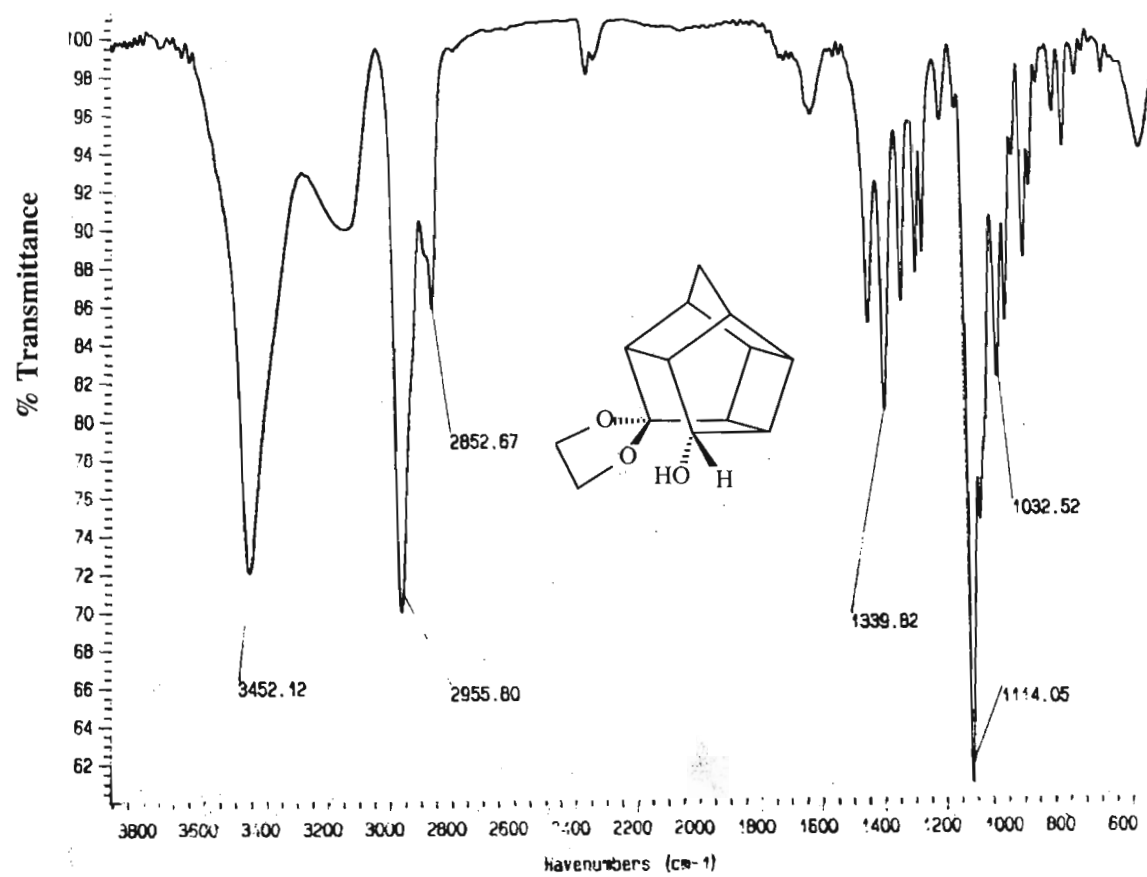
Spectrum 9: Infrared spectrum (KBr) of the keto-ketal (2.31)



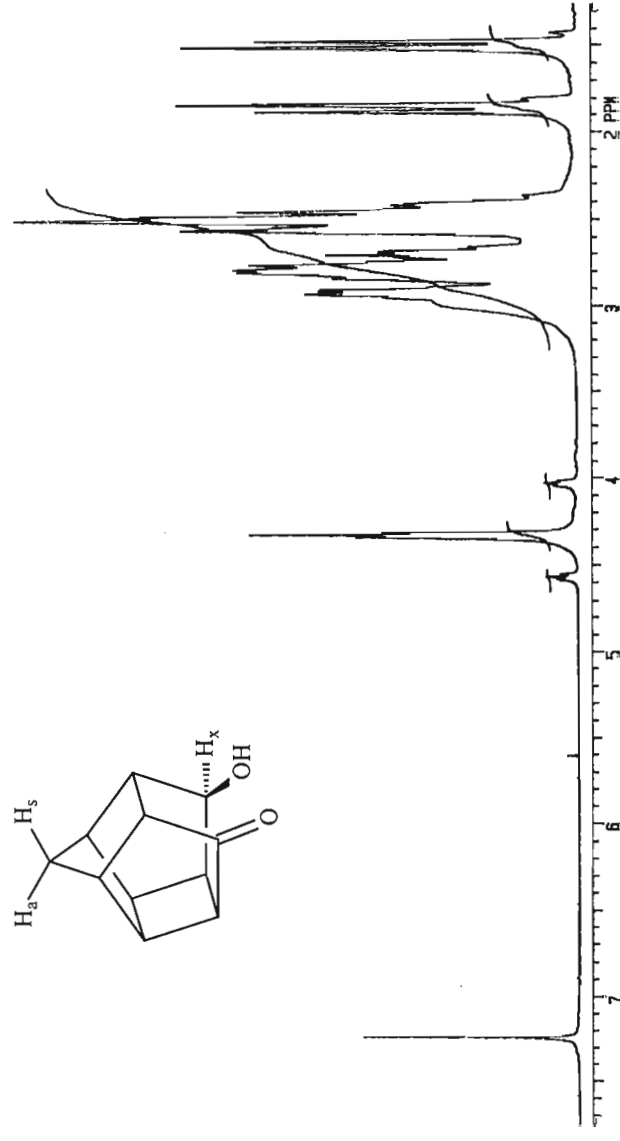
Spectrum 10: ^1H NMR spectrum of the hydroxy-ketal in CDCl_3 (2.34)



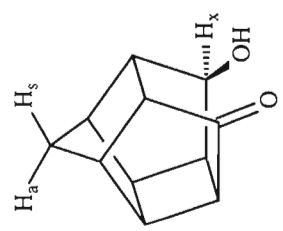
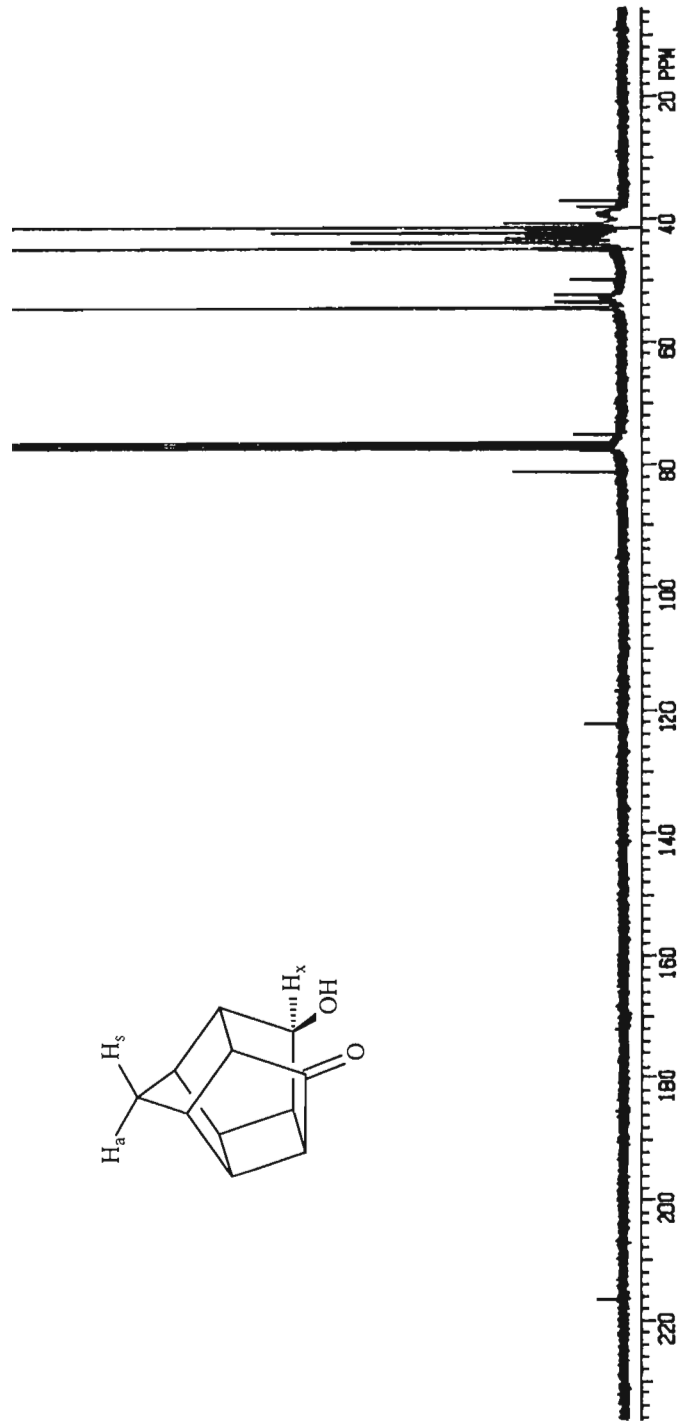
Spectrum 11: ^{13}C NMR spectrum of the hydroxy-ketal in CDCl_3 (2.34)



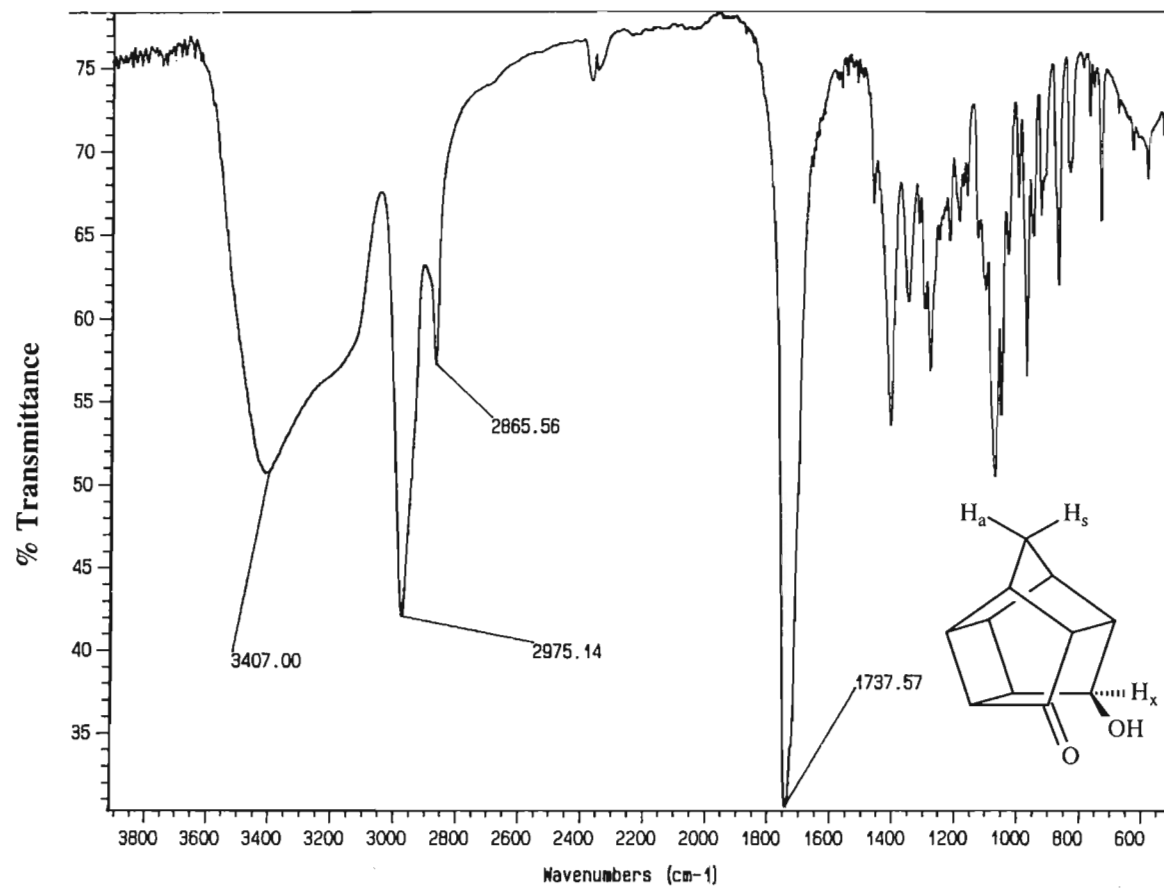
Spectrum 12: Infrared spectrum (KBr) of the hydroxy-ketal (2.34)



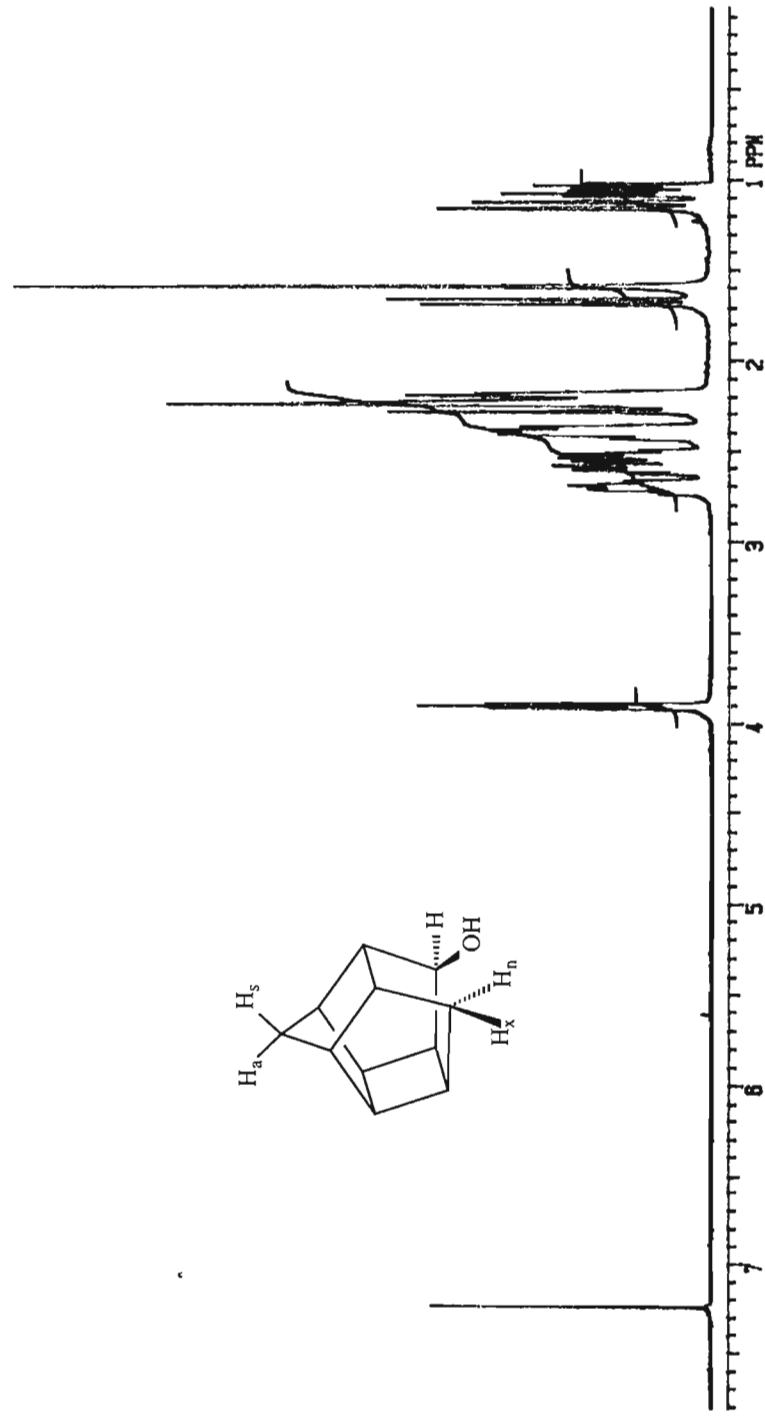
Spectrum 13: ^1H NMR spectrum of the hydroxy-ketone in CDCl_3 (2.40)



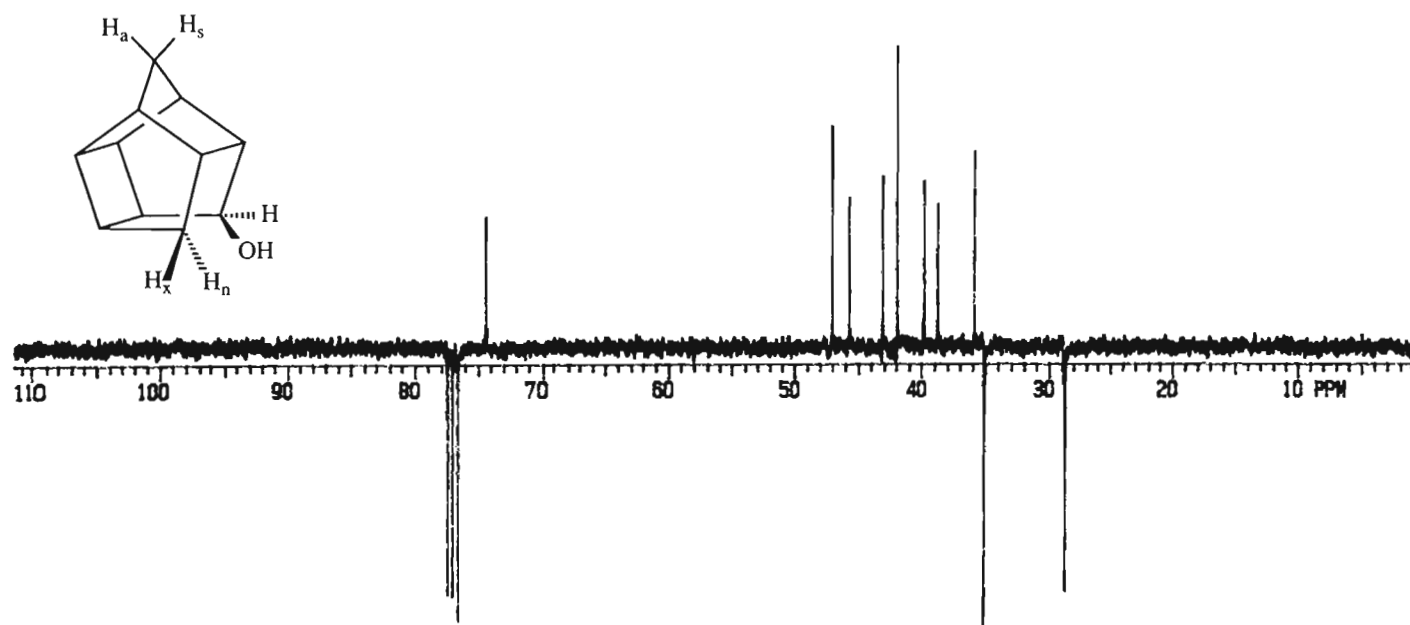
Spectrum 14: ^{13}C NMR spectrum of the hydroxy-ketone in CDCl_3 (2.40)



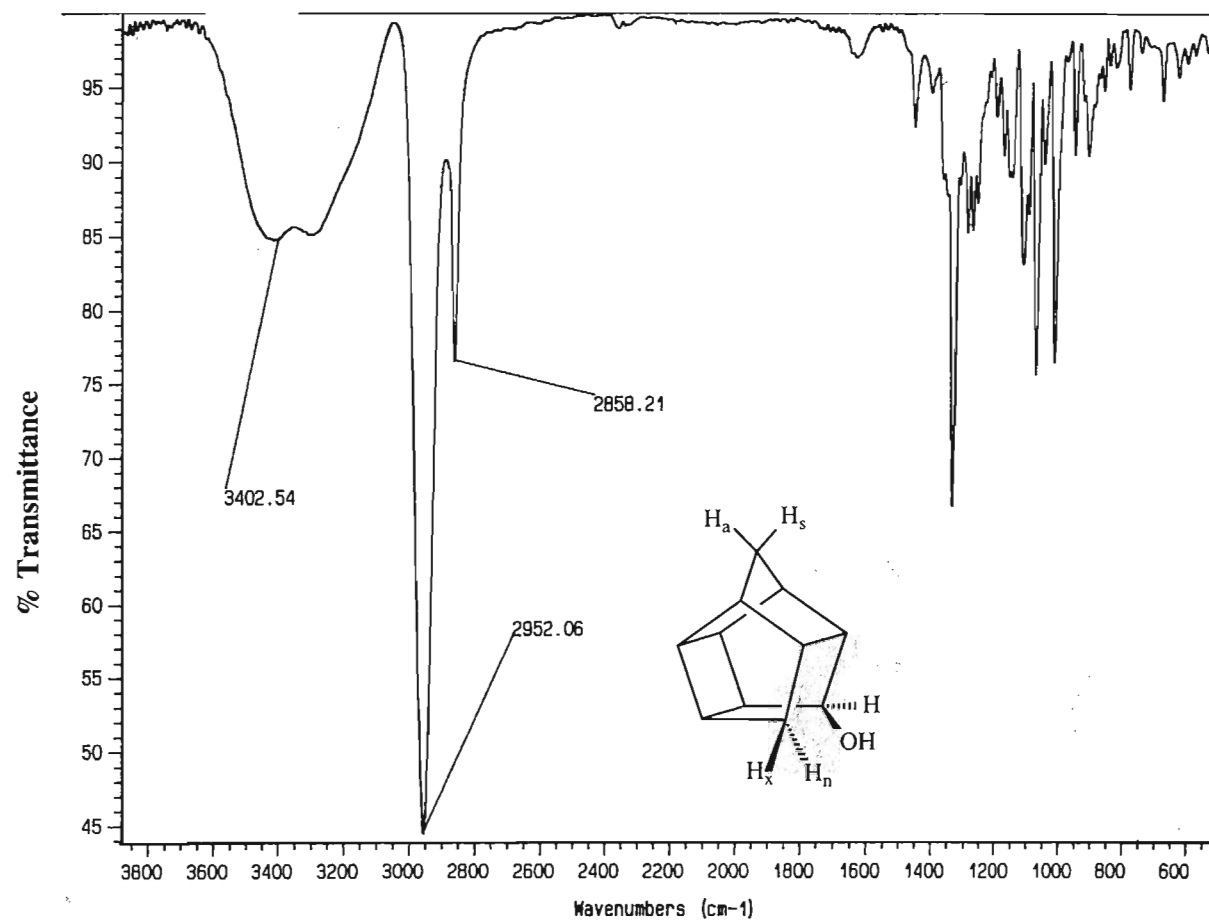
Spectrum 15: Infrared spectrum (KBr) of the hydroxy-ketone (2.40)



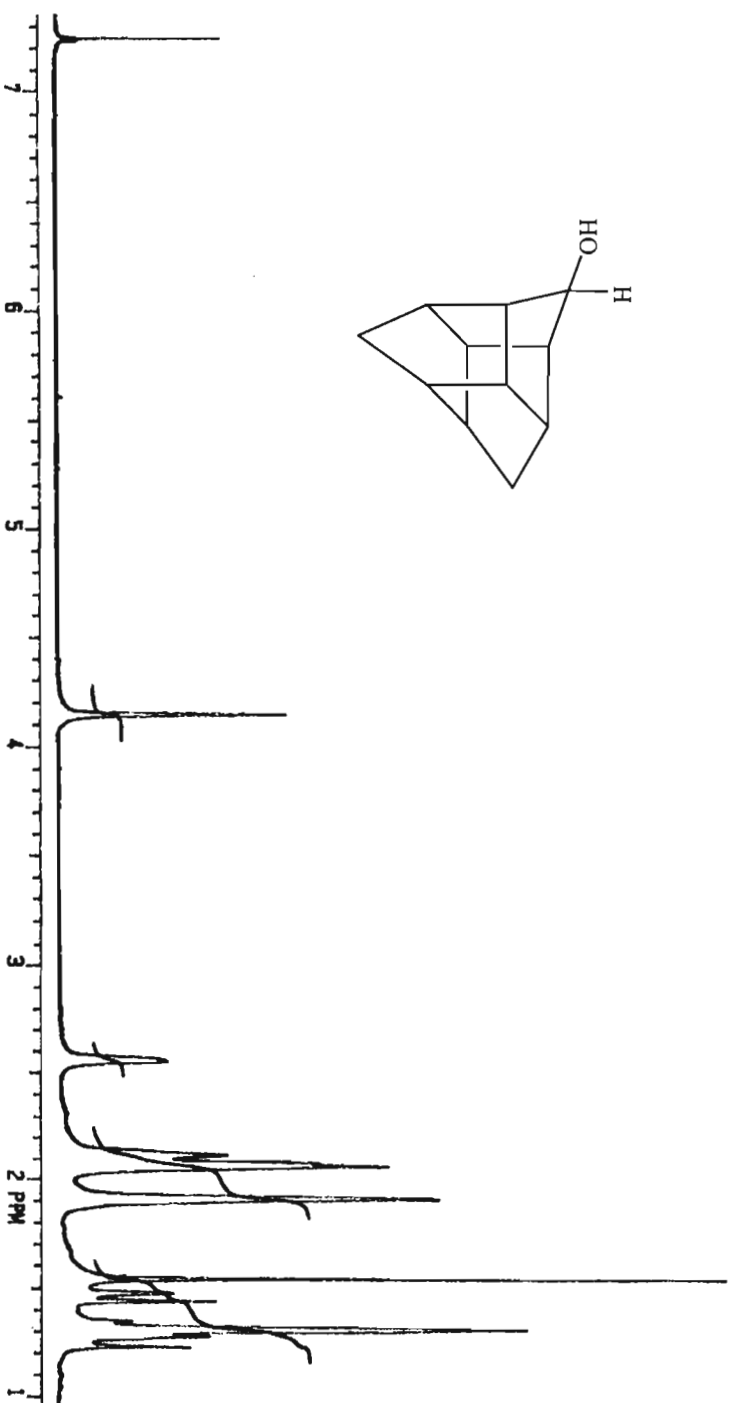
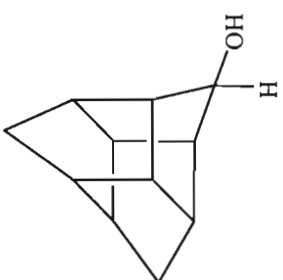
Spectrum 16: ^1H NMR spectrum of the *endo*-PCU alcohol in CDCl_3 (2.46)



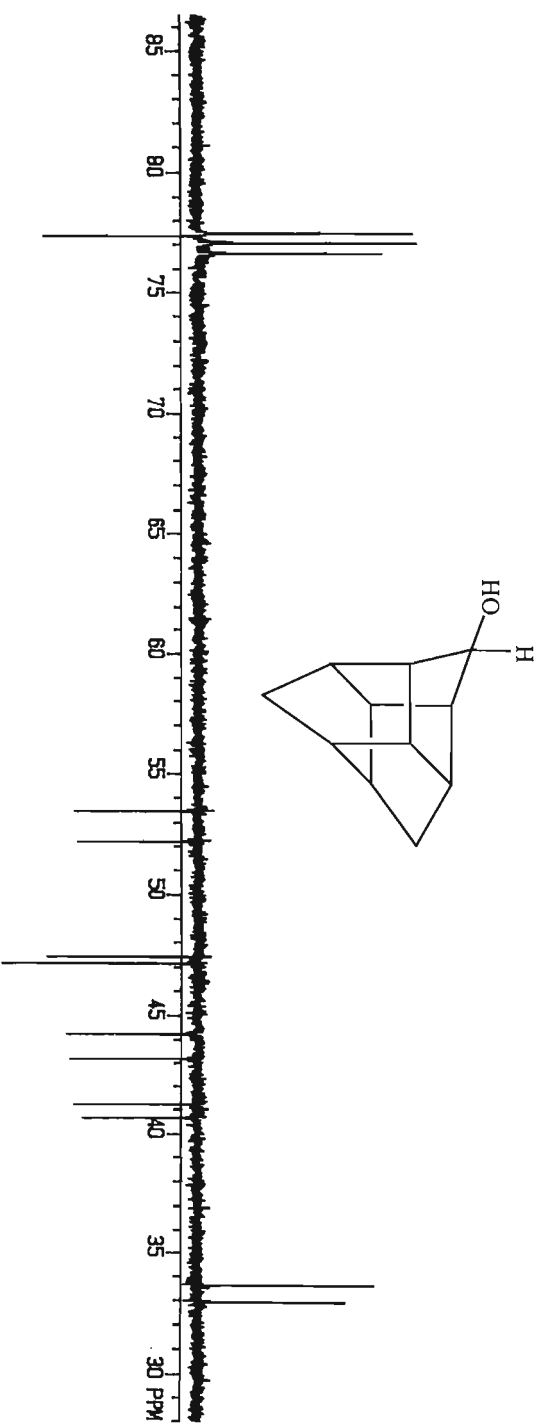
Spectrum 17: ^{13}C NMR spectrum of the *endo*-PCU alcohol in CDCl_3 (2.46)



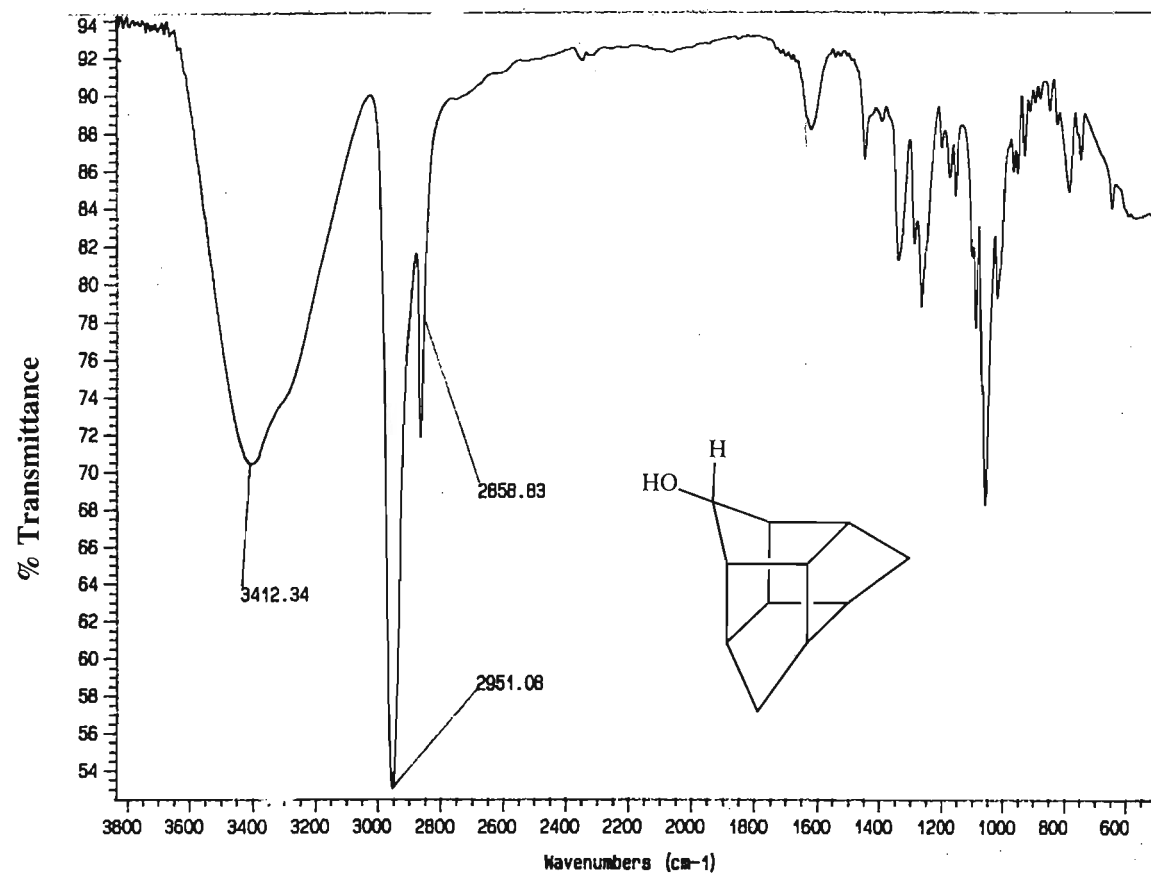
Spectrum 18: Infrared spectrum (KBr) of the *endo*-PCU alcohol (2.46)



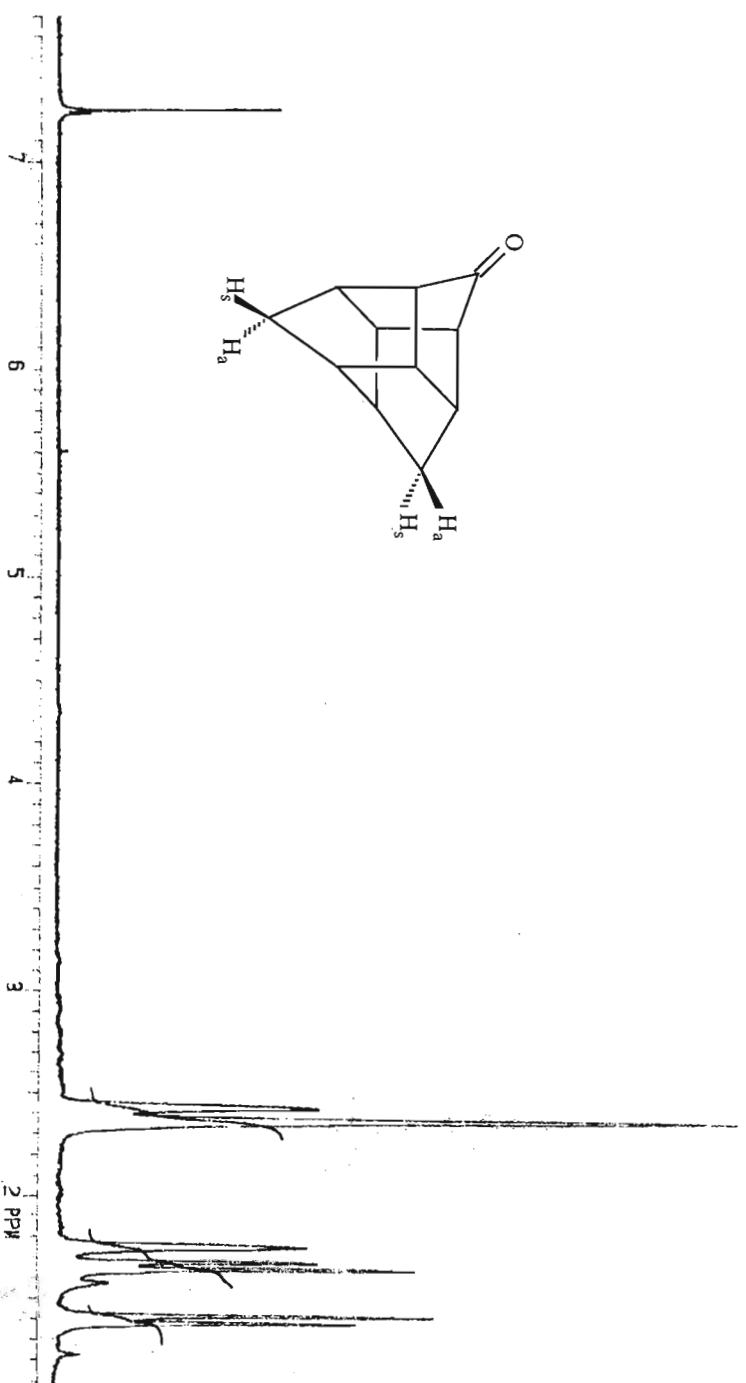
Spectrum 19: ^1H NMR spectrum of trishomocuban-4-ol in CDCl_3 (2.53)



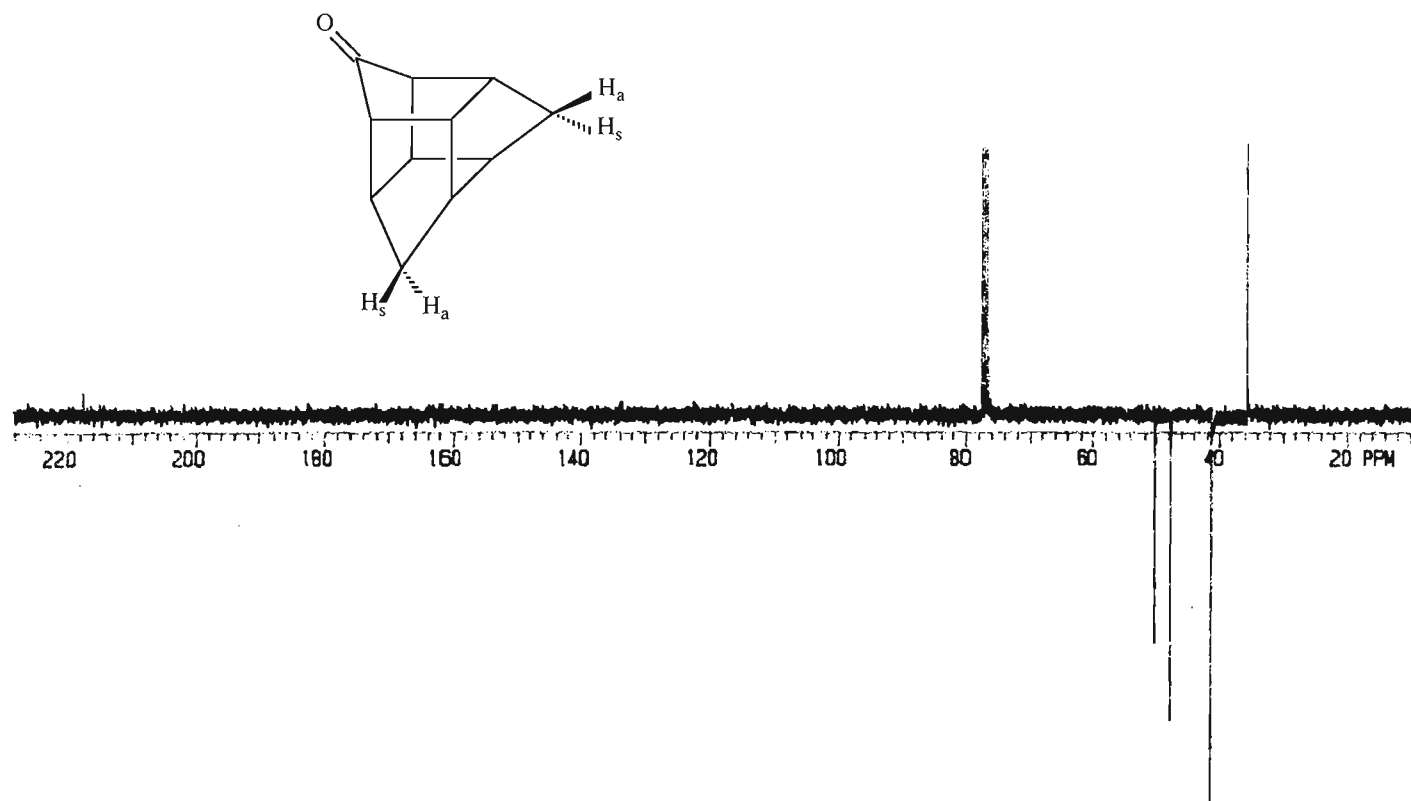
Spectrum 20: ^{13}C NMR spectrum of trishomocuban-4-ol in CDCl_3 (2.53)



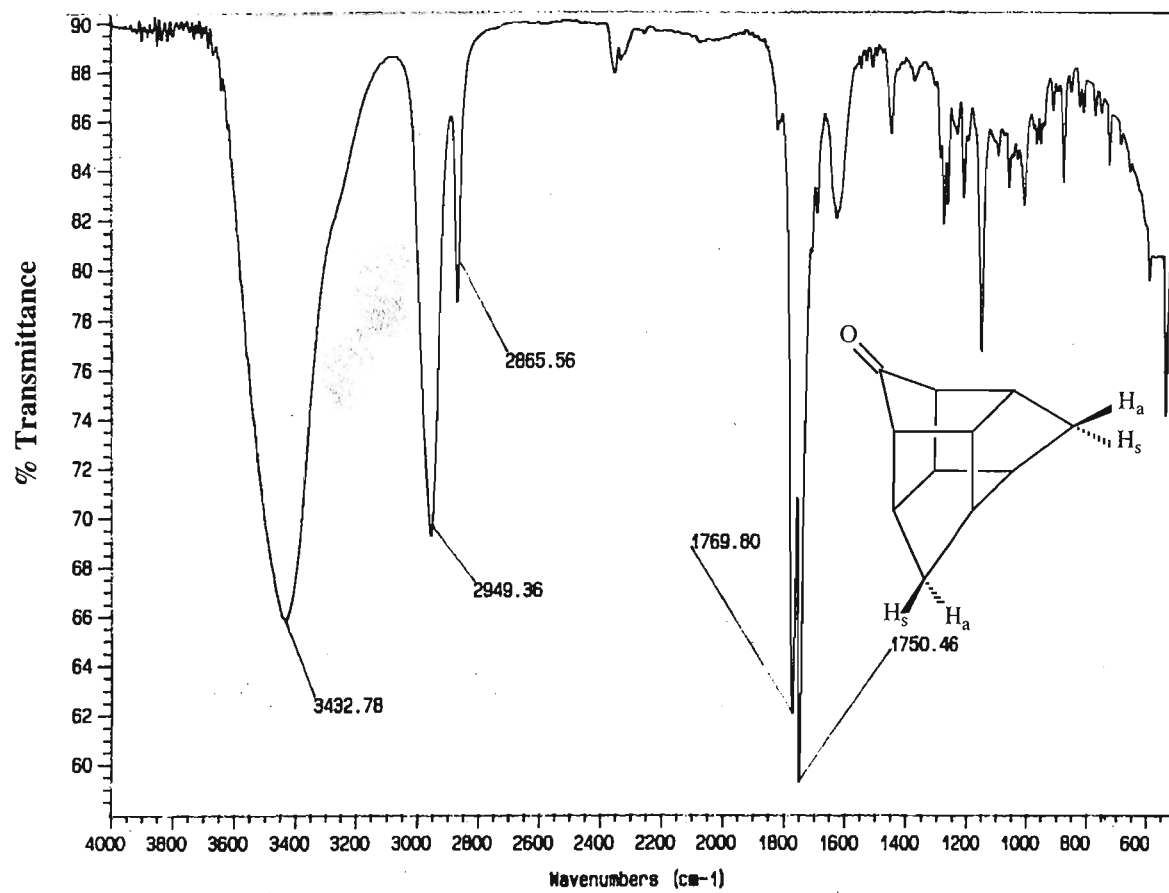
Spectrum 21: Infrared spectrum (KBr) of trishomocuban-4-ol (2.53)



Spectrum 22: ^1H NMR spectrum of trishomocubaneone in CDCl_3 (2.55)

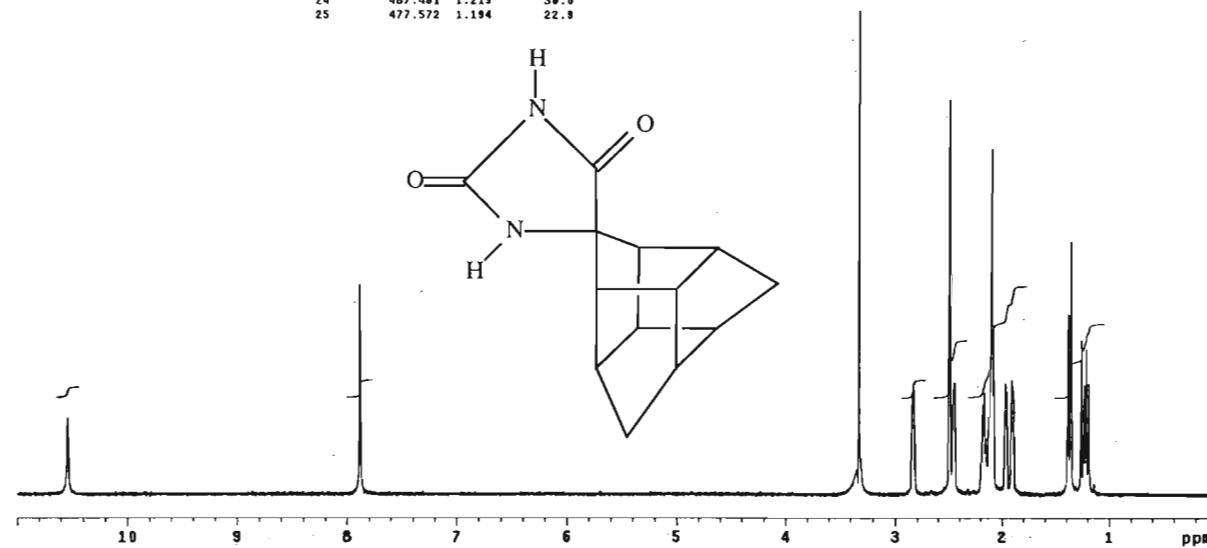


Spectrum 23: ^{13}C NMR spectrum of trishomocubanone in CDCl_3 (2.55)

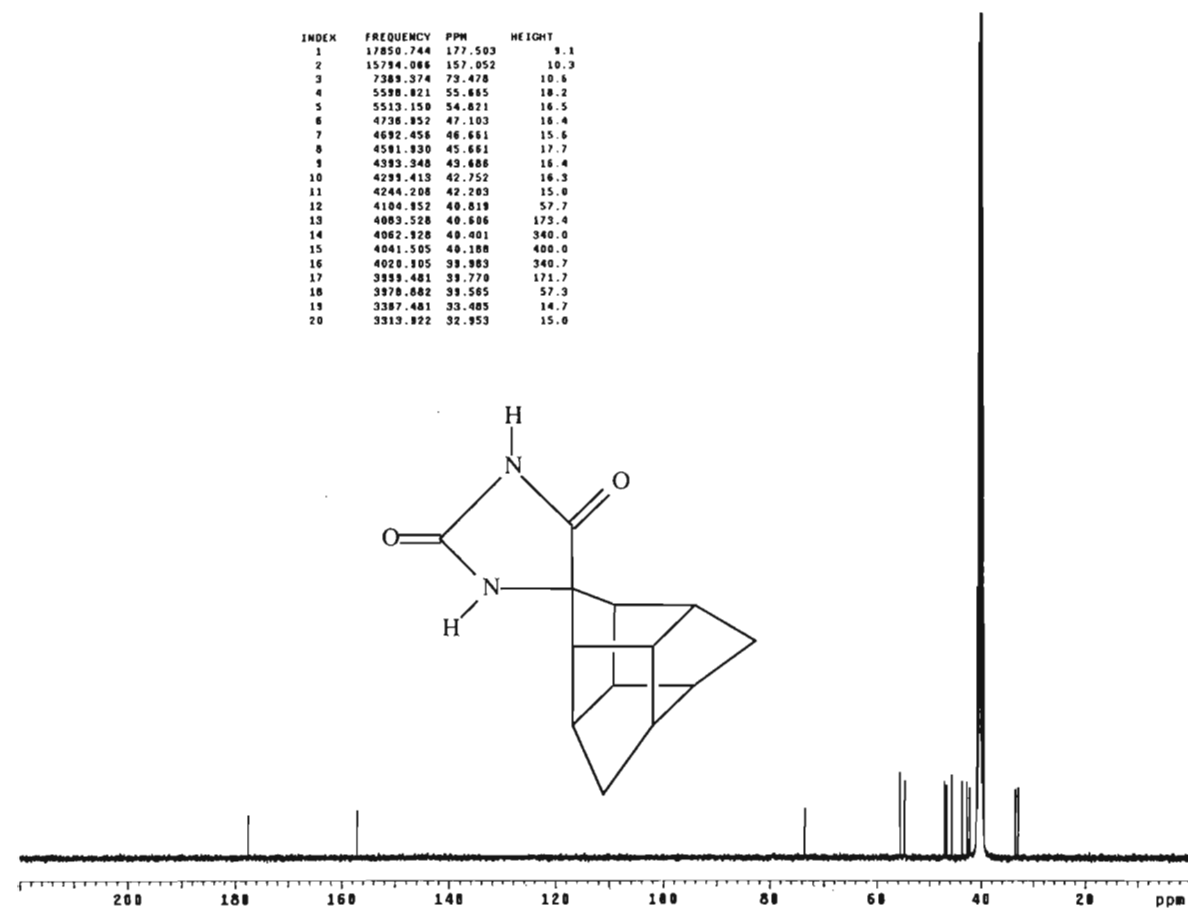


Spectrum 24: Infrared spectrum (KBr) of trishomocubanone (2.55)

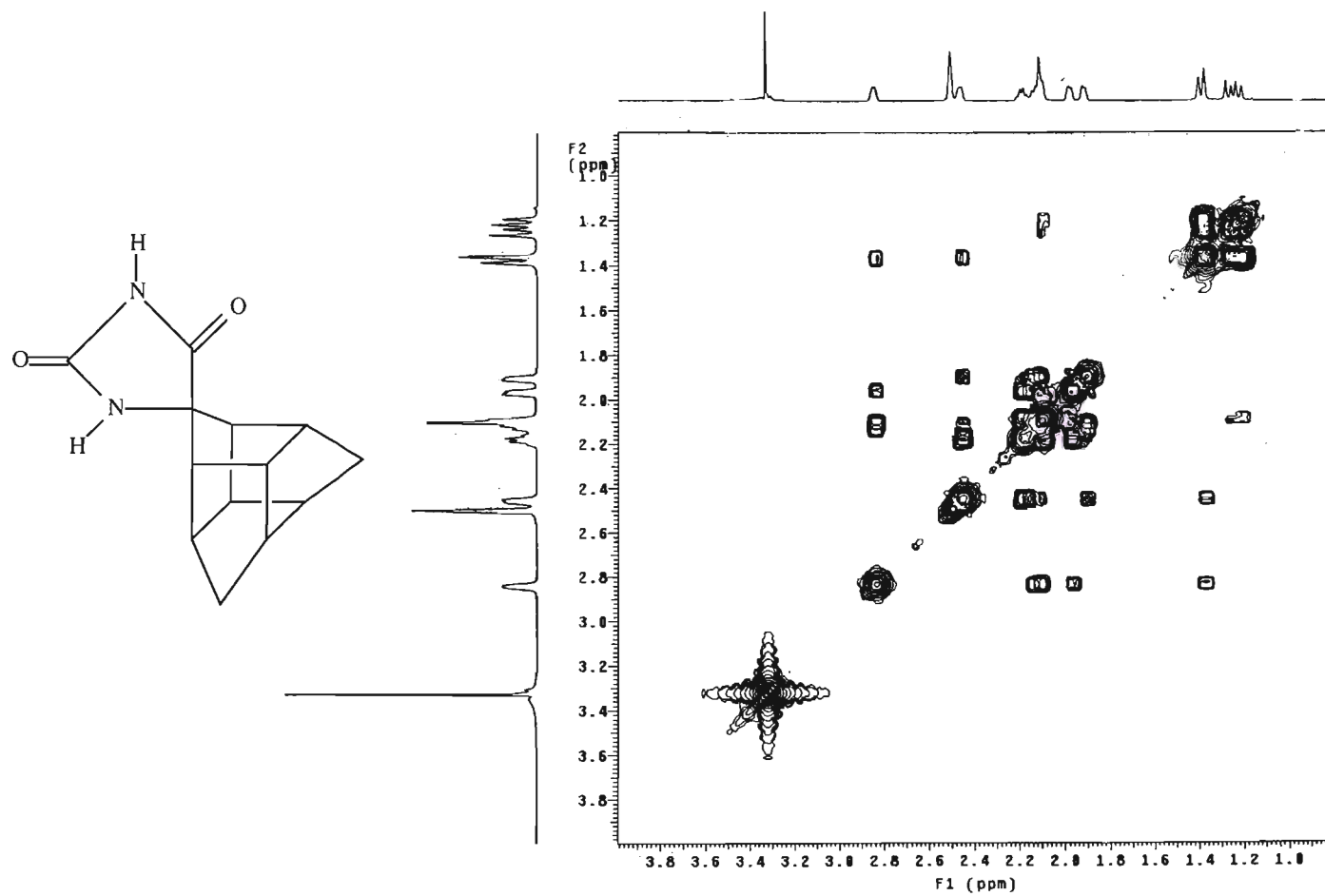
INDEX	FREQUENCY	PPM	HEIGHT
1	4216.708	10.543	15.8
2	3152.543	7.882	43.2
3	1331.595	3.328	100.0
4	1330.589	3.327	95.9
5	1328.391	3.321	12.7
6	1136.655	2.842	22.8
7	998.857	2.500	81.6
8	978.347	2.449	23.0
9	980.079	2.451	23.2
10	874.414	2.186	18.4
11	868.553	2.172	21.0
12	868.920	2.179	21.1
13	863.249	2.158	19.2
14	852.621	2.132	16.1
15	846.578	2.117	24.3
16	840.901	2.103	71.4
17	789.808	1.975	22.9
18	784.497	1.962	21.1
19	783.620	1.959	23.6
20	554.853	1.387	37.2
21	544.598	1.362	52.0
22	505.957	1.285	31.8
23	495.702	1.239	22.7
24	487.461	1.219	38.9
25	477.572	1.194	22.9



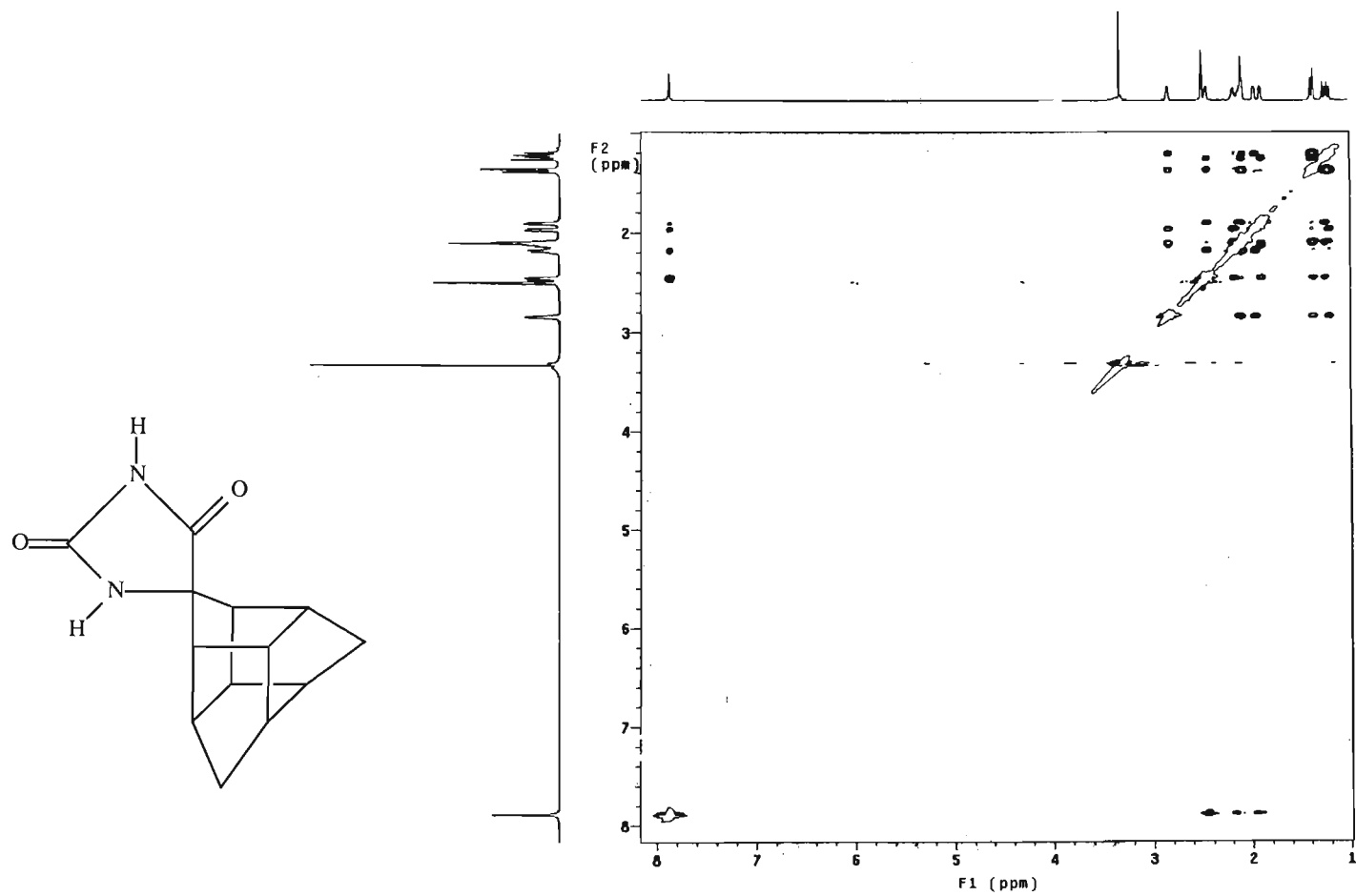
Spectrum 25: ^1H NMR spectrum of tris-hydantoin in $[(\text{CD}_3)_2\text{SO}]$ (2.12)



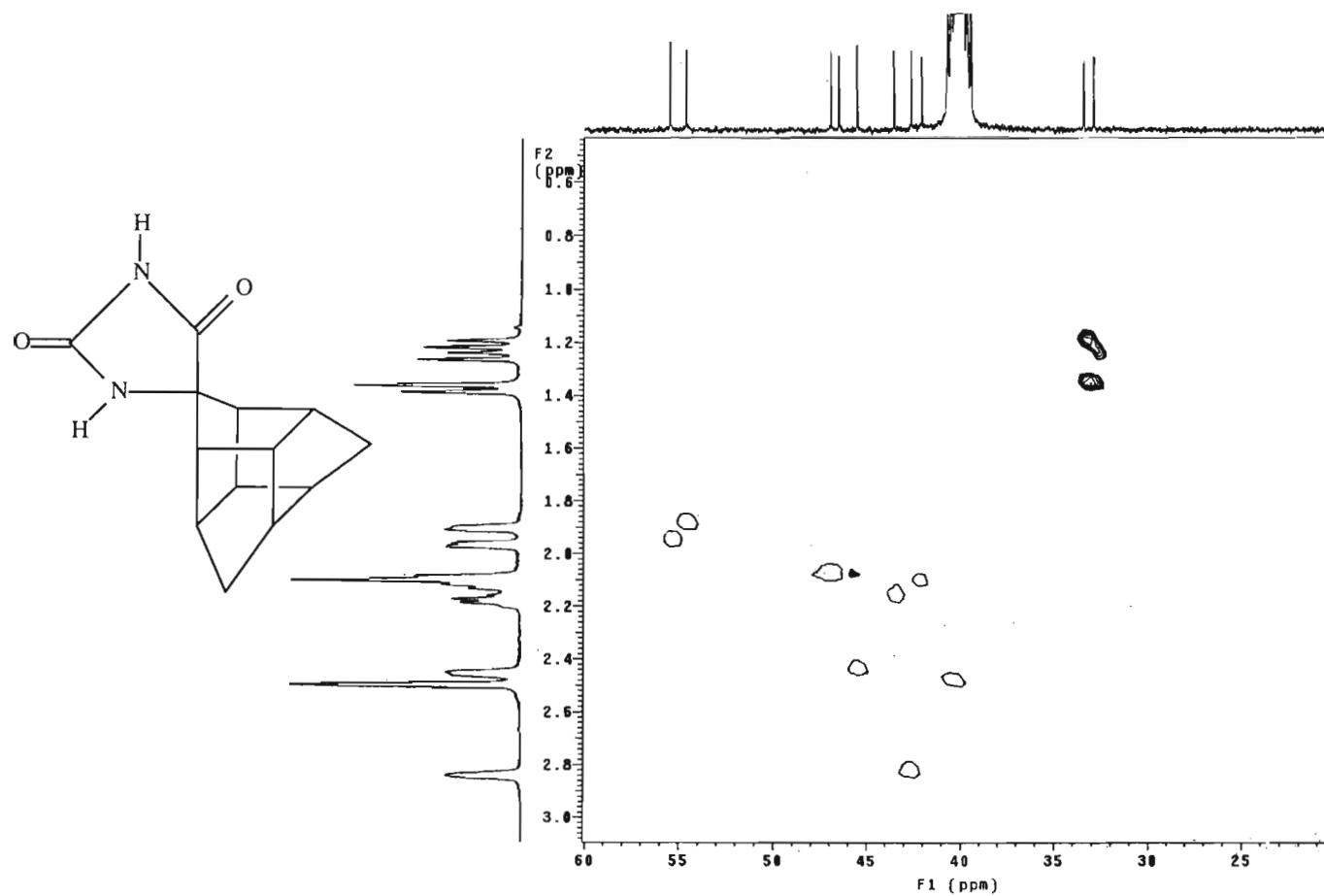
Spectrum 26: ^{13}C NMR spectrum of tris-hydantoin in $[(\text{CD}_3)_2\text{SO}]$ (2.12)



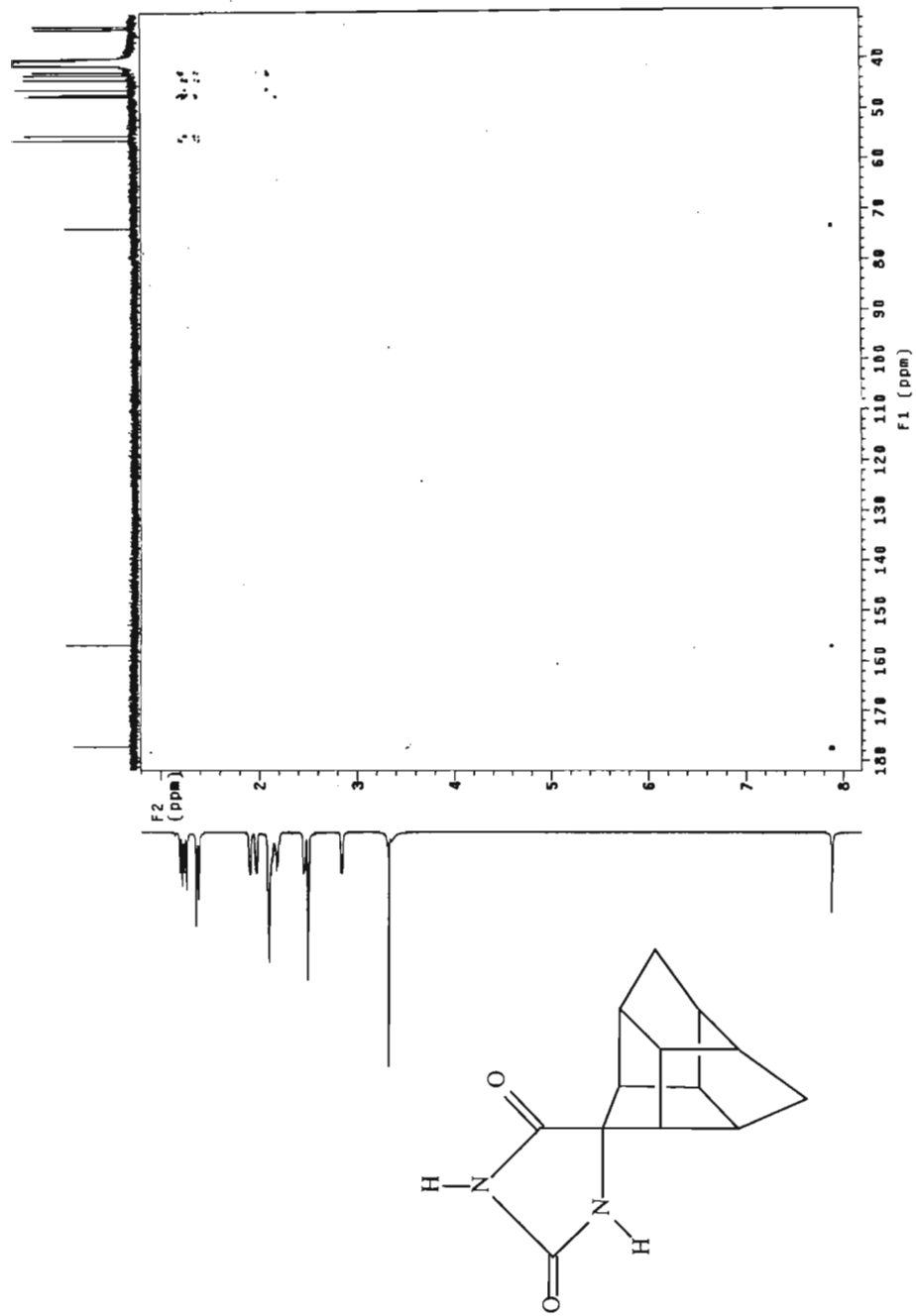
Spectrum 27: COSY spectrum of tris-hydantoin in $[(\text{CD}_3)_2\text{SO}]$ (2.12)

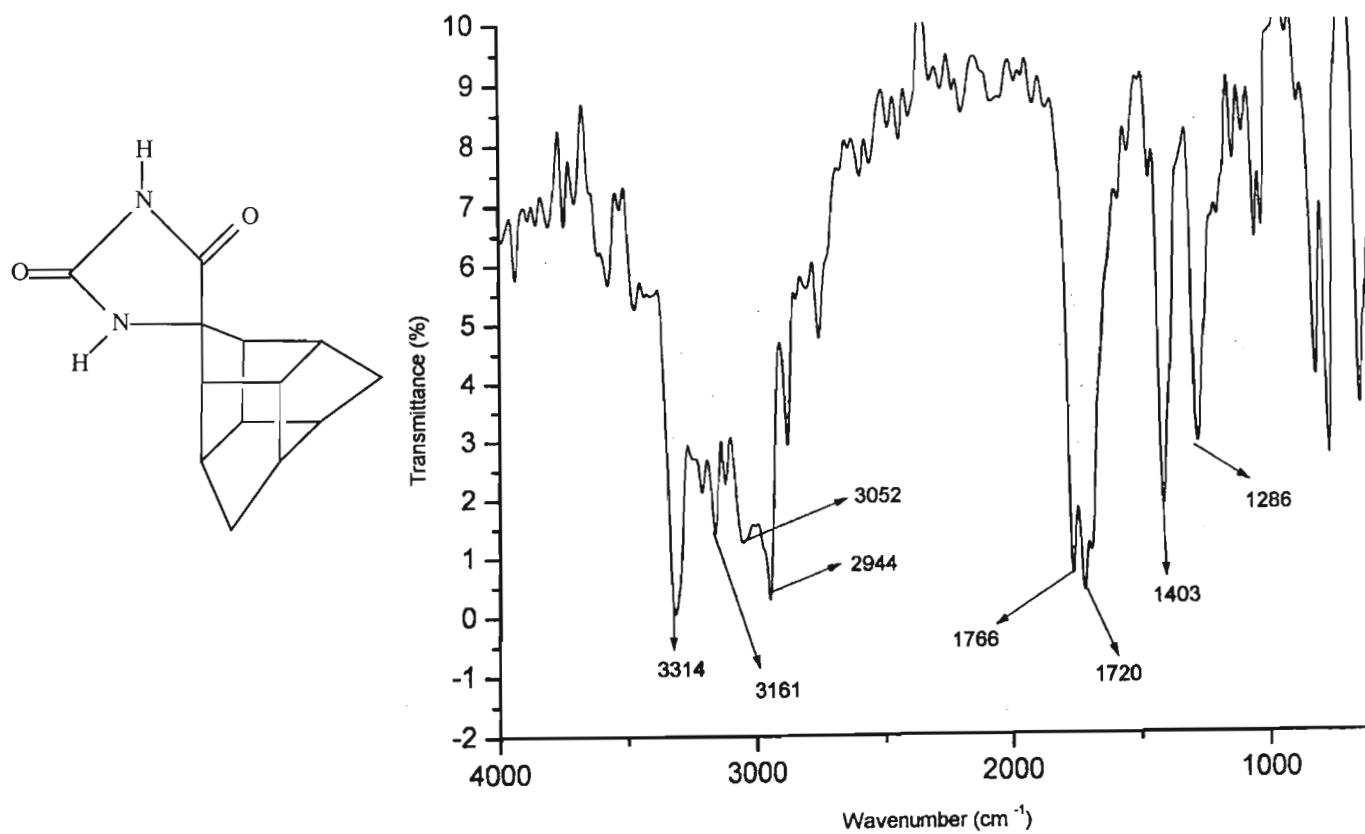


Spectrum 28: NOESY spectrum of tris-hydantoin in $[(\text{CD}_3)_2\text{SO}]$ (2.12)

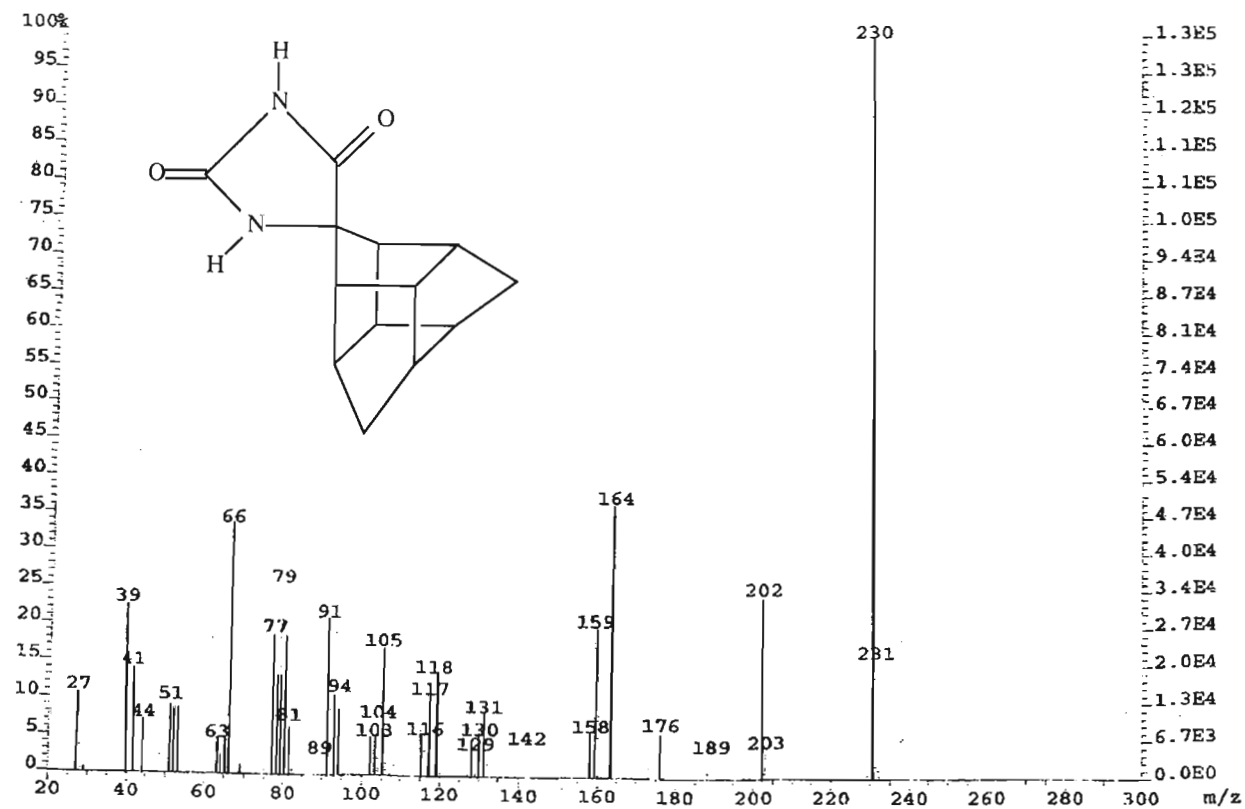


Spectrum 29: HSQC spectrum of tris-hydantoin in $[(\text{CD}_3)_2\text{SO}]$ (2.12)

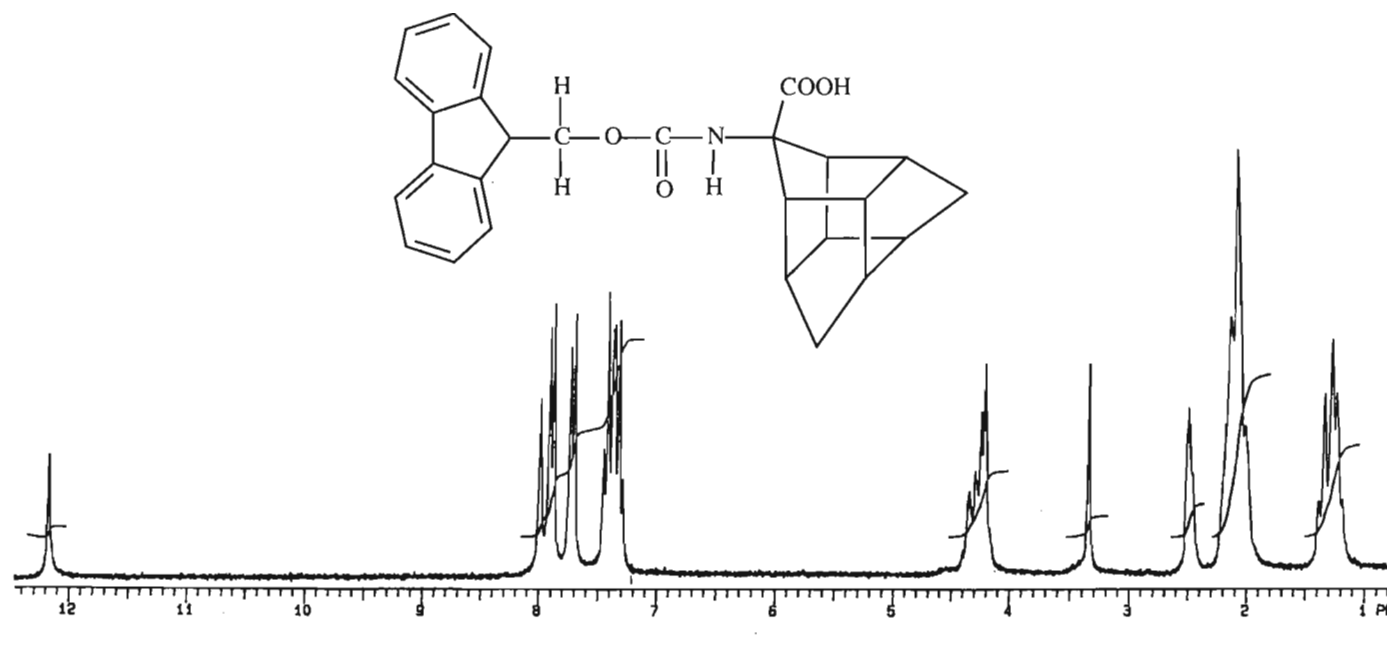




Spectrum 31: Infrared spectrum (KBr) of tris-hydantoin (2.12)

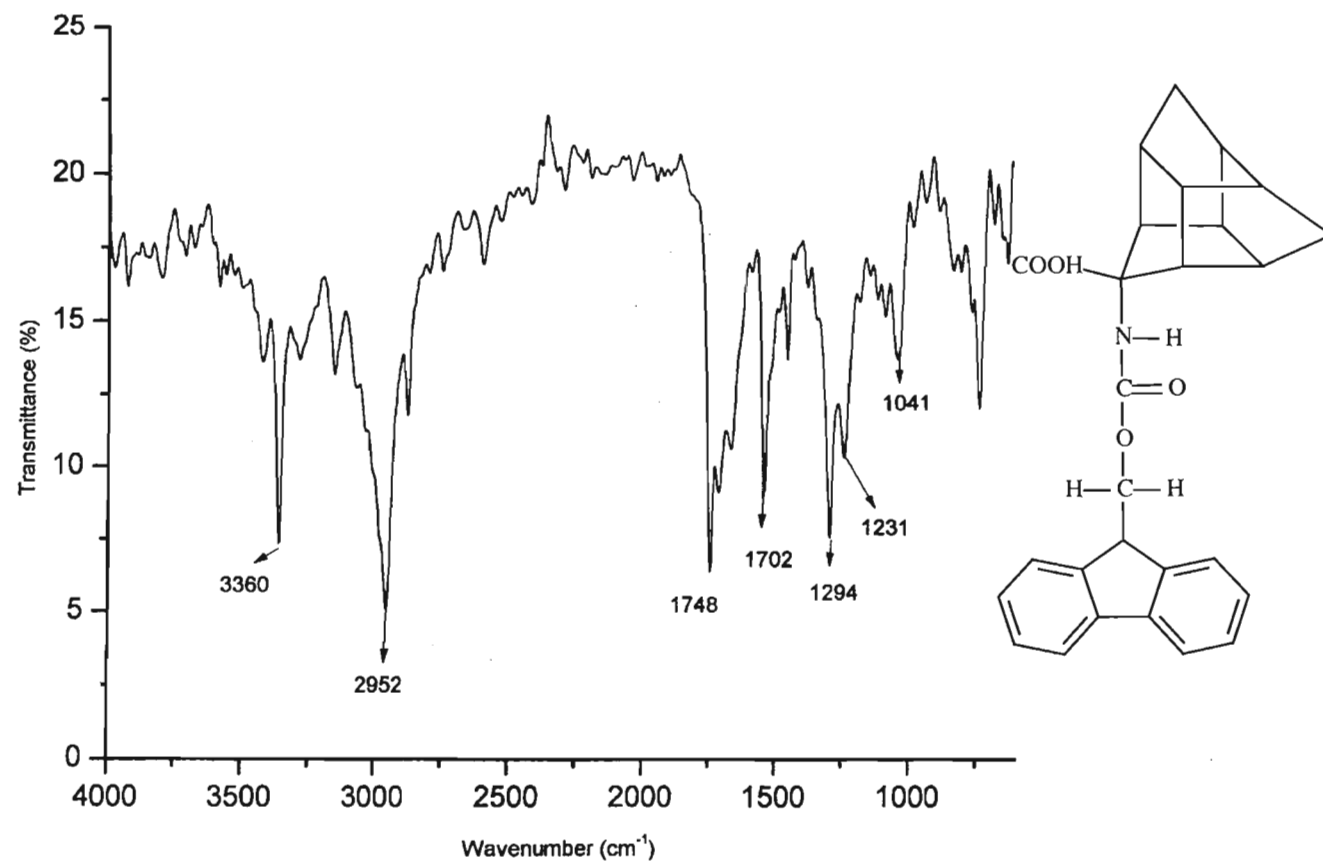


Spectrum 32: Mass spectrum (MS-TOF) of tris-hydantoin (2.12)

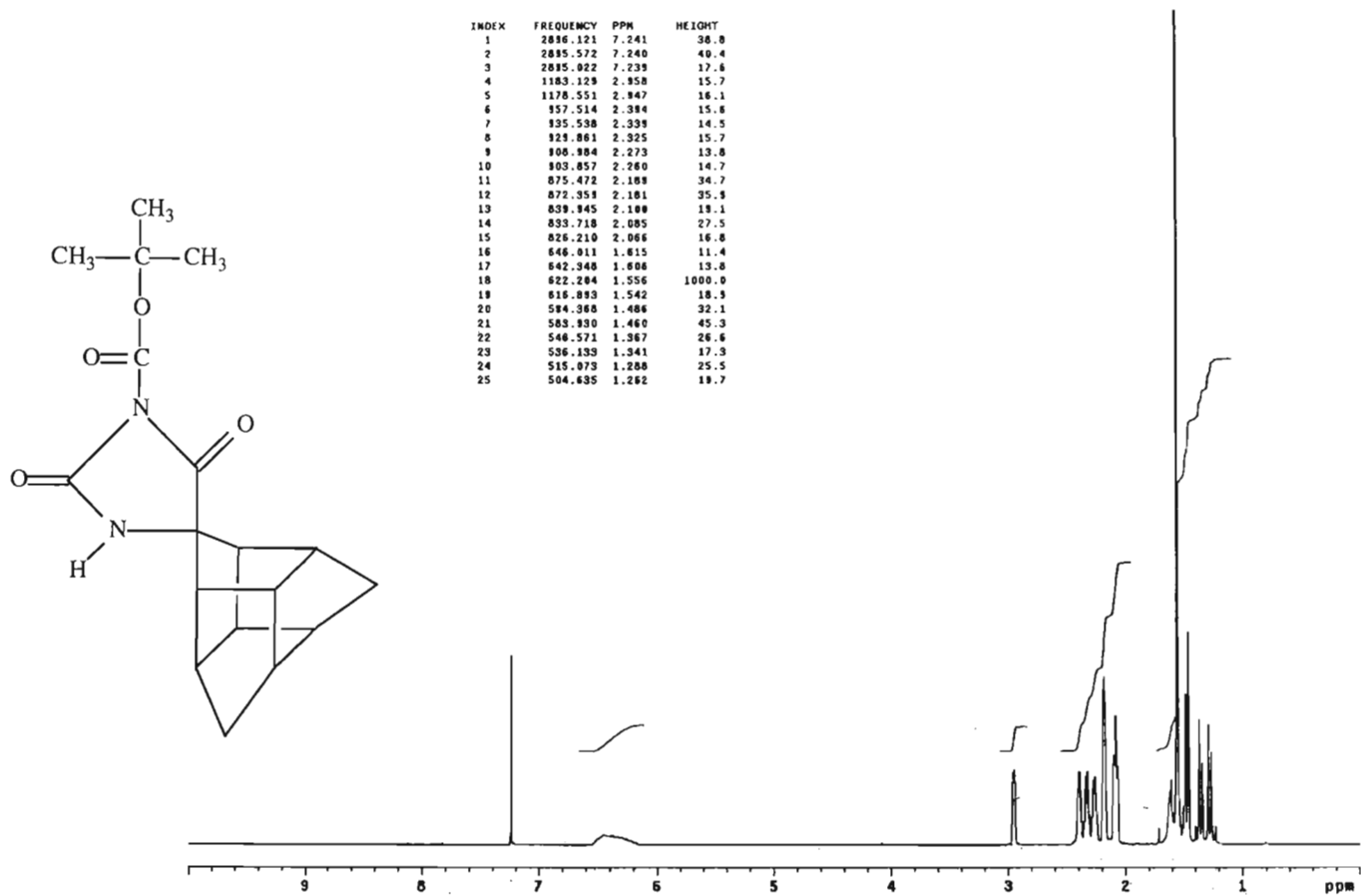


Spectrum 34: ^1H NMR spectrum of Fmoc-tris-amino acid in $[(\text{CD}_3)_2\text{SO}]$ (2.65)



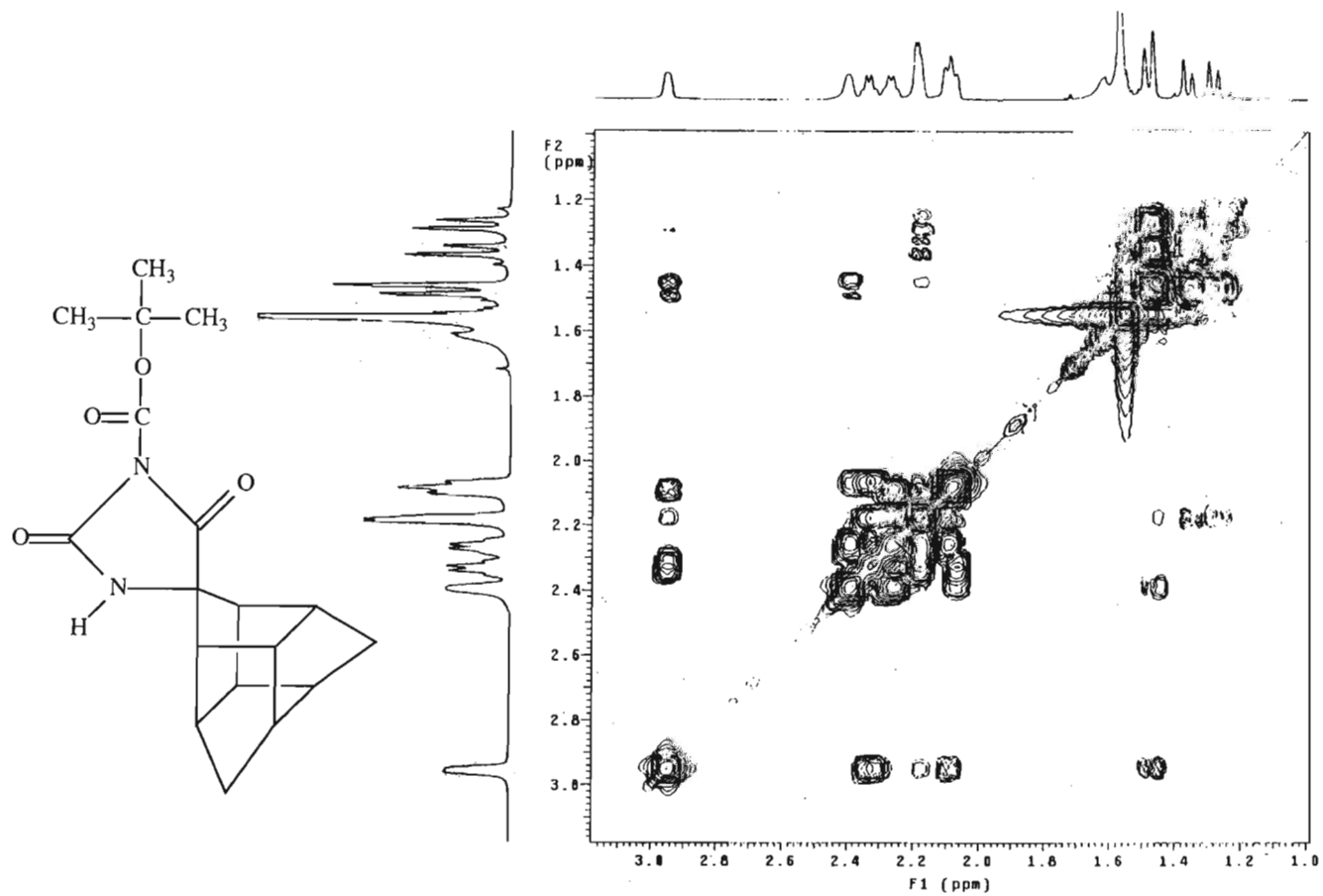


Spectrum 36: Infrared spectrum (KBr) of Fmoc-tris-amino acid (2.65)

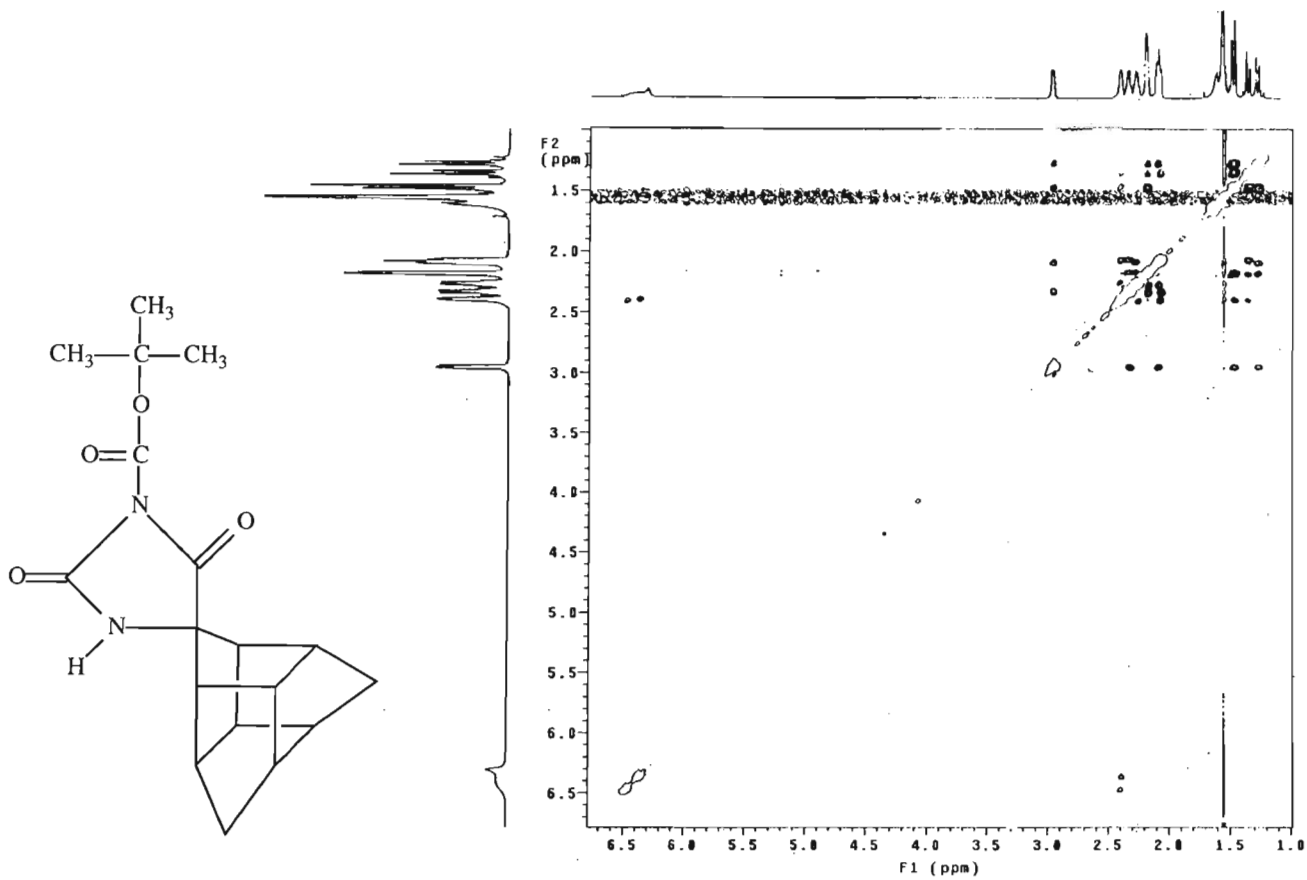


Spectrum 37: ^1H NMR spectrum of Novel Compound 1 in CDCl_3 (2.66)

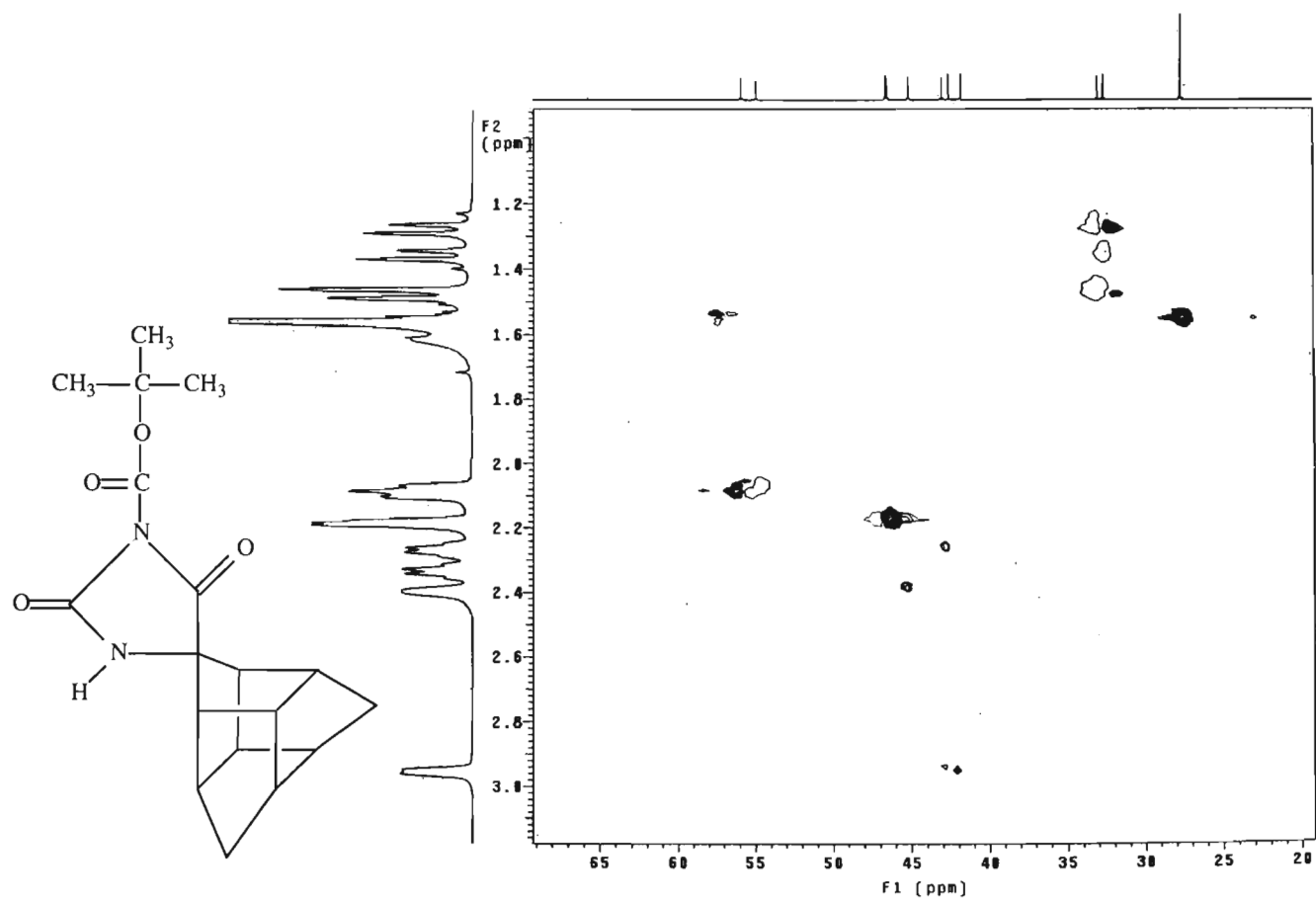
CC(C)OC(=O)N1C(=O)N(C23C4C1CC5C3C2CC6C4C5C7C6C)C(=O)N2



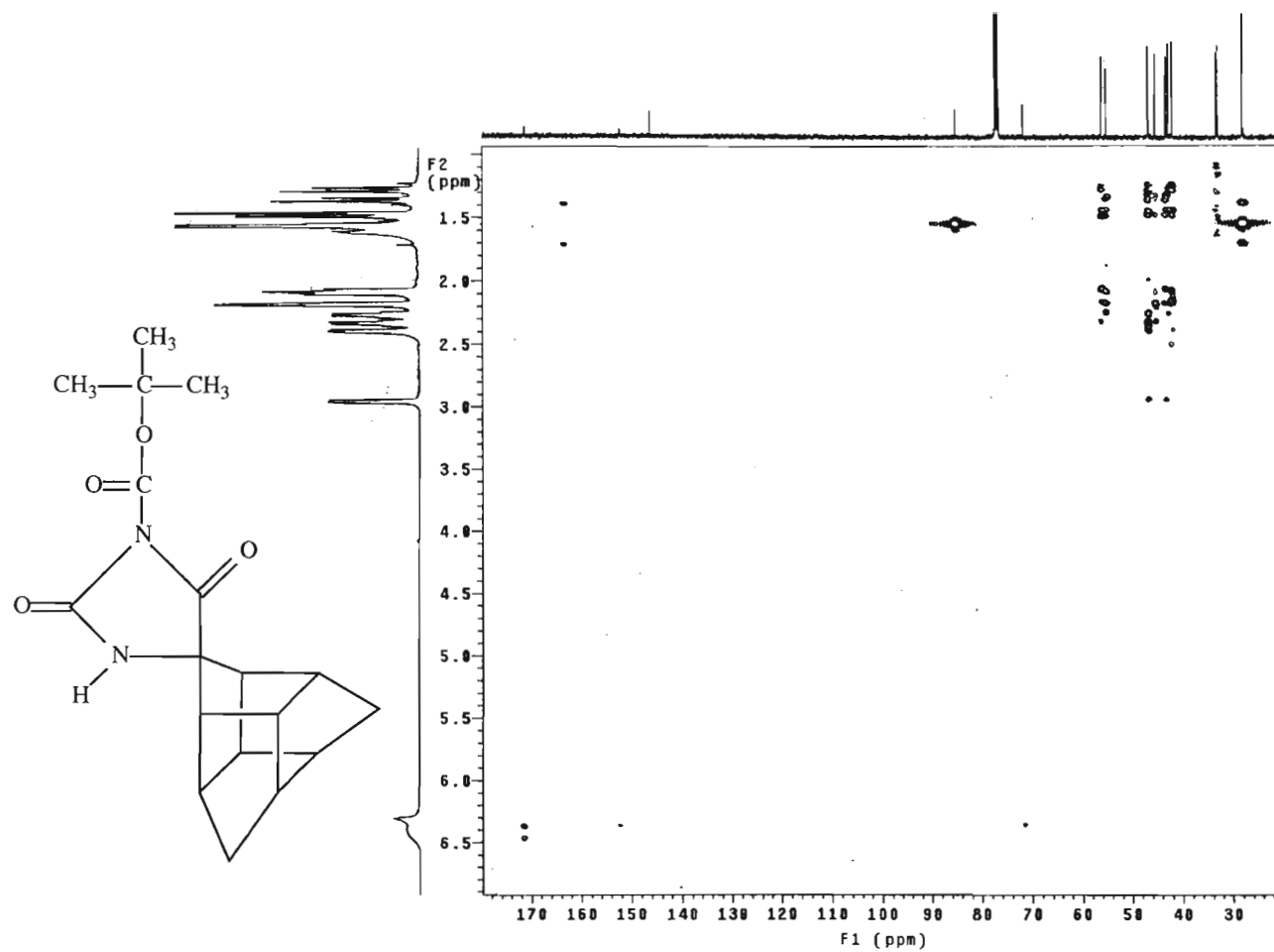
Spectrum 39: COSY spectrum of Novel Compound 1 in CDCl₃ (2.66)



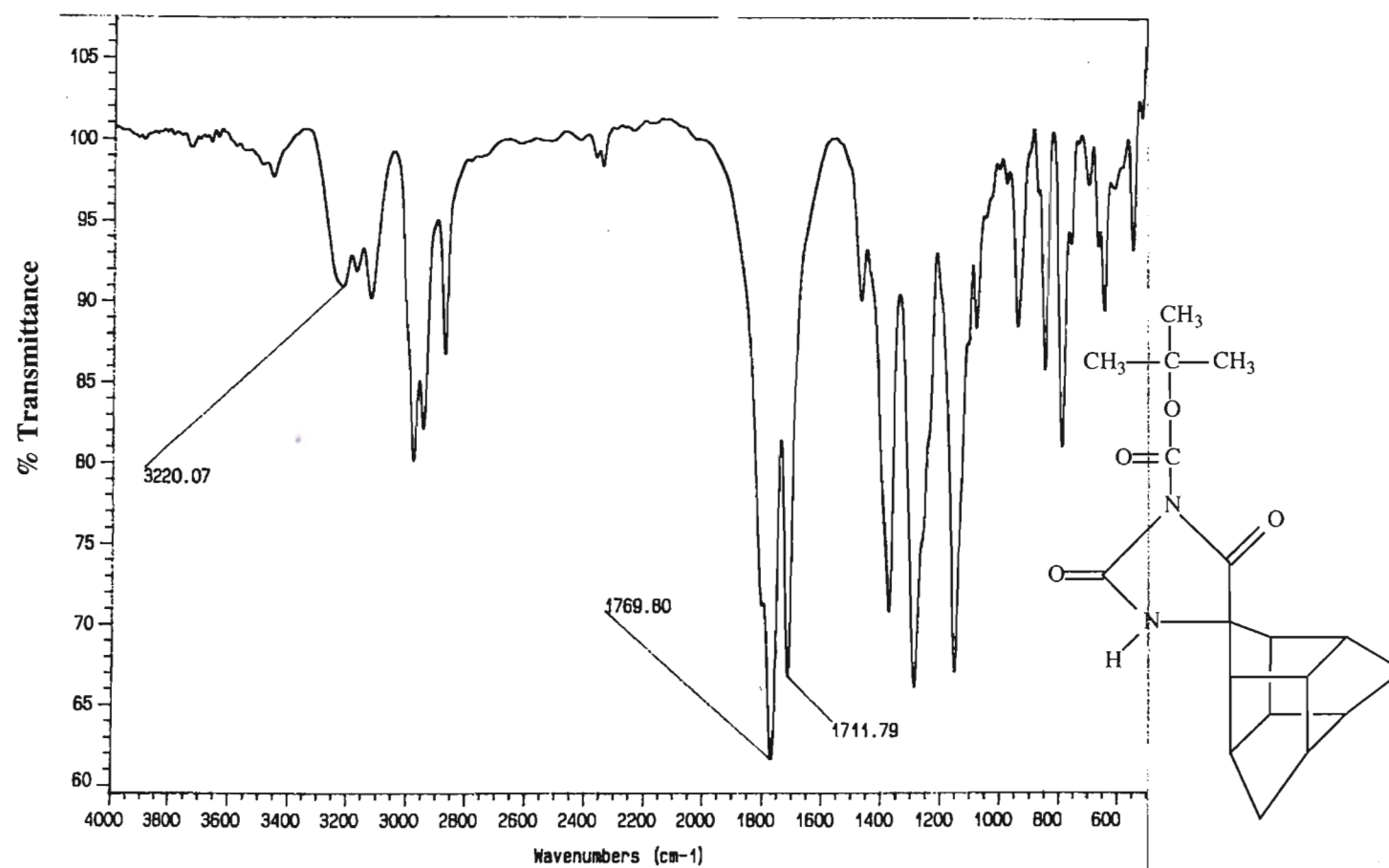
Spectrum 40: NOESY spectrum of Novel Compound 1 in CDCl₃ (2.66)



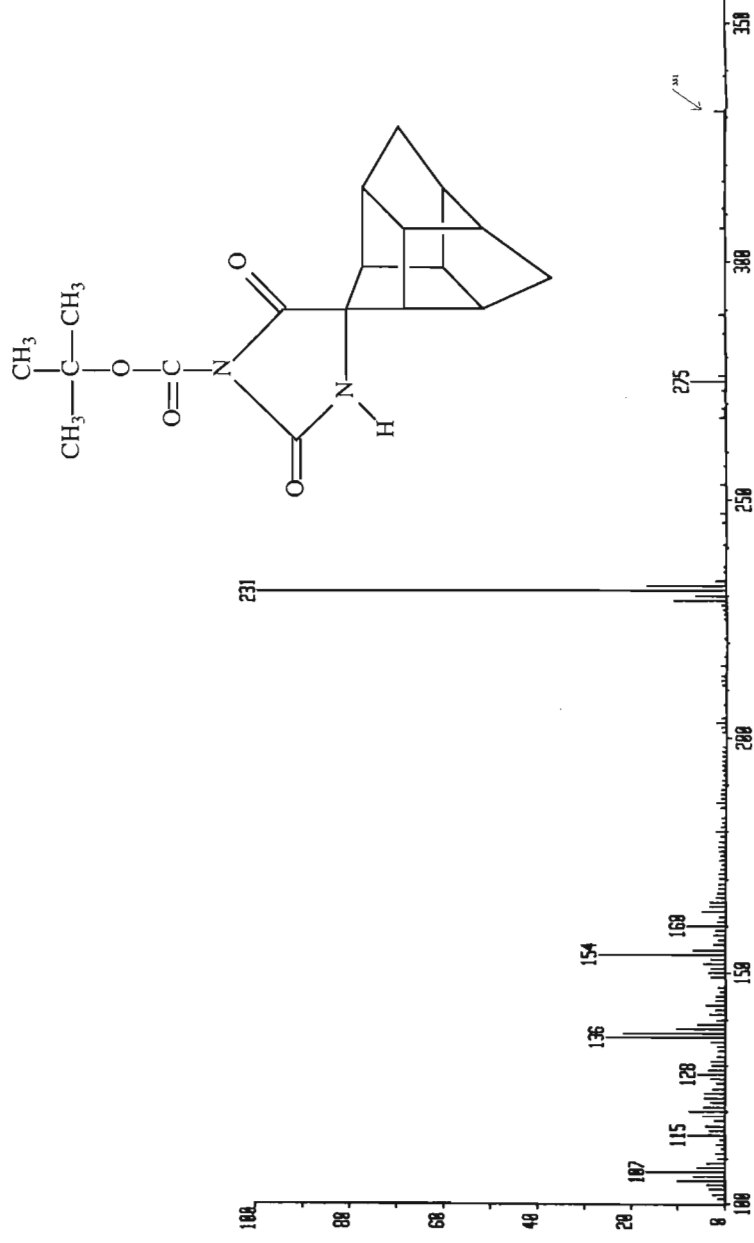
Spectrum 41: HSQC spectrum of Novel Compound 1 in CDCl_3 (2.66)



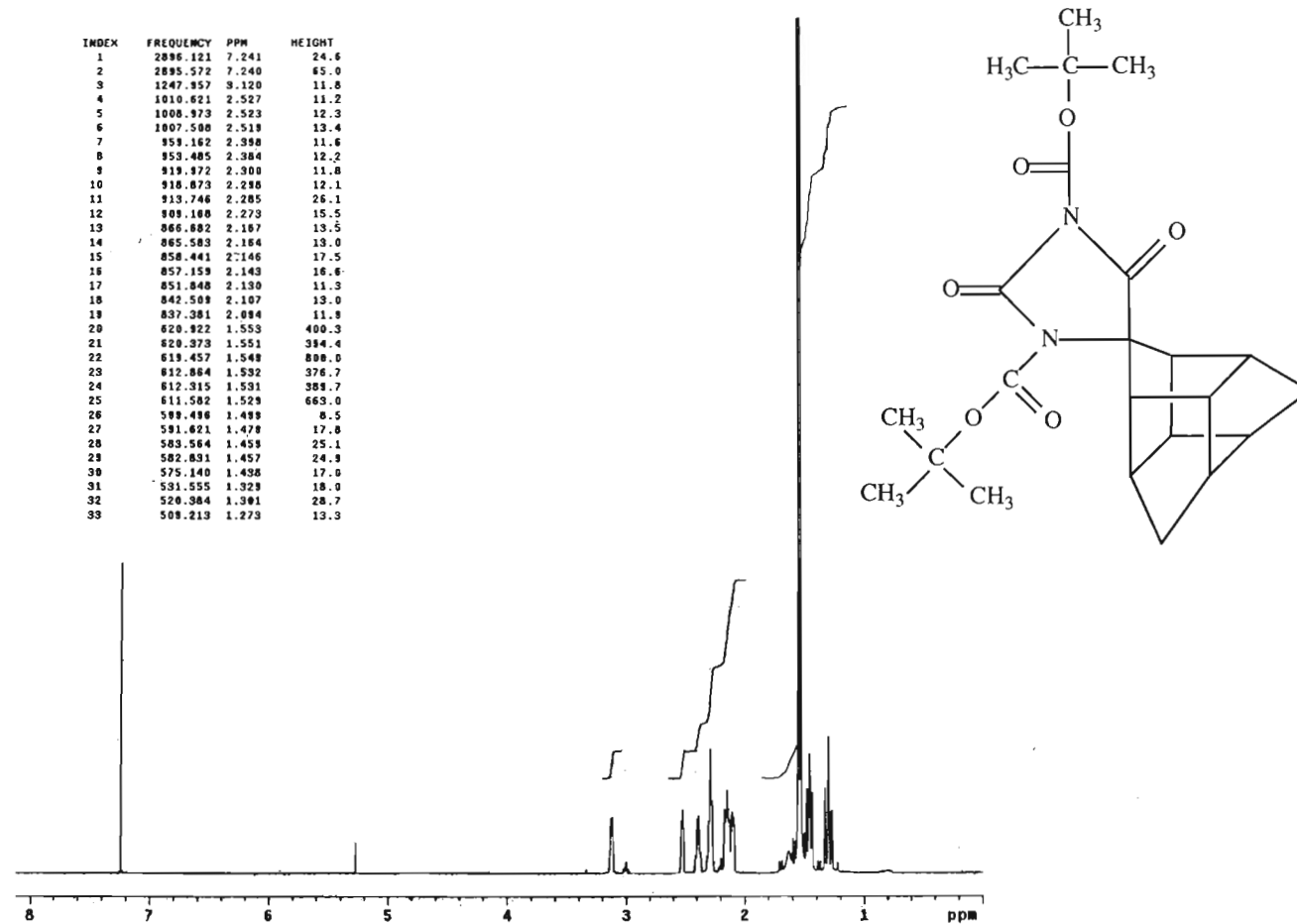
Spectrum 42: HMBC spectrum of Novel Compound 1 in CDCl_3 (2.66)



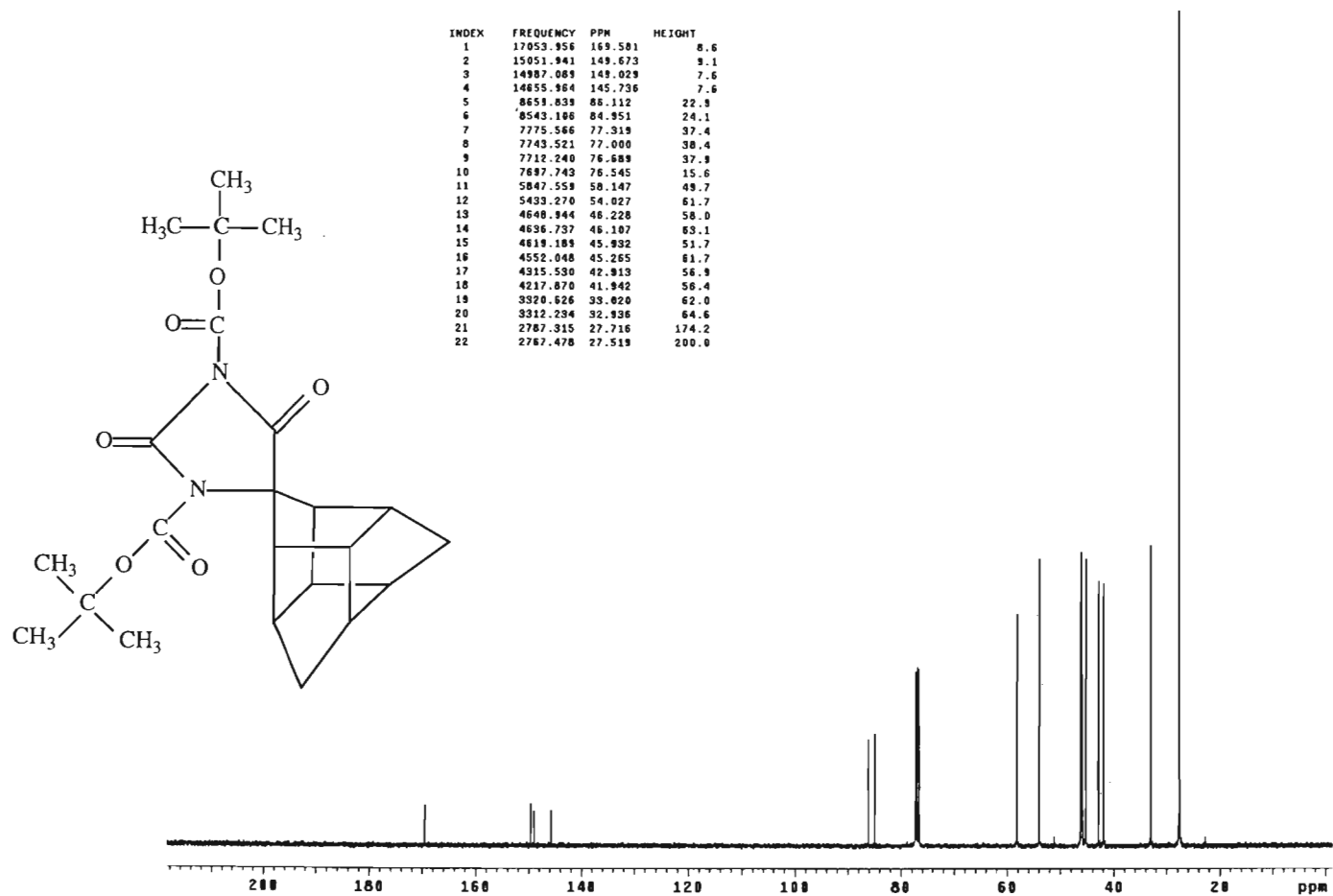
Spectrum 43: Infrared spectrum (KBr) of Novel Compound 1 (2.66)



Spectrum 44: Mass spectrum (FAB) of Novel Compound 1 (2.66)

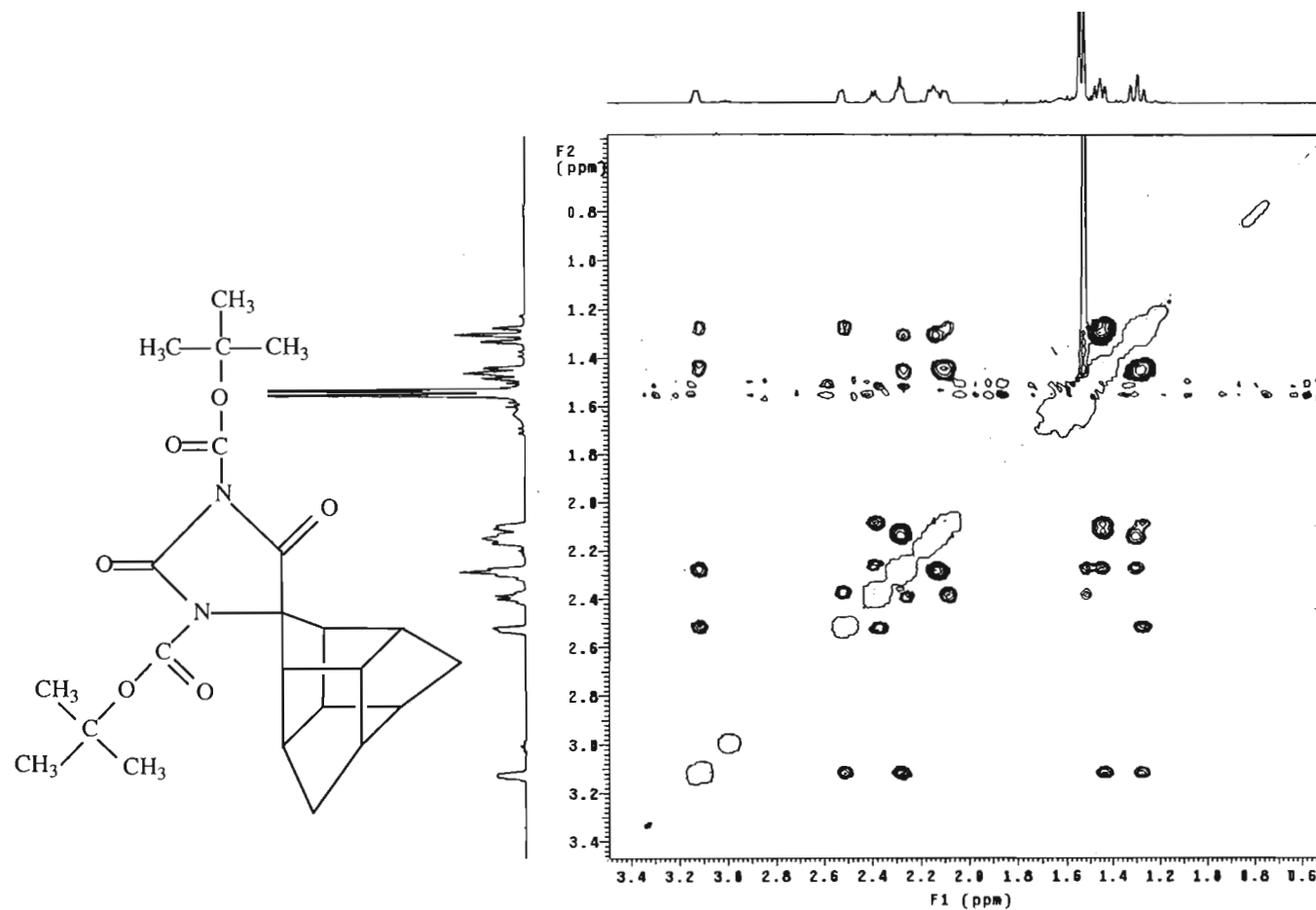


Spectrum 45: ¹H NMR spectrum of Novel Compound 2 in CDCl₃ (2.67)

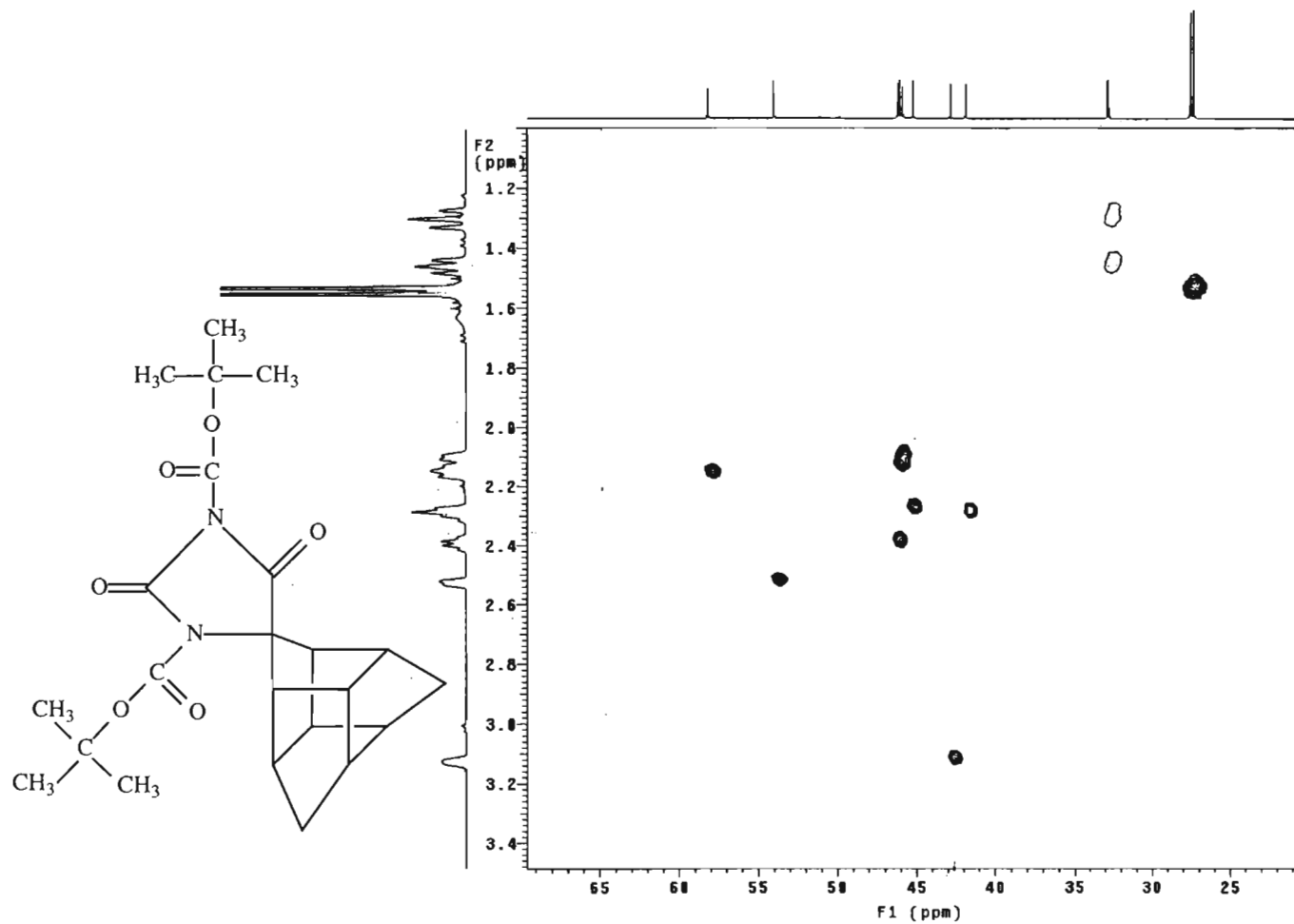


Spectrum 46: ^{13}C NMR spectrum of Novel Compound 2 (2.67)

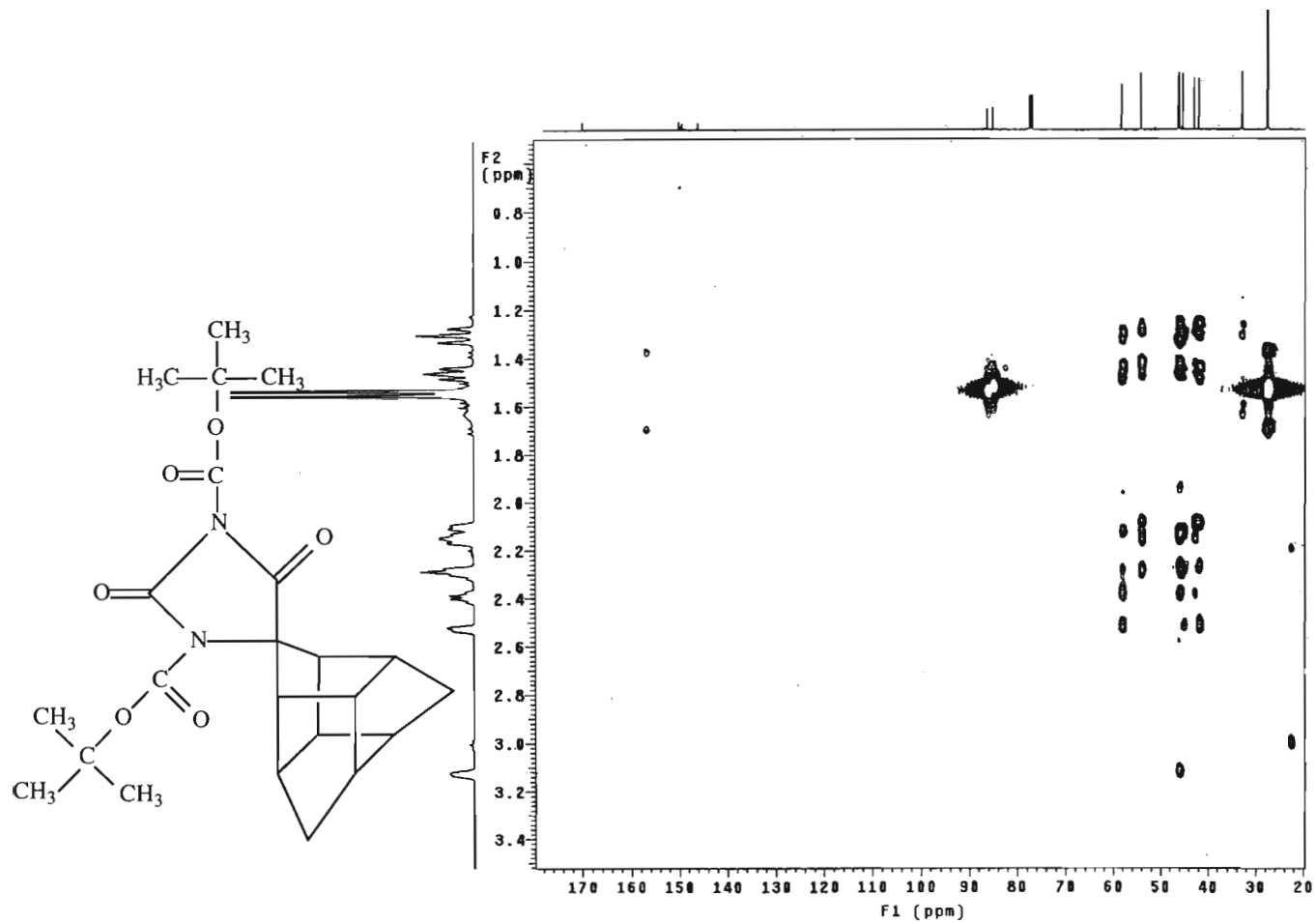




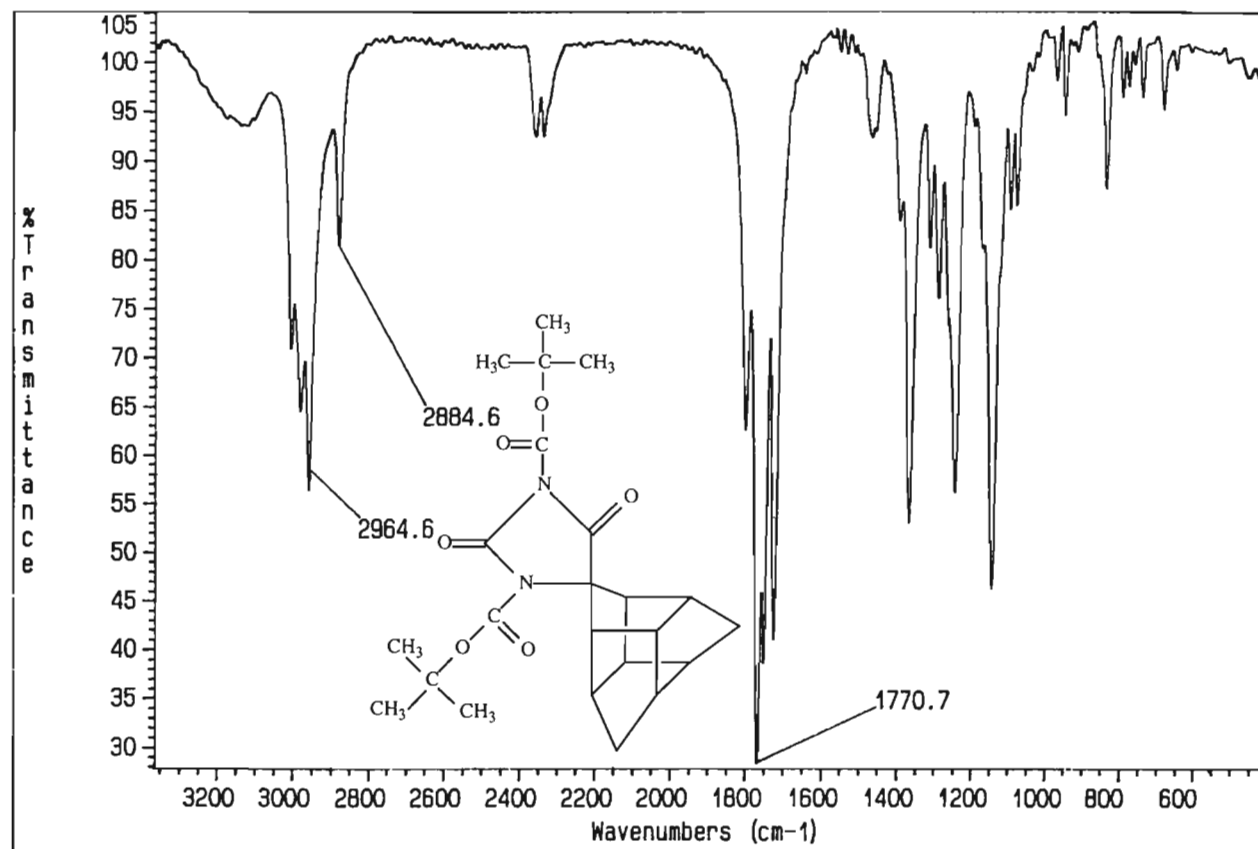
Spectrum 48: NOESY spectrum of Novel Compound 2 in CDCl₃ (2.67)



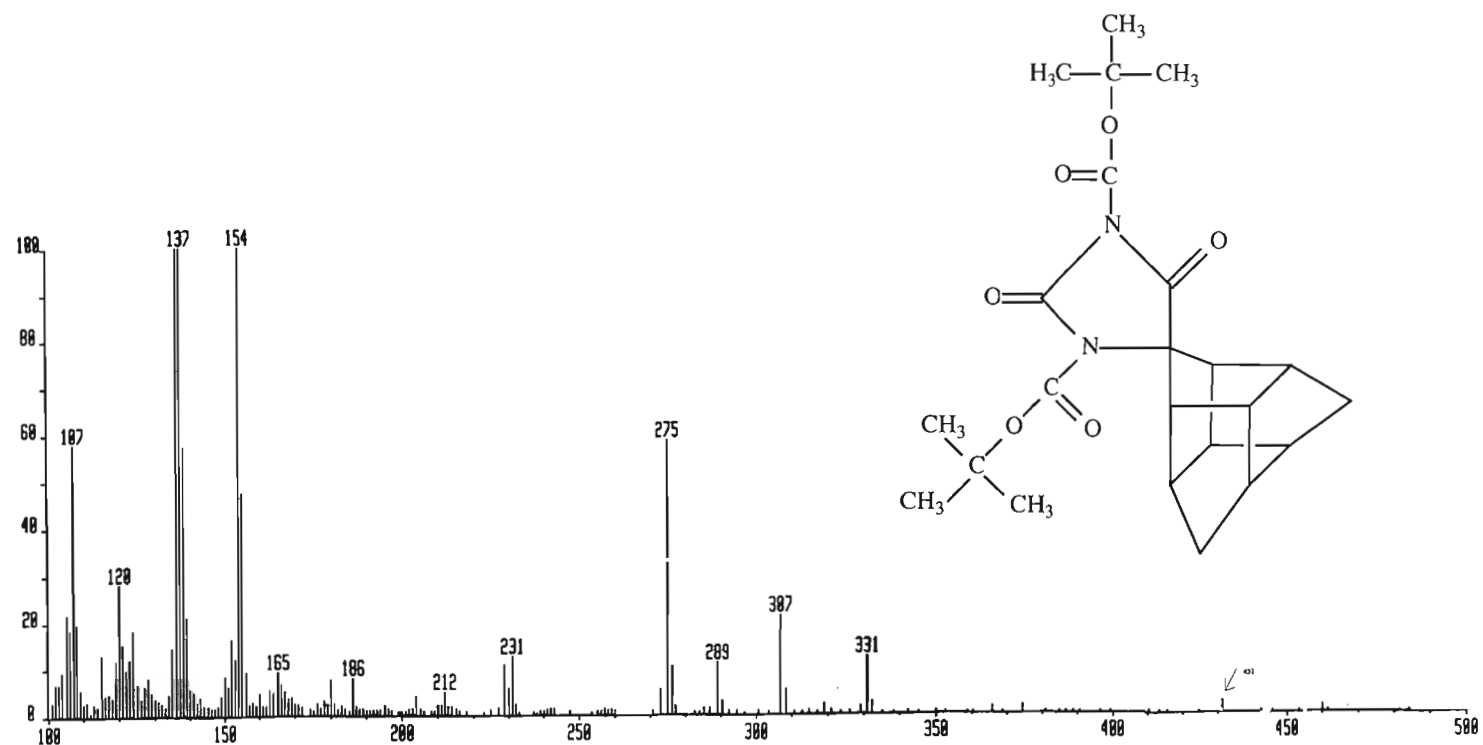
Spectrum 49: HSQC spectrum of Novel Compound 2 in CDCl₃ (2.67)



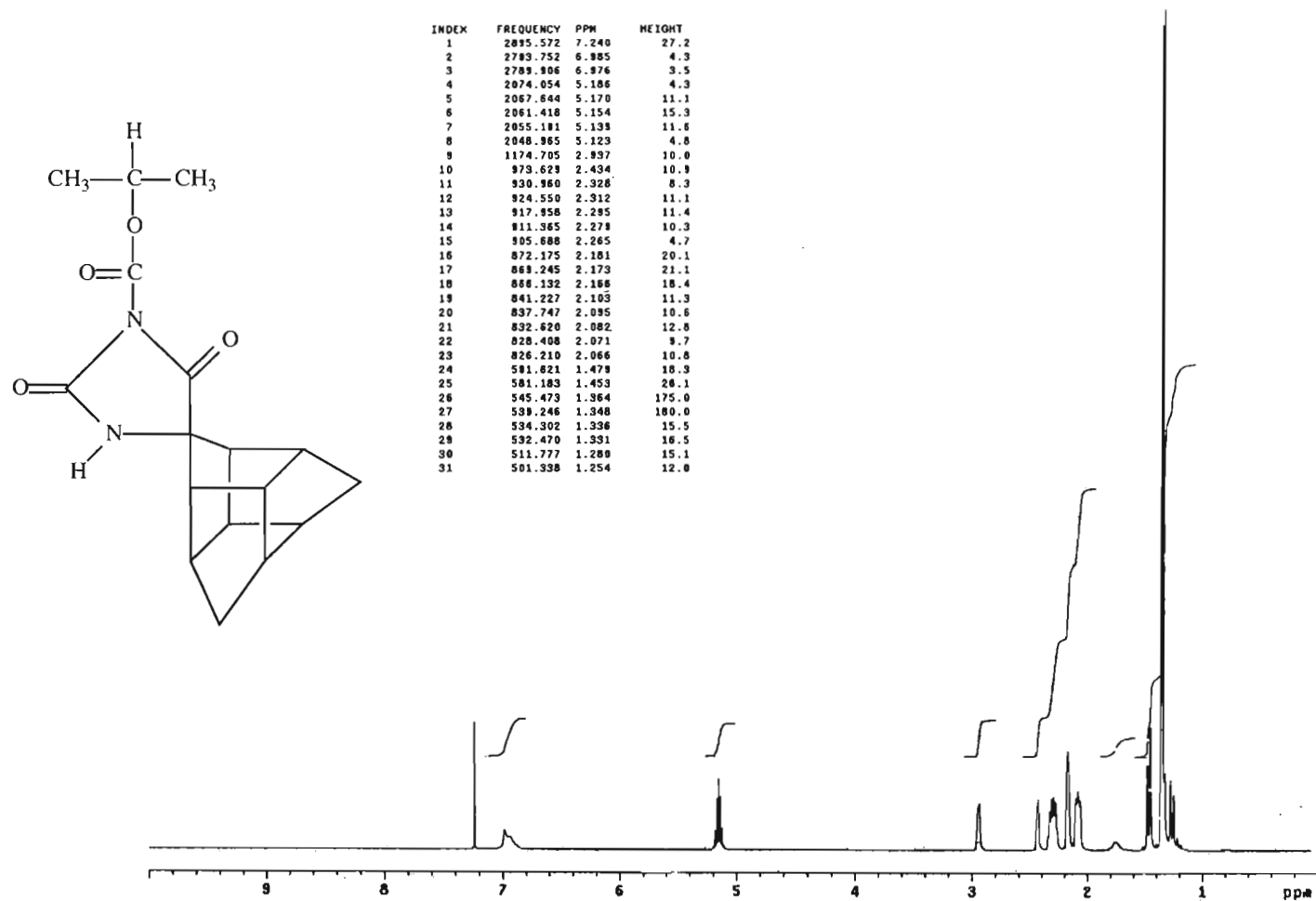
Spectrum 50: HMBC spectrum of Novel Compound 2 in CDCl_3 (2.67)



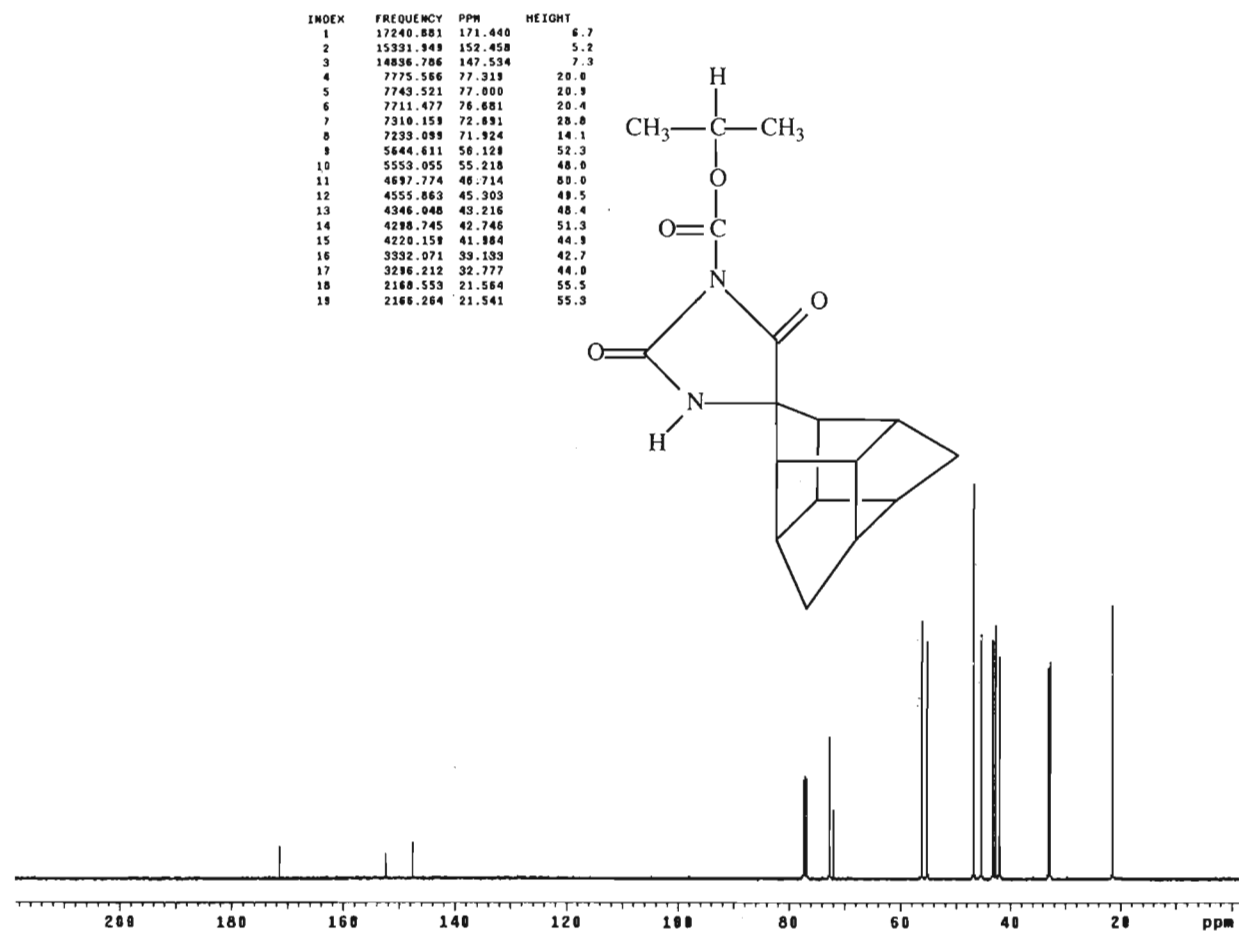
Spectrum 51: Infrared spectrum (KBr) of Novel Compound 2 (2.67)



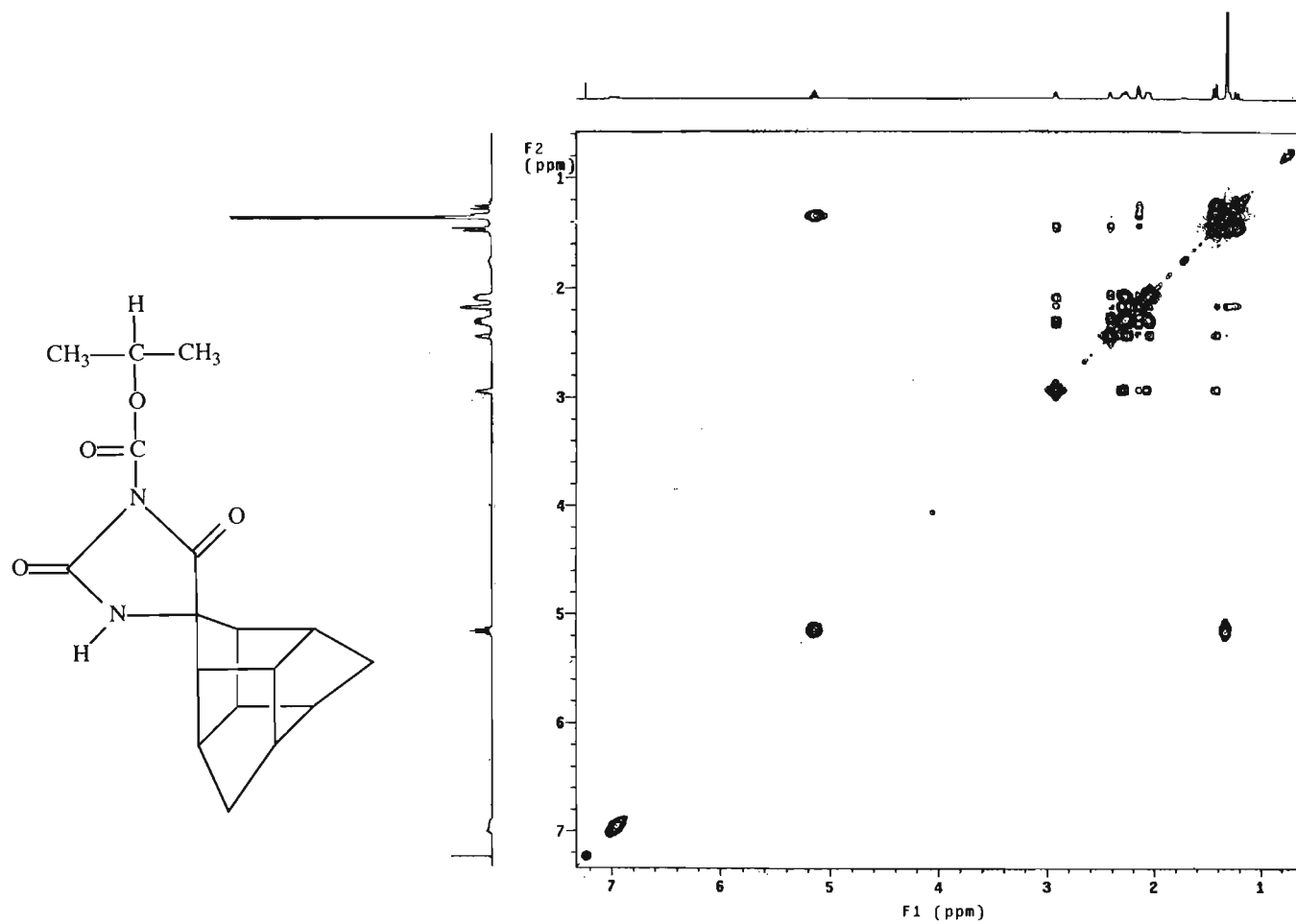
Spectrum 52: Mass spectrum (FAB) of Novel Compound 2 (2.67)



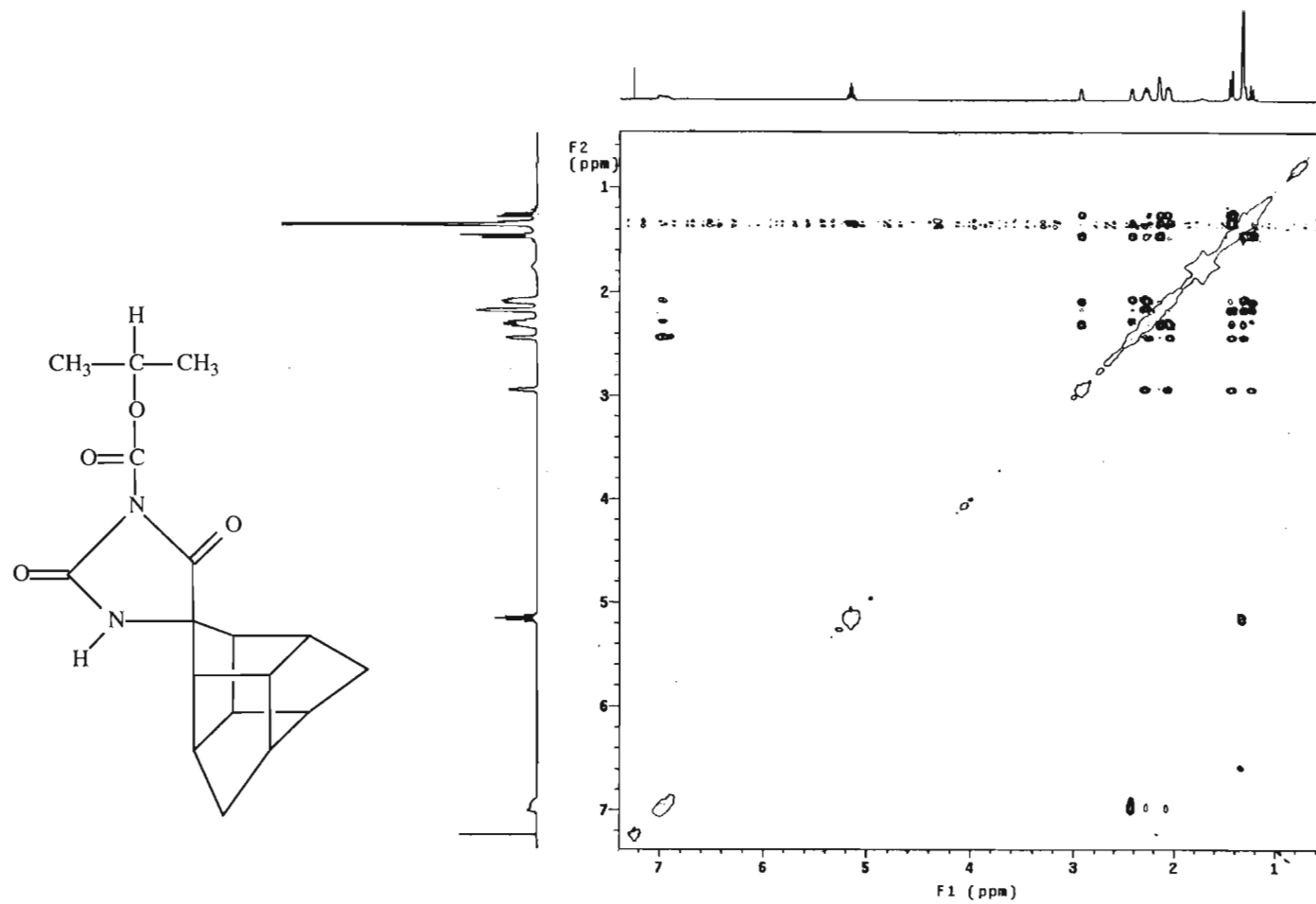
Spectrum 53: ^1H NMR spectrum of Novel Compound 3 in CDCl_3 (3.14)



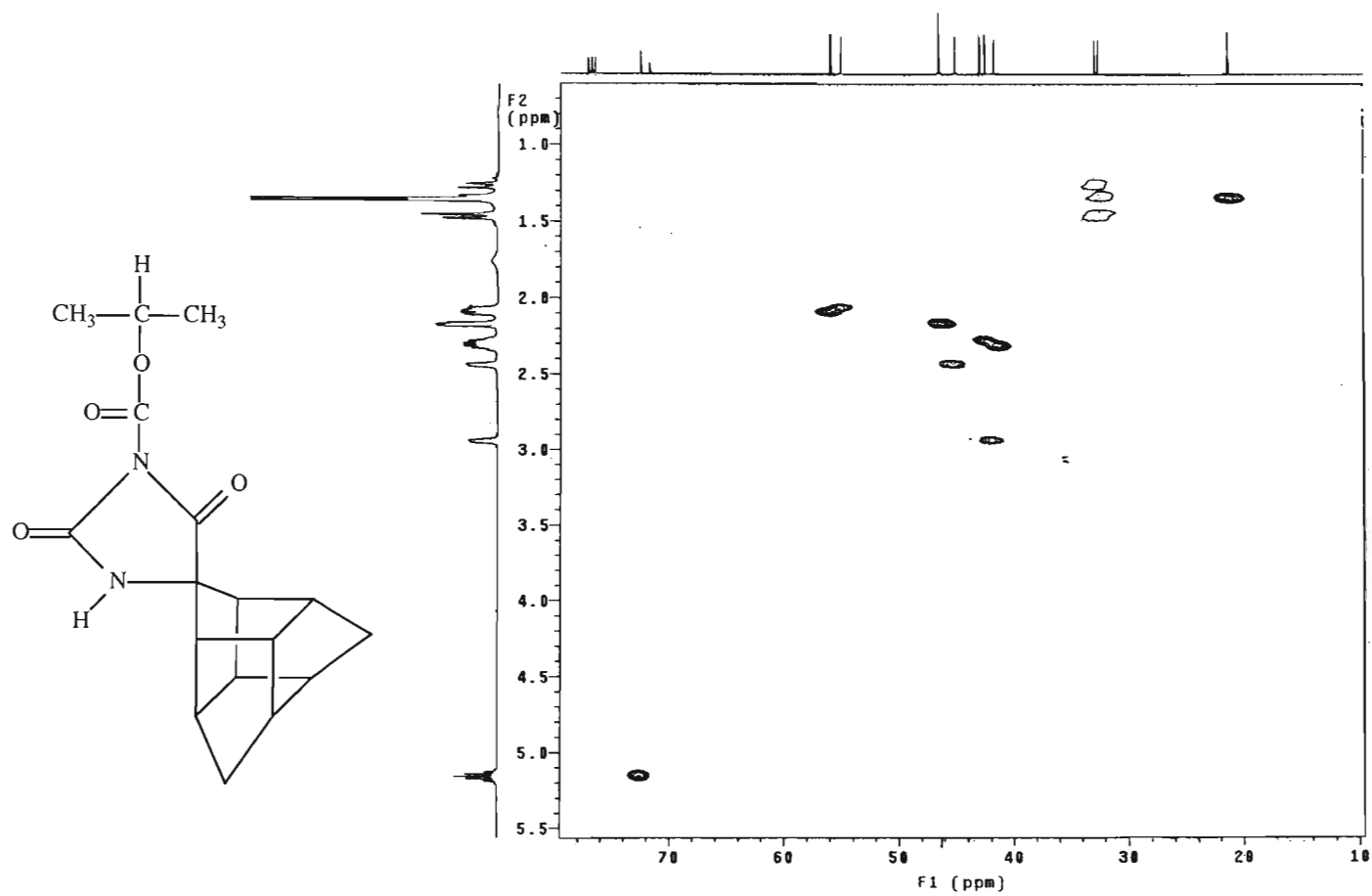
Spectrum 54: ^{13}C NMR spectrum of Novel Compound 3 in CDCl_3 (3.14)



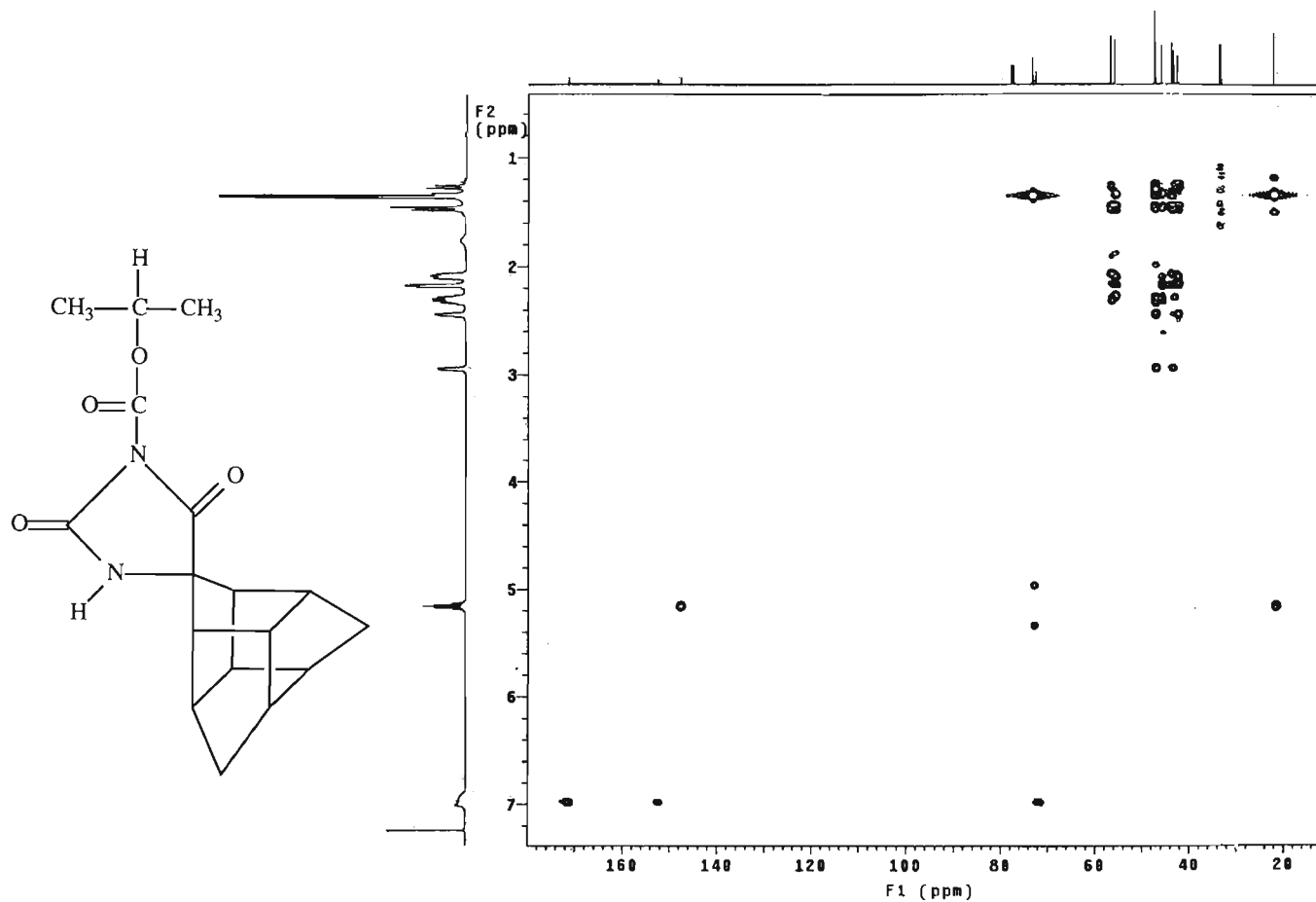
Spectrum 55: COSY spectrum of Novel Compound 3 in CDCl₃ (3.14)



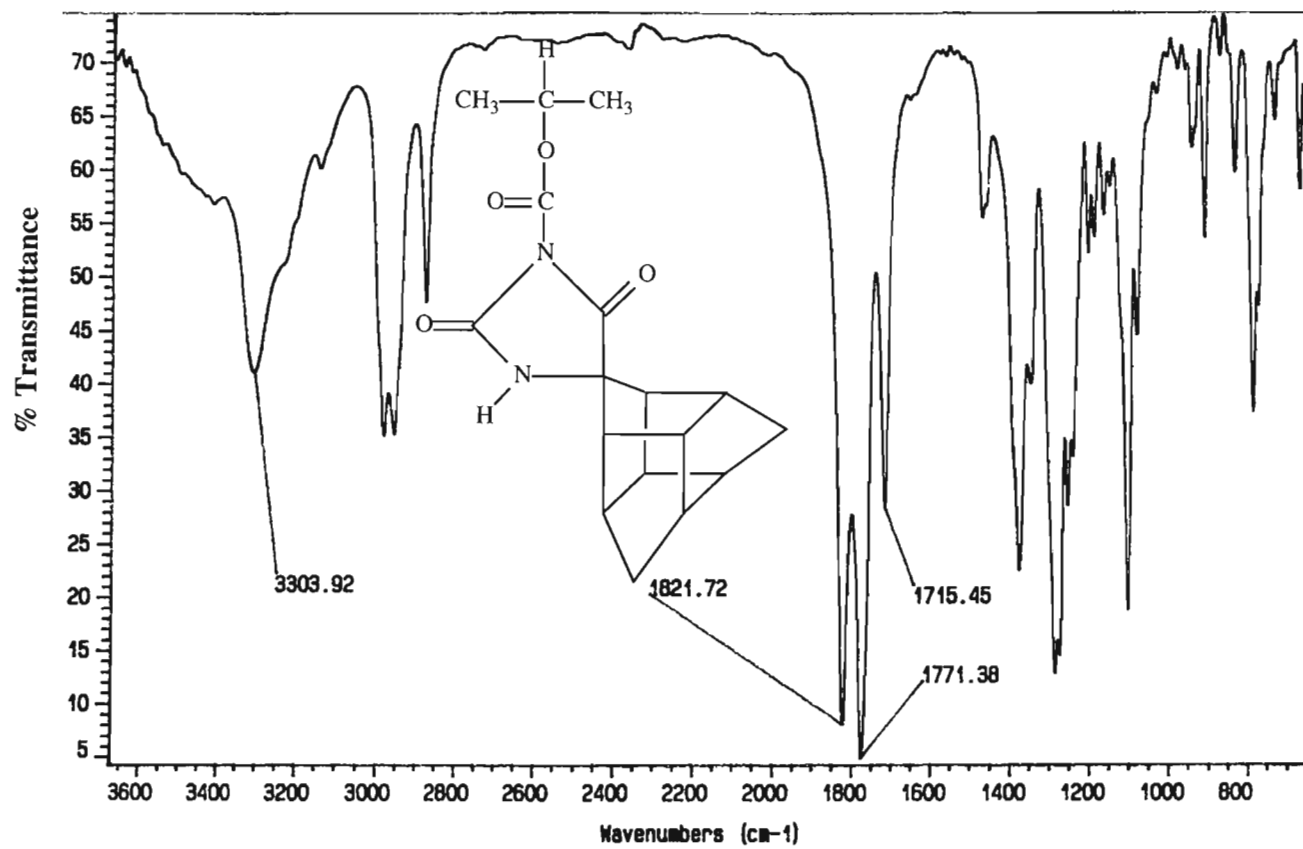
Spectrum 56: NOESY spectrum of Novel Compound 3 in CDCl₃ (3.14)



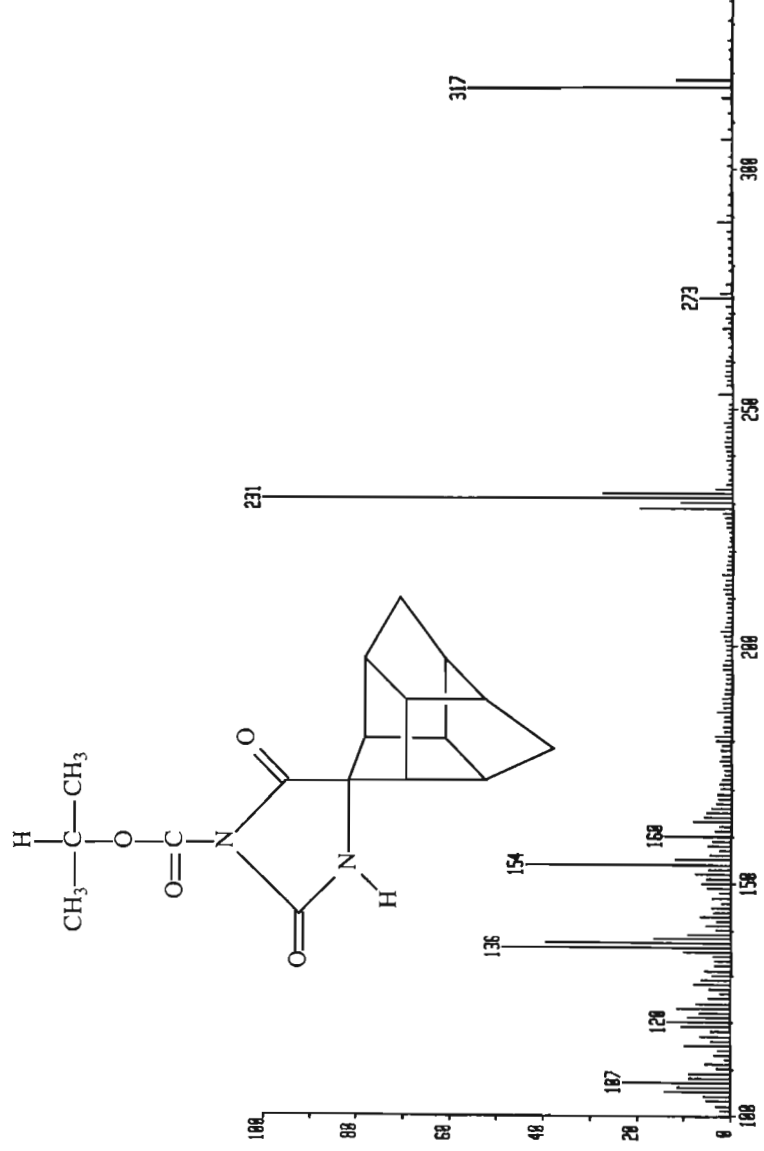
Spectrum 57: HSQC spectrum of Novel Compound 3 in CDCl_3 (3.14)



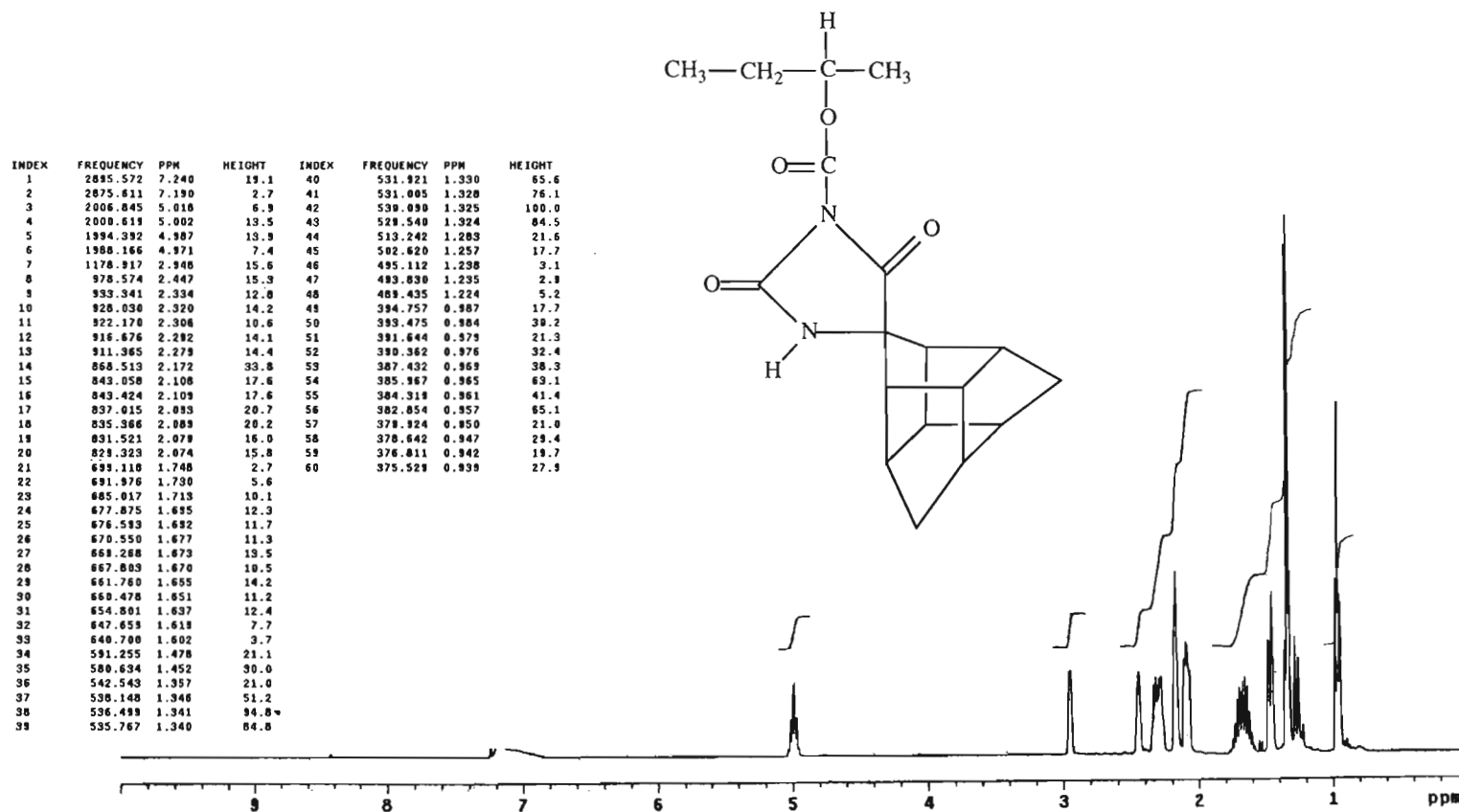
Spectrum 58: HMBC spectrum of Novel Compound 3 in CDCl₃ (3.14)



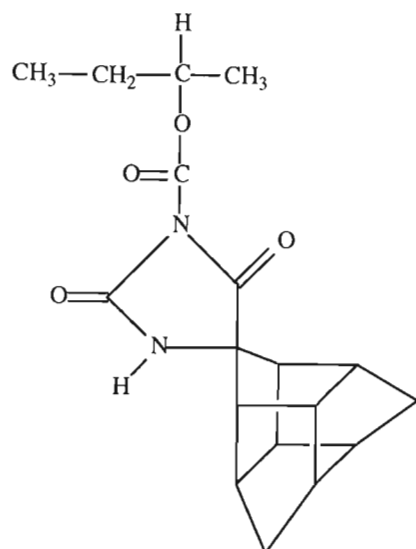
Spectrum 59: Infrared spectrum (KBr) of Novel Compound 3 (3.14)



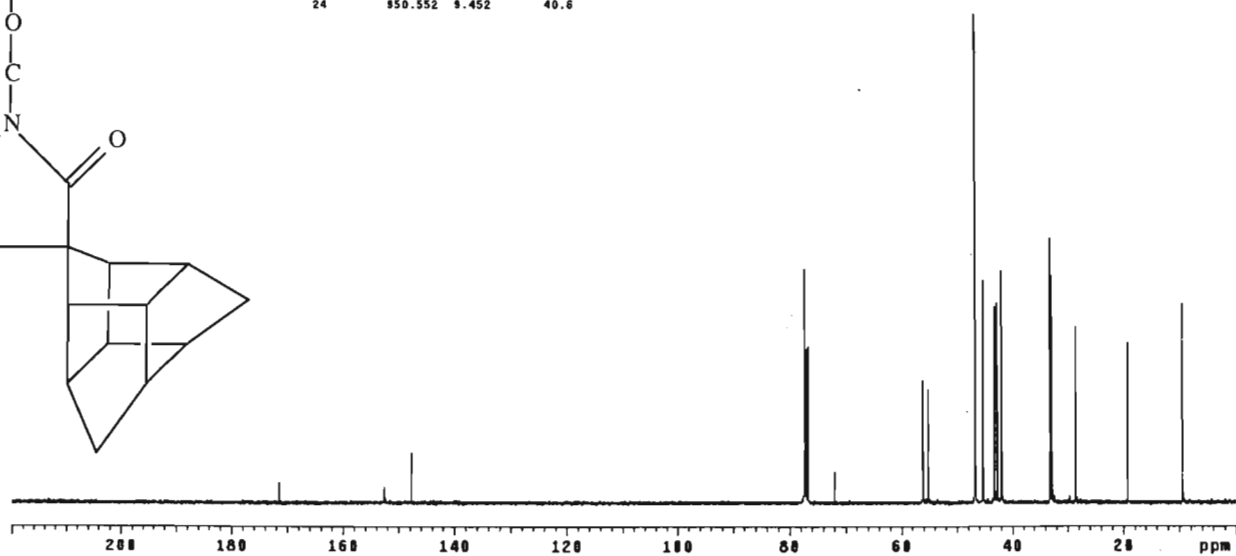
Spectrum 60: Mass spectrum (FAB) of Novel Compound 3 (3.14)



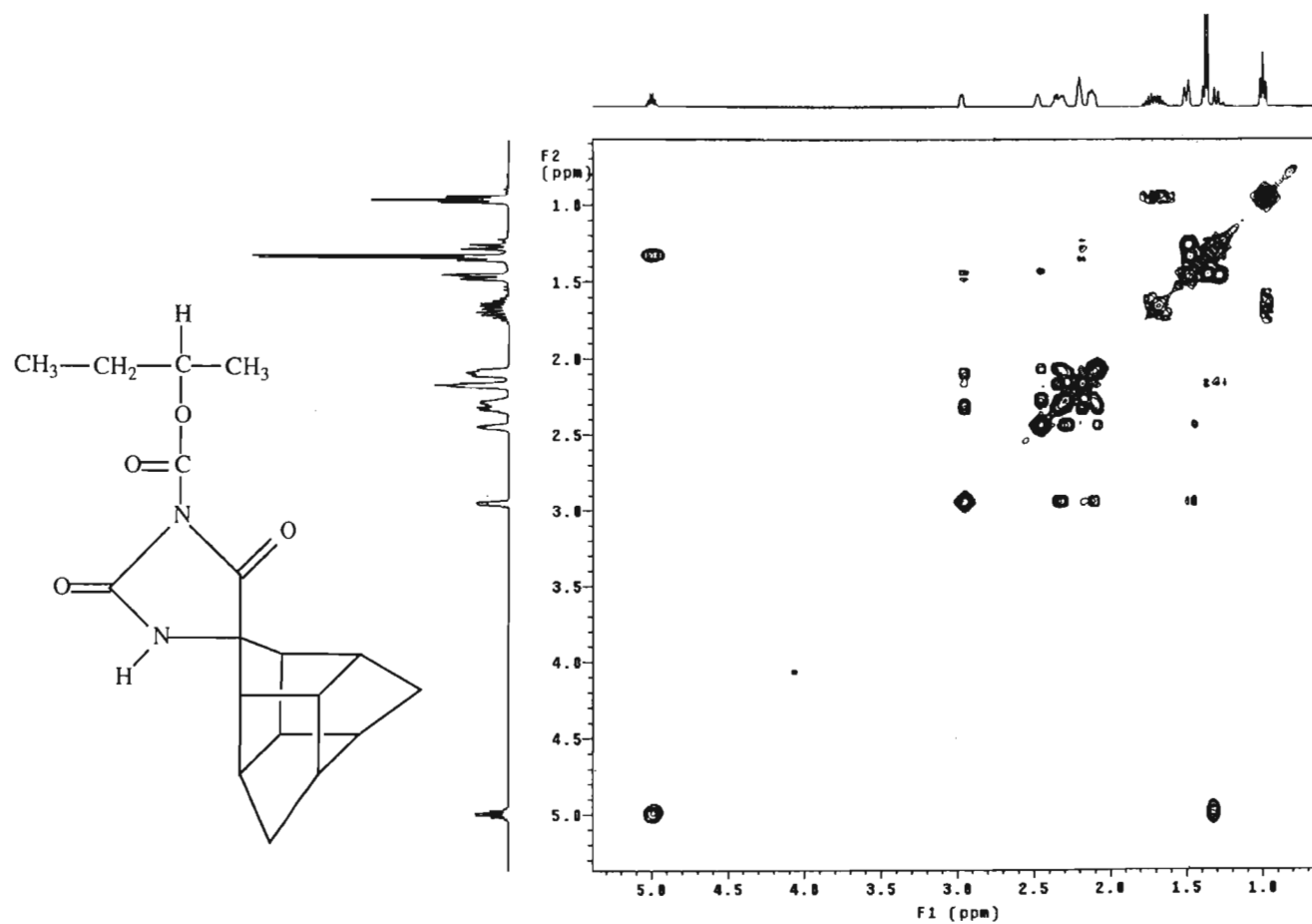
Spectrum 61: ^1H NMR spectrum of Novel Compound 4 in CDCl_3 (3.15)



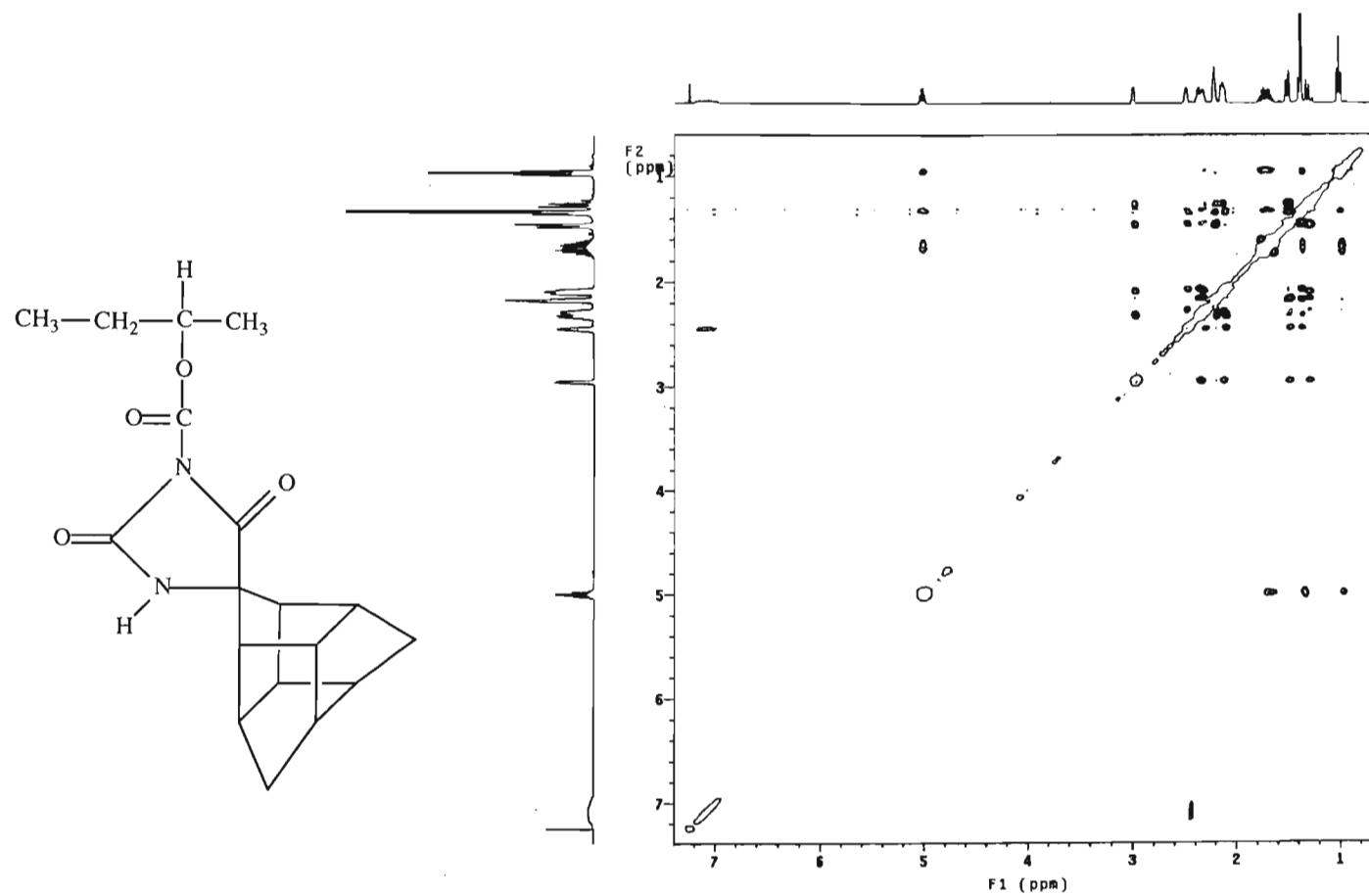
INDEX	FREQUENCY	PPM	HEIGHT
1	17246.591	171.497	4.2
2	15348.120	152.619	3.3
3	14857.846	147.743	10.2
4	7775.857	77.320	48.4
5	7744.945	77.008	31.4
6	7712.289	76.689	31.8
7	7240.887	72.002	5.8
8	7236.767	71.961	6.4
9	5648.940	56.172	25.0
10	5643.172	56.115	24.8
11	5555.828	55.246	22.1
12	5551.708	55.205	23.2
13	4689.704	46.733	100.0
14	4559.628	45.349	45.4
15	4347.880	43.234	40.0
16	4299.245	42.751	40.8
17	4221.790	41.981	47.5
18	3339.528	33.140	54.1
19	3287.274	32.787	46.6
20	2873.743	28.576	34.9
21	2871.271	28.551	36.0
22	1938.515	19.276	26.4
23	1931.923	19.211	32.7
24	950.552	9.452	40.6



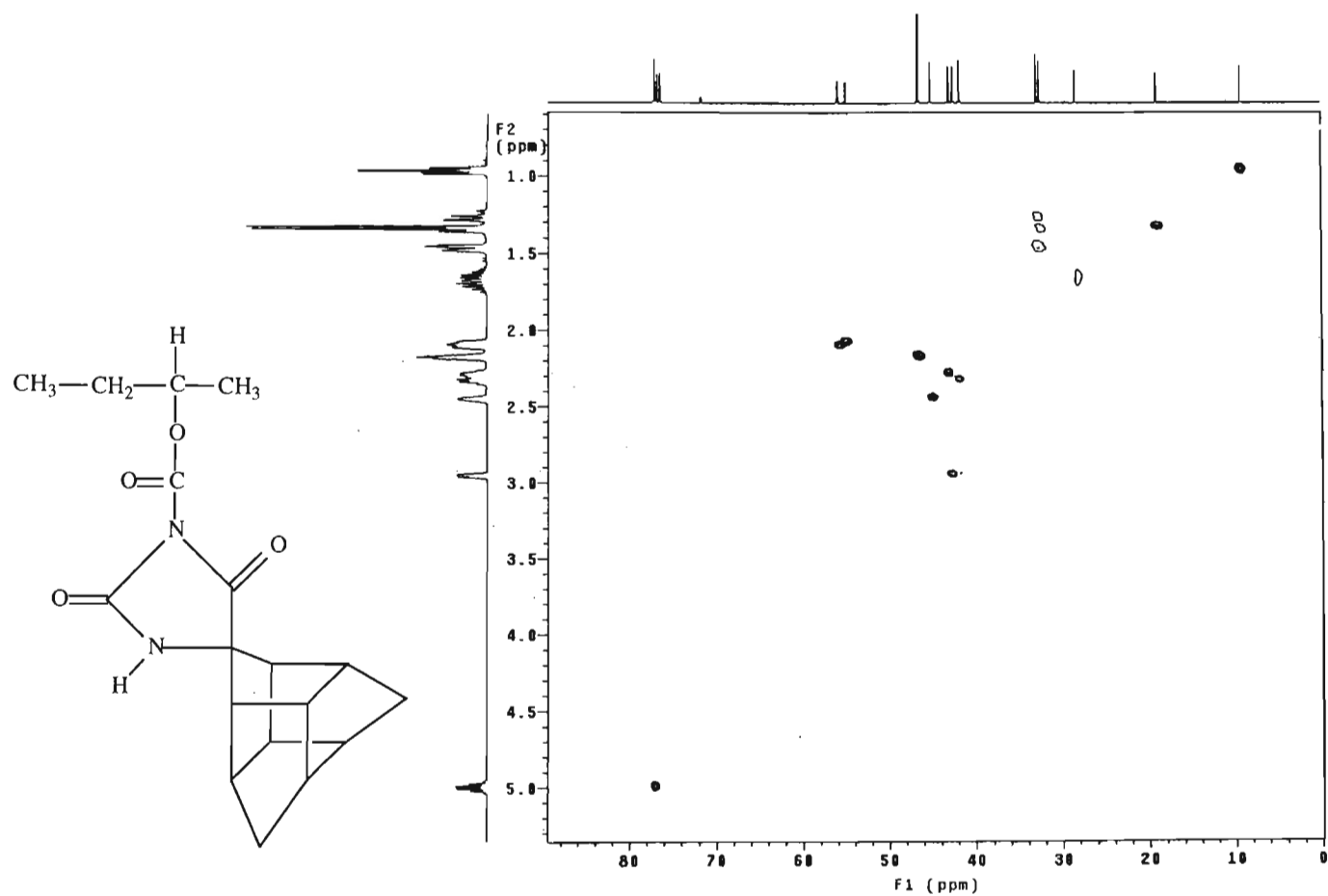
Spectrum 62: ^{13}C NMR spectrum of Novel Compound 4 in CDCl_3 (3.15)



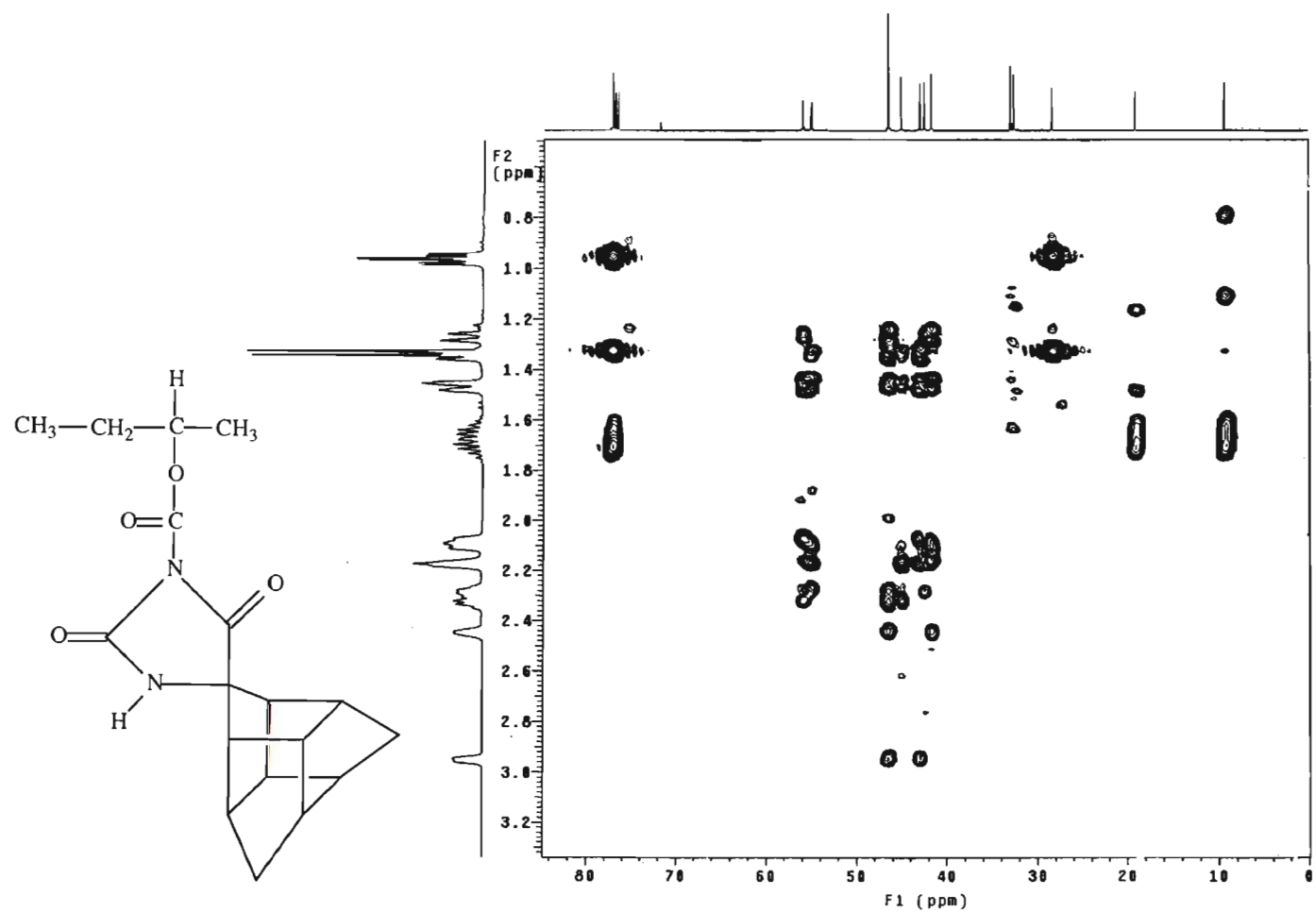
Spectrum 63: COSY spectrum of Novel Compound 4 in CDCl₃ (3.15)



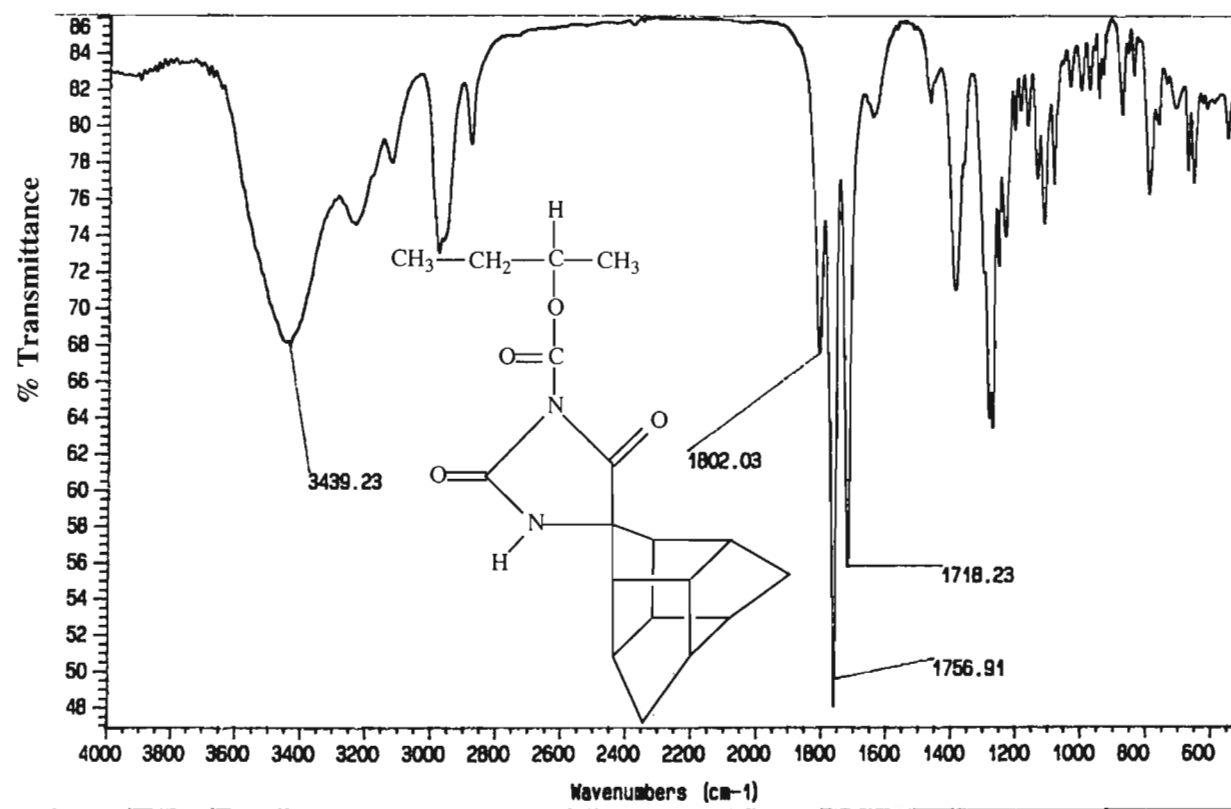
Spectrum 64: NOESY spectrum of Novel Compound 4 in CDCl₃ (3.15)



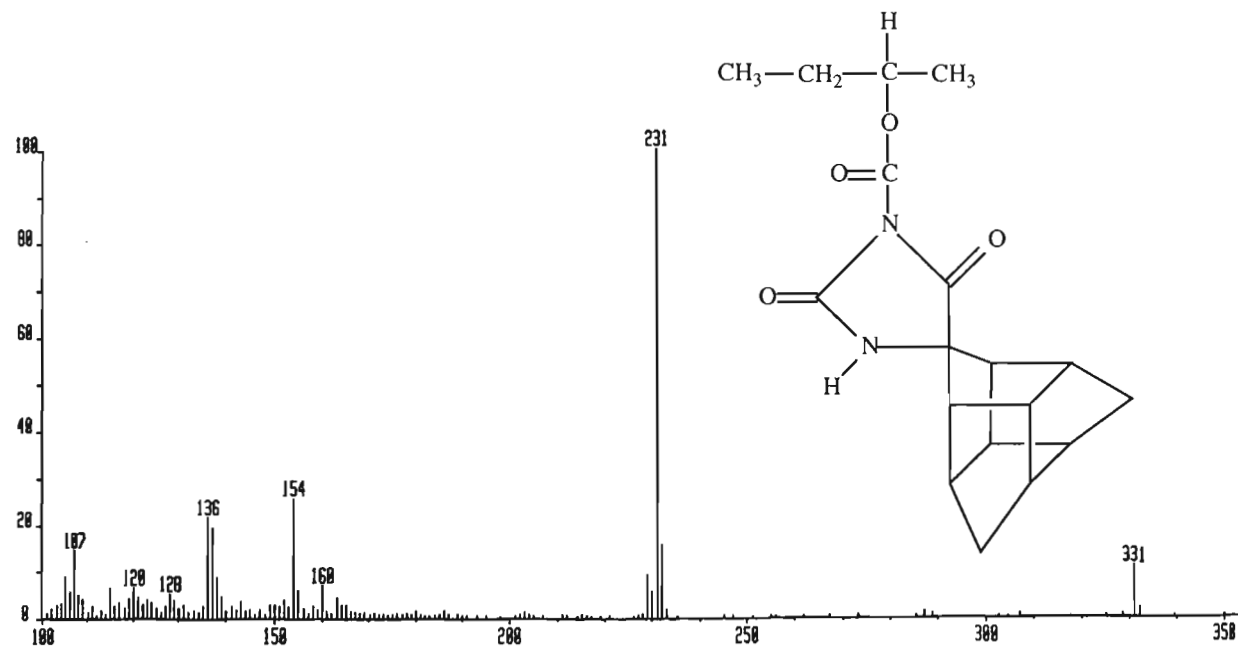
Spectrum 65: HSQC spectrum of Novel Compound 4 in CDCl_3 (3.15)



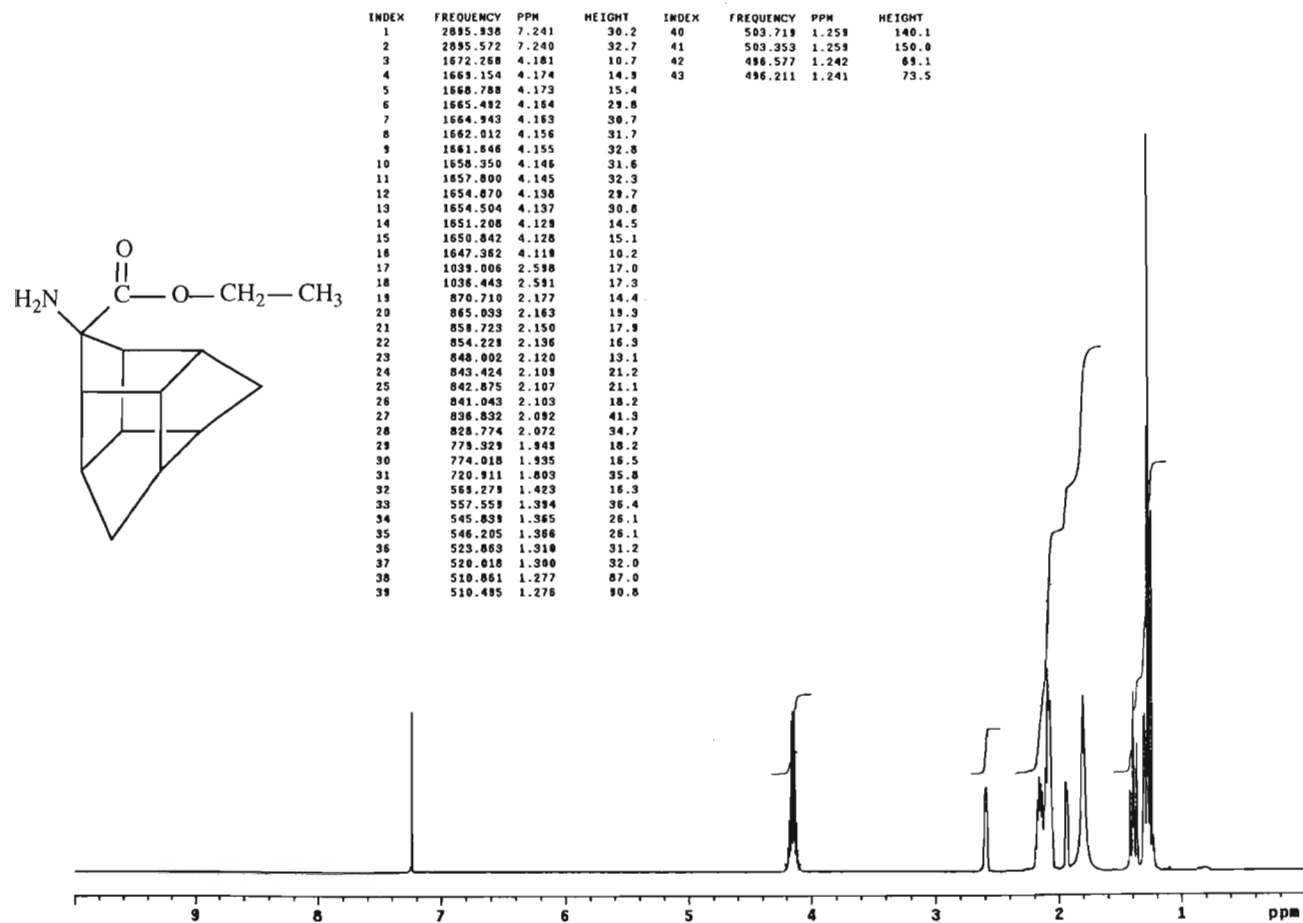
Spectrum 66: HMBC spectrum of Novel Compound 4 in CDCl₃ (3.15)



Spectrum 67: Infrared spectrum (KBr) of Novel Compound 4 (3.15)

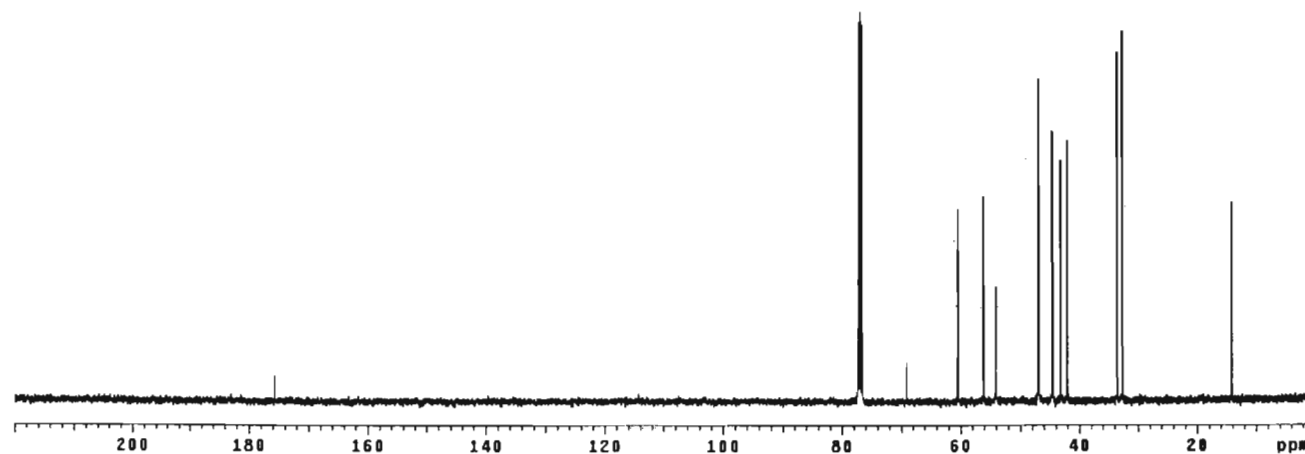
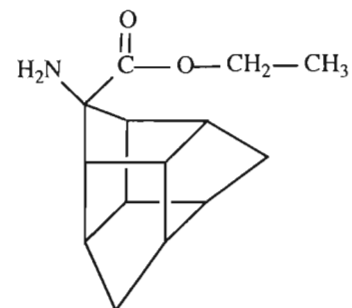


Spectrum 68: Mass spectrum (FAB) of Novel Compound 4 (3.15)

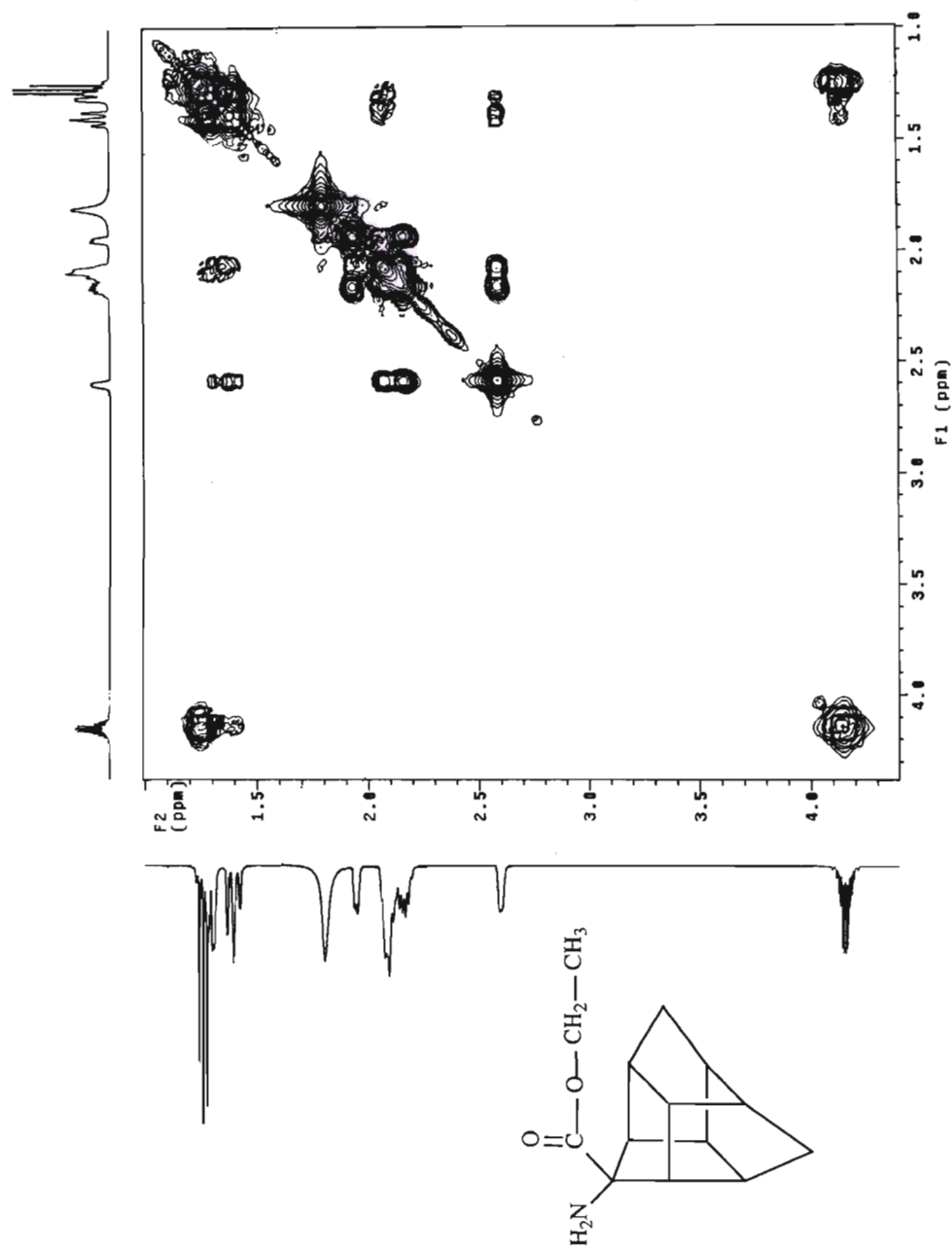


Spectrum 69: ^1H NMR spectrum of Novel Compound 5 in CDCl_3 (4.10)

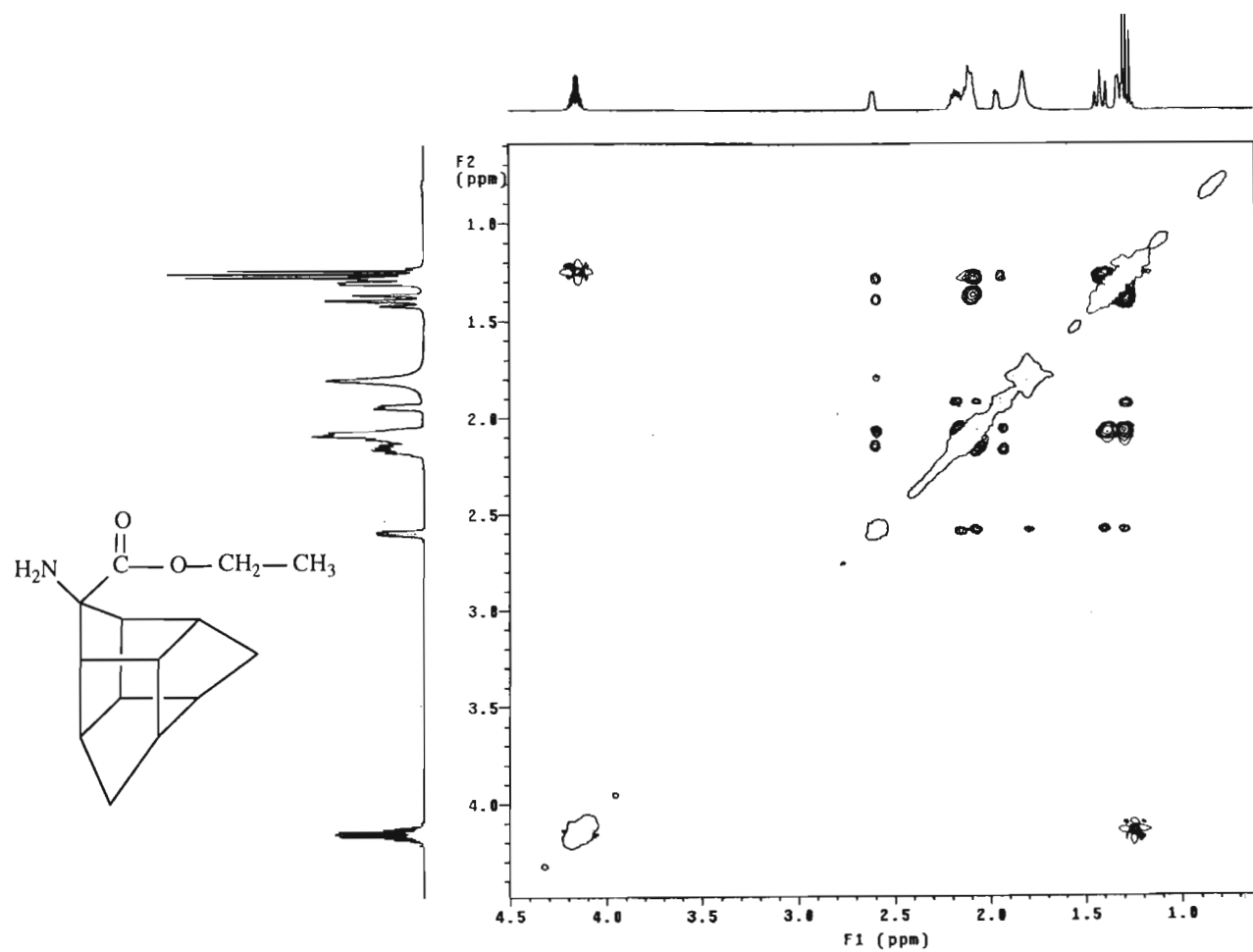
INDEX	FREQUENCY	PPM	HEIGHT
1	17673.418	175.741	4.8
2	7775.857	77.320	73.1
3	7743.521	77.000	75.0
4	7711.385	76.680	72.5
5	6945.888	68.069	7.3
6	6080.710	60.465	36.8
7	5851.412	56.196	39.2
8	5434.703	54.042	21.9
9	4722.776	46.962	62.1
10	4718.656	46.921	58.7
11	4488.763	44.835	51.8
12	4482.171	44.570	47.1
13	4346.213	43.218	46.2
14	4233.326	42.095	50.0
15	3978.849	39.599	67.1
16	3288.210	32.697	71.3
17	1426.818	14.188	38.0



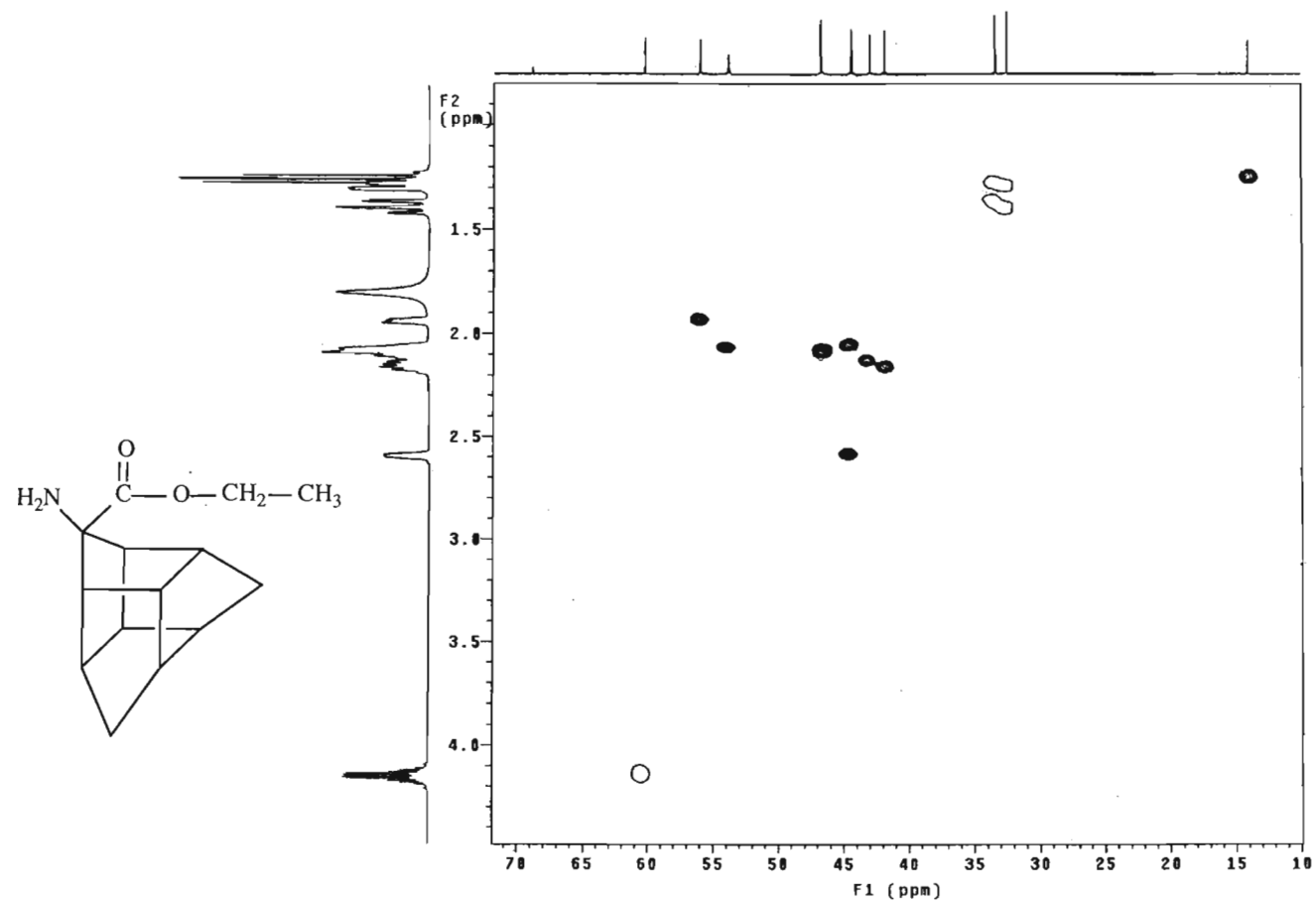
Spectrum 70: ^{13}C NMR spectrum of Novel Compound 5 in CDCl_3 (4.10)



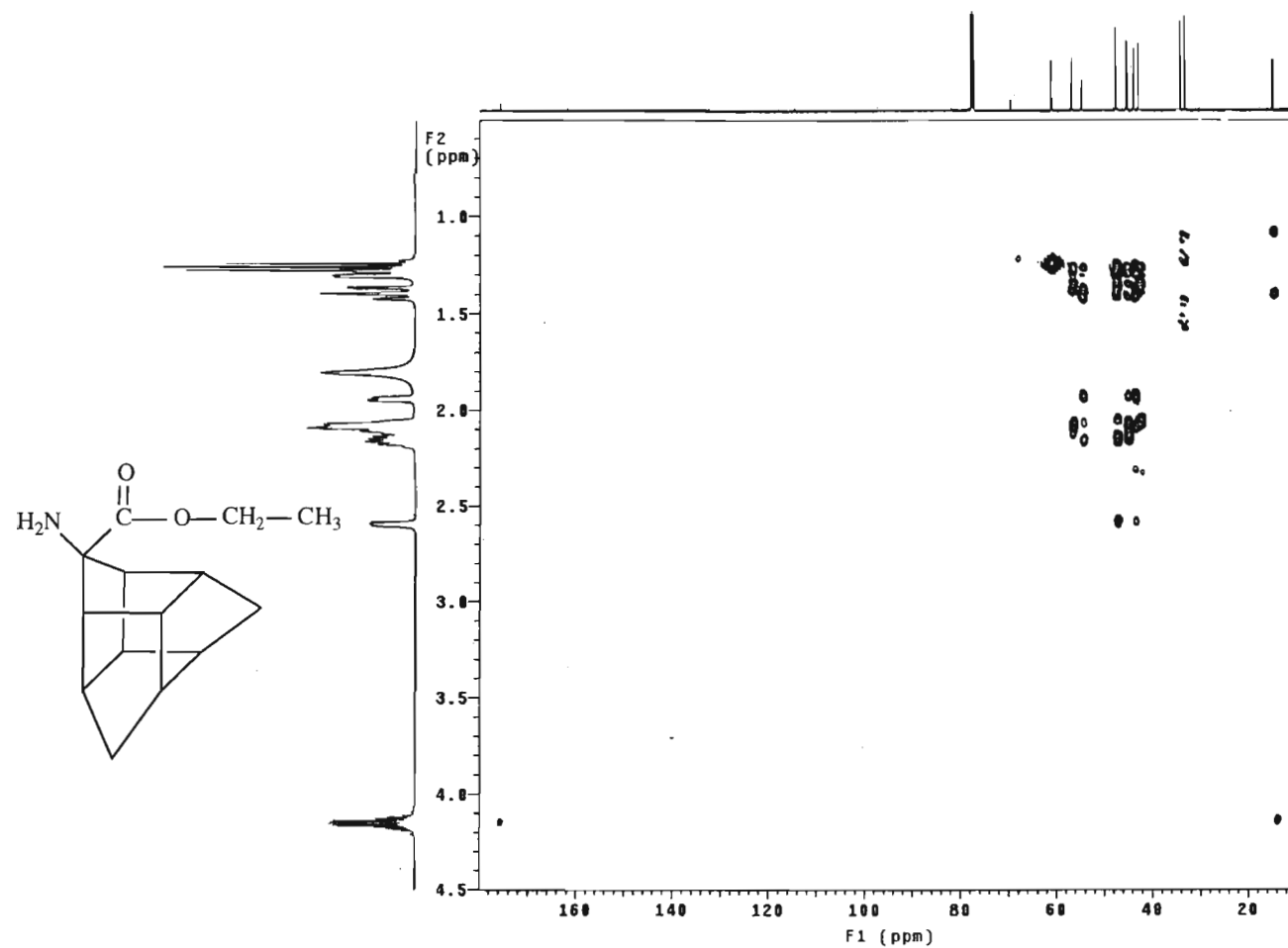
Spectrum 71: COSY spectrum of Novel Compound 5 in CDCl_3 (4.10)



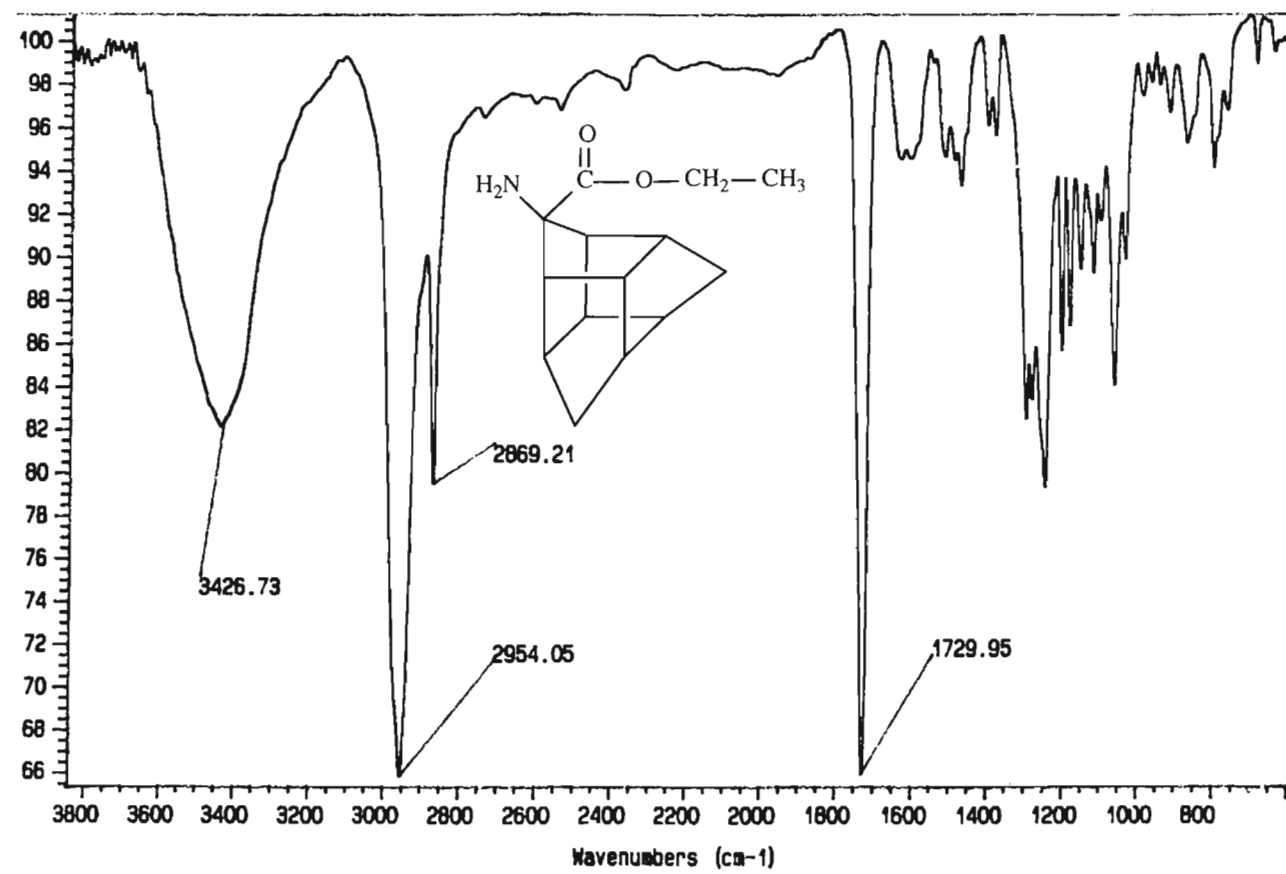
Spectrum 72: NOESY spectrum of Novel Compound 5 in CDCl₃ (4.10)



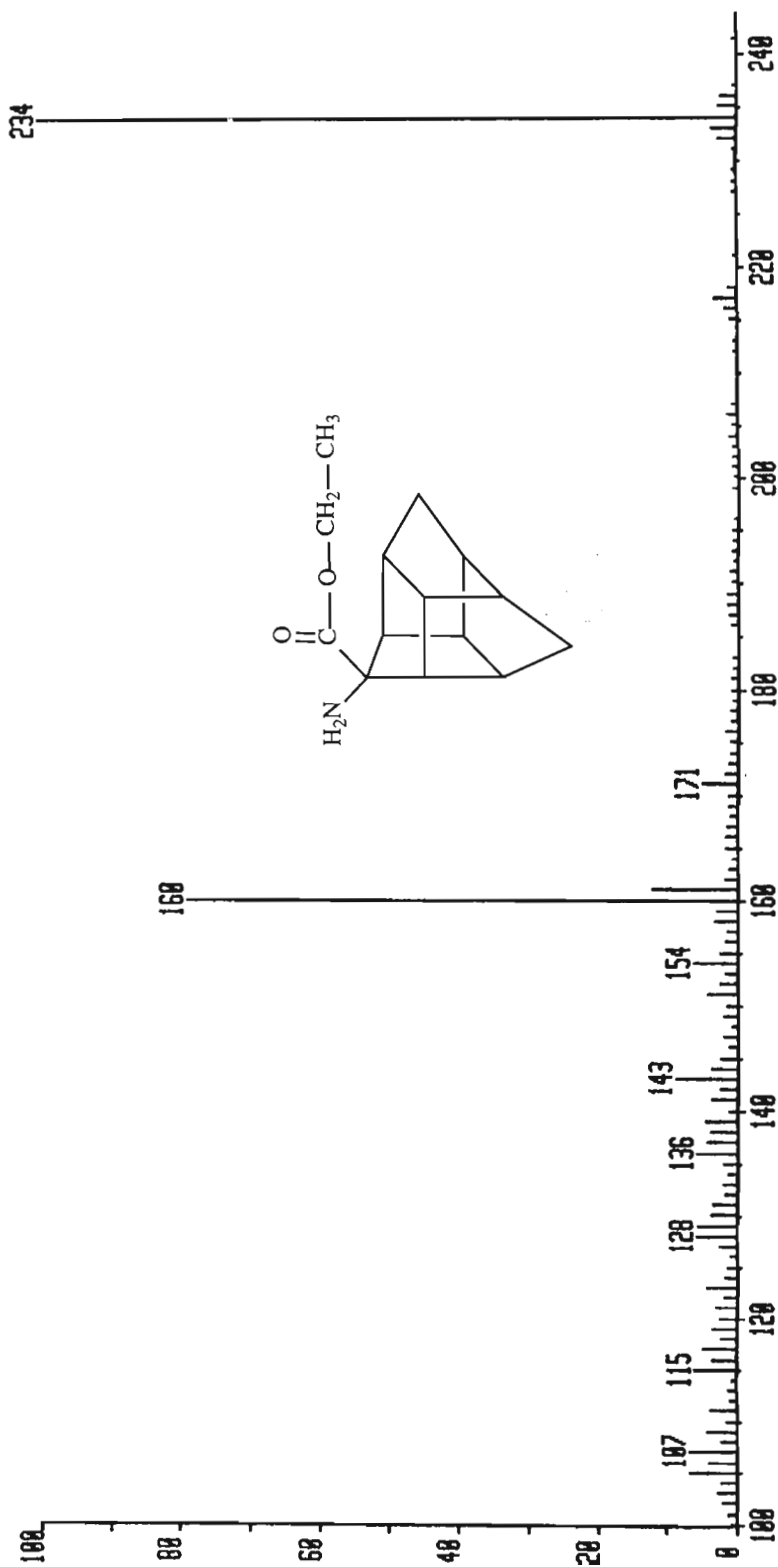
Spectrum 73: HSQC spectrum of Novel Compound 5 in CDCl_3 (4.10)



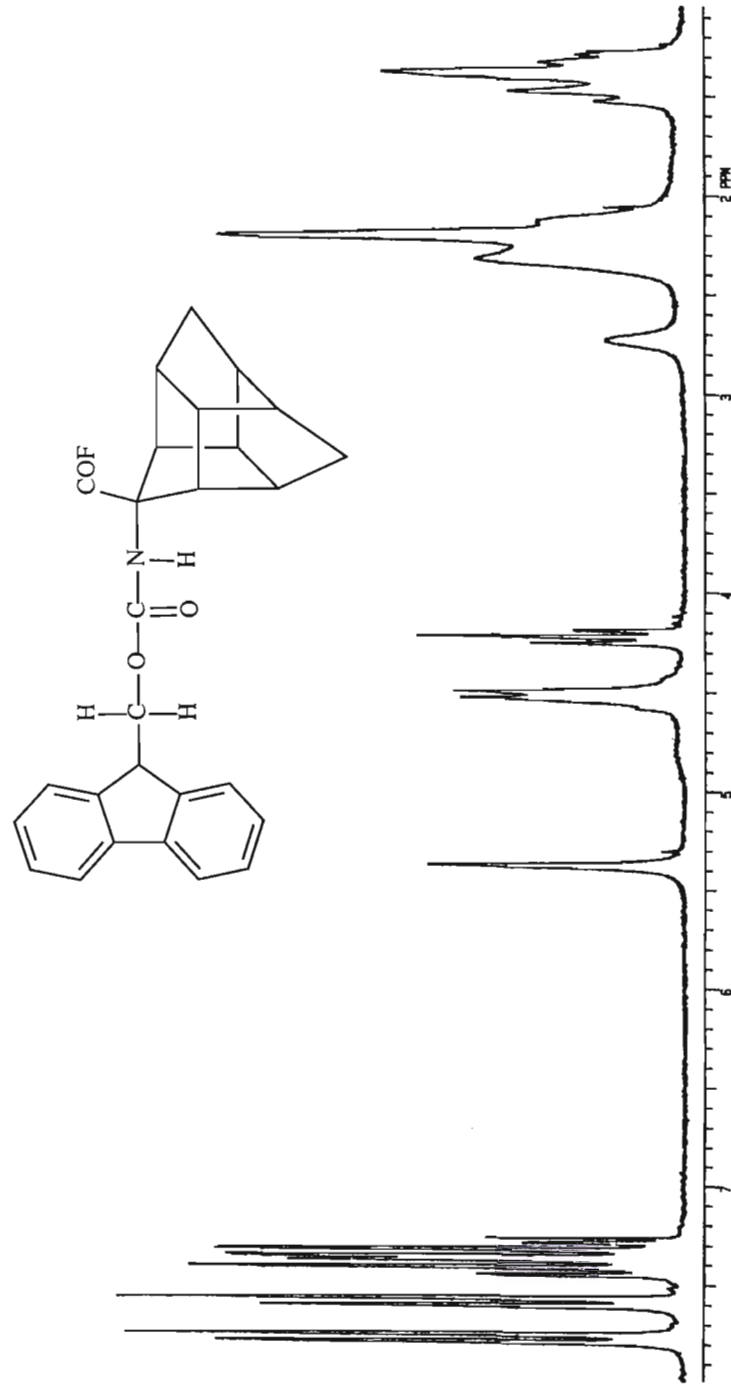
Spectrum 74: HMBC spectrum of Novel Compound 5 in CDCl_3 (4.10)



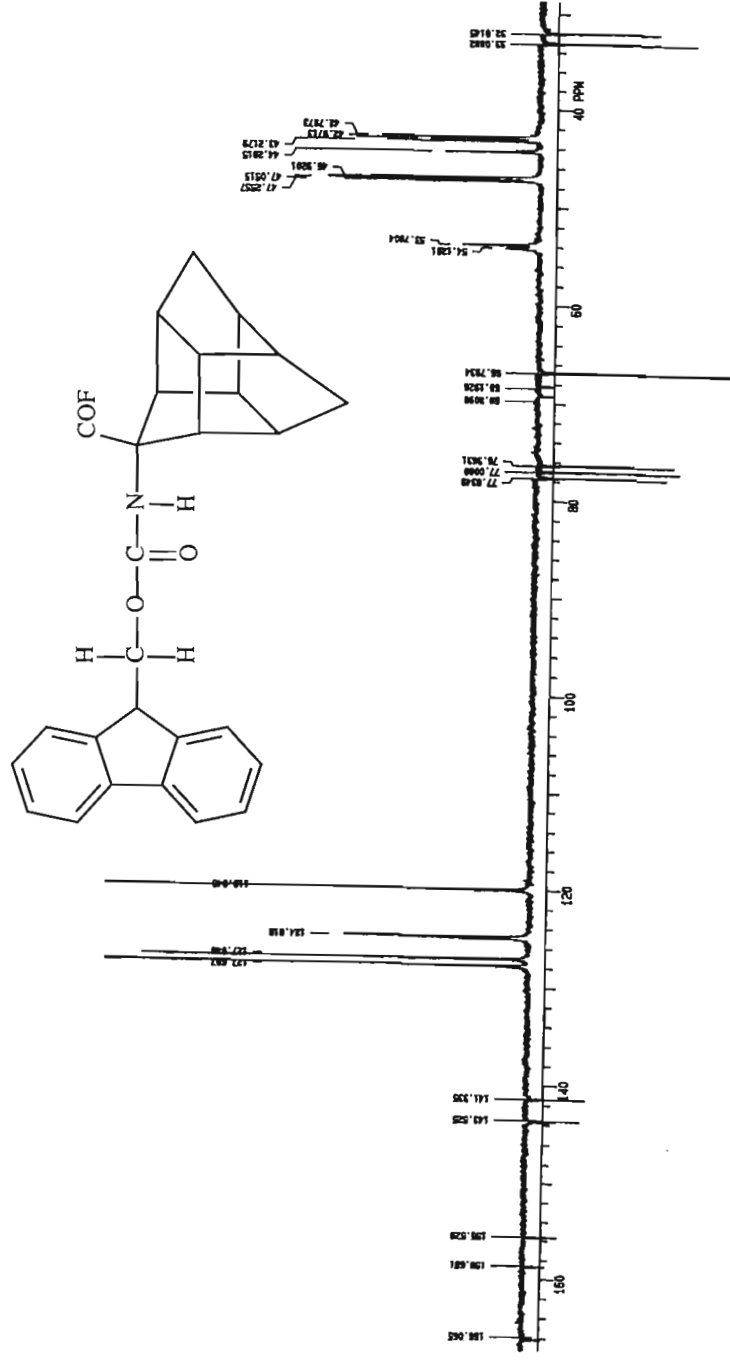
Spectrum 75: Infrared spectrum (KBr) of Novel Compound 5 (4.10)



Spectrum 76: Mass spectrum (FAB) of Novel Compound 5 (4.10)

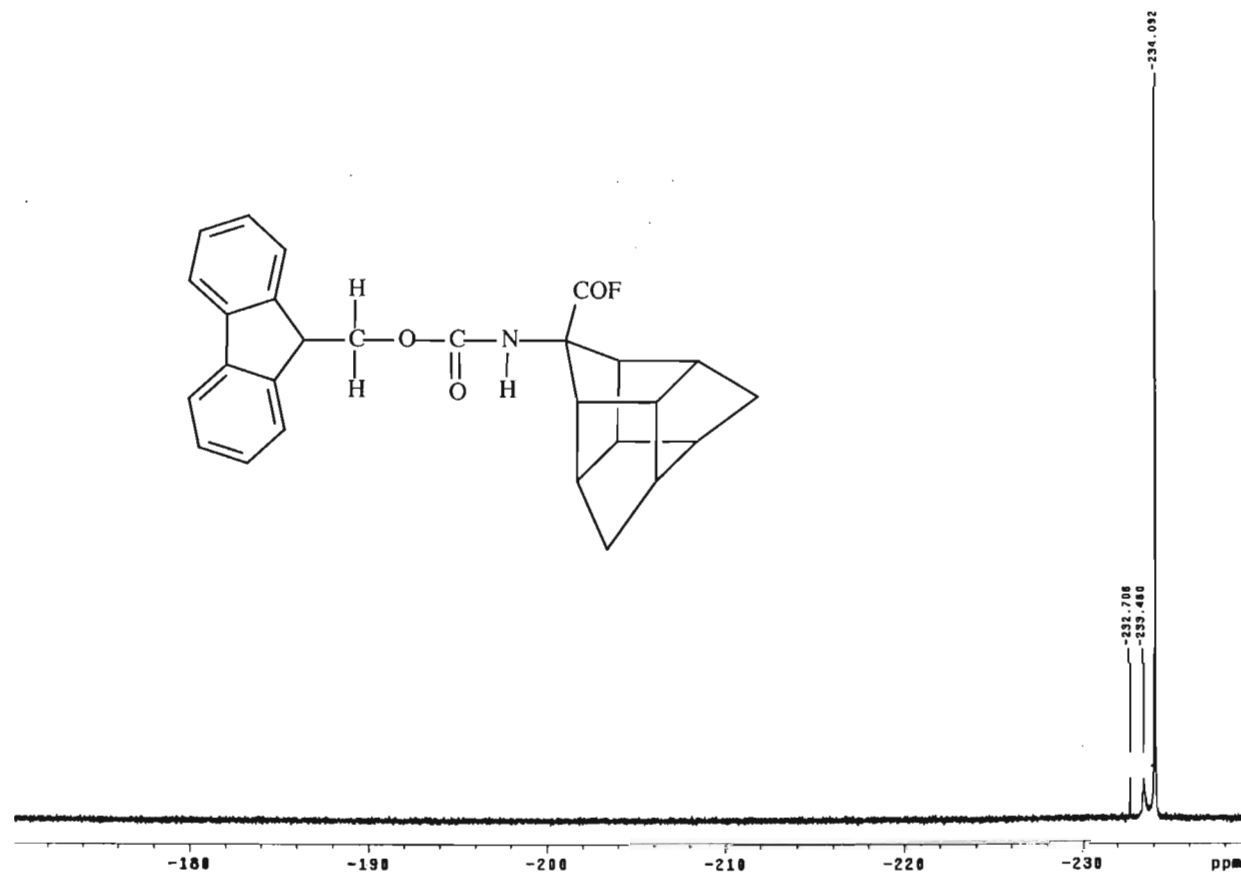


Spectrum 77: ¹H NMR spectrum of the Fmoc-tris-acid fluoride in CDCl₃

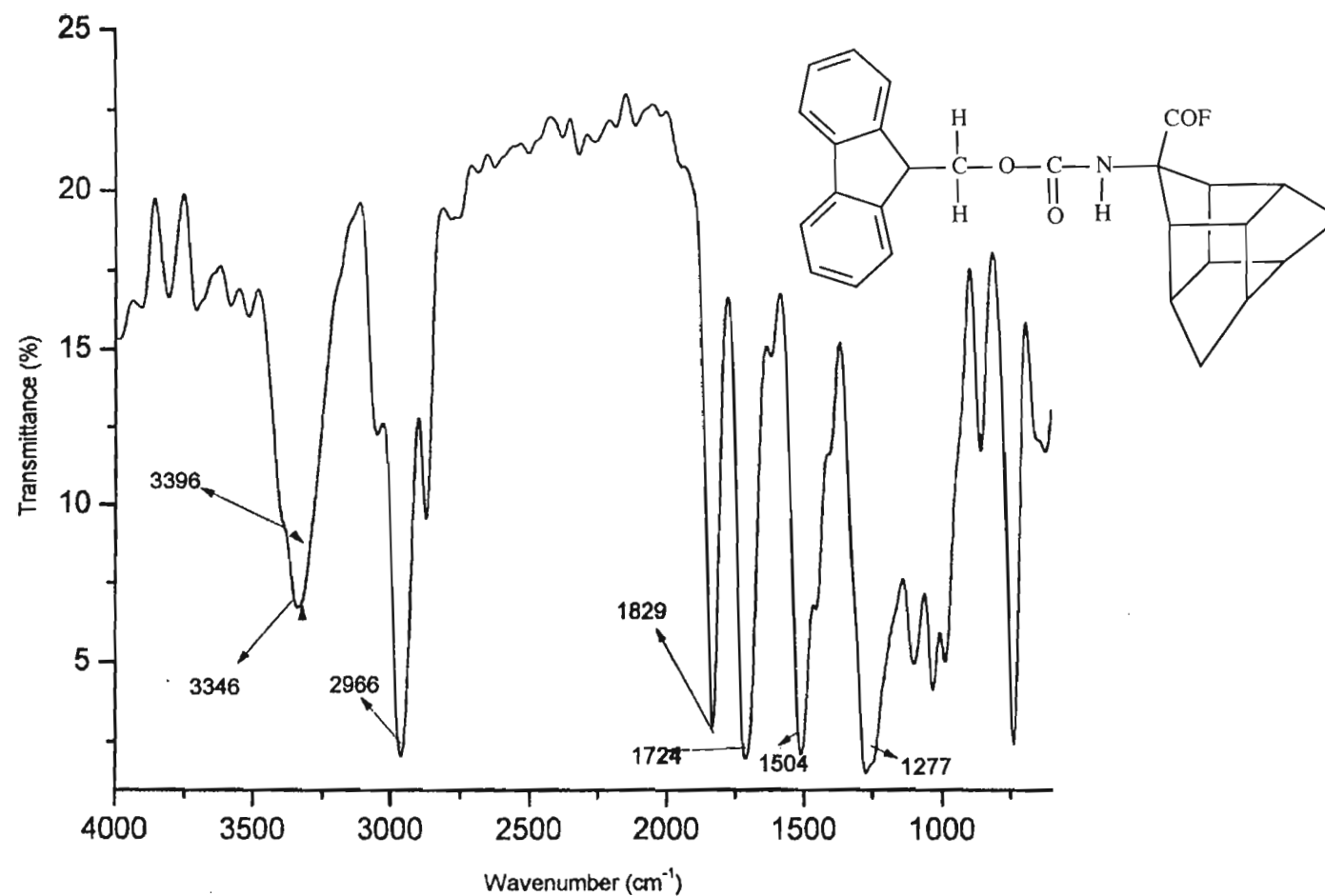


Spectrum 78: ^{13}C NMR spectrum of the Fmoc-tris-acid fluoride in CDCl_3

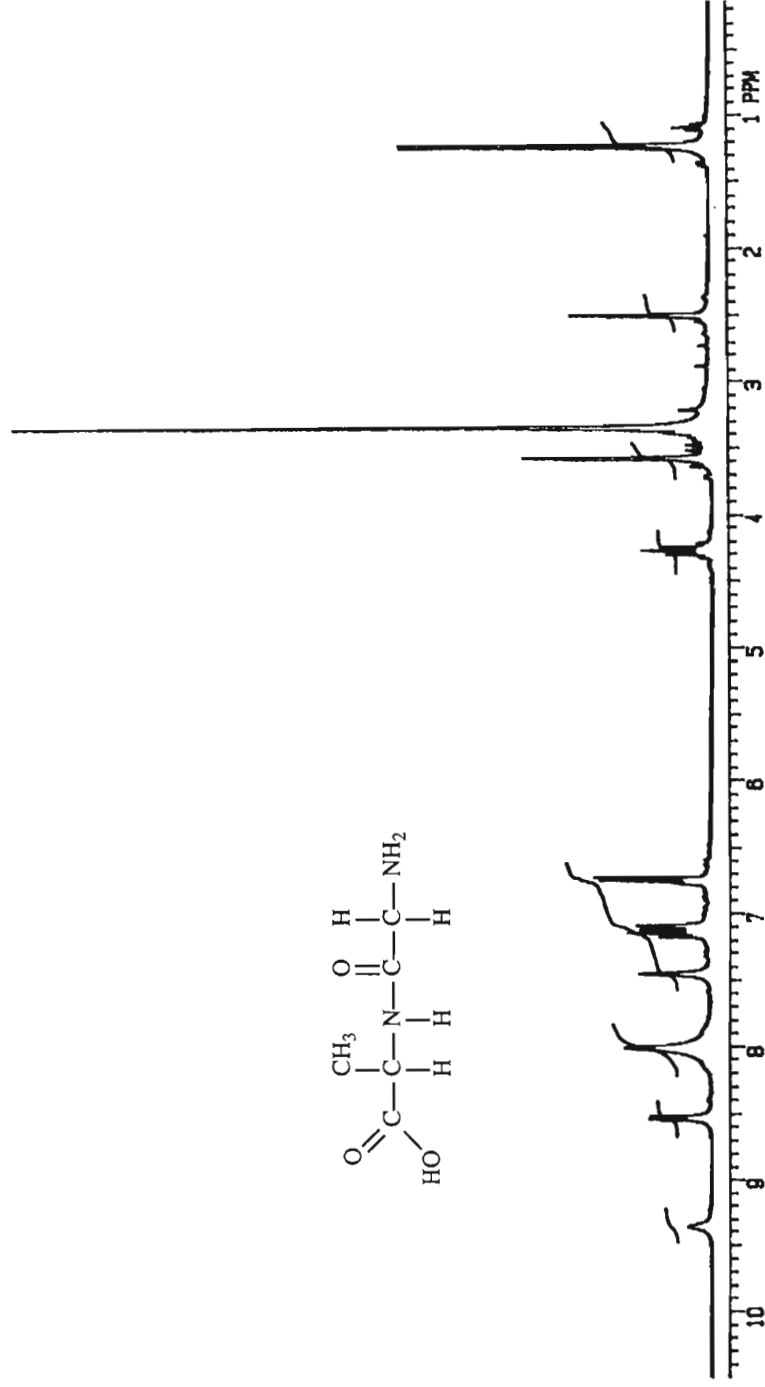
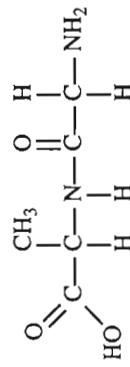
Ref. frequency TFA=-78.2561 ppm



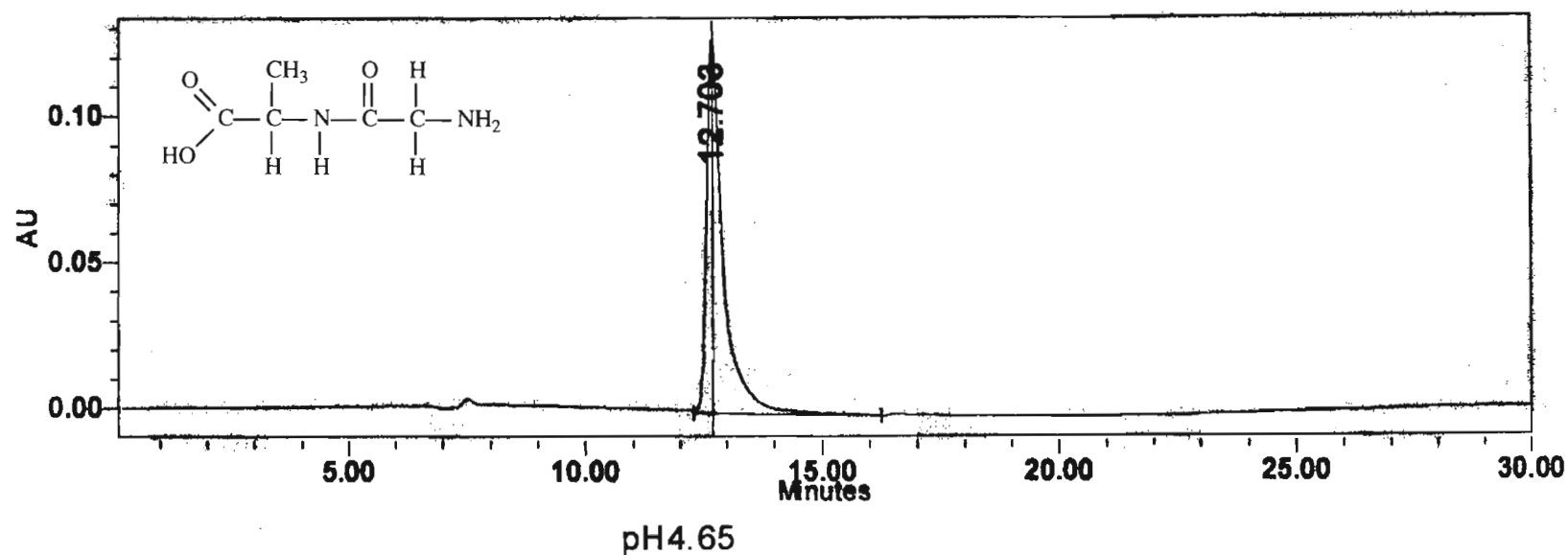
Spectrum 79: ^{19}F NMR spectrum of the Fmoc-tris-acid fluoride in CDCl_3



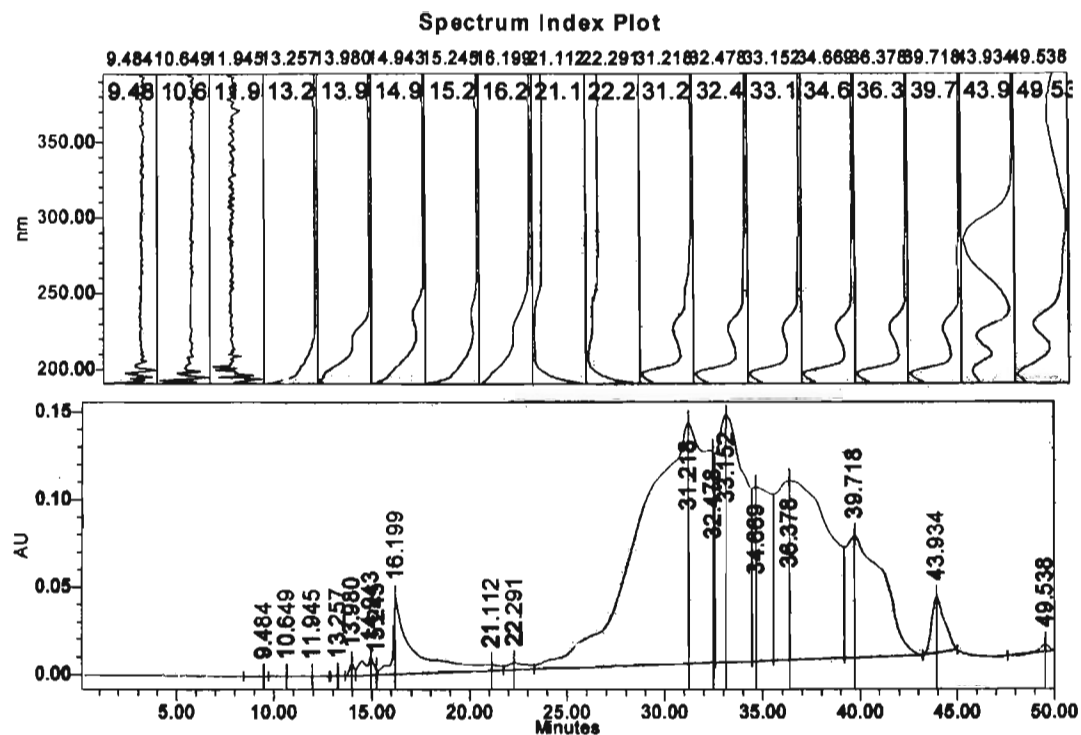
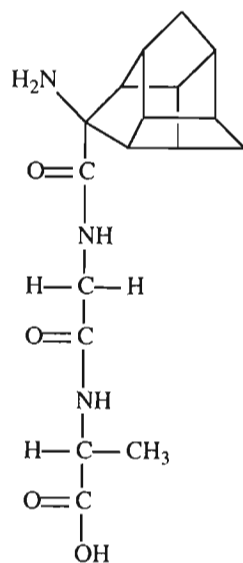
Spectrum 80: Infrared spectrum (KBr) of the Fmoc-tris-acid fluoride



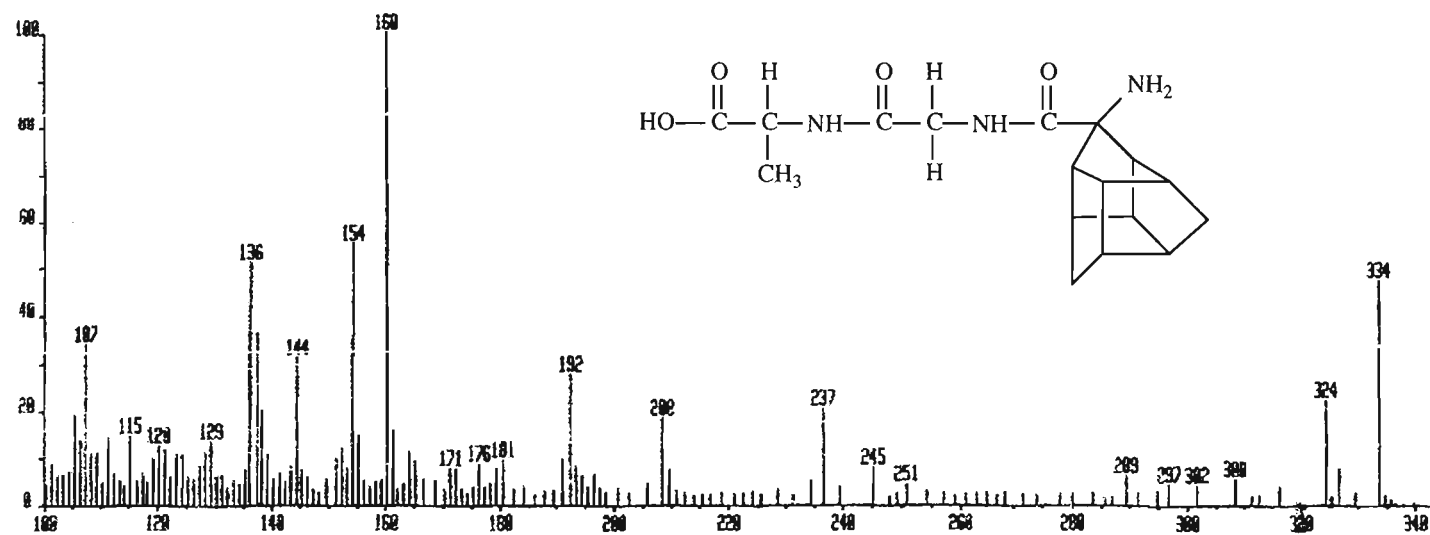
Spectrum 81: ^1H NMR spectrum of Alanine-Glycine in $[(\text{CD}_3)_2\text{SO}]$



Chromatogram 82: HPLC chromatogram of alanine-glycine from an 80 % (v/v) acetonitrile/20 % (v/v) water/0.1 % (v/v) trifluoroacetic acid (solution A) and 100 % water (solution B) gradient system: 80 % solution A and 20 % solution B was changed linearly to 40 % solution A and 60 % solution B at 1.00 ml min⁻¹ over 30 minutes.



Chromatogram 84 : HPLC chromatogram of alanine-glycine-tris-amino acid from an 80 % (v/v) acetonitrile/20 % (v/v) water/0.1 % (v/v) trifluoroacetic acid (solution A) and 100 % water (solution B) gradient system: 80 % solution A and 20 % solution B was changed linearly to 40 % solution A and 60 % solution B at 1.00 ml min^{-1} over 50 minutes.



Spectrum 85 : Mass spectrum (FAB) of alanine-glycine-tris-amino acid

Appendix 2

Commands for Gaussian 98

1.1 Commands for Gaussian 98

1.1.1 *TS*

This command is used to request the use of a mathematical search algorithm, which aims to find a local maximum on the potential energy surface (transition state) rather than a local minimum for a normal optimisation.

1.1.2 *Opt*

This instruction requests that a geometry optimisation is performed.

1.1.3 *Modredundant (modred)*

MODRED is used in conjunction with a geometry optimisation, specifying the specific co-ordinates that are to be constrained during a SCAN calculation, while the remaining co-ordinates are optimised. Bonds, bond angles and dihedral angles can be used as reaction co-ordinates. These co-ordinates could also be fixed for the duration of a calculation using MODRED.

1.1.4 *Noeigentest*

The default algorithm in G98¹ uses a test to determine the number of negative eigenvalues. If more than one negative eigenvalue is found, the program automatically terminates the calculation since it assumes the wrong negative eigenvalue (solution of the wave function) might be followed to produce a wrong result. Since there can be only one true transition state, there can only be one negative eigenvalue associated with a transition state. The problem is, except when the starting structure of the transition state calculation is very close to the real transition state, that more than one negative eigenvalues will in practice be found. The result is that very few transition state optimisations proceed to the end. To avoid this, one should turn the default eigentest off by using the "noeigentest" command.

Note that some programs have better algorithms to find transition states. For example, once a frequency calculation is performed, one is allowed to choose the negative eigenvalue representing the correct transition state. The software code will then ensure that the wave function involving the correct transition is solved.

1.1.5 *GDIIS*

This specifies the use of the modified GDIIS algorithm, which is recommended during the processing of large systems and molecules with a flat potential energy surface. It makes use of a smaller step size down (for local minima) or up (for local maxima) the potential energy surface.

1.1.6 *SCAN Calculation*

This is used to find a starting structure for a transition state optimisation. This command changes the specified reaction co-ordinate in a number of steps as the reaction proceeds from reactants to products. The rest of the molecule is optimised to find the lowest possible energy for the structure. A plot of energy for each step *versus* reaction co-ordinate reveals the approximate transition state as a maximum on the graphical plot.

-
- 1) Gaussian 98, Revision A.9, Frisch, M.J., Trucks, G.W., Schlegel, H.B., Scuseria, G.E., Robb, M.A., Cheeseman, J.R., Zakrzewski, V.G., Montgomery, Jr., J.A., Stratmann, R.E., Burant, J.C., Dapprich, S., Millam, J.M., Daniels, A.D., Kudin, K.N., Strain, M.C., Farkas, O., Tomasi, J., Barone, V., Cossi, M., Cammi, R., Mennucci, B., Pomelli, C., Adamo, C., Clifford, S., Ochterski, J., Petersson, G.A., Ayala, P.Y., Cui, Q., Morokuma, K., Malick, D.K., Rabuck, A.D., Raghavachari, K., Foresman, J.B., Cioslowski, J., Ortiz, J.V., Baboul, A.G., Stefanov, B.B., Liu, G., Liashenko, A., Piskorz, P., Komaromi, I., Gomperts, R., Martin, R.L., Fox, D.J., Keith, T., Al-Laham, M.A., Peng, C.Y., Nanayakkara, A., Challacombe, M., Gill, P.M.W., Johnson, B., Chen, W., Wong, M.W., Andres, J.L., Gonzalez, C., Head-Gordon, M., Replogle, E.S., Pople, J.A., Gaussian, Inc., Pittsburgh PA, **1998**.

Appendix 3

Cartesian Co-ordinates for Computational Structures

Co-ordinates for DFT optimised tris-hydantoin (2.64)

b3lyp/6-31+g(d) opt=restart pop=full gfprint (-763.8105618a.u.)

C, -1.193546, -1.403636, 0.496093
 C, -0.891161, -2.489253, 1.533748
 C, 0.628165, -2.381062, 1.383295
 C, 0.852441, -2.682643, -0.115436
 C, -0.226862, -1.699572, -0.724913
 H, -2.247028, -1.248678, 0.244792
 H, -1.273089, -3.481868, 1.265200
 H, -1.267945, -2.229058, 2.530479
 H, 0.728032, -3.732304, -0.398852
 C, 2.204906, -2.027448, -0.402094
 H, 3.012677, -2.443774, 0.212198
 H, 2.514125, -2.067504, -1.454145
 C, 1.760368, -0.624815, 0.026381
 C, 0.578788, -0.344953, -0.922938
 C, -0.260558, 0.712219, -0.171861
 C, -0.463708, -0.171892, 1.075969
 C, 0.943735, -0.830101, 1.368207
 H, 2.521080, 0.154277, 0.069321
 H, 0.843428, -0.095543, -1.954853
 H, 1.442419, -0.446812, 2.259233
 H, 1.244072, -2.971636, 2.068083
 H, -0.954883, 0.308859, 1.926364
 H, -0.722467, -2.070265, -1.625700
 C, 0.417790, 2.072839, 0.079528
 O, 1.437748, 2.299520, 0.704021
 N, -1.491666, 1.135580, -0.842689
 N, -0.379402, 3.017749, -0.532949
 C, -1.527634, 2.472647, -1.138217
 O, -2.361761, 3.090376, -1.774725
 H, -0.190255, 4.012088, -0.523548
 H, -2.096927, 0.505752, -1.350046

Co-ordinates for volume of trishomocubane

rhf/3-21+g scf=tight volume (-422.3703658a.u.)

C, 1.322402, -0.267346, -2.830973
 H, 2.298043, -0.683981, -2.691547
 C, 0.149199, -1.096494, -2.260161
 H, 0.017948, -2.092609, -2.628166
 C, -1.051231, -0.230749, -2.519923

H, -1.305937, -0.192595, -3.558465
 C, -0.539657, 1.099767, -1.930207
 H, -0.860945, 1.981966, -2.443431
 C, 0.994831, 0.898842, -1.870980
 H, 1.567056, 1.798256, -1.963241
 C, -2.117852, -0.777121, -1.538807
 H, -3.047457, -0.247545, -1.521966
 H, -2.357605, -1.808960, -1.689559
 C, -1.201262, -0.471554, -0.333444
 H, -1.538941, -0.764441, 0.638714
 C, -0.967200, 1.005569, -0.439489
 H, -1.823191, 1.605259, -0.210248
 C, 0.304330, 1.198449, 0.412089
 H, 0.198222, 0.801156, 1.399915
 C, 1.132022, 0.280398, -0.504048
 C, 0.227070, -0.980963, -0.723937
 H, 0.549807, -1.865501, -0.215672
 H, 2.138763, 0.052904, -0.221879
 H, 1.230799, -0.048935, -3.874431
 H, 0.654031, 2.209622, 0.400311

Co-ordinates for the transition state of the protonated trishomocubanol (6.11)

rhf/3-21+g opt=(ts,noeigentest,gdiis) freq optcyc=100 (-499.8554894a.u.)

C, -0.474635, 1.324753, -0.826928
 C, 0.677770, 1.380022, 0.151918
 C, 1.442904, 0.058812, -0.073580
 C, 0.254694, -0.906222, -0.399822
 C, -0.789669, 0.013453, -1.025284
 C, -0.303281, -1.322013, 1.011100
 C, -1.747103, -0.839010, 1.046624
 C, 0.449607, -0.324306, 1.910838
 C, -0.167186, 1.018588, 1.402229
 C, -1.485350, 0.618241, 0.669702
 C, 1.867329, -0.321635, 1.342003
 H, -1.001231, 2.162047, -1.246146
 H, 1.263939, 2.285564, 0.177544
 H, 2.207064, 0.106145, -0.837415
 H, 0.499273, -1.735508, -1.046520
 O, 0.214749, -0.364864, -3.823040
 H, -1.599631, -0.317980, -1.644527
 H, -0.147017, -2.361694, 1.262736
 H, -2.159256, -0.845112, 2.052810
 H, -2.434839, -1.363467, 0.397525

H, 0.344846, -0.501214, 2.972768
 H, -0.298610, 1.796125, 2.141025
 H, -2.322582, 1.295131, 0.641548
 H, 2.521804, 0.413878, 1.796876
 H, 2.344664, -1.292863, 1.407584
 H, 0.862896, -0.977619, -4.149309
 H, -0.149789, 0.051372, -4.594978

Co-ordinates for the transition state of the *exo-endo* PCU diol (6.12)

rhf/3-21+g opt=(ts,noeigentest,gdiis) freq optcyc=100 (-670.7193615a.u.)

C, 0.277999, 1.160234, 0.813842
 C, -1.180608, 0.857513, 0.493741
 C, -1.275256, -0.686625, 0.530150
 C, 0.154448, -1.088204, 0.022189
 C, 1.035410, 0.037537, 0.525443
 C, 0.052360, -0.933975, -1.548480
 C, 1.005827, 0.188213, -1.953730
 C, -1.336328, -0.267330, -1.700732
 C, -1.056132, 1.129099, -1.039633
 C, 0.504767, 1.298177, -1.037514
 C, -2.195398, -0.996872, -0.656251
 H, 0.640171, 2.029405, 1.312894
 H, -1.912700, 1.384351, 1.075277
 H, -1.522624, -1.080560, 1.500536
 H, 0.506106, -2.046343, 0.361695
 O, 1.231124, -1.054399, 2.766029
 H, 2.094293, -0.015337, 0.608997
 H, 0.169106, -1.861817, -2.090626
 H, 0.833286, 0.496501, -2.981181
 H, -1.713758, -0.232584, -2.712904
 H, -1.606879, 1.961314, -1.449794
 H, 0.951705, 2.267258, -1.168301
 H, -3.183018, -0.565394, -0.540430
 H, -2.290254, -2.056389, -0.865367
 H, 1.660372, -1.481369, 3.513244
 H, 0.565963, -0.308412, 3.047806
 F, -0.339679, 0.771126, 3.108325
 O, 2.410429, -0.069878, -1.747387
 H, 2.810395, -0.623140, -2.430065

Co-ordinates for the transition state of the *exo-exo* PCU diol (6.13)

rhf/3-21+g opt=(ts,noeigentest,gdiis) freq optcyc=100 (-670.7166734a.u.)

C, -0.551659, 1.059959, -0.892533
 C, 0.922343, 1.030033, -0.502997
 C, 1.330895, -0.459618, -0.609924
 C, -0.009707, -1.171069, -0.214521
 C, -1.074214, -0.212142, -0.720282
 C, -0.029481, -1.093770, 1.364082
 C, -1.231437, -0.236541, 1.734898
 C, 1.180437, -0.170646, 1.641947
 C, 0.664498, 1.173559, 1.032763
 C, -0.894726, 1.032712, 0.926738
 C, 2.224911, -0.651049, 0.621354
 H, -1.050414, 1.862048, -1.386648
 H, 1.561529, 1.726409, -1.011820
 H, 1.705815, -0.738508, -1.579722
 H, -0.142370, -2.156761, -0.624760
 O, -1.065282, -1.112417, -2.961138
 H, -2.100040, -0.458654, -0.876656
 H, 0.011306, -2.048842, 1.864317
 H, 1.471581, -0.123194, 2.677668
 H, 1.005718, 2.071367, 1.522641
 H, -1.524263, 1.889839, 1.093946
 H, 3.109999, -0.026044, 0.590937
 H, 2.522067, -1.680903, 0.784193
 H, -1.337861, -1.629737, -3.724807
 H, -0.508221, -0.257526, -3.209223
 F, 0.201809, 0.924425, -3.214789
 H, -2.190444, -0.682443, 1.515757
 O, -1.135263, 0.071147, 3.146738
 H, -1.937474, 0.454721, 3.523330

Co-ordinates for transition state in Chapter 6, Figure 6.10, letter 'a'

rhf/gen opt=(ts,noeigentest,gdiis) freq optcyc=100 (-3131.8607671)

C, 0.996524, 0.079265, -2.382304
 H, 2.005893, -0.209895, -2.146795
 C, -0.057108, -0.976491, -2.032221
 H, 0.035081, -1.891521, -2.602561
 C, -1.400389, -0.228206, -2.261659

H, -1.717121, -0.205753, -3.291183
 C, -1.071853, 1.160476, -1.649689
 H, -1.637021, 1.989779, -2.042176
 C, 0.489825, 1.281402, -1.602797
 H, 0.931513, 2.215299, -1.908727
 C, -2.352504, -0.861328, -1.238690
 H, -3.289722, -0.323619, -1.142950
 H, -2.558531, -1.907726, -1.432526
 C, -1.450130, -0.640322, -0.021326
 H, -1.779459, -0.972132, 0.947038
 C, -1.108403, 0.888721, -0.105560
 H, -1.663460, 1.521829, 0.562117
 C, 0.485276, 1.026433, -0.053706
 H, 0.895232, 1.774316, 0.599383
 C, 0.776612, -0.369077, 0.324300
 H, 1.105671, -0.616552, 1.307717
 C, -0.067019, -1.282267, -0.484885
 H, 0.030158, -2.325625, -0.235617
 O, 2.899350, -0.677013, -0.090258
 H, 3.301841, -1.429085, 0.368418
 Br, -0.062800, 0.108678, 3.299199
 H, 3.451277, 0.114431, 0.000286
 O, 0.897493, 0.451797, -3.786600
 H, 1.266910, -0.207387, -4.388283

Co-ordinates for transition state in Chapter 6, Figure 6.10, letter 'b'

rhf/gen opt=(ts,noeigentest,gdiis) freq optcyc=400 (-3131.86866a.u.)

C, 1.604054, 0.361154, -1.921991
 C, 0.622315, -0.738146, -2.346894
 H, 1.094133, -1.535712, -2.900509
 C, -0.456498, 0.047535, -3.135189
 H, -0.189017, 0.256484, -4.160366
 C, -0.627645, 1.305388, -2.232022
 H, -0.984491, 2.194277, -2.726420
 C, 0.652175, 1.404350, -1.335960
 H, 1.087539, 2.377191, -1.175533
 C, -1.748496, -0.746211, -2.906467
 H, -2.637251, -0.223389, -3.244021
 H, -1.724739, -1.737487, -3.342112
 C, -1.653434, -0.758023, -1.376876
 H, -2.425715, -1.267848, -0.823868
 C, -1.455073, 0.761382, -1.017972
 H, -2.330654, 1.286400, -0.678817

C, -0.137854, 0.869410, -0.091138
 H, -0.183472, 1.466110, 0.798721
 C, -0.012284, -0.568155, 0.131874
 H, -0.188120, -0.980977, 1.109110
 C, -0.174993, -1.320752, -1.120250
 H, -0.124692, -2.391017, -1.018850
 O, 2.084779, -0.505340, 1.533183
 H, 2.783434, -1.080968, 1.870703
 Br, -0.513469, 0.060861, 3.356557
 H, 1.485154, -0.211303, 2.270295
 H, 2.067953, 0.766142, -2.811093
 O, 2.673087, -0.079391, -1.084302
 H, 2.504825, -0.077791, -0.120471

Co-ordinates for the transition state of the 8-*exo*-fluoro-11-*exo*-hydroxy-PCU (6.16)

rhf/3-21+g opt=(ts,noeigentest,gdiis) freq optcyc=100 (-770.2721304a.u.)

C, -0.027602, -1.135451, 0.627338
 C, 1.287802, -0.510605, 0.179253
 C, 1.023766, 1.015285, 0.215314
 C, -0.488604, 1.070493, -0.204157
 C, -1.045539, -0.253275, 0.317035
 C, -0.452545, 0.965029, -1.775146
 C, -1.205949, -0.312279, -2.110739
 C, 1.028374, 0.596757, -2.018860
 C, 1.086787, -0.812958, -1.341668
 C, -0.406202, -1.295894, -1.228483
 C, 1.774203, 1.506436, -1.028798
 H, -0.137492, -2.064132, 1.141614
 H, 2.173036, -0.856938, 0.678051
 H, 1.233182, 1.482870, 1.164032
 H, -1.043924, 1.899146, 0.196894
 F, -1.854918, 0.933012, 2.286082
 H, -2.079234, -0.446986, 0.493303
 H, -0.790993, 1.842378, -2.303720
 H, -2.266068, -0.279578, -1.910770
 H, 1.332158, 0.619215, -3.051663
 H, 1.749865, -1.527992, -1.800772
 H, -0.642318, -2.340478, -1.330322
 H, 2.837931, 1.304641, -0.979185
 H, 1.620318, 2.558759, -1.237181
 F, 1.115745, -1.337341, 3.024639
 O, -0.319082, 0.284932, 3.946806

H, 0.502691, -0.609035, 3.533318
 H, -0.407277, 0.552291, 4.862727
 H, -1.084382, 0.639545, 3.227798
 O, -0.956565, -0.643379, -3.495716
 H, -1.586697, -1.268397, -3.875863

Co-ordinates for the transition state of the 8-*exo*-fluoro-11-*endo*-hydroxy-PCU (6.17)

rhf/3-21+g opt=(ts,noeigentest,gdiis) freq optcyc=100 (-770.2726247a.u.)

C, -0.015637, 1.172843, 0.536305
 C, -1.365376, 0.569235, 0.170825
 C, -1.111643, -0.958191, 0.163633
 C, 0.369480, -1.015094, -0.358215
 C, 0.972029, 0.287116, 0.148791
 C, 0.224869, -0.877061, -1.921998
 C, 0.927012, 0.422440, -2.308603
 C, -1.271087, -0.506494, -2.054319
 C, -1.276054, 0.899477, -1.352868
 C, 0.223615, 1.375531, -1.348424
 C, -1.951797, -1.427871, -1.029662
 H, 0.135773, 2.096801, 1.047474
 H, -2.207146, 0.913760, 0.739865
 H, -1.260410, -1.436342, 1.118187
 H, 0.939710, -1.860866, -0.019490
 F, 1.792719, -1.105568, 2.105642
 H, 2.017526, 0.461584, 0.243733
 H, 0.523720, -1.753980, -2.478443
 H, 0.673137, 0.725290, -3.320889
 H, -1.658866, -0.519363, -3.062797
 H, -1.975800, 1.620158, -1.745918
 H, 0.470684, 2.418137, -1.431198
 H, -3.008167, -1.221026, -0.903680
 H, -1.817750, -2.477028, -1.265730
 F, -1.014418, 1.291330, 2.931891
 O, 0.365355, -0.378982, 3.806298
 H, -0.380264, 0.494860, 3.442838
 H, 0.461308, -0.600333, 4.733373
 H, 1.130327, -0.794305, 3.010161
 O, 2.353530, 0.462062, -2.124447
 H, 2.847965, -0.055438, -2.772894

Appendix 4
Compact Disk